School of Chemical, Materials and Biological Engineering.

For the degree of Doctor of Philosophy (PhD)

Expanding the Enzymatic Toolbox for β-amino Acids and Unnatural Amino Acids Manufacturing

Fangyi Zhang

Submission Date 05.02.2025

Declaration

I, Fangyi Zhang, declare that the thesis is my own work. I am aware of the University's Guidance on the Use of Unfair Means (www.sheffield.ac.uk/ssid/unfair-means). This work has not previously been submitted for any other degrees.

Abstract

β-Amino acids, characterized by the separation of their terminal carboxylic acid and amino groups by two carbon atoms (Cα and Cβ), exhibit remarkable structural versatility. This arrangement allows for R or S isomers at both Cα and Cβ positions, resulting in up to four diastereomers for a given side chain. Such diversity facilitates the generation of a broad array of stereo- and regio-isomers, alongside the potential for di-substitution, making β-amino acids highly valuable in molecular design. Their incorporation into peptidomimetics has led to compounds with potent biological activity and enhanced resistance to proteolysis. Furthermore, β-amino acids and their derivatives serve as essential chiral building blocks in pharmaceutical synthesis, highlighting their significance in drug discovery and development.

This study focuses on enzymatic approaches to β-amino acid production as a sustainable alternative to traditional chemical synthesis, which often suffers from low carbon efficiency. Leveraging both wildtype and engineered variants of aspartase and 3-methylaspartate ammonia-lyase (MAL), this project explores their catalytic potential for industrial applications. Aspartase catalyzes the reversible deamination of L-aspartic acid via a carbanion mechanism to produce fumaric acid and ammonium ion, while MAL facilitates the α,β-elimination of ammonia from 3-methylaspartate to form mesaconate.

Novel aspartase and MAL enzymes sourced from thermophilic organisms were identified and characterized. Protocols for their recombinant expression and purification were established, and their enzymatic activities were validated through NMR and spectrometric assays. This research provides critical insights into the catalytic mechanisms and industrial applicability of aspartase and MAL, offering a foundation for environmentally friendly and efficient production of β-amino acids and other unnatural amino acids.

Acknowledgements

The past four years have flown by in the blink of an eye, leaving me deeply grateful for the journey and the people who have made it so meaningful. I feel incredibly fortunate to have encountered so many individuals who offered me encouragement, guidance, and support along the way. Every staff member, colleague, and friend—whether from within or beyond the University—has been a beautiful brushstroke in the canvas of my life, painting a picture of inspiration, resilience, and joy that I will cherish forever.

First and foremost, I would like to express my deepest gratitude to my PhD academic supervisors, Prof. Tuck Seng Wong and Dr. Kang Lan Tee, for their invaluable guidance, unwavering support, and insightful feedback throughout my research journey. Their expertise and encouragement have been instrumental in shaping this thesis and in helping me navigate the challenges of this academic pursuit. I am truly grateful for their mentorship, which has not only enriched my scientific knowledge but also inspired me to push the boundaries of my potential.

I would also like to extend my heartfelt thanks to my colleagues in our research group. Your camaraderie, collaboration, and shared enthusiasm for science have made this journey immensely enjoyable and rewarding. The stimulating discussions and moments of teamwork have left a lasting impression on me.

My sincere appreciation goes to the University of Sheffield and the School of Chemical, Materials and Biological Engineering for providing an exceptional academic environment. The resources and opportunities I have been afforded here have played a pivotal role in the success of my research.

Lastly, I want to say thank you and love you to my parents Min Zhang and Fang Wang, as well as my partner Andi, whose unwavering support and unconditional love have been my greatest source of strength throughout this journey.

Contents

List of Figures

List of Tables

Abbreviations

6× His Tag	Hexa-histidine tag for protein purification
APS	Ammonium Persulfate
AspB	Aspartase B
ATPE	Aqueous Two-Phase Extraction
BABA	β-Aminobutyric Acid
BLAST	Basic Local Alignment Search Tool (sequence analysis)
Cry/MagR	Cryptochrome/Magnetic receptor complex
D_2O	Deuterium Oxide
DKR	Dynamic kinetic resolution
dtMAL Lyase	*Dictyoglomus thermophilum* Methylaspartate Ammonia
E.Z.N.A.	E.Z.N.A.® Plasmid DNA Mini Kit
E. coli	*Escherichia* coli
ee	Enantiomeric excess
Fe_2O_3	Maghemite
Fe_3O_4	Magnetite
GABA	Gamma-aminobutyric acid
H_2O_2	Hydrogen peroxide
HIC	Hydrophobic Interaction Chromatography
HILIC	Hydrophilic Interaction Liquid Chromatography
HisTrap	HisTrap High Performance column
HiFi	High-Fidelity DNA Assembly
IMAC	Immobilized Metal Affinity Chromatography
IPTG	Isopropyl β-D-1-thiogalactopyranoside
KanR	Kanamycin resistance gene
K^+	Potassium ion
K_m	Michaelis constant
MagR	Magnetic receptor protein
MAL	Methylaspartate Ammonia Lyase

MD Simulations	Molecular Dynamics Simulations
Mg^{2+}	Magnesium ion
MIO	4-Methylideneimidazole-5-one
MNPs	Magnetic Nanoparticles
MSC	multiple cloning site
NMR	Nuclear Magnetic Resonance spectroscopy
N-substituted aspartic acids	Aspartic acid derivatives with added nucleophiles
OD	Optical Density
PCR	Polymerase Chain Reaction
PLGA	Poly(lactide-co-glycolide)
PmAspA	*Pasteurella multocida* Aspartase A
R-BABA	(R)-β-Aminobutyric Acid
SDM	Site-Directed Mutagenesis
SDS-PAGE	Sodium Dodecyl Sulfate-Polyacrylamide Gel Electrophoresis
SEC	Size-Exclusion Chromatography
SPE	Solid-Phase Extraction
T7	T7 promoter for protein expression
TCA Cycle	Tricarboxylic Acid Cycle
TEMED	Tetramethylethylenediamine
TIM barrel	Triose phosphate isomerase barrel
TYE	Tryptone Yeast Extract
V_{max}	Maximum reaction velocity
VWR	Gel documentation system (VWR, part of Avantor, USA)

1 Introduction and Literature Review: Unnatural Amino Acids and the Manufacturing of Unnatural Amino Acids.

1.1 Introduction to the β-amino acids and unnatural amino acids

1.1.1 Background on β-amino acids and unnatural amino acids.

Amino acids serve as the essential building blocks of proteins and play a crucial role in living organisms. While the twenty proteinogenic α-amino acids are the most common, there is growing interest in β-amino acids and other unnatural amino acids due to their unique properties and potential applications. β-amino acids differ from α-amino acids in that they contain an additional carbon atom between the amino and carboxyl groups (Cheng *et al.* 2001). As shown in Figure 1-1, in the presence of substituents, the two obtained regioisomers are called β^2 and β^3-amino acids (Clerici *et al.* 2016). The structural difference leads to distinct folding patterns, increased stability against proteolytic degradation, and altered physicochemical properties compared to α-amino acids (Seebach and Gardiner 2008).

Figure 1-1 The structure comparisons between α-amino acid and β-amino acids.

β-amino acids have been discovered in various natural products, such as the antifungal cispentacin (Oki *et al.* 1989) and the antitumor agent paclitaxel (Wani *et al.* 1971). Unnatural amino acids encompass a broader category of non-proteinogenic amino acids, including β-amino acids, D-amino acids, and those with modifications to the side chain or backbone (Blaskovich *et al.* 2016). These artificial amino acids expand the structural and functional diversity beyond what is available with the 20 natural amino acids. Incorporation of unnatural amino acids into peptides and proteins enables the fine-tuning of properties such as stability, bioactivity, and catalytic functions (Liu and Schultz 2010).

In summary, β-amino acids and unnatural amino acids provide vast opportunities to expand the structural and functional scope of peptides and proteins. This chapter will discuss the applications of unnatural amino acids and the methods for their manufacture.

1.1.2 Importance of β-amino acids and unnatural amino acids in pharmaceuticals, biocatalysis, and synthetic chemistry.

β-Amino acids and unnatural amino acids have garnered significant attention due to their versatile applications in pharmaceuticals, biocatalysis, and synthetic chemistry. Their distinctive structural and functional properties have facilitated advancements in drug discovery, enzyme engineering, and the synthesis of novel compounds. These amino acids offer a unique platform to enhance the stability, specificity, and efficacy of pharmaceutical agents, while also enabling the design of biocatalysts with improved activity and selectivity. Moreover, their integration into synthetic chemistry has expanded the repertoire of accessible chemical scaffolds, paving the way for innovative methodologies and applications.

1.1.2.1. Pharmaceuticals

In the pharmaceutical industry, β-amino acids and unnatural amino acids have been utilized to develop peptide-based therapeutics with enhanced pharmacological properties. The incorporation of these non-natural building blocks into peptide drugs improves their stability, bioavailability, and target specificity (Luca *et al.* 2010). For example, peptides containing β-amino acids exhibit remarkable resistance to proteolytic degradation, as the backbone extension (–CH_2– insertion between the carbonyl and amino group) disrupts the recognition and cleavage sites of most endo- and exopeptidases (Cheng *et al.* 2001). This structural modification prevents common proteases such as trypsin, chymotrypsin, and pepsin from effectively binding and hydrolyzing the peptide bond. As a result, β-peptide–containing therapeutics maintain their structural integrity for significantly longer periods in biological fluids, thereby prolonging their half-life in vivo and improving oral bioavailability and dosing intervals compared to conventional α-peptides.

Furthermore, unnatural amino acids with tailored functional groups enable the design of peptide-drug conjugates, which facilitate targeted drug delivery while reducing off-target effects. β-amino acids have also been explored as standalone therapeutic agents. A notable example is cispentacin, a naturally occurring β-amino acid first isolated from Streptomyces species (Oki *et al.* 1989). Structurally, cispentacin is a conformationally constrained cyclic β-amino acid (Figure 1-2), consisting of a

cyclopentane ring bearing an amino group (–NH_2) and a carboxyl group (–COOH) in a trans-relationship. This rigid framework distinguishes cispentacin from flexible linear β-AAs, conferring metabolic stability and reducing its susceptibility to enzymatic degradation. Pharmacologically, cispentacin displays potent antifungal activity, particularly against Candida albicans and other pathogenic yeasts, by disrupting fungal cell wall biosynthesis. Importantly, it shows low mammalian toxicity, highlighting its potential as a safe therapeutic lead.

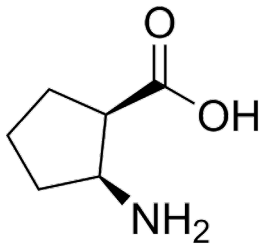

Figure 1-2 Structure of cispentacin.

Additionally, synthetic β-peptides have demonstrated significant antimicrobial properties (Porter *et al*. 2002). Porter and colleagues reported that oligomers of β-amino acids can fold into stable secondary structures, most notably the 14-helix, which mimics the amphipathic α-helices found in natural antimicrobial peptides. Unlike linear α-peptides, these β-peptides are highly resistant to proteolytic degradation, enabling them to retain activity in biological fluids where α-helical peptides are rapidly cleaved. Moreover, by presenting alternating hydrophobic and cationic residues along the helix, β-peptides replicate the amphipathic topology critical for interaction with bacterial membranes.

Magainins, a class of antimicrobial peptides discovered in the African clawed frog (*Xenopus laevis*), exhibit broad-spectrum antibacterial activity (Zasloff 1987). The unique folding patterns of β-peptides, including their ability to form stable helical structures, have been exploited to develop inhibitors of protein-protein interactions (PPI), which are often considered challenging targets for traditional small-molecule drugs (Kritzer *et al.* 2004). For example, Kritzer *et al.* demonstrated this concept by targeting the p53·hDM2 interaction. The tumor suppressor p53 is inactivated in many cancers through binding of its N-terminal transactivation domain (p53AD) to the E3 ubiquitin ligase hDM2, which promotes p53 degradation. Blocking this PPI is a validated anticancer strategy. Instead of trying to mimic the primary sequence of the p53AD (residues 15–29), Kritzer *et al.* built β^3-peptides that folded into a stable 14-helix, presenting key side chains (Phe19, Trp23, Leu26) at the correct helical periodicity to match their arrangement in the native α-helix of p53. This secondary

structure homology approach yielded β³-peptides with nanomolar affinity for hDM2, resistant to proteolysis, and significantly more stable than natural α-helices. Importantly, this work established β-peptides as modular scaffolds for designing PPI inhibitors, with advantages in stability and pharmacokinetics over peptide or small-molecule mimics.

1.1.2.2. Biocatalysis

In the field of biocatalysis, unnatural amino acids have been employed to expand the catalytic capabilities of enzymes. By incorporating unnatural amino acids with novel functional groups, researchers have successfully developed enzymes with enhanced or entirely new catalytic activities (Wang *et al.* 2006). This approach, known as enzyme engineering, has been used to develop biocatalysts for the synthesis of pharmaceuticals, fine chemicals, and biofuels (Bornscheuer *et al.* 2012).

For example, fluorinated amino acids such as trifluoroleucine have been introduced into enzymes to improve thermal stability, as the strong electronegativity and unique packing properties of fluorine strengthen hydrophobic interactions within the protein core, thereby stabilizing the folded state (Montclare and Tirrell 2006). Beyond side-chain modification, altering the peptide backbone itself can yield additional benefits: Buß *et al.*combined computational design with directed evolution to integrate β-amino acids into a lipase scaffold, generating variants that not only exhibited increased thermostability but also displayed enhanced catalytic activity toward non-natural esters, thus broadening substrate scope (Buß *et al.* 2018).

More radically, unnatural amino acids with novel chemical functionalities have been employed to create enzymes capable of catalyzing entirely abiological reactions. By introducing residues that can coordinate metals or participate in bioorthogonal chemistry, enzymes have been engineered to promote transformations such as C–C bond formation, cyclopropanation, and nitrene insertion, reactions absent from the natural enzymatic toolkit (Drienovská and Roelfes 2020).

Unnatural amino acids have also been utilized to expand the genetic code of microorganisms, enabling the incorporation of novel functional groups into enzymes. For example, Xie *et al.* incorporated p-acetylphenylalanine into a lipase using an engineered tRNA/tRNA synthetase pair. The acetyl group on this residue provided a chemically orthogonal handle that enabled site-specific immobilization of the enzyme on solid supports through covalent attachment. This strategy not only improved the enzyme's operational stability but also enhanced its reusability, making it particularly attractive for industrial biocatalysis where immobilized enzymes are routinely employed (Xie *et al.* 2007). Beyond immobilization, unnatural amino acids have also been exploited to construct artificial metalloenzymes, wherein a residue bearing a

metal-binding moiety is strategically introduced into a protein scaffold. For instance, Drienovská *et al.* demonstrated that such approaches can yield hybrid catalysts with tailored catalytic properties, combining the structural precision of enzymes with the broad reactivity of transition metals. These artificial metalloenzymes have been designed to perform transformations not accessible to natural biocatalysts, including abiological reactions such as olefin metathesis and selective C–H functionalization (Drienovská *et al.* 2018).

1.1.2.3. Synthetic chemistry

β-Amino acids and other unnatural amino acids have found broad utility in synthetic chemistry as versatile chiral building blocks for the construction of complex and bioactive molecules. Their extended backbone and stereochemical richness enable unique conformational control in target synthesis. A notable example is the synthesis of the antitumor agent (-)-bestatin, a natural aminopeptidase inhibitor with immunomodulatory properties. For example, Juaristi et al. demonstrated that enantiomerically pure (S)-β-phenylalanine could be employed as a chiral precursor to assemble (-)-bestatin with the correct stereochemistry (Figure 1-3) underscoring the value of β-amino acids in stereoselective synthesis (Juaristi *et al.* 1996).

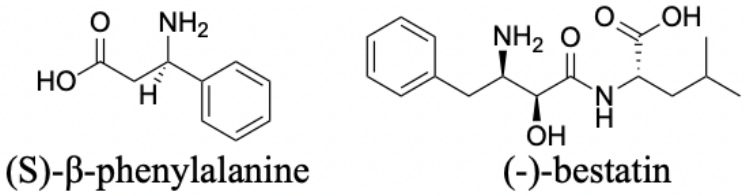

Figure 1-3 The structure of (S)-β-phenylalanine (*left*) and (-)-bestatin (*right*).

Beyond bestatin, β-amino acids have been incorporated into the synthesis of alkaloids, β-lactams, peptidomimetics, foldamers, and functional materials with properties that surpass those of natural peptides. Unlike natural peptides, which are often unstable outside physiological conditions, β-peptides can adopt highly stable helices, sheets, and turns that are resistant to proteolysis. This structural robustness makes them attractive as scaffolds for a variety of applications. For example, Guichard and Huc 2011 highlighted the use of foldamers—synthetic oligomers that mimic peptide secondary structures—for the creation of bioactive molecules, molecular recognition systems, and supramolecular assemblies. Similarly, Martinek and Fülöp 2012 demonstrated that β-peptides can form well-defined helical conformations (such as the 14-helix), which can be exploited to design nanostructured materials, self-assembling

systems, and functional polymers with tunable mechanical or electronic properties (Martinek and Fülöp 2012).

Unnatural amino acids have also been used as chiral building blocks in asymmetric synthesis, enabling the stereoselective preparation of pharmaceuticals and natural products (Shibasaki and Kanai 2008). A classic example is the development of chiral phosphinooxazoline (PHOX) ligands, in which oxazoline units derived from unnatural α-amino acids provide a stereogenic element (Helmchen and Pfaltz 2000). Helmchen and Pfaltz (2000) demonstrated that these ligands, when complexed with palladium, enabled asymmetric allylic alkylations with excellent enantioselectivities, cementing PHOX ligands as one of the most influential ligand classes in asymmetric catalysis. In addition to their role in chiral ligand synthesis, β-amino acids have been used as chiral scaffolds for the preparation of organocatalysts. For example, β-amino acid-derived chiral imidazolidinones, which have been used as organocatalysts in asymmetric Diels-Alder reactions (Córdova *et al.* 2002). Furthermore, the incorporation of unnatural amino acids into peptide-based catalysts has enabled the development of efficient and selective organocatalysts for a variety of synthetic transformations (Wennemers 2011). As highlighted by Wennemers (2011), these systems leverage the tunable nature of peptide backbones to achieve efficient and selective catalysis in transformations such as Michael additions and aldol reactions, while offering a sustainable, metal-free alternative.

In conclusion, β-amino acids and unnatural amino acids have proven to be valuable chiral building blocks in organic synthesis. Their unique structural features and the ability to introduce stereochemical complexity have enabled the synthesis of a wide range of chiral compounds, including bioactive natural products, chiral ligands, organocatalysts, auxiliaries, and peptidomimetics.

1.2 The synthetic methods of β-amino acid

1.2.1 Introduction of β-amino butyric acid (BABA).

β-amino butyric acid (BABA) is a non-proteinogenic amino acid that has been widely studied for its potential applications in agriculture, medicine, and materials science. As shown in Figure 1-4, BABA is an isomer of the inhibitory neurotransmitter γ-Aminobutyric acid (GABA) and has been shown to exhibit a range of biological activities (Watanabe *et al.* 2002). BABA is a synthetic compound (Meyer *et al.* 2006), its natural occurrence is very rare (Jisha and Puthur 2016).

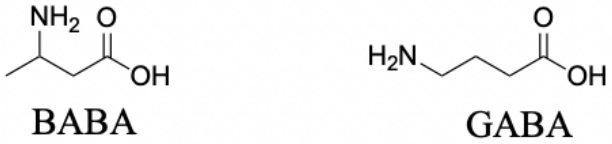

Figure 1-4 Structure of BABA (*left*) and GABA (*right*).

One of the most promising applications of BABA is in agriculture as a plant defense activator. Several studies have shown that treatment of plants with BABA induces resistance to a variety of pathogens, including fungi, bacteria, and viruses (Cohen 2002, Koen *et al.* 2014). BABA activates the plant's innate defense mechanisms, including the production of pathogenesis-related proteins and the reinforcement of cell walls (Zimmerli *et al.* 2000). For example, Sahebani et al. investigated the effects of β-amino-butyric acid (BABA) on cucumber resistance against the root-knot nematode (Meloidogyne javanica) (Sahebani *et al.* 2011). Their findings revealed that BABA treatment significantly reduced nematode infection levels, stimulated the accumulation of defense compounds such as hydrogen peroxide (H_2O_2) and phenolics, and increased the activity of defense-related enzymes, including peroxidase, polyphenol oxidase, and catalase, in cucumber roots. These results suggest that BABA enhances nematode resistance by stimulating plant defense mechanisms, offering a potential alternative to chemical nematode management.

In addition to its agricultural applications, BABA demonstrates complex biological effects on gastrointestinal tissues and bacterial populations. A recent rat study (Al-Dulaimy and Jasim 2022) evaluated the impact of BABA on gastrointestinal tissue integrity and enteric bacterial populations. At varying concentrations, BABA exhibited minimal effects on stomach tissue but progressively altered the structures of the small and large intestines, particularly at higher concentrations (200–300 mg/kg). These alterations were characterized by inflammatory cell infiltration, endothelial cell shedding, and villous adhesion. Furthermore, BABA demonstrated significant antimicrobial properties, markedly reducing populations of three pathogenic enteric bacteria—Escherichia coli, Klebsiella pneumoniae, and Brucella melitensis. At the highest concentrations tested, bacterial growth was nearly eliminated. These findings highlight BABA's potential as a novel antimicrobial agent with broad applications in medicine.

1.2.2 β-amino acids synthetic methods.

β-Amino acids are essential building blocks in medicinal chemistry, peptidomimetics, and the synthesis of natural products; they are distinguished from α-amino acids by an additional methylene group between the amino and carboxyl groups. This structural feature imparts unique properties containing β-amino acids, such as enhanced

metabolic stability and improved biological activities, to peptides containing β-amino acids. These unique properties have driven significant progress in the development of synthetic methods for β-amino acids, addressing the growing demand for compounds with precise stereochemical purity.

The β-amino acids synthetic strategies can be broadly classified into several key approaches (Table 1). Homologation of α-amino acids, leveraging the chiral pool of natural amino acids, is a foundational technique that preserves stereochemical integrity. Methods such as Arndt-Eistert homologation exemplify this approach, enabling the conversion of α-amino acids into their β-amino acid counterparts. Asymmetric synthesis, particularly through conjugate additions of nitrogen nucleophiles to α,β-unsaturated esters or acids, is another widely used strategy. This method provides access to diverse β-amino acid derivatives with excellent stereocontrol, typically facilitated by chiral catalysts or auxiliaries.

Chemoenzymatic methods have also emerged as powerful tools for β-amino acid synthesis. These approaches utilize biocatalysts such as lipases and aminomutases to achieve highly enantioselective transformations under mild conditions. However, substrate specificity can sometimes limit their broader applicability. Modern catalytic approaches, including transition metal-catalyzed and organocatalytic transformations, have further expanded the synthetic toolbox. These methodologies offer advantages such as enhanced atom economy, operational simplicity, and precise stereochemical control, making them highly attractive for both academic and industrial applications.

In this chapter, representative examples of manufacturing methods for β-amino acids and unnatural amino acids will be discussed, showcasing their diverse synthetic strategies and practical applications.

Table 1 Main strategies to prepare β-amino acid building blocks.

Method	Description	Starting Materials
Arndt–Eistert Homologation	Extend α-amino acids by one carbon via diazoketone formation and Wolff rearrangement	Natural α-amino acids
Michael Addition	Nucleophilic addition to α,β-unsaturated esters or nitriles	Acrylates, acrylonitrile, fumarates
Asymmetric Hydrogenation	Catalytic hydrogenation of dehydro-β-amino acid derivatives	Dehydroamino acids or β-enamides

Chiral Auxiliary Approach	Alkylation of chiral imide or oxazolidinone to control β-center	Chiral imide and electrophile
Reductive Amination	Reductive amination of β-keto esters or acids	β-Keto esters or β-keto acids
Strecker-type Synthesis	Multicomponent formation of β-amino nitriles and hydrolysis to acids	Aldehyde with NH_3 and HCN or TMSCN

1.2.3 The chiral pool synthesis method.

The chiral pool synthesis approach is a well-established and reliable method for preparing β-amino acids. This method utilizes readily available natural α-amino acids as starting materials while preserving their stereochemical integrity. Extensively reviewed by Juaristi and López-Ruiz, this strategy often employs Arndt-Eistert homologation as the key reaction (Juaristi and López-Ruiz 1999). As shown in the Figure 1-5, the process begins with the conversion of the carboxylic acid group of an α-amino acid into an acyl chloride. The acyl chloride is then treated with diazomethane to produce a diazoketone intermediate, which undergoes a Wolff rearrangement. This rearrangement, performed by sonicating the diazoketone with a silver catalyst under dark conditions, yields the corresponding β3-amino acid with high stereochemical fidelity.

While the Arndt-Eistert homologation is a powerful technique, it has limitations due to the use of diazomethane. Diazomethane is highly toxic, extremely volatile, and prone to explosive decomposition when exposed to heat, light, or sharp surfaces. Its instability requires that it be freshly prepared before use, further complicating its application. The handling of diazomethane necessitates strict safety protocols, including the use of specialized equipment such as explosion-proof glassware and fume hoods, which significantly increase operational complexity and cost. Additionally, environmental concerns arise from the careful disposal required to neutralize its residues, adding further challenges to its practical application.

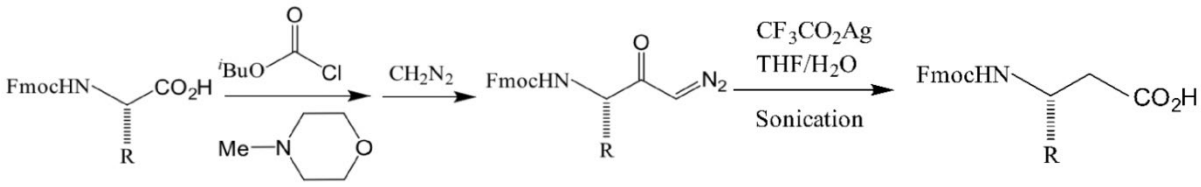

Figure 1-5 Arndt-Eistert homologation.

1.2.4 The asymmetric synthesis methods.

As shown in Figure 1-6, the asymmetric reduction of β-enamino esters enabling the conversion of β-enamino esters—compounds containing a C=C double bond adjacent to an amino group—into enantiomerically enriched β-amino esters. This process utilizes chiral catalysts or reagents to achieve precise stereochemical control, producing β-amino esters as key intermediates for pharmaceuticals and natural products. The reaction typically involves the selective reduction of the C=C double bond via hydrogenation or hydride transfer while preserving the amino and ester functional groups.

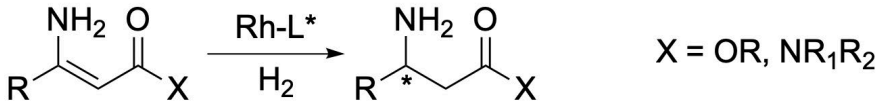

Figure 1-6 Asymmetric hydrogenation of unprotected enamine esters and amides.

Schematic representation of the Rh–Josiphos catalyzed asymmetric hydrogenation of unprotected enamino esters and amides. In the presence of Rh complexes with chiral Josiphos-type ligands (Rh–L*), the reaction proceeds with molecular hydrogen (H_2) to afford β-amino esters and β-amino amides in high yield and excellent enantioselectivity (93–97% ee). The process does not require protection or deprotection steps, making it a highly efficient synthetic route for the preparation of enantiomerically enriched β-amino acid derivatives.

Chiral transition metal catalysts, including rhodium (Rh), ruthenium (Ru), and iridium (Ir) complexes, are widely employed for their ability to achieve high stereoselectivity. Ligands such as BINAP and DuanPhos play a critical role in enhancing the

enantioselectivity of these catalysts. For instance, a study (Gao *et al.* 2017) demonstrated asymmetric hydrogenation of β-acetylamino vinylsulfides to synthesize chiral β-acetylamino sulfides using a Rh-DuanPhos catalyst, achieving exceptional enantioselectivity of up to 99% enantiomeric excess (*ee*). The use of chiral transition metal catalysts in synthesizing chiral β-acetylamino sulfides shows high efficiency and stereocontrol.

Another notable contribution to asymmetric synthesis is the proline-catalyzed direct asymmetric three-component Mannich reaction (List *et al.* 2002). This method enables the synthesis of β-amino carbonyl compounds with enantioselectivities up to 99% ee. The reaction employs simple ketones, aldehydes, and amines as substrates, with proline serving as an inexpensive, non-toxic catalyst. Key optimizations include reducing catalyst loading and substrate quantities without compromising yield or stereoselectivity, thereby enhancing the process's efficiency and practicality. Furthermore, the reaction's broad scope accommodates various aldehydes and ketones, achieving high chemo-, regio-, and diastereoselectivity.

1.2.5 Cycloaddition reactions.

Shindo *et al.* introduced an innovative anionic inverse electron-demand 1,3-dipolar cycloaddition of nitrones with ynolates to synthesize substituted 5-isoxazolidinones with high regio- and stereoselectivity (Figure 1-7). These cycloadducts were subsequently converted into β-amino acids via reduction, providing a short and efficient synthetic route. The reaction involves the generation of ynolates from dibromoesters, followed by their reaction with nitrones (Shindo *et al.* 2002). The selective protonation of intermediates was shown to determine the diastereomeric outcome. Optimization of the quenching conditions revealed that protonation with tert-butyl alcohol predominantly yielded trans-5-isoxazolidinones with excellent stereocontrol. The scope of the reaction was evaluated using a variety of nitrones and ynolates, achieving moderate to high yields. The resulting 5-isoxazolidinones were demonstrated to be versatile intermediates, enabling further functionalization and the synthesis of diverse β-amino acids.

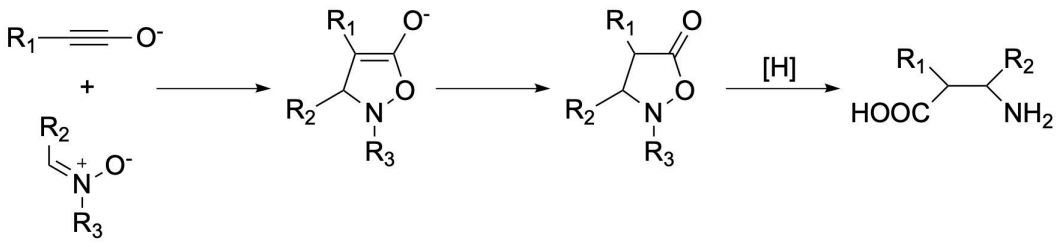

Figure 1-7 Anionic inverse electron-demand 1,3-dipolar cycloaddition of ynolates with nitrones leading to β-amino acids.

The scheme illustrates the first reported inverse electron-demand [3+2] cycloaddition of ynolates with nitrones to form 5-isoxazolidinones as key intermediates. Subsequent reduction of these heterocycles provides access to synthetically valuable β-amino acids. This strategy offers a novel and efficient route to β-amino acid scaffolds using ynolate chemistry, expanding the synthetic toolbox for nitrogen-containing building blocks.

Another example of using cycloaddition reactions was reported by He et al. who explored a copper(I)-catalyzed asymmetric 1,3-dipolar cycloaddition of azomethine ylides with β-phthaliminoacrylate esters. This method produced pyrrolidine β-amino acid derivatives with exceptional stereoselectivity (dr >20:1, ee >99%). Utilizing a Cu(I)/Ph-Phosferrox catalytic system, the reaction achieved high yields (up to 98%) under mild conditions and exhibited a broad substrate scope, tolerating various ester and imino groups (He *et al.* 2017), . The resulting cycloadducts were efficiently converted into pyrrolidine β-amino acids through deprotection and hydrogenolysis, providing a scalable and versatile method for synthesizing these valuable compounds.

1.2.6 The chemoenzymatic methods.

Biocatalytic strategies have emerged as versatile and sustainable approaches for the synthesis of β-amino acids, offering high stereoselectivity, mild reaction conditions, and alignment with green chemistry principles. A variety of enzyme classes—including lipases, proteases, and dehydrogenases—have been harnessed to transform simple precursors into enantiopure β-amino acids or their derivatives, each method providing distinct advantages in terms of efficiency, selectivity, and substrate scope. Table 2 summarizes representative examples of these enzymatic approaches.

Lipase-catalyzed kinetic resolution is a powerful technique that utilizes the selective hydrolysis or acylation of racemic β-amino acid derivatives. Lipases such as Candida antarctica lipase B (CAL-B) and Pseudomonas cepacia lipase display remarkable enantioselectivity and broad substrate tolerance. For example, CAL-B has been applied to the resolution of β-amino esters, affording products with high optical purities (Forró and Fülöp 2007). The dynamic kinetic resolution (DKR) approach further enhances efficiency by combining enzymatic resolution with in situ racemization, enabling yields of up to 100% for the desired enantiomer (Strompen 2012).

Beyond lipases, protease-catalyzed amidation offers another powerful route to β-amino acid derivatives. Nuijens *et al.* introduced the method to synthesize C-terminal arylamides of amino acids and peptides using the industrial serine protease Alcalase under near-anhydrous conditions. This method achieves high yields (50–95%) and excellent chemical, enantiomeric, and diastereomeric purity without racemization. The process accommodates unprotected side-chain functionalities such as β/γ-carboxyl, hydroxyl, and guanidino groups, highlighting its flexibility. The study also demonstrates the versatility of other enzymes, such as papain and CAL-B, in efficiently producing anilides under optimized conditions (Nuijens *et al.* 2009) .

Dehydrogenase-based methods represent another innovative approach for the synthesis of β-amino acid precursors. These methods rely on the reduction of β-iminoesters to β-amino acid precursors using NADH-dependent reductases, often supported by cofactor recycling systems to enhance efficiency and reduce costs. For example, Zhang *et al.* described the development of a novel β-amino acid dehydrogenase (β-AADH) for the synthesis of chiral β-amino acids via reductive amination of β-keto acids (Zhang *et al.* 2015). Through domain scanning mutagenesis of L-erythro-3,5-diaminohexanoate dehydrogenase from *Candidatus Cloacamonas acidaminovorans*, mutants with significantly enhanced activity toward non-native β-amino acid substrates were identified. The engineered β-AADH catalyzed the reductive amination of β-keto acids derived from stable precursors such as β-keto esters and nitriles, with D-glucose dehydrogenase used for cofactor regeneration. This process facilitated the synthesis of various chiral β-amino acids, including (R)-β-homomethionine, (R)-β-phenylalanine, and (S)-β-aminobutyric acid, with preparative yields ranging from 12% to 22%. This method represents a significant advancement in the efficient and stereoselective production of β-amino acids, providing a scalable and environmentally friendly alternative to traditional chemical synthesis.

Table 2 Chemoenzymatic methods for β-amino acid synthesis.

Enzyme Example(s)	Substrate(s)	Reaction Type	Products	Reference(s)
Lipases: *Candida antarctica* lipase B (CAL-B), *Pseudomonas cepacia* lipase	Racemic β-amino esters	Enantioselective hydrolysis or acylation; DKR combines enzymatic resolution with in	Enantiopure β-amino esters	(Forró and Fülöp 2007)

		situ racemization		
Alcalase (serine protease)	Amino acids and peptides (C-terminal) and arylamines	Amidation under near-anhydrous conditions	C-terminal arylamides of amino acids and peptides	(Forró and Fülöp 2007)
Engineered β-amino acid dehydrogenase (β-AADH) and glucose dehydrogenase (for NADH recycling)	β-Keto acids (from β-keto esters or nitriles)	NADH-dependent reductive amination	Chiral β-amino acids, e.g., (R)-β-homomethionine, (R)-β-phenylalanine, (S)-β-aminobutyric acid	(Zhang *et al.* 2015)

1.2.7 Ammonia lyases and aminomutases for α- and β-Amino acid synthesis.

The synthesis of β-amino acids has long attracted interest due to their value as building blocks for pharmaceuticals, peptidomimetics, and functional materials. However, traditional chemical methods for β-amino acid synthesis are often hampered by several limitations. Many strategies, such as asymmetric hydrogenation, cycloaddition, or chiral auxiliary-based routes, require multi-step sequences, stoichiometric amounts of chiral reagents, and harsh reaction conditions (e.g., strong bases, high temperatures, or metal catalysts). These approaches frequently suffer from poor atom economy, generate significant chemical waste, and may rely on toxic or precious transition metals, making large-scale applications less sustainable. In addition, achieving high stereocontrol remains challenging, often necessitating extensive use of protecting groups or resolution steps, which further reduces efficiency and increases environmental impact.

In contrast, biocatalytic approaches provide a sustainable and efficient alternative for the synthesis of β-amino acids. Enzyme-catalyzed reactions operate under mild, aqueous conditions and typically exhibit high regio- and stereoselectivity, thereby

eliminating the need for protecting groups and minimizing waste. Enzymes such as transaminases, aminomutases, and hydrolases have been engineered or repurposed to enable direct access to enantiopure β-amino acids from simple precursors. To provide a clear overview of these strategies, Table 3 summarizes the key enzymes, substrates, products, and outcomes reported for β-amino acid synthesis, which will be referred to in subsequent sections for detailed discussion. These biocatalytic processes align strongly with the principles of green chemistry, offering improvements in atom economy, energy efficiency, and the use of renewable catalysts (enzymes). Furthermore, biocatalysis can be integrated into chemoenzymatic cascades, enabling streamlined one-pot syntheses that reduce solvent use and purification steps.

Ammonia lyases and aminomutases represent two distinct but mechanistically related classes of enzymes that have emerged as powerful biocatalysts for the stereoselective synthesis of amino acids. These enzymes share a common 4-methylideneimidazole-5-one (MIO) cofactor and exhibit remarkable specificity in their transformations.

Ammonia lyases, such as phenylalanine ammonia lyase (PAL) (D'Cunha *et al*. 1994) and tyrosine ammonia lyase (TAL), catalyse the reversible addition of ammonia to cinnamic acid derivatives, producing L-phenylalanine and L-tyrosine respectively. These enzymes are widespread across plants, fungi, and prokaryotic organisms, and their synthetic utility has garnered increasing attention for producing diverse *L*-arylalanine derivatives. For instance, enantiopure L-arylalanines have been synthesized from arylaldehydes through a one-pot process combining chemical and enzymatic reactions (Paizs *et al.* 2006). The process begins with a Wittig reaction, a classical carbon–carbon bond-forming reaction in which an arylaldehyde reacts with a phosphonium ylide to produce an α,β-unsaturated ester. This step introduces the key carbon–carbon double bond adjacent to the ester group, which is essential for downstream biotransformation. The unsaturated ester is then subjected to porcine liver esterase (PLE)-catalyzed hydrolysis, yielding the corresponding cinnamic acid derivative. Finally, PAL from parsley catalyzes the stereoselective amination of the cinnamic acid to furnish enantiopure L-arylalanines. This combined chemical–enzymatic process achieved high yields across a range of substrates: phenyl (88%), 4-chlorophenyl (78%), 3-fluorophenyl (72%), and thiophen-2-yl (91%), after purification by ion-exchange chromatography.

Table 3 Enzymatic reactions for the synthesis of β-amino acids and derivatives.

Enzyme	Reaction type	Substrate(s)	Product(s)	Reference(s)
Phenylalanine ammonia lyase	Reversible amination	Cinnamic acid derivatives	L-Phenylalanine (and analogues)	(D'Cunha *et al*. 1994)

(PAL)				
Tyrosine ammonia lyase (TAL)	Reversible amination	p-Coumaric acid derivatives	L-Tyrosine and derivatives	(D'Cunha *et al.* 1994)
Aspartase B (AspB)	Hydroamination /Michael addition	Fumarate, acrylates	L-Aspartate, N-substituted aspartates, β-AAs	(Li *et al.* 2018)
3-Methylaspartate ammonia lyase (MAL)	Reversible amination	Mesaconate	(2S,3S)- & (2S,3R)-3-methylaspartic acids	(Raj *et al.* 2012)
Phenylalanine aminomutase (PAM), Tyrosine aminomutase (TAM)	2,3-Amino shift (α→β)	(S)-α-arylalanines	(R)-β-arylalanines	(Parmeggiani *et al.* 2018)
Engineered C–N lyases	Hydroamination	Acrylates, β-keto acids, industrial substrates	ncAAs, β-AAs, β-lactam precursors	(Drienovská and Roelfes 2020)

Aspartase B from *Bacillus sp.* YM55-1 catalyzes the enantioselective addition of ammonia to fumarate, yielding L-aspartate. AspB has also been shown to mediate Michael-type additions, in which nucleophiles such as primary or secondary amines attack the activated double bond of fumarate. This process forms C–N bonds at the β-position, producing N-substituted aspartic acids with high regio- and stereoselectivity. Importantly, AspB tolerates a broad range of amine nucleophiles—including benzylamine, allylamine, and heteroaryl-substituted amines—while consistently delivering products with enantiomeric excesses ranging from 97% to >99% (Weiner *et al.* 2008). These biotransformations highlight the enzyme's utility not only for L-aspartate production but also as a versatile biocatalyst for constructing structurally diverse β-amino acid derivatives, which are valuable as pharmaceutical building blocks (Weiner *et al.* 2008). Structure-based computational enzyme design has further expanded AspB's substrate scope, enabling the asymmetric addition of ammonia to substitute acrylates to produce enantiopure β-amino acids. The redesigned enzymes exhibited excellent substrate tolerance (up to 300 g/L), conversion rates (up to 99%), β-regioselectivity (>99%), and enantiomeric excess (>99%), demonstrating their

industrial applicability. Details of these engineered AspB enzymes will be discussed in Section 1.3.3.

Additionally, 3-methylaspartate ammonia lyase (MAL) has been engineered to create mutants with enhanced diastereoselectivity for the reversible amination of mesaconate. Wild-type MAL produces both (2S,3S)- and (2S,3R)-3-methylaspartic acid (Raj *et al.* 2009). Structural analysis led to the design of active-site mutants (K331A, H194A, and Q329A) that significantly improved diastereoselectivity. Two additional mutants, Q73A and L384A, developed through structure-based mutagenesis, expanded the enzyme's nucleophile and electrophile acceptance, respectively (Raj *et al.* 2012). The Q73A mutant efficiently catalyzed the addition of various amines to mesaconate, producing *N*-substituted 3-methylaspartic acids with high regio- and stereoselectivity, while the L384A mutant demonstrated a broadened substrate scope. The details of MAL and its engineering will be further discussed in Section 1.4.

More recently, Drienovská and Roelfes presented the development of a versatile enzyme platform for synthesizing non-canonical amino acids (ncAAs), which are essential building blocks in pharmaceuticals and bioactive compounds. Approximately 12% of top-selling drugs contain ncAA components, yet traditional chemical synthesis methods face challenges with stereoselectivity, functional group compatibility, and the need for complex protection/deprotection steps (Drienovská and Roelfes 2020). Computational redesign of AspB has addressed these limitations by creating improved C–N lyases capable of hydroamination reactions. Using molecular dynamics simulations to predict beneficial mutations, these redesigned enzymes achieved high conversion rates (up to 99%) and excellent enantioselectivity (>99%) under scalable, industrially relevant conditions. The platform has also been integrated into cascade reactions for β-lactam synthesis and pharmaceutical precursor production, demonstrating its practical utility at the kilogram scale.

Complementing ammonia lyases, aminomutases catalyze the remarkable conversion of α-amino acids to their respective β-amino acid derivatives via a 2,3-amino shift mechanism. These enzymes, including phenylalanine aminomutase (PAM) and tyrosine aminomutase (TAM), also utilize the MIO prosthetic group to achieve high stereoselectivity, although their substrate scope remains limited (Parmeggiani *et al.* 2018). For example, *Chondromyces crocatus* and *Myxococcus fulvus* produce opposite stereochemical forms of β-tyrosine, used as building blocks for secondary metabolites. In *C. crocatus*, the enantiomeric excess of (R)-β-tyrosine can be influenced by mutating a single residue in its aminomutase enzyme CmdF. PAM can convert (S)-α-arylalanines to (R)-β-arylalanines (Cox *et al.* 2009, Krug and Müller 2009). When racemic starting materials are used, the conversion is limited by the accumulation of nonproductive (R)-α-arylalanine. Coupling PAM with alanine

racemase from *Pseudomonas putida* addresses this issue by converting (R)-α-arylalanine into the (S)-form, enhancing yields by 4–19% depending on the substrate.

In conclusion, the studies in ammonia lyases and aminomutases have demonstrated their immense potential in amino acid synthesis. However, several challenges remain, including restricted substrate scope, stability issues under harsh conditions, and equilibrium control between α- and β-amino acids (Turner 2009, Reetz 2011). Innovative solutions, such as directed evolution, computational enzyme design, and tandem catalytic processes, offer promising pathways to overcome these hurdles. Expanding substrate scope and optimizing catalytic efficiency will be critical for realizing the full industrial potential of these enzymatic systems.

1.3 The aspartate ammonia lyase (aspartases): An enzyme can be engineered to producing β-amino acids.

1.3.1 Overview of aspartases.

Aspartase (EC 4.3.1.1), also known as aspartate ammonia-lyase, belongs to the aspartase/ fumarase superfamily. This superfamily comprises enzymes such as aspartase, fumarase, and argininosuccinate lyase, which share structural and mechanistic features. These enzymes catalyze reactions involving succinyl-containing substrates, often producing fumarate, through a general base-catalyzed mechanism that stabilizes an aci-carboxylate intermediate. A conserved serine within a flexible SS loop acts as the catalytic base, while a histidine-glutamate pair serves as the catalytic acid in some members. Structural studies reveal a shared active-site architecture among these enzymes, with specific adaptations for their distinct functions.

As shown in the Figure 1-8, aspartase catalyses the reversible deamination of L-aspartate to form fumarate and ammonia (Quastel and Woolf 1926). This reaction plays a critical role in microbial nitrogen metabolism.

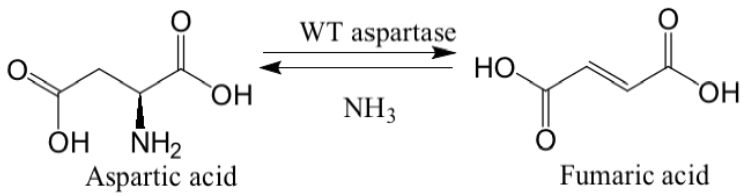

Figure 1-8 Wildtype aspartase catalyses the reversible deamination of L-aspartate to form fumarate and ammonia.

Aspartases have been purified and characterized from various Gram-negative and Gram-positive bacteria, including *Escherichia coli*, *Hafnia alvei*, *Pseudomonas fluorescens*, *Bacillus subtilis*, and *Bacillus sp.* YM55-1. The most extensively studied aspartases are AspA from *Escherichia coli* (Jayasekera *et al.* 1997, Shi *et al.* 1997) and AspB from *Bacillus sp.* YM55-1 (Kawata *et al*. 2000, Fujii *et al*. 2003, Puthan Veetil *et al.* 2009).

For both enzymes, the crystal structures of their unliganded forms have been resolved. More recently, the structure of AspB bound to L-aspartate has also been elucidated, providing deeper insights into its catalytic mechanism (Fibriansah *et al.* 2011).

Other members of this aspartase/ fumarase superfamily catalyze diverse array of reactions, including various C−N lyase reactions, C−O lyase reactions, and unrelated transformations. Among these, aspartase is noted for its remarkable specificity. The enzyme's primary practical application lies in utilizing the reverse of its natural reaction for the asymmetric synthesis of *L*-aspartic acid, a process that has proven invaluable for industrial biocatalysis. Despite numerous engineering attempts to create more versatile biocatalysts, the specificity of aspartase has limited its broader applicability. Nevertheless, aspartases have been used to synthesize a restricted range of aspartic acid analogs.

1.3.1.1 Overview of aspartase A

The conversion of *L*-aspartic acid to succinic acid was first reported in 1901 (Harden 1901). This process involves two steps: the action of aspartase followed by a reductase, utilizing *Escherichia coli* (then referred to as *Bacillus coli communis*). In 1926, researchers reported the equilibrium reaction between *L*-aspartate, fumarate, and ammonia facilitated by resting cells of the same organism (Quastel and Woolf 1926). By 1971, AspA had been successfully isolated and purified from *E. coli*, revealing that the enzyme requires a divalent metal ion for activity, has a molecular weight of 170,000, and is composed of four subunits of 45,000 each (Rudolph and Fromm 1971).

As shown in Figure 1-9, the first crystal structure of AspA was solved by Shi et al. The 2.8 Å resolution structure of *L*-aspartate ammonia-lyase (aspartase) from *E. coli* revealed a tetrameric enzyme, with each monomer comprising three α-helical domains. The smallest domain, the C-terminal domain, is composed of two helix-turn-helix motifs oriented approximately 90° to each other (Shi *et al.* 1997). The central helix domain, the largest of the three, consists of five long α-helices and constitutes over half of the subunit's total residues. The N-terminal domain features a short two-stranded antiparallel β-sheet followed by five α-helices.

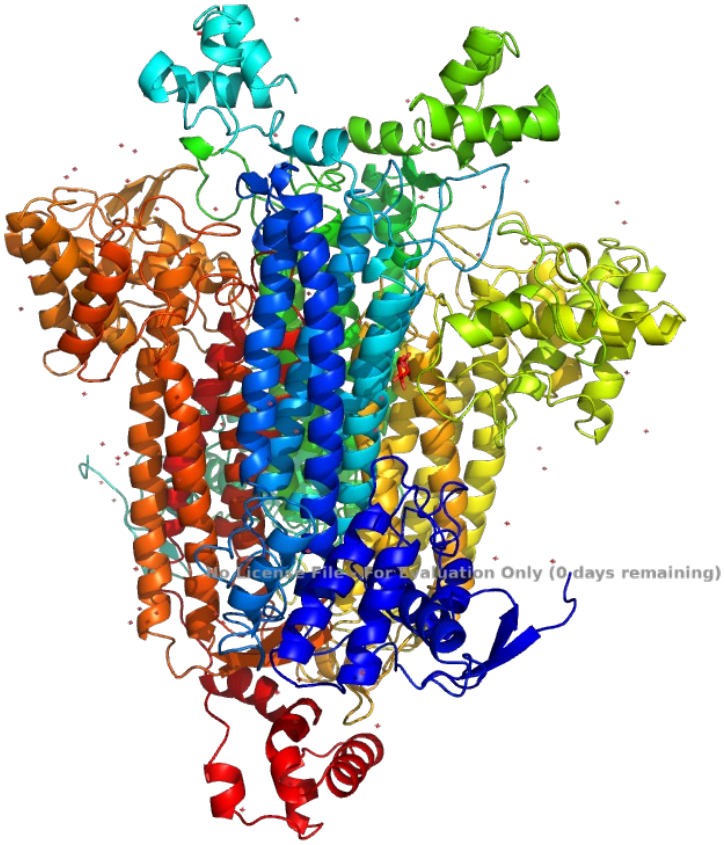

Figure 1-9 X-ray crystal structure of AspA homotetramer.

Representation of the AspA homotetramer (PDB ID: 1JSW), highlighting the domains of each subunit. The structure was visualized and rendered using PyMOL software.

The active site, formed by residues from three subunits, binds the α- and β-carboxylate groups and facilitates the reversible deamination of L-aspartate to fumarate and ammonia. Unlike fumarase, aspartase stabilizes its high-energy intermediate without requiring metal ion cofactors. This crystal structure of AspA showed that the enzyme shares structural features with several other proteins, now collectively referred to as the aspartase/fumarase superfamily. As the high-resolution structure of L-aspartate ammonia-lyase from *Escherichia coli* has been determined (Shi *et al.* 1997), site-directed mutagenesis of AspA identified several key residues: lysine 327 is critical for substrate binding, while arginine 29 interacts with the β-carboxylate group of aspartates (Jayasekera *et al.* 1997). Residues such as serine 143 and aspartate 10 have been proposed to function as an acid catalyst and for structural stabilization, respectively. Mutagenesis results show that some substitutions have

minimal effects but replacing aspartate 10 with alanine significantly impairs catalytic activity (Jayasekera *et al.* 1997).

Kinetic studies revealed that AspA exhibits non-Michaelis−Menten kinetics for the deamination reaction at high pH. In the amination reaction, a time lag before reaching a steady-state rate is observed, suggesting allosteric activation. *L*-Aspartate and Mg^{2+} bind to a distinct activator site separate from the active site, with *L*-aspartate acting as both a substrate and an activator (Ida and Tokushige 1985, Karsten *et al.* 1986). While the crystal structure of unliganded AspA does not identify the activator-binding site, it is proposed that Cys430 is located near this region (Shi *et al.* 1997). Comparisons with fumarase C revealed that Arg126 and Asn135 in fumarase correspond to Gln129 and Asn138 in AspA, forming part of a short helix segment in the activator-binding site (Shi *et al.* 1997, Weaver *et al.* 1997).

A general acid-base mechanism has been proposed for aspartases and related enzymes, supported by pH-rate profiles and inhibition studies (Yoon *et al.* 1995, Puthan Veetil *et al.* 2012). Upon substrate binding and loop closure, the catalytic base on the flexible loop abstracts the pro-*R* proton at the β-position, forming a carbanion stabilized as an enediolate intermediate. This intermediate undergoes rearrangement, breaking the C−N bond (or C−O bond in fumarases) and releasing the nucleophile (ammonia, amine, or water), forming fumarate. This elimination occurs in an "anti" manner, requiring distinct residues to facilitate proton abstraction and donation.

While most aspartase/fumarase superfamily members require a general acid for catalysis, the role of such an acid in aspartase remains unclear. Whether the leaving group is released as ammonium ion (NH_4^+) or free ammonia (NH_3) has yet to be resolved. If NH_3 is the product, the necessity of a general acid to protonate the α-amino group is eliminated. To date, mutagenesis studies have not identified a catalytically essential acidic residue in the AspA active site.

The structural studies of AspA have been unable to address these questions due to the lack of a crystal structure of AspA in complex with its substrate or product (Shi *et al.* 1997). To overcome these limitations, recent research has focused on AspB, which offers a simpler system due to its lack of allosteric activation (Kawata *et al.* 1999). The unliganded crystal structure of AspB has already been resolved, and the putative active site was predicted through comparisons with AspA and other members of the aspartase/fumarase superfamily.

1.3.1.2 Overview of aspartase B

Aspartase B (AspB) is derived from the thermophilic bacterium *Bacillus sp.* YM55-1 and was successfully purified for the first time in 1999 (Kawata *et al.* 1999). AspB was the first thermostable aspartase that had been identified. It is a homotetrameric enzyme with subunits of 51 kDa, resulting in a total molecular weight of 200 kDa. AspB exhibits remarkable thermostability, retaining 80% of its activity after 60 minutes at 55°C, and demonstrates resistance to chemical denaturants such as guanidine hydrochloride (Kawata *et al.* 1999). It operates with high efficiency, showing *Vmax* of 2200 U/mg at 55°C, surpassing other aspartases. (Kawata *et al.* 1999). Additionally, AspB follows Michaelis–Menten kinetics and does not require allosteric activation, unlike other members of the aspartase family (Kawata *et al.* 1999). Its high activity and robust stability make it suitable for industrial applications such as L-aspartate production, while its structural resilience provides valuable insights into the design and function of thermophilic enzymes.

Manual docking of *L*-aspartate into the active site of AspB, as shown in Figure 1-10, highlights specific hydrogen-bonding interactions that stabilize the substrate and facilitate catalysis. The α-carboxylate group of *L*-aspartate forms hydrogen bonds with Thr187 and Lys324, while the β-carboxylate group interacts with the hydroxyl groups of Ser140 and Thr141. Additionally, the amino group of L-aspartate forms hydrogen bonds with the side chains of Thr101, Asn142, and His188 (Fujii *et al.* 2003).

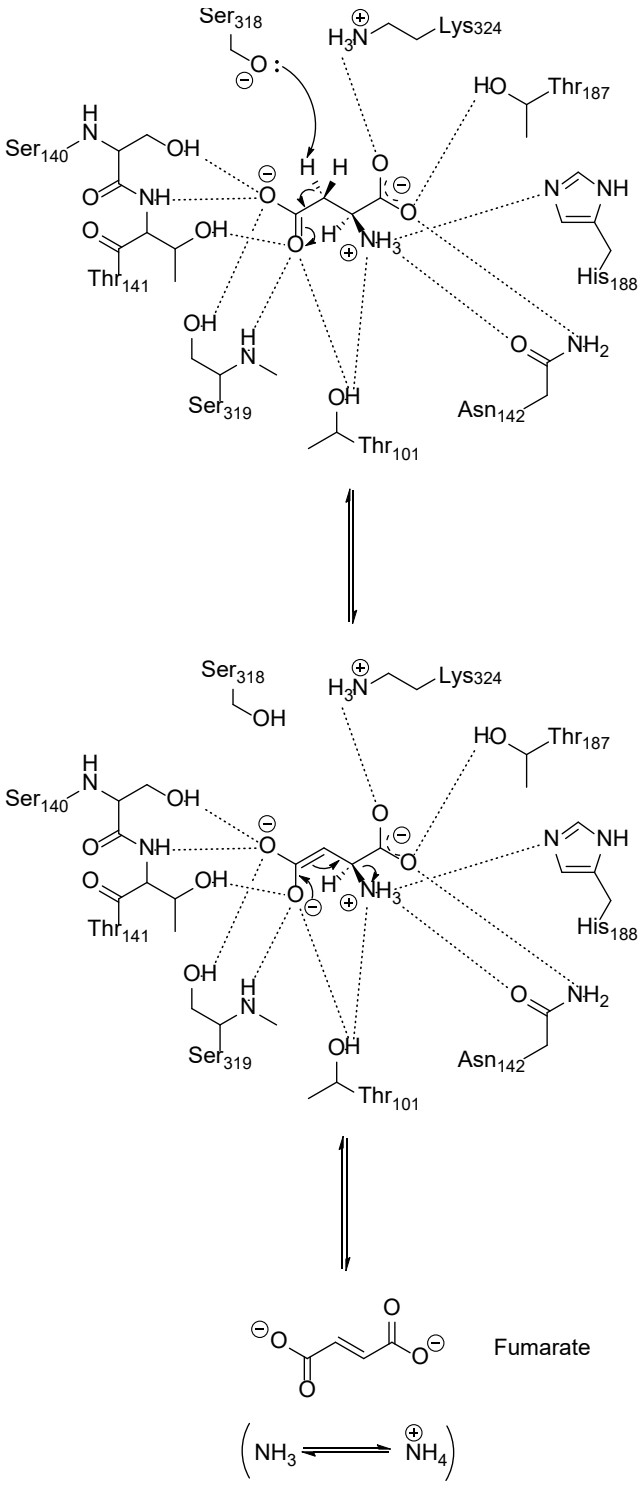

Figure 1-10 Catalytic mechanism of AspB.

The catalytic mechanism of AspB involves Ser318 acting as the catalytic base, abstracting the pro-R proton from the C3 position of the substrate. This generates an enolate anion intermediate, stabilized by hydrogen bonding with active-site residues. The collapse of intermediate leads to cleavage of the Cα−N bond, yielding fumarate and ammonia as the final products.

To confirm the role of these residues and elucidate the catalytic mechanism, site-directed mutagenesis, pH-rate profile analyses, and inhibition studies were conducted on AspB (Puthan Veetil *et al.* 2009). As shown in Figure 1-11, the X-ray crystal structure of AspB bound to *L*-aspartate reveals the substrate in a distorted conformation resembling the ene-diolate intermediate. This intermediate is stabilized by a network of hydrogen bonds involving Thr101, Ser140, Thr141, and Ser319, which interact with the substrate's β-carboxylate group (Fibriansah *et al.* 2011).

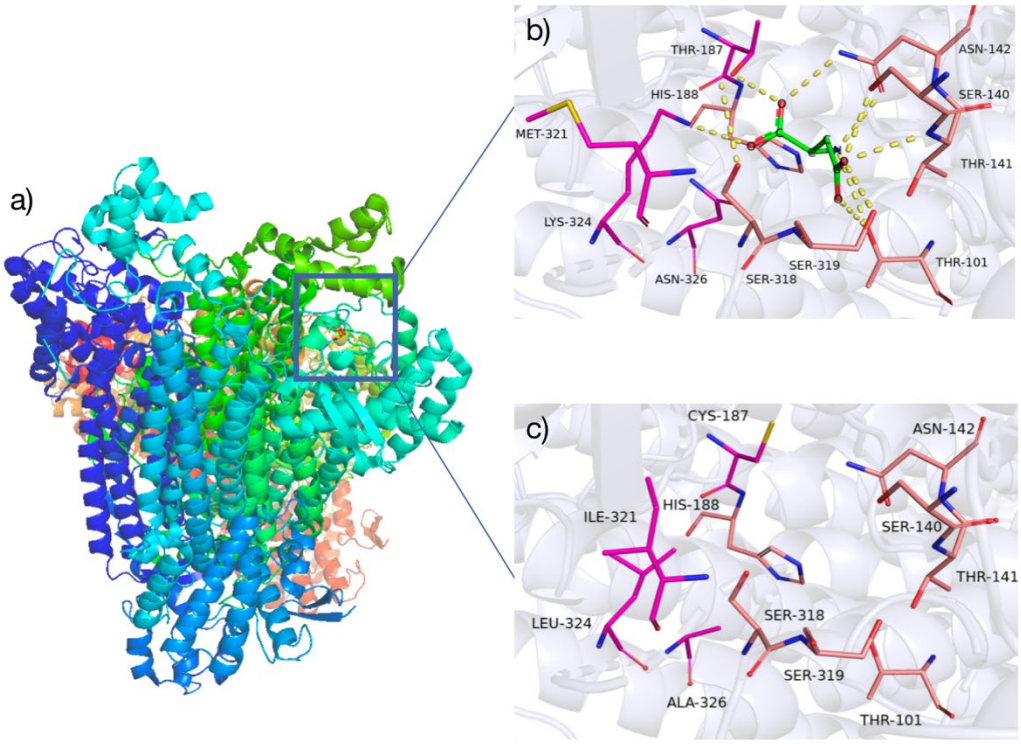

Figure 1-11 Structural analysis of AspB and the active site modifications in AspB-M1.

a) The functional tetrameric structure of AspB is depicted, with each monomer represented in a different color. One of the four active sites within the homotetramer is highlighted (Fibriansah, Veetil et al. 2011).
b) Detailed view of the active site in wild-type AspB bound to L-aspartate (green), showing key residues involved in catalysis and substrate binding (PDB: 3R6V).
c) Mutated active site of AspB-M1, incorporating the mutations T187C, M321I, K324L, and N326A, highlighting the structural adjustments to the catalytic environment.

All visualizations were generated using PyMOL.

The distorted conformation of the substrate is proposed to facilitate proton abstraction from the sp^3 carbon, forcing it into an sp^2 ene-diolate-like conformation (Fibriansah *et*

al. 2011). The structure also shows the enzyme in a closed conformation, a state previously observed in other superfamily members such as adenylosuccinate lyase. Within this closed conformation, the conserved Ser318 acts as the essential catalytic base, abstracting the Cβ proton in the reaction's first step. This was confirmed through mutagenesis studies, where the Ser318Ala mutant exhibited no enzymatic activity, demonstrating the critical role of Ser318 in catalysis (Fibriansah *et al.* 2011).

Substrate binding induces a significant conformational change in the SS loop (residues G317SSIMPGKVN326), transitioning it from an open to a closed state over the active site. This repositioning places Ser318 in an optimal position to act as a catalytic base. However, for Ser318 to function in this capacity, it must be deprotonated to form the corresponding oxyanion. The exact mechanism by which this serine anion is formed and stabilized remains unclear and warrants further investigation.

1.3.2 Biocatalytic, synthetic and therapeutic applications of aspartase.

In industry, aspartase is a crucial biocatalyst for producing enantiopure *L*-aspartic acid, a key precursor in the synthesis of artificial sweeteners such as N-(L-α-aspartyl)-L-phenylalanine 1-methyl ester, commonly known as aspartame (Wubbolts 2002). N-substituted and 3-substituted derivatives of *L*-aspartic acid are also vital for biological research and serve as chiral building blocks in pharmaceuticals. However, their enantiopure synthesis remains a significant challenge (Mavencamp *et al.* 2008, Shimamoto 2008, Spengler *et al.* 2010). Aspartase-catalyzed stereo- and regioselective addition of amine nucleophiles to fumarate derivatives offers a promising approach for the synthesis of these derivatives. However, this strategy is constrained by the enzyme's narrow substrate range (Weiner *et al.* 2008). The ability of aspartase to accept various nucleophiles has been tested. For example, aspartase from *Bacillus cadaveris* catalyzes the condensation of fumaric acid with hydroxylamine, producing N-hydroxyaspartic acid—the first enzymatic synthesis of a hydroxamino acid (Emery 1963). Additionally, AspB from *Bacillus sp.* YM55-1 catalyzes the Michael addition of various nucleophiles to fumarate with high enantioselectivity (>97% ee), including hydroxylamine, hydrazine, methoxylamine, methylamine, ethylamine, and propylamine (Weiner *et al.* 2008). As shown in Figure 1-12 the Michael addition is a classic conjugate addition reaction in which a nucleophile attacks the β-carbon of an α,β-unsaturated carbonyl compound, forming a stable 1,4-addition product. Traditionally applied in organic synthesis for constructing C–C and C–X bonds, the reaction has also been adapted in biocatalysis, where enzymes such as aspartase B (AspB) catalyze the addition of nucleophiles to fumarate. Compared with chemical methods such as metal-catalyzed hydrogenation or ynolate

cycloadditions, the enzymatic Michael addition offers significant advantages in terms of green chemistry, stereoselectivity, and process simplicity, though challenges remain in improving enzyme stability and solubility for industrial application. This positions AspB-mediated Michael addition as a powerful and sustainable route to access diverse β-amino acids. Hydroxylamine and hydrazine demonstrate the highest catalytic efficiency. Kinetic studies indicate that AspB efficiently catalyzes reactions with small, uncharged nucleophiles, comparable to its natural substrate, ammonia. The resulting N-substituted aspartic acids are valuable for pharmaceutical applications and peptide mimetics, though the enzyme's substrate range remains a limitation for broader synthetic applications (Weiner *et al.* 2008).

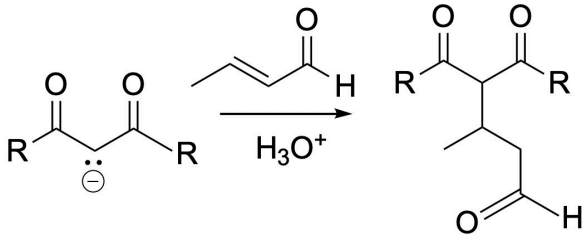

Figure 1-12 General mechanism of the Michael addition reaction.

In a typical Michael addition, a nucleophilic donor (Michael donor) attacks an electron-deficient α,β-unsaturated carbonyl compound (Michael acceptor), resulting in the formation of a new carbon–carbon bond at the β-position.

Aspartase has also been employed at an industrial scale for producing *L*-aspartic acid from fumaric acid and ammonium salts. On a laboratory scale, aspartase has been utilized for the stereospecific synthesis of ^{13}C-labeled *L*-aspartic acid from [1,4-$^{13}C_2$]fumaric acid and for producing L-β([^{13}C]cyano)alanine as a precursor to *L*[4-^{13}C]aspartic acid (Röhm and van Etten 1985).

Aspartase's high substrate specificity has also facilitated its integration into multienzymatic cascade processes, minimizing cross-reactions with other enzymatic systems. For example, a co-immobilization strategy combining aspartase (AspB) with transaminase (TA) was developed for the one-pot synthesis of *L*-phenylalanine. Under optimized conditions (pH 7.5, 37°C, with 0.15 M fumarate, 0.3 M NH_4Cl, and 0.1 M phenylpyruvate), this system achieved a reaction yield of 79.5%, comparable to reactions using free enzymes (Cárdenas-Fernández *et al.* 2015).

In another application, aspartase was utilized in a tandem reaction with nitrilase BjNIT3397 from *Bradyrhizobium japonicum* to improve the biocatalytic hydrolysis of 3-aminopropionitrile to β-alanine (Han *et al.* 2015). BjNIT3397 demonstrates high

efficiency at substrate concentrations up to 3 M under optimal conditions (pH 7.3, 30°C). However, the reaction typically produces a byproduct, 3-aminopropanamide. To mitigate this issue, aspartase was used in combination with fumaric acid to consume ammonia, thereby shifting the equilibrium toward β-alanine production. This tandem reaction reduced byproduct levels from 33% to 3%, enabling the simultaneous production of β-alanine and *L*-aspartic acid.

In summary, the ability of aspartase to catalyze stereospecific and regioselective reactions, combined with its integration into cascade processes, highlights its utility in both industrial and pharmaceutical applications. However, challenges such as its narrow substrate scope remain a limitation, underscoring the need for further enzyme engineering to broaden its applicability.

1.3.3 Engineering of aspartases for β-amino acids manufacturing.

Although aspartases hold significant potential for synthesizing enantiomerically pure *L*-aspartic acid derivatives, their utility is limited by a narrow substrate range. Redesigning these enzymes to process novel unnatural substrates could greatly expand their biocatalytic applications and enhance their industrial relevance (Turner 2011)

In 2005, directed evolution was applied to alter the substrate specificity of aspartase AspA from *Escherichia coli* (Asano *et al.* 2005). Through random mutagenesis and screening, a mutant (MA2100) with a K327N substitution was identified, enabling the enzyme to process *L*-aspartic acid-α-amide, a substrate not recognized by the wild-type enzyme. However, while the mutation allowed for new substrate recognition, it significantly compromised the enzyme's catalytic performance. The K327N mutant exhibited a 14-fold increase in the Michaelis constant (K_m) and a 560-fold decrease in maximum reaction velocity (V_{max}) for *L*-aspartic acid. Additionally, its K_m for *L*-aspartic acid-α-amide was 50 times higher than that of wild-type AspA for its natural substrate. The mutant displayed optimal activity at pH 6.0, but no further AspA variants with altered substrate specificity have been reported to date.

In 2014, researchers successfully engineered aspartase AspB from *Bacillus sp.* YM55-1 into a β-amino acid lyase capable of synthesizing (R)-3-aminobutyrate from crotonic acid and ammonia (Vogel *et al.* 2014). Using combinatorial mutagenesis and high-throughput cluster screening of 300,000 clones, the mutant BSASP-C6 was identified. This mutant featured four key mutations (T187C, M321I, K324M, N326C) that reshaped the substrate-binding pocket, enabling it to accommodate crotonic acid. While the mutant exhibited significantly lower activity compared to the wild-type enzyme with fumarate, it maintained high regio- and enantioselectivity for (R)-3-

aminobutyrate, demonstrating the potential of substrate-pocket engineering to expand enzyme functionality.

The Rosetta Enzyme Design approach is a computational protein engineering framework that allows researchers to redesign enzymes with tailored catalytic properties. It works by first defining the idealized transition state geometry of the desired reaction (for example, hydroamination of an α,β-unsaturated acid). The program then searches through the enzyme's active site and identifies positions where amino acid side chains can be placed to optimally stabilize that transition state through hydrogen bonding, electrostatics, or steric interactions. Using this information, Rosetta suggests mutations—often at residues surrounding the active site—that remodel the binding pocket to accommodate new substrates or improve stereocontrol. The most promising variants are then experimentally tested and refined through iterative rounds of computation and laboratory validation. In the case of AspB (Li *et al.* 2018), this approach was used to redesign the enzyme to accept a broader range of α,β-unsaturated carboxylic acids. The engineered variants gained the ability to catalyze regio- and enantioselective hydroamination, efficiently producing diverse β-amino acids (e.g., (R)-β-aminobutanoic acid, β-aminopentanoic acid, (S)-β-asparagine, and (S)-β-phenylalanine) at high substrate concentrations, with conversions up to 99% and enantiomeric excess >99% (Figure 1-13).

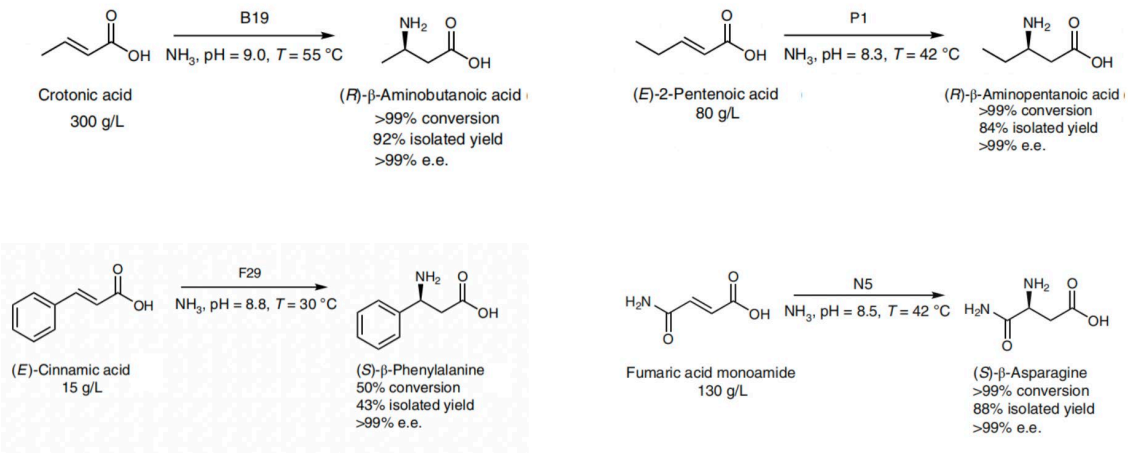

Figure 1-13 Substrate scope and product formation catalyzed by engineered AspB mutants.

Engineered AspB variants (B19, P1, F29, and N5) catalyze the enantioselective hydroamination of unsaturated acids and derivatives, yielding β-amino acids with high conversion rates and excellent enantiomeric excess. AspB-B19 efficiently converts crotonic acid (300 g/L) to (R)-β-aminobutanoic acid with >99% conversion, 92% isolated yield, and >99% e.e. AspB-P1 catalyzes the transformation of (E)-2-

pentenoic acid (80 g/L) to (R)-β-aminopentanoic acid with >99% conversion, 84% isolated yield, and >99% e.e. AspB-F29 processes (E)-cinnamic acid (15 g/L) to (S)-β-phenylalanine with 50% conversion, 43% isolated yield, and >99% e.e. Finally, AspB-N5 enables the conversion of fumaric acid monoamide (130 g/L) into (S)-β-asparagine with >99% conversion, 88% isolated yield, and >99% e.e. These results highlight the catalytic versatility of AspB mutants in producing structurally diverse β-amino acids under mild conditions, illustrating their potential for industrial biocatalysis.

1.4 The methylaspartate ammonia lyase (MAL): An enzyme can be engineered for the asymmetric synthesis of unnatural amino acids.

1.4.1 Overview of MAL.

Methylaspartate ammonia-lyases (MALs), also known as 3-methylaspartate ammonia-lyases (EC 4.3.1.2), share mechanistic and structural similarities with the enolase superfamily (de Villiers *et al.* 2012). As illustrated in Figure 1-14, the proposed catalytic mechanism of both aspartase and MAL begins with a general base in the active site (B:) abstracting the pro-*R* proton from the C3 position of the substrate, forming a carbanion stabilized as an aci-carboxylate intermediate. This intermediate, resembling an enolate anion, rearranges, cleaving the Cα–N bond and releasing ammonia (NH_3). A general acid facilitates the Cα–N bond cleavage by donating a proton to ammonia, forming ammonium ion (NH_4^+), with this step being the rate-limiting part of the reaction. The reaction ultimately produces fumarate or its methylated counterpart, depending on the substrate.

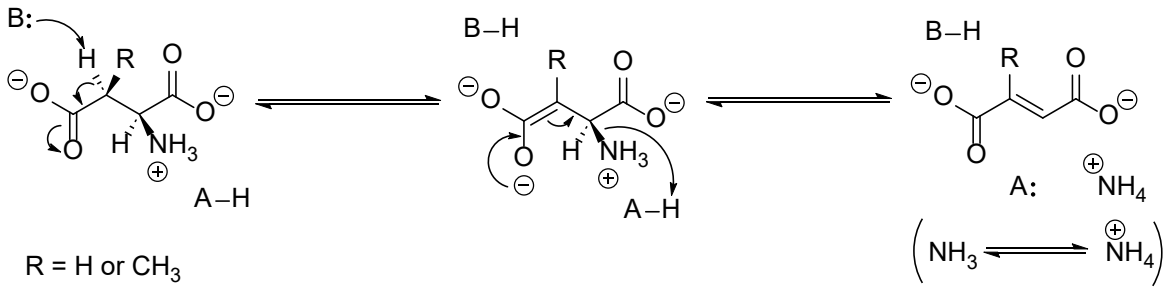

Figure 1-14 Proposed catalytic mechanism of aspartase and methylaspartase.

In certain aspartases, a general acid (A-H) may facilitate the elimination of ammonia by donating a proton to the leaving group. The mechanism ultimately produces fumarate or a methylated counterpart, depending on the substrate.

MALs were first identified in the anaerobic bacterium *Clostridium tetanomorphum* H1 by Barker et al. (Barker *et al.* 1959). They were subsequently detected in various facultative anaerobic organisms, including *Morganella morganii*, *Citrobacter amalonaticus*, *Fusobacterium varium*, and *Hafnia alvei* (Asano and Kato 1994, Kato and Asano 1995, Raj *et al.* 2012).

MALs were later found to be oxygen-insensitive and present in various non-anaerobic species. Beyond the characterized MALs, over 100 putative MAL sequences are available in various databases. For example, MAL from the thermophilic bacterium *Carboxydothermus hydrogenoformans* Z-2901 (Ch-MAL) was cloned and overproduced in *Escherichia coli* (Raj *et al.* 2012). Ch-MAL is a homodimer in solution, with ~49 kDa subunits, requiring Mg^{2+} and K^{+} ions for optimal activity. It exhibits maximum activity at pH 9.0 and 70°C (k_{at} = 78 s^{-1}, K_m = 16 mM) and retains stability at 50°C for over 4 hours, making it the most thermally stable MAL identified to date.

MAL catalyzes the deamination of (2S,3S)-threo-3-methylaspartate to mesaconic acid (2-methylfumaric acid) and requires divalent (Mg^{2+}) and monovalent (K^{+}) cations as cofactors. Structurally distinct from aspartate ammonia-lyase, MAL is more closely related to the enolase superfamily, which performs diverse reactions such as dehydrations, racemizations, and cycloisomerizations (Babbitt *et al.* 1996).

In 2012, the structure of *Citrobacter amalonaticus* MAL, resolved to 1.3 Å, revealed a dimeric enzyme with each subunit comprising two domains. The larger domain adopts a TIM barrel fold, with the active site located at the C-terminal end, while the smaller domain, rich in β-strands, partially occludes the barrel's C-terminus, forming a large cleft where the metal ion site resides (Levy *et al.* 2002). Despite minimal sequence similarity, this structure closely resembles other members of the enolase

superfamily, suggesting a mechanism involving proton abstraction at the C3 position of the substrate, forming an enolate intermediate.

Additionally, the structure of *Clostridium tetanomorphum* MAL has been resolved to 1.9 Å using the single-wavelength anomalous diffraction method, along with a divalent metal ion complex of the protein. As shown in Figure 1-15, MAL is a homodimer, and each monomer comprising two domains, which is α/β-barrel and a smaller β-strand-rich domain. The smaller domain partially occludes the barrel's C-terminus, forming a large cleft where the metal ion site is located. Structural analysis places MAL in the enolase superfamily, with the metal ions coordinating the carboxylic acid of the substrate. A base, likely Lys331 in MAL, abstracts the α-proton of methylaspartic acid, a defining mechanistic feature of this enzyme family.

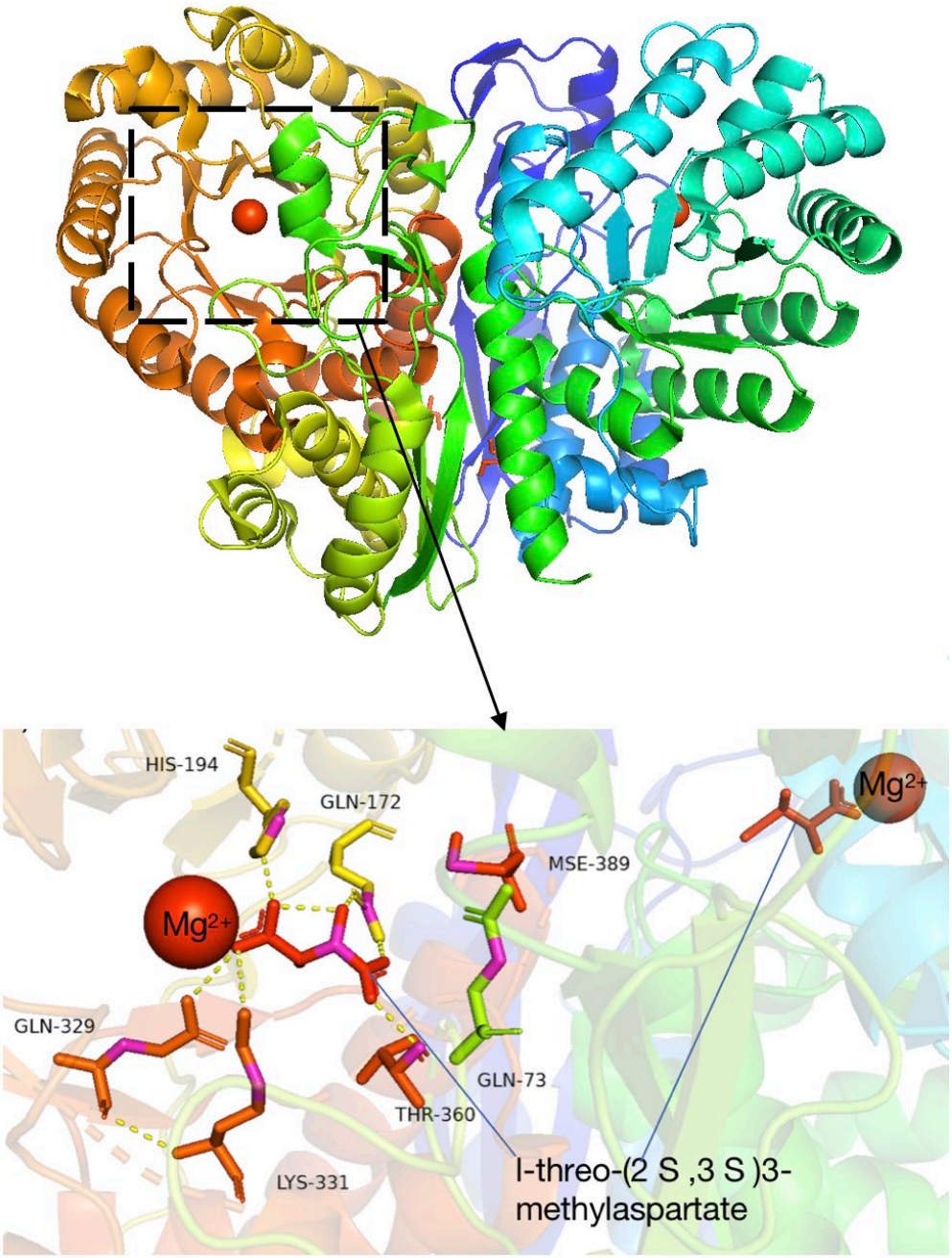

Figure 1-15 Structural analysis of CtMAL and its interaction with the natural substrate.

Top: X-ray crystal structure of CtMAL (PDB ID: 1KCZ) represented as a homodimer. Each subunit is color-coded to highlight its structural domains. Red spheres indicate Mg^{2+} ions, which are crucial for catalytic activity.
Bottom: Close-up view of the active site of CtMAL in complex with its natural substrate, *L-threo-(2S,3S)-3-methylaspartate* (green) (PDB ID: 1KKR). Key residues involved in substrate binding and catalysis, including His-194, Gln-172, Gln-329, Thr-360, Lys-331, and Gln-73, are shown, along with interactions stabilizing the substrate (Raj and Poelarends 2013).

All structures and annotations were prepared using PyMOL

The structure of the MAL-substrate complex (Levy *et al.* 2002), combined with structural alignment of MAL with other enolase superfamily members (Asuncion *et al.* 2002), suggests that Lys331 serves as the S-specific base catalyst, responsible for abstracting the C3 proton from substrate L -threo-3-methylaspartate (Figure 1-16). Additionally, structural analysis indicates that His194 is positioned to stabilize the aci-carboxylate intermediate as an electrophile, which is a key step in the enzyme's catalytic mechanism. Therefore, it is hypothesized that His194 may act as the R-specific base catalyst, abstracting the C3 proton from L-erythro-3-methylaspartate. This hypothesis is supported by structural comparisons with other enolase superfamily enzymes, where the main chain of His194 aligns with Lys164 of mandelate racemase (a secondary base) and Lys213 of glucarate dehydratase (a primary base).

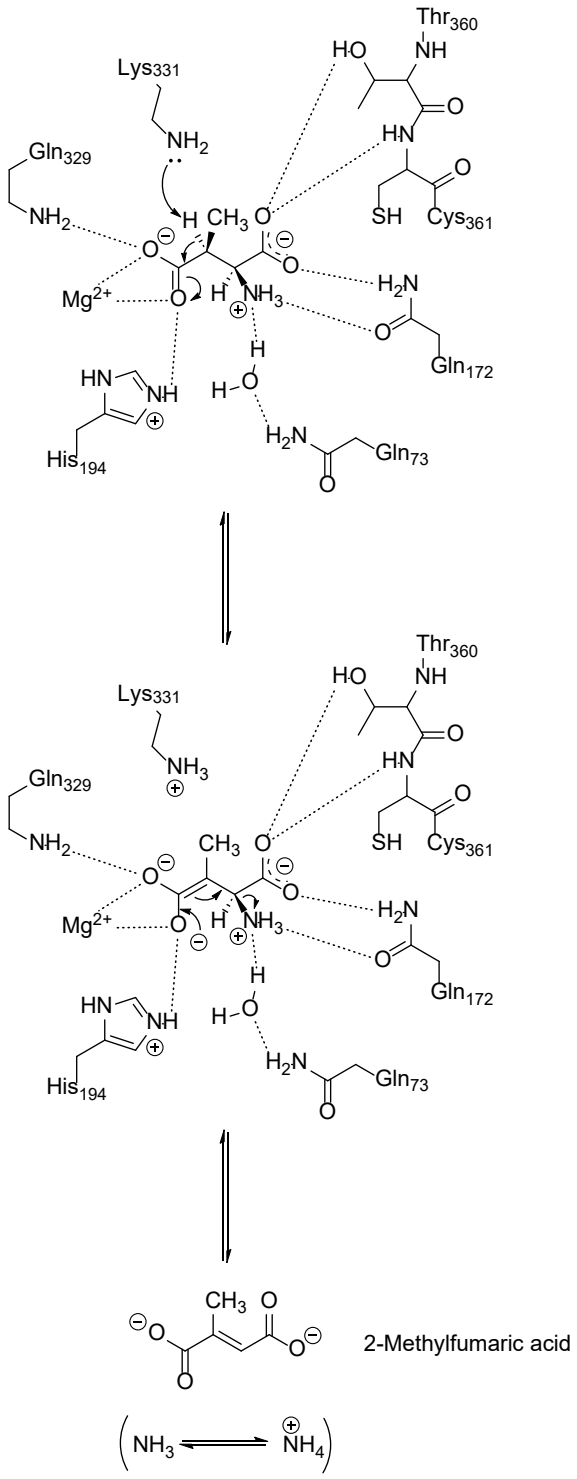

Figure 1-16 Catalytic mechanism of methylaspartate ammonia-lyase (MAL).

The residue Lys331 acts as the catalytic base, abstracting the C3 proton from the substrate to form an enolate anion intermediate. This intermediate is stabilized by interactions with both the Mg^{2+} ion and specific amino acid residues in the active site. The intermediate subsequently collapses, leading to Cα–N bond cleavage and the release of ammonia (NH_3), resulting in the formation of 2-methylfumaric acid

(mesaconate). The stabilization and catalytic precision highlight the essential roles of the active-site residues and metal ion coordination.

On top of that, Site-directed mutagenesis has identified the key residues contributes to MAL's catalytic mechanism (Raj *et al.* 2009). Mutations of Lys331, His194, and Gln329 to alanine or other residues preserved the enzyme's structural integrity but significantly altered catalytic efficiency (k_{at} and k_{at}/K_m) and diastereoselectivity. These mutants exclusively catalyzed the conversion of mesaconate to (2S,3S)-3-methylaspartic acid without forming the (2S,3R) isomer. The findings suggest that Lys331 serves as the S-specific general base/acid catalyst, while His194 acts as the R-specific catalyst.

Additionally, MAL does not directly catalyze the epimerization of *L-threo*-(2S,3S)-3-methylaspartate to *L-erythro*-(2S,3R)-3-methylaspartate. Instead, these products are formed through the anti- and syn-addition of ammonia to mesaconate. Structural studies also identified key interactions between the substrate and residues Gln329, His194, and Mg^{2+} ions, which stabilize the enolate intermediate and assist substrate binding. The active site Mg^{2+} ion, located at the mouth of the TIM barrel, is coordinated by Asp238, Glu273, Asp307, and three water molecules in the unliganded structure (Asuncion *et al.* 2002). Upon substrate binding, the substrate β-carboxyl oxygen atom replaces one water molecule as a ligand, completing the typical hexagonal coordination of Mg^{2+}. The substrate's α-carboxylate group forms hydrogen bonds with the NH of Cys361, the Oγ atom of Thr360, and the Nε2 atom of Gln172 in main chain, while its C2 amino group forms hydrogen bonds with Gln172 and Gln73 by one water molecule. The substrate's 3-methyl group has Van der Waals interactions with the Leu384 and Gln172 in side chains, which further stabilize the substrate (Raj and Poelarends 2013).

To summarise, MALs are versatile enzymes that catalyze reversible deamination reactions with broad substrate tolerance and high stereoselectivity. Structural and mutational studies have elucidated key residues, such as Lys331 and His194, that mediate catalytic activity and diastereoselectivity. These insights have advanced our understanding of MAL's role within the enolase superfamily and its potential for biocatalytic applications, including the synthesis of substituted aspartic acids and other valuable compounds.

1.4.2 Biocatalytic, synthetic and therapeutic applications of MAL.

MAL from *Clostridium tetanomorphum* has been utilized as a biocatalyst to catalyze the reversible deamination of (2S,3S)-3-methylaspartic acid to mesaconic acid and to facilitate the aminative addition of ammonia to various fumaric acid derivatives (Akhtar *et al.* 1987). This enzyme exhibits high stereospecificity, selectively producing (2S,3S)-configured products. Substrates with smaller substituents, such as chloro- and bromo-fumaric acids, demonstrate the highest efficiency, while larger groups, such as iodine, exhibit reduced reactivity due to steric hindrance.

MAL has also been employed for the enzymatic synthesis of N-substituted aspartic acids. It catalyzes the anti-addition of various N-nucleophiles, such as hydrazines, hydroxylamines, and alkylamines, to fumaric acids, producing highly enantiospecific (2S,3S)-configured products via a concerted mechanism (Saeed Gulzar *et al.* 1997). The enzyme's active site imposes strict spatial constraints, which influence substrate compatibility and reactivity. These constraints result in either stable or unstable products, depending on the nucleophile used.

In addition to the MAL from *C. tetanomorphum*, the enzyme sourced from *Carboxydothermus hydrogenoformans* Z-2901 has demonstrated significant biocatalytic versatility. This MAL catalyzes ammonia addition to fumarate, mesaconate, ethylfumarate, and propylfumarate, enabling the synthesis of various product. Moreover, this MAL efficiently utilizes nucleophiles such as methylamine, ethylamine, hydrazine, hydroxylamine, and methoxylamine to produce N-substituted methylaspartic acids with diastereomeric excesses exceeding 98% (Raj *et al.* 2012).

1.4.3 Engineering of MAL for the asymmetric synthesis of unnatural amino acids.

Unlike aspartases, which rely on substrate-induced closure of the SS-loop to align catalytic and substrate-binding residues, methylaspartate ammonia-lyase (MAL) retains an intact catalytic machinery in its unbound state and does not undergo significant conformational changes during substrate binding. This structural feature makes MAL a more promising template for redesign to accommodate and convert novel unnatural substrates (Glasner *et al.* 2006).

1.4.3.1 Structure-based engineering of MAL mutants

The Q73A mutation in *Clostridium tetanomorphum* MAL represents a breakthrough in enzyme engineering, significantly expanding the enzyme's nucleophile scope (Raj *et al.* 2012). In the wild-type enzyme, glutamine at position 73 forms part of the

amine-binding pocket, interacting with the substrate's amino group via a water molecule. Structure-guided saturation mutagenesis at position 73 led to the identification of the Q73A variant, in which the replacement of glutamine with the smaller alanine created an enlarged binding pocket while maintaining the enzyme's selective properties. The Q73A mutation enabled the enzyme to process an impressive array of amine nucleophiles, including linear alkylamines (methyl through hexyl), branched amines (isopropyl), cyclic amines (cyclobutyl through cyclohexyl), and functionalized amines (cyclopropylmethyl, benzyl, ethoxy, hydroxyethyl, hydroxypropyl, methoxyethyl, and aminoethyl derivatives).

The Q73A variant maintained excellent stereoselectivity, producing the *threo* isomers of N-substituted 3-methylaspartic acids with >95% diastereomeric excess and >99% enantiomeric excess. Under optimized conditions, such as with methylamine or ethoxyamine substrates, the enzyme achieved nearly 100% conversion within 20–60 minutes. This expanded substrate scope, combined with high selectivity, highlights the potential of the Q73A variant for synthesizing diverse N-substituted aspartic acids, which are valuable building blocks in pharmaceutical and chemical synthesis.

On the other hand, the L384A mutation in *C. tetanomorphum* MAL expanded the enzyme's electrophile scope (Raj *et al.* 2012). In the wild-type enzyme, leucine at position 384 forms part of the alkyl-binding pocket that accommodates the substrate's methyl group. Saturation mutagenesis identified the L384A variant, where replacing leucine with alanine enlarged the binding pocket while preserving the enzyme's catalytic architecture. The L384A mutant showed activity with fumarates containing varying alkyl chain lengths (from methyl to hexyl), as well as derivatives with aryl, alkoxy (ethoxy), aryloxy (phenoxy), benzyloxy, alkylthio (ethylthio), arylthio (phenylthio), benzylthio, and benzyl substituents at the C2 position.

The mutant exhibited higher affinity and activity toward substrates with longer alkyl chains, achieving at least a 13-fold increase in catalytic efficiency (k_{cat}/K_m) for these substrates compared to shorter-chain derivatives. Under optimized conditions with 5 M ammonia and 30 mM substrate, the L384A variant achieved 85–100% conversion within 10–60 minutes, maintaining excellent regioselectivity and >99% enantiomeric excess, though diastereoselectivity varied depending on the substrate.

1.4.3.2 Engineering MAL from escherichia coli O157:H7

In addition to *C. tetanomorphum* MAL, the enzyme from *Escherichia coli* O157:H7 was engineered to improve its activity and selectivity for bulky substrates (Ni *et al.* 2020, Ni *et al.* 2021). Using structure-guided protein engineering, researchers simultaneously modified residues in the binding pocket (positions 73, 170, 172, 194, 329, and 384) and substrate tunnel (positions 196, 198, 199, 240, 277, 307, 308, 356, 365, and 389) to expand the enzyme's substrate scope(Ni *et al.* 2021).

Five aromatic unsaturated carboxylic acids were tested as substrates: caffeic acid, cinnamic acid, p-hydroxycinnamic acid, methylcinnamic acid, and acrylic acid. Iterative rounds of mutation and screening identified the M8 variant (E172R/Y240S/D307L/Q329F/Y356S/C361L) as the most successful. This variant demonstrated a 15-fold increase in catalytic activity compared to earlier versions, particularly with caffeic acid. The M8 variant achieved >50% conversion within 12 hours, maintaining 99% enantiomeric excess. Kinetic analysis revealed improved catalytic efficiency ($kcat/Km = 46.8\ min^{-1}\ mM^{-1}$) for caffeic acid, while another variant, M6, showed superior activity toward cinnamic acid ($kcat/Km = 34.6\ min^{-1}\ mM^{-1}$). Structural analysis indicated that these improvements were due to enhanced hydrophobic interactions and π–π stacking between the modified enzyme and substrates, achieved by replacing polar residues with non-polar ones near the active center(Ni *et al.* 2021).

In conclusion, the engineering of MAL using structure-guided approaches and efficient screening methods has demonstrated its potential for the asymmetric synthesis of unnatural amino acids. The Q73A and L384A mutants of *C. tetanomorphum* MAL, along with the M8 variant of *E. coli* O157:H7 MAL, showcase the power of enzyme engineering to expand substrate scope while maintaining high regio- and stereoselectivity. These advances bring us closer to more sustainable and efficient processes to produce pharmaceutical intermediates and fine chemicals.

1.5 Application of magnetic protein (MagR) for purification and immobilization of aspartase.

1.5.1 Techniques of enzymes immobilization.

Enzyme immobilization is a pivotal biotechnological advancement that enhances enzyme reusability, stability, and functionality. By anchoring enzymes to inert supports, immobilization overcomes limitations associated with free enzymes, such as low operational stability and challenges in recovery and reuse. While protein engineering and mutagenesis approaches, such as those described in Section 1.4, are powerful for expanding enzyme activity and substrate scope, immobilization provides a complementary strategy that ensures enzymes remain practical and efficient in industrial bioprocesses. Together, these approaches illustrate how modern biocatalyst design integrates both molecular-level modifications and process-level optimizations to maximize performance.

As summarized in Figure 1-17, enzyme immobilization can be categorized into three primary approaches: binding to a support, entrapment, and cross-linking. Binding to a support involves attaching enzymes to carriers or matrices through adsorption, ionic binding, affinity binding, or covalent bonding. Adsorption relies on weak interactions, ionic binding utilizes electrostatic forces, affinity binding depends on specific ligand interactions, and covalent bonding provides stable chemical linkages. Entrapment methods encapsulate enzymes within structures such as microcapsules, gel matrices, or channels, enabling substrate diffusion while retaining the enzymes. Cross-linking, on the other hand, involves directly connecting enzymes to one another using chemical cross-linkers, forming a stable enzyme network without requiring a carrier.

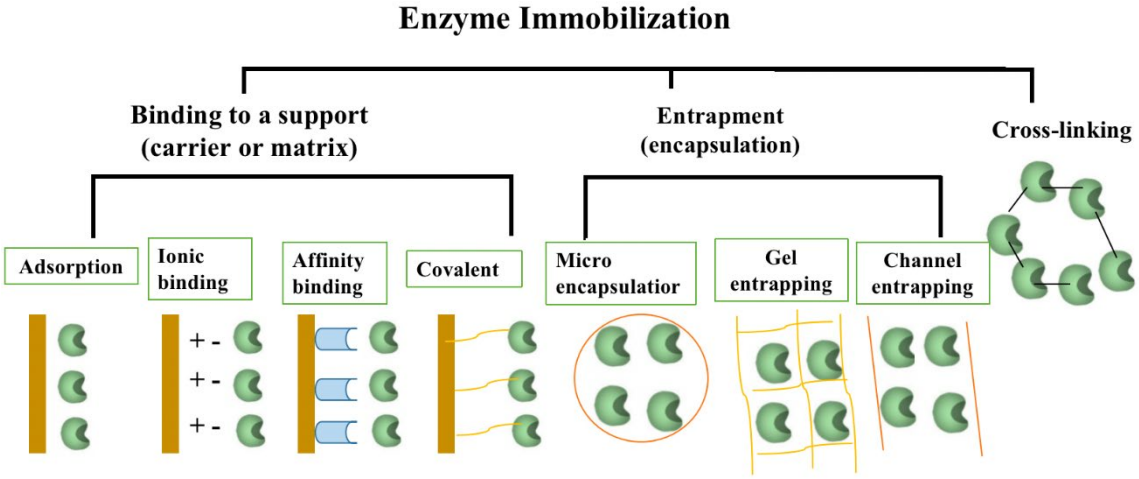

Figure 1-17 Different methods of enzyme immobilization.

This schematic illustrates the major approaches to enzyme immobilization, categorized into three primary strategies: binding to a support, entrapment, and cross-linking.

1.5.1.1 Enzyme immobilization using adsorption

Enzyme immobilization through adsorption is one of the oldest and simplest methods for enhancing enzyme stability, reusability, and functionality. This technique relies on weak physical interactions between the enzyme and support materials, such as van der Waals forces, hydrogen bonding, and ionic interactions. While adsorption is cost-effective and preserves enzyme activity, it also presents challenges, such as enzyme leaching under changing environmental conditions. The adsorbed enzymes may exhibit reduced stability at extreme pH or temperature, and not all enzymes are amenable to adsorption, as binding efficiency depends on the enzyme's surface properties.

The mechanism of adsorption immobilization involves non-covalent binding of enzymes to solid supports, influenced by the physicochemical properties of both the enzyme and the support material. Hydrophobic, ionic, and polar interactions facilitate enzyme binding, with adsorption strength impacting enzyme stability and activity (Jesionowski *et al.* 2014). Organic supports, such as polymers like chitosan, offer tunable charge properties, enabling adsorption of enzymes with varying isoelectric points. Charge-controllable carriers based on carboxymethyl chitosan have demonstrated potential for immobilizing enzymes with enhanced catalytic efficiency (Wang *et al.* 2024). In addition to this, combining adsorption with covalent binding has been shown to mitigate enzyme leaching while maintaining high activity. For example, tyrosinase immobilized on magnetic nanoparticles through adsorption followed by cross-linking exhibited improved pH and thermal stability (Liu *et al.* 2017). Similarly, adsorption onto halloysite nanotubes followed by entrapment in cellulose nanocrystals enhanced enzyme storage stability and activity (Tizchang *et al.* 2021).

The industrial applications of adsorption-based immobilization are diverse and impactful. Adsorbed enzymes are commonly utilized in biocatalysis for processes such as biodiesel synthesis, juice clarification, and pharmaceutical manufacturing. Lipases adsorbed on hydrophobic supports have shown high activity in anhydrous media (Fernandez-Lorente *et al.* 2020). Additionally, adsorption onto nanomaterials has enabled the development of biosensors for detecting glucose and cholesterol. Enzymes adsorbed onto metal-organic frameworks have maintained activity and stability under harsh conditions, making them ideal for biosensing applications (Zhao *et al.* 2019). In environmental applications, adsorbed enzymes have been effectively employed in wastewater treatment and soil remediation. For instance, laccase adsorbed onto iron and aluminum minerals has been used to degrade soil phenolic compounds (Wu, Jiang et al. 2014). Similarly, cellulose-based adsorbents enhance the removal of heavy metals and organic pollutants, providing a versatile solution for environmental challenges(Varghese *et al.* 2018).

Despite its advantages, adsorption-based immobilization faces challenges, including enzyme leaching and reduced stability under extreme conditions. To address these limitations, hybrid approaches integrating adsorption with covalent bonding or entrapment have been used. The development of nanotechnology and material science offers further opportunities to design tailored supports with enhanced binding capacities and improved environmental stability.

1.5.1.2 Enzyme immobilization using covalent binding

Covalent binding is a widely used technique for enzyme immobilization, characterized by the formation of stable covalent bonds between enzymes and support materials. This method provides significant advantages, including high enzyme stability, resistance to environmental stresses, and reusability, making it highly suitable for industrial applications. However, covalent immobilization can sometimes lead to enzyme inactivation due to structural distortions.

The process of covalent immobilization involves the chemical attachment of enzyme molecules to a support material through reactive groups on the enzyme surface, such as amino, carboxyl, or hydroxyl groups. Commonly used reagents for this purpose include glutaraldehyde, cyanogen bromide, and carbodiimides. Multipoint covalent attachment has been shown to further improve enzyme stability by rigidifying the enzyme structure and preventing conformational changes (Rodrigues *et al.* 2021).

As discussed in section 1.5.1.1, combining covalent immobilization with other techniques, such as adsorption or entrapment, can reduce enzyme leaching while maintaining activity. For example, tyrosinase immobilized on magnetic nanoparticles enhanced thermal stability and reusability (Wu *et al.* 2015). Similarly, site-directed covalent immobilization using the PRECISE (Protein Residue-Explicit Covalent Immobilization for Stability Enhancement) system improved enzyme orientation, leading to higher activity and stability (Wu *et al.* 2015). Covalent attachment also protects enzymes from denaturation under extreme pH and temperature conditions, significantly extending their operational lifespan (Rodrigues *et al.* 2021). Unlike adsorption, covalent binding establishes permanent bonds between the enzyme and support bonds, thereby eliminating the risk of enzyme leaching (Hosseini *et al.* 2018). Covalently immobilized enzymes have found wide application in various industries, including food, pharmaceuticals, and textiles. For example, immobilized cellulase demonstrated enhanced enzymatic performance in the breakdown of cellulose for biofuel production (Sannino *et al.* 2020).

However, covalent binding can induce conformational changes in the enzyme, potentially reducing catalytic activity, particularly in cases where sensitive active sites are affected (Naghshbandi and Moghimi 2020). For instance, vinyl sulfone-activated silica often results in reduced activity when enzyme orientation is not well-controlled (Santos-Moriano *et al.* 2016). Additionally, the functionalization of support materials can be complex and costly, particularly when using advanced systems like magnetic nanocomposites, which require specialized reagents and processes (Hosseini *et al.* 2018). Furthermore, the chemical reagents and functionalization steps required for covalent immobilization can significantly increase costs compared to simpler methods like adsorption (Maghraby *et al.* 2023). Another limitation is mass transfer resistance, which can occur in dense or poorly porous support matrices, where substrate

accessibility to immobilized enzymes is restricted. For example, covalent organic frameworks (COFs), while offering high stability, may experience diffusion constraints in reactions involving large substrates (Gan *et al.* 2020). Similarly, hybrid approaches that combine covalent binding with encapsulation can face substrate diffusion challenges in tightly packed systems (Hosseini *et al.* 2018).

Scaling up covalent binding immobilization for industrial applications presents additional challenges. The precision required for enzyme attachment and the need for expensive materials and reagents can significantly increase costs, posing a barrier to widespread adoption. Addressing these challenges through advancements in material science, enzyme engineering, and process optimization will be crucial for unlocking the full potential of covalent immobilization in industrial biocatalysis.

1.5.1.3 Enzyme immobilization using encapsulation

Encapsulation is a promising technique for enzyme immobilization, involving the enclosure of enzymes within semi-permeable matrices or membranes. This method protects enzymes from external stresses while permitting the diffusion of substrates and products, thereby maintaining their catalytic activity. Encapsulation immobilization involves enclosing biomolecules within polymeric matrices, offering a controlled microenvironment for sensitive enzymes and biomolecules (Brady and Jordaan 2009). Like entrapment, encapsulation allows enzymes to remain freely suspended in solutions but confines them within a defined physical structure, typically tiny vesicles with porous membranes. These semi-permeable membranes allow smaller molecules, such as substrates and products, to diffuse freely while retaining larger enzyme molecules within the encapsulated structure (Akram *et al.* 2019, Kurzbaum *et al.* 2020).

Various materials, including cellulose nitrate and nylon, are used to create microcapsules ranging in size from 10 to 100 μm (Rother and Nidetzky 2014). Hydrogels such as alginate, agarose, and polyacrylamide are widely used for enzyme encapsulation due to their biocompatibility, ease of preparation and adaptability for diverse applications. Silica-based sol-gels are also extensively used for encapsulating enzymes and offering high mechanical strength, chemical inertness, and compatibility with various operational environments. For instance, silica-based matrices have been successfully utilized to immobilize oxidoreductases, significantly enhancing their operational stability in bioreactor systems (Rother and Nidetzky 2014). Encapsulation not only maintains the integrity of biological systems but also protects enzymes from environmental factors such as temperature fluctuations, pH changes, and exposure to contaminants, thereby enhancing their durability and efficiency.

However, enzyme encapsulation immobilization faces several challenges. Restricted substrate and product diffusion through the semi-permeable membrane can limit reaction rates, particularly for large or highly viscous substrates. Additionally, the mechanical fragility of certain encapsulation materials, such as hydrogels, can lead to structural degradation over time, especially under industrial-scale operations. Enzyme leakage through the encapsulating material is another concern, potentially reducing efficiency and stability. Furthermore, scaling up encapsulation methods remains complex and costly due to the precision required in fabrication and the high costs associated with advanced materials. Limited thermal stability of some encapsulating matrices and compatibility issues with specific enzymes or substrates further constrain the widespread application of this technique. Uniformity in microcapsule size and structure is critical for ensuring consistent performance, yet achieving this uniformity can be challenging (Rother and Nidetzky 2014). Variations in size and structural integrity can impact the diffusion properties and mechanical stability of the capsules, ultimately affecting enzyme activity and reusability.

1.5.1.4 Enzyme immobilization using entrapment

Entrapment is an irreversible enzyme immobilization technique that involves confining enzymes within a network of fibers or matrices through covalent or noncovalent bonds (Won *et al.* 2005). This method can be further described as the immobilization of enzymes within support material, such as lattices or polymer membranes, which retain the enzyme molecules while allowing the diffusion of substrates and products. Entrapment matrices include hydrogels, sol-gels, and synthetic polymers, each designed to ensure enzyme stability and functionality. For instance, enzyme immobilization using agar-agar has demonstrated high catalytic efficiency and enhanced thermal stability, making it suitable for applications in extreme environments (Sattar *et al.* 2018).

The use of polymer-based matrices has become a significant area of research in enzyme entrapment, offering enhanced stability and broader applicability. A notable development is the entrapment of enzymes using a cationic polymer, poly(2-(dimethylamino)ethyl methacrylate) (MADQUAT), incorporated into a single-wall carbon nanotube and reduced graphene oxide (SWCNT-rGO) nanohybrid thin film, which effectively reduces enzyme leakage (Adhikari *et al.* 2017). Compared to free enzymes, polymer-immobilized enzymes exhibit superior thermal and operational stability, enabling their functionality under challenging conditions such as extreme pH, high temperatures, and variable substrate concentrations (Lyu *et al.* 2021). Additionally, ionic liquid gels have emerged as innovative entrapment matrices, facilitating the development of recyclable biocatalysts with prolonged activity and operational lifespans (Imam *et al.* 2023).

Entrapment is environmentally sustainable due to the use of non-toxic materials, aligning with green chemistry principles (Trivedi *et al.* 2023). Techniques like gel entrapment enable enzymes to be used for multiple cycles without significant loss of activity (Sattar *et al.* 2018). For example, protease enzymes immobilized on k-carrageenan beads via entrapment have demonstrated sustained functionality and reusability over repeated cycles, further emphasizing the eco-friendly nature of the approach (Trivedi *et al.* 2023).

However, the entrapment technique is limited by challenges such as enzyme leakage and high mass transfer resistance to substrates. Certain matrices, such as hydrogels, may degrade under prolonged operational conditions, compromising enzyme stability and activity (Lyu *et al.* 2021). Additionally, inadequate control over pore size in the matrix can lead to reduced enzyme activity and efficiency over time (Imam *et al.* 2023).

1.5.1.5 Enzyme immobilization using cross-linking

For cross-linking, the enzymes are chemically bonded to each other or to support materials via cross-linking agents which do not require carriers. This technique enhances enzyme stability, reusability, and functionality under challenging conditions. Cross-linking immobilization involves the formation of stable covalent bonds between enzyme molecules or between enzymes and support matrices. Commonly used cross-linking agents include glutaraldehyde, carbodiimide, and dextran-based polymers, which react with functional groups (e.g., amino groups) on the enzyme surfaces. This method stabilizes the enzyme structure, minimizes leakage, and enhances resistance to environmental stresses (Aissaoui *et al.* 2014).

Cross-linked enzyme aggregates (CLEAs) are widely utilized, which are a carrier-free immobilization technique applicable to a diverse range of enzymes. Over the past two decades, extensive research has focused on identifying and optimizing the key variables in the CLEA preparation to develop robust and efficient immobilized biocatalysts. Each enzyme immobilized using the CLEA method required specific conditions and protocols to ensure optimal activity (Velasco-Lozano 2020). Enzymes can also be immobilized on functional nanofibers or nanoparticles cross-linker to further enhance their performance. For instance, poly (vinyl alcohol) (PVA) nanofibers with cross-linked enzymes exhibit improved thermal resistance and stability under extreme conditions (Tang *et al.* 2014). This method is effective at elevated temperatures, up to 105 °C. Using α-galactosidase from *Thermotoga maritima* as a model, immobilization within chemically cross-linked PVA nanofibers provides not only thermal stability but also provides a high specific surface area, further improving enzymatic functionality (Tang *et al.* 2014).

Cross-linked layer-by-layer (cLbL) deposition offers another immobilization strategy, allowing controlled and efficient enzyme stabilization under mild conditions. This technique has demonstrated its potential for immobilizing enzymes such as acid phosphatase and β-galactosidase on biocompatible, monodisperse sub-micrometer poly(lactide-co-glycolide) (PLGA) particles (Sieber *et al.* 2017). Such immobilized PLGA-enzyme systems are evaluated based on parameters such as size, surface charge, enzyme activity, storage stability, reusability, and stability across varying pH and temperature conditions. The cLbL protocol is highly versatile and can be readily adapted to immobilize a wide range of enzymes under similar conditions, making it particularly suitable for biomedical applications (Sieber *et al.* 2017).

The cross-linking method for enzyme immobilization offers advantages, including enhanced stability, minimized enzyme leakage, and high reusability, making it a preferred choice for various industrial and biotechnological applications. Cross-linking stabilizes enzymes against extreme pH and temperature conditions, with studies showing that aldehyde-dextran polymers can enhance the thermal stability of immobilized lipases by up to 250-fold (Orrego *et al.* 2018). Additionally, the formation of strong covalent bonds prevents enzyme leaching, ensuring consistent performance over repeated cycles (Sun *et al.* 2017). Cross-linked enzyme aggregates (CLEAs) retain substantial activity over multiple uses, with lipase CLEAs maintaining 70% of their activity after ten cycles (Rehman *et al.* 2016).

However, the method also has some drawbacks. Harsh cross-linking conditions can compromise enzyme structure, leading to reduced catalytic efficiency (Tang *et al.* 2014). Dense cross-linked matrices may impede substrate diffusion, limiting reaction rates (Velasco-Lozano 2020). Furthermore, the initial costs of this method can be prohibitive, as high-quality cross-linking agents and materials are often required (Sieber *et al.* 2017).

Recent developments in cross-linking agents, including the use of green and biocompatible materials, aim to mitigate enzyme deactivation and address environmental concerns. Additionally, combining cross-linking with other immobilization techniques, such as encapsulation, offers potential solutions to challenges related to mass transfer and stability (Jie *et al.* 2020).

1.5.1.6. Enzyme immobilization using nanotechnology-based immobilization

Nanotechnology-based enzyme immobilization leverages nanomaterials as immobilization supports. This technique offers unique advantages, including high surface area for enzyme attachment, minimal mass transfer resistance, and robust enzyme-substrate interactions.

Unlike conventional methods, enzyme immobilization in inorganic hybrid nanoflowers involves a biomimetic mineralization approach under mild reaction conditions (Liang *et al.* 2021). This technique results in the formation of biocatalysts with superior characteristics, including enhanced stability and catalytic efficiency. Another application involves the use of metal-organic frameworks (MOFs) to co-immobilize multiple enzymes, enabling the creation of cascade biocatalytic systems for complex multistep reactions (Hao *et al.* 2024). Cross-linked poly(vinyl alcohol) nanofibers, discussed earlier, have been used to immobilize hyperthermophilic enzymes, enabling them to retain activity at elevated temperatures of up to 105°C, making this method highly effective for extreme environmental conditions (Tang *et al.* 2014).

Magnetic nanoparticles (MNPs) represent another innovative platform for enzyme immobilization, allowing for easy recovery and reuse of enzymes under the influence of external magnetic fields. This property makes MNPs highly scalable and practical for industrial applications (Vaghari *et al.* 2015). Commonly used MNPs include magnetite (Fe_3O_4) and maghemite (γ-Fe_2O_3), which are biocompatible and exhibit low toxicity. Functionalized Fe_3O_4 nanoparticles have demonstrated enhanced enzyme-substrate affinity, maintaining over 80% of enzymatic activity even after six weeks of storage (Zhu *et al.* 2014). Furthermore, coating MNPs with polymers or zwitterionic materials improves their biocompatibility and minimizes enzyme denaturation, making them suitable for use in complex biological systems (Zhang *et al.* 2018). However, the synthesis and functionalization of MNPs often require specialized techniques and materials, leading to increased production costs and posing challenges for large-scale adoption (Suo *et al.* 2020).

In conclusion, each immobilization technique offers different unique advantages and limitations based on the application context. Adsorption and encapsulation are cost-effective but suffer from stability issues. Covalent binding and cross-linking provide superior stability but may impact enzyme activity due to structural alterations. Nanotechnology-based approaches represent cutting-edge solutions, combining stability and efficiency but with higher complexity and cost. The choice of technique depends on factors such as enzyme type, application, operational conditions, and overall cost-effectiveness.

1.5.2 Techniques of enzyme purification.

1.5.2.1 Enzyme purification via extraction

The purification of enzymes is a critical step in both research and industrial applications, as it ensures the isolation of biologically active and pure enzymes for

downstream processes. Among various purification techniques, extraction methods—particularly aqueous two-phase extraction (ATPE) and solid-phase extraction (SPE)—have emerged as valuable approaches due to their scalability, cost-effectiveness, and ability to maintain enzyme activity.

ATPE has garnered significant attention in enzyme purification due to its mild separation conditions and potential for large-scale applications. The method relies on the formation of two immiscible aqueous phases, typically created using polymer-polymer or polymer-salt combinations. Recent advancements have focused on improving ATPE systems to enhance efficiency and sustainability. For example, He et al. developed a recyclable ATPE system using pH-responsive copolymers to purify the Cap protein of Porcine Circovirus Type 2 (PCV2) (He *et al.* 2018). Additionally, Baskaran et al. investigated the use of polyethylene glycol (PEG 600) and ammonium sulfate-based ATPE for protein partitioning from aqua waste (Baskaran *et al.* 2018). Another study employed a citrate buffer (13.5%), PEG 2000 (8%), and varying NaCl concentrations (5–13.5%) to purify immunoglobulin G (IgG) from human serum albumin. This optimized system, using 13.5% NaCl, achieved a 98.9% IgG recovery with 92.6% selectivity, demonstrating ATPE as a cost-effective alternative to traditional chromatography techniques (Kress *et al.* 2017).

Solid-phase extraction (SPE) has also evolved significantly as a purification technique, particularly with the integration of advanced materials and surface modifications. Kanazawa et al. introduced a temperature-responsive SPE system using poly(N-isopropylacrylamide)-based hydrogel-coated aminopropyl silica beads for the selective separation of drugs and proteins from biological fluids (Akimaru *et al.* 2015). This system demonstrated precise control over analyte retention through temperature and salt content adjustments, showing promise for applications such as serum drug level measurements (Akimaru *et al.* 2015). Further advancements in SPE include the use of magnetic nanoparticles (MNPs) functionalized with Cu^{2+} and citric acid. This magnetic solid-phase extraction (MSPE) method offers rapid and efficient protein recovery with minimal operational complexity, highlighting its potential for large-scale applications (García-Nicolás *et al.* 2023).

In summary, ATPE offers scalability and cost-effectiveness, with ongoing innovations addressing its limitations in phase recovery and selectivity. SPE, on the other hand, benefits from advancements in material science, such as temperature-responsive systems and magnetic nanoparticles, to enhance selectivity and operational efficiency.

1.5.2.2 Enzyme purification via precipitation

Precipitation is a technique that leverages changes in solubility induced by pH, organic solvents, salt concentrations, or other additives to selectively separate proteins from complex mixtures. Among precipitation methods, isoelectric precipitation,

organic solvent precipitation, and salting out have proven particularly effective for protein purification.

Isoelectric precipitation separates proteins by adjusting the solution's pH to the isoelectric point (pI), where proteins exhibit minimal solubility. This approach has been extensively applied for protein purification. For example, a novel method employing phosphate salts and a freeze-thaw procedure under neutral or mildly acidic conditions achieved over 90% yield in precipitating caseins while preserving bioactivity (Yen *et al.* 2015). Pereira, Lisboa et al. (Pereira *et al.* 2018), demonstrated the effectiveness of isoelectric solubilization/precipitation (ISP) in producing protein isolates with excellent solubility at neutral pH and suitable foaming stability, in which protein concentrates (83.9%) and isolates (91.3%) were successfully derived from *Spirulina sp. LEB 18* biomass through solubilization at pH 11 and precipitation at pH 4.2, resulting in enhanced protein solubility, improved foam stability, and greater resistance to thermal denaturation. Similarly, isoelectric precipitation was employed to produce detoxified jatropha protein isolate (DJP), significantly reducing antinutritional factors while preserving functionality. Feeding trials using *L. rohita* fingerlings demonstrated that DJP supplemented with lysine could fully replace soybean protein isolate without adversely affecting growth, organ integrity, or enzyme activity, except for minor changes in intestinal alkaline phosphatase and serum alanine transaminase (Fawole *et al.* 2018).

Organic solvent precipitation disrupts protein hydration shells by reducing the solution's dielectric constant, causing proteins to aggregate and precipitate. This method is advantageous for its simplicity, scalability, and mild operating conditions, making it suitable for large-scale applications. However, careful optimization of solvent type and conditions is essential to prevent protein denaturation. An example is the PRotein Organic Solvent Precipitation (PROSPR) method, which uses cold acetone to purify extracellular vesicles (EVs) from human plasma. This approach had efficiently removed soluble proteins while retaining EV integrity and biomarker content, offering a viable alternative to traditional ultracentrifugation methods (Gallart-Palau *et al.* 2015).

Another application of organic solvent precipitation involved the production of protein-rich powders from *Chlorella protothecoides*. Using an ethanol: acetone (1:1, v/v) mixture, researchers achieved high protein content powders (67.2 ± 1.0 g/100 g for insoluble fractions and 46.3 ± 0.1 g/100 g for soluble fractions). This method effectively reduced the dielectric constant, promoting protein aggregation while removing pigments, making it ideal for food applications (Grossmann *et al.* 2018). However, organic solvents can denature proteins by disrupting hydration shells,

necessitating careful optimization of solvent concentrations and precipitation conditions to preserve protein functionality (Kim *et al.* 2022).

Salting out employs high salt concentrations to modulate protein solubility, which weaken electrostatic interactions and promote hydrophobic aggregation. The salting-out method for protein purification, emphasizing the role of salt concentration, ion size, and electrostatic interactions in influencing protein solubility (Dahal and Schmit 2018). For instance, ammonium sulfate precipitation at pH 6.5 was used to extract lactoperoxidase (LP) from bovine milk, achieving an 87.93% activity recovery and a purification fold of 3.13. Subsequent cation exchange chromatography enhanced the purification fold to 126.65 while maintaining an 82.62% activity recovery (Li *et al.* 2019).

Homogeneous liquid-liquid extraction (h-LLE) methods, such as salting-out (SALLE) and sugaring-out (SULLE), have been applied to extract proteins and other biomolecules. For example, NaCl was found to be the most effective salt for extracting 10-hydroxy-2-decenoic acid (10-HDA) from royal jelly, achieving high recovery with minimal protein co-extraction (Tu *et al.* 2018). More recently, Kinugasa, Kiyohito et al. used a salting-out method with sodium di(2-ethylhexyl) sulfosuccinate (AOT) to precipitate a protein-surfactant complex, followed by dissolution in acetone and reprecipitation with aqueous NaCl to recover lysozyme denatured by urea and GuHCl (Kinugasa *et al.* 2023). This approach achieved high protein recovery and retained lysozyme's enzymatic activity and native conformation under optimized conditions.

1.5.2.3 Enzyme purification via membrane separation

Membrane separation techniques, such as dialysis and ultrafiltration, are extensively utilized in protein purification due to their efficiency and ability to maintain protein activity. These methods provide gentle and effective means of separating proteins from impurities, such as salts, small molecules, and other undesired components, without compromising protein functionality.

Dialysis relies on a concentration gradient as the driving force to remove small molecules, such as salts, while retaining proteins through a semi-permeable membrane. This method is often combined with other purification techniques, such as ion exchange chromatography or salting-out, to enhance protein purity. For example, El-Ahmady El-Naggar et al. utilized ammonium sulfate precipitation and dialysis to purify *L-asparaginase* from a crude enzyme preparation. The purified enzyme was subsequently analyzed for its kinetic properties using ion exchange chromatography, demonstrating the utility of dialysis in conjunction with other purification methods (El-Naggar *et al.* 2016).

Recent advancements in dialysis membranes have further improved their efficacy. (Kidambi *et al.* 2017) utilized nanoporous atomically thin graphene membranes (NATMs) with size-selective pores for protein purification via dialysis, enabling efficient separation of small molecules from larger proteins like lysozyme. The NATMs demonstrated significantly improved permeance and selectivity compared to traditional dialysis membranes, making them effective for biochemical separations, including desalting and purifying peptides and proteins while retaining their structure and functionality.

On the other hand, ultrafiltration, driven by pressure or centrifugal force, separates proteins based on molecular weight through selective filtration. This technique is particularly effective for desalination, concentrating proteins, and removing small molecules. Ultrafiltration membranes are characterized by their molecular weight cut-off (MWCO), which determines the size range of molecules retained or removed.

For example, (Teng *et al.* 2006) applied cross-flow ultrafiltration (UF) enhanced by ultrasonic waves to separate bovine serum albumin (BSA) and lysozyme (Ly), achieving a 135% increase in flux in the upward mode and 120% in the downward mode. The ultrasonic irradiation minimized protein aggregation on the membrane surface and improved acoustic streaming.

Ultrafiltration has also been utilized for protein desalination, such as the removal of salt from salted duck egg white (SDEW). Using a 100 kDa MWCO membrane, researchers achieved 92.93% salt removal, reducing salt content from 9.2% to 0.65%, while retaining protein integrity (Thammasena *et al.* 2020).

Recent innovations in membrane technology have further expanded the scope of ultrafiltration for protein purification. For instance, polymer blend ultrafiltration membranes, made from polysulfone and sulfonated poly(arylsulfone)s, were employed to separate proteins like BSA and hemoglobin (Hb) based on size exclusion and charge selectivity (Emin *et al.* 2018). Additionally, titanium oxide (TiO_2) nanoparticles have been incorporated into membrane structures to improve performance across diverse applications, including catalysis, photocatalysis, and electrocatalysis. TiO_2 enhances membrane durability, selectivity, and efficiency, making it an essential component in modern membrane engineering (Bet-moushoul *et al.* 2016).

1.5.2.4 Enzyme purification via chromatography

Enzyme purification via chromatography offers high specificity and efficiency in isolating target enzymes from complex mixtures. The technique relies on the interaction between enzymes and chromatographic media, such as ion-exchange,

affinity, size-exclusion, and hydrophobic matrices, to achieve separation based on properties like charge, size, binding affinity, and hydrophobicity. With its scalability and precision, chromatography has become a cornerstone in the production of highly pure enzymes for research, therapeutic applications, and industrial use.

Ion-exchange chromatography (IEC) utilizes charged resins or cellulose matrices to separate proteins based on their surface charge. Depending on the nature of the charged groups in the matrix, IEC is classified as anion-exchange chromatography (AEC) or cation-exchange chromatography (CEC). Proteins bind to oppositely charged groups within the ion exchanger, and selective elution is achieved by modifying the salt gradient or pH of the eluent (Lou *et al.* 2018) For example, Ilicheva *et al.* demonstrated the use of IEC to purify the recombinant protein udTRF2 through optimized salt gradient elution (Ilicheva *et al.* 2018). Similarly, Özkan *et al.* enhanced the adsorption capacity of lysozyme using humic acid-modified poly (2-hydroxyethyl methacrylate) matrices (Özkan *et al.* 2018). In another study, pneumococcal surface protein A (PspA) of clade 4 was produced using *Escherichia coli* and purified via hydroxylapatite and ion-exchange chromatography, achieving a purity of over 95% in a single step (Xi *et al.* 2018).

Hydrophobic interaction chromatography (HIC) separates proteins based on differences in surface hydrophobicity under high-salt conditions (King *et al.* 2018). Proteins bind to hydrophobic chromatographic media through their hydrophobic regions, and elution is achieved by reducing ionic strength (Rodler *et al.* 2018). HIC operates under mild conditions, preserving protein structure and activity. For instance, Lei Wang *et al.* used HIC with polyethylene terephthalate (PET) capillary polymer fibers to efficiently separate exosomes from human plasma, achieving comparable yields with reduced impurities and faster processing compared to traditional methods (Wang *et al.* 2019). While HIC preserves protein functionality, its mobile phase is often incompatible with mass spectrometry, which limits its combined applicability in combined analyses (Rodler *et al.* 2018).

Hydrophilic Interaction Liquid Chromatography (HILIC) is a specialized chromatographic technique introduced by Dr. Andrew Alpert in 1990, designed to bridge the principles of normal phase chromatography with aqueous mobile phases (Alpert 1990). HILIC combines the principles of normal-phase chromatography with aqueous mobile phases to separate hydrophilic and polar compounds. This technique employs hydrophilic stationary phases, such as silica gel or polar polymers, and operates with an aqueous-organic solvent gradient (Xiong *et al.* 2018). HILIC provides enhanced resolution and specificity, making it particularly useful for analyzing complex biochemical samples. For example, crude sialylglycopeptides

(SGPs) were extracted from egg yolk and purified using a cotton-based HILIC column, yielding 300 mg of SGPs with 95% purity (Han *et al.* 2020).

Affinity chromatography is a highly selective method that utilizes specific and reversible interactions between biological macromolecules and ligands immobilized to a matrix. First introduced by Cuatrecasas et al. in 1968, affinity chromatography (AC) has become a standard technique for antibody purification due to its selectivity, stability, and efficiency (Ayyar *et al.* 2012, Grom *et al.* 2018). For instance, IMACM@mPEG, a magnetic immobilized metal affinity chromatography matrix, was used to purify angiotensin I-converting enzyme (ACE) inhibitory peptides from casein hydrolysate, demonstrating improved purification efficiency and identification of a novel peptide (Liu *et al.* 2020).

Size-exclusion chromatography (SEC), also known as gel permeation chromatography, separates molecules based on size using porous materials as the stationary phase (Cai *et al.* 2017). Large molecules elute first, as they are excluded from the pores, while smaller molecules experience delayed elution; when the porous material is a gel, this process is known as gel permeation chromatography (Hall 2018). SEC is particularly useful for mild separation, as it preserves the structural integrity of macromolecules. For example, SEC was combined with bind-elute techniques to purify extracellular vesicles (EVs), achieving high yields (~80%) and greater purity than ultracentrifugation methods (Corso *et al.* 2017). SEC has also been employed to isolate small extracellular vesicles (sEVs) from rat plasma, providing higher yields and improved marker signals compared to traditional methods (Takov *et al.* 2019).

High-performance liquid chromatography (HPLC) is a powerful technique used for separating and purifying proteins and peptides with high precision. HPLC operates by exploiting differences in the affinity between protein mixtures in the mobile phase and the stationary phase in the column. It is widely used for analytical and preparative purposes. For example, HPLC combined with ion-exchange chromatography successfully separated acidic proteins, demonstrating its utility in resolving complex mixtures (Bai *et al.* 2018).

Other chromatographic techniques, such as gel chromatography can be divided into gel filtration chromatography and gel permeation chromatography (GPC) based on the mobile phase (Barth 2018). Gel chromatography, also known as SEC, separates molecules based on their size and shape using a porous gel as the stationary phase (Kahle and Wätzig 2018). Supercritical fluid chromatography (SFC) is another emerging technique, particularly useful in the food and pharmaceutical industries for the rapid and cost-effective separation of chiral and achiral molecules (Manjare and Dhingra 2019).

1.5.2.5 Enzyme purification via electrophoresis and capillary electrophoresis

Electrophoresis is a highly effective analytical and preparative technique for enzyme purification that exploits the differential migration of charged particles in an electric field. It operates based on the principles of charge, size, and shape, which influence the movement of proteins and other biomolecules. Beyond traditional electrophoresis methods, advanced capillary electrophoresis (CE) techniques have been developed to offer enhanced resolution and precision in enzyme separation and purification.

As amphoteric molecules, proteins have charges that are influenced by the pH of the solution relative to their isoelectric point (pI). Proteins carry a positive charge at pH values below their pI and a negative charge at pH values above it. The magnitude of charge and mobility increases as the pH deviates further from the pI, enabling separation based on electrophoretic mobility (Kotz *et al.* 2018).

Two-dimensional electrophoresis (2-DE) is a widely used proteomic method for separating complex protein mixtures. It integrates isoelectric focusing (IEF) and sodium dodecyl sulfate-polyacrylamide gel electrophoresis (SDS-PAGE) to provide high-resolution separation based on both charge and molecular weight (Katorcha and Baskakov 2018, Yang *et al.* 2018). IEF separates proteins by their pI, while SDS-PAGE resolves proteins by their size under denaturing conditions, making the combination a powerful tool for characterizing enzyme purity and composition.

In contrast, capillary electrophoresis (CE) is a modern liquid-phase separation technique that employs narrow capillary tubes and a high-voltage direct current electric field to achieve rapid and precise separation (Moser *et al.* 2018). CE provides significant advantages, including high resolution, minimal sample requirements, and short analysis times. Its separation mechanism combines electrophoresis and electroosmotic flow (EOF).

In CE, the negatively charged inner surface of a quartz capillary generates EOF in the presence of a buffer at pH > 3. Positively charged ions move toward the cathode, while negatively charged ions migrate toward the anode. Neutral molecules move with the EOF. The overall migration velocity of particles depends on the combined effects of EOF and their electrophoretic mobility (Schejbal and Glatz 2018, Voeten *et al.* 2018). This versatility enables CE to separate a wide range of biomolecules, including enzymes, with high resolution and specificity.

Modifications to the capillary surface and buffer composition further enhance CE's capabilities. Surface modifications and the addition of additives to the buffer system enable improved control over protein distribution and separation (Ramos-Payán *et al.*

2018). These advancements have expanded CE's applications to challenging separation tasks, including resolving closely related protein isoforms and analyzing complex enzyme mixtures.

In conclusion, the progression of protein separation technologies reflects significant advancements in biotechnology and a deeper understanding of protein behavior. Traditional methods such as salting out, isoelectric precipitation, and organic solvent precipitation remain cost-effective for crude protein isolation but often require complementary techniques, such as dialysis or ultrafiltration, to achieve high purity. Modern high-precision methods, such as chromatography, electrophoresis, and microfluidics, have revolutionized protein separation with greater efficiency and resolution. High-performance liquid chromatography (HPLC) is the dominant tool in laboratories, whereas capillary electrophoresis offers excellent separation resolution despite its limited capacity. No single method can universally address all protein purification challenges, which has led to the development of integrated approaches tailored to the unique properties of target proteins. As protein purification evolves, continued innovation and optimization will provide solutions to increasingly complex challenges with greater precision and efficiency.

1.5.3 Why chose MagR for aspartase purification and immobilization?

The magnetic protein MagR has emerged as a multifunctional tool for protein purification and immobilization. First identified as a magnetoreceptor involved in magnetosensing, MagR forms a rod-like complex with cryptochromes (Cry), which are proteins associated with light and circadian rhythms (Qin *et al.* 2016). MagR naturally binds iron-sulfur (Fe–S) clusters, endowing it with unique magnetic properties that allow manipulation via external magnetic fields. A structural model of the Cry/MagR magnetosensor complex illustrates how 10 cryptochromes helically bind to the MagR rod polymer, which consist of 20 MagR molecules and is stabilized by helix-helix interactions (Figure 1-18). The Fe–S clusters are integral to MagR’s magnetism, and their arrangement in an “iron-loop” structure is highlighted in the figure.

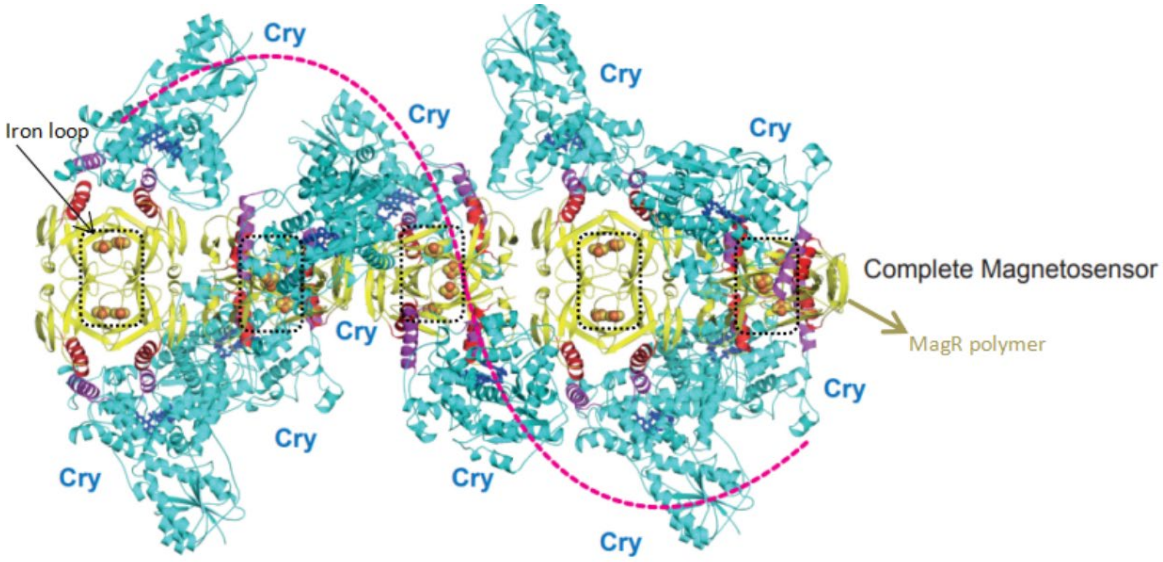

Figure 1-18 The structural model of the Cry/MagR magnetosensor protein complex (adapted from Qin *et al.*, 2016).

Ten cryptochromes (blue) helically bind the rod-like MagR polymer (yellow), consisting of 20 MagR units. The Fe–S clusters in MagR are represented as spheres, and the "iron-loop" structures are highlighted with dashed black ovals.

MagR's utility extends to protein purification and enzyme immobilization, particularly when fused with target proteins. As demonstrated by Jiang *et al.*, MagR fusion proteins facilitate one-step purification by adsorption to magnetic nanoparticles (Figure 1-19), bypassing traditional chromatographic methods (Jiang *et al.* 2017). For instance, GFP and three enzymes of varying molecular sizes—lipase, α-L-arabinofuranosidase, and pullulanase—were expressed in *E. coli* and successfully immobilized on Fe_3O_4 nanoparticles via physical adsorption. The immobilized enzymes exhibited enhanced stability under extreme pH and temperature conditions, retaining 71% of their activity after 20 cycles of resue. This simplified process achieved high purification efficiency while preserving enzymatic activity, highlighting MagR's robustness in biotechnological applications.

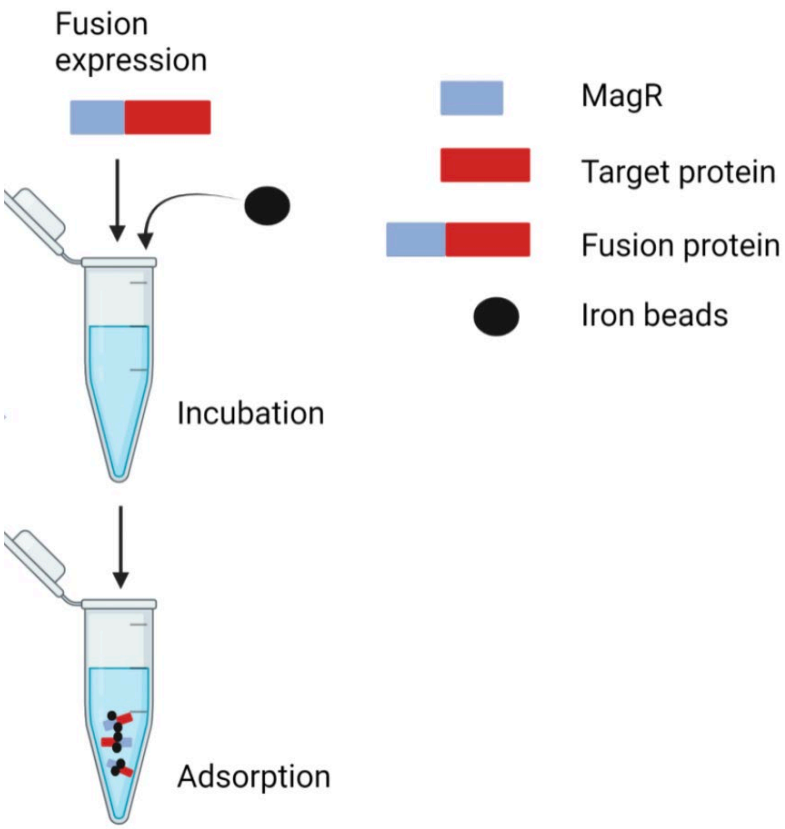

Figure 1-19 Schematic representation of one-step rrotein purification and immobilization.

A target protein (red) is fused to MagR (blue), forming a fusion protein. Then, the fusion protein is expressed and mixed with magnetic nanoparticles (black). The MagR's inherent magnetic properties enable the fusion protein to bind the nanoparticles through physical adsorption. Application of an external magnetic field facilitates the separation of fusion proteins bound to nanoparticles from unbound components, achieving efficient purification.

MagR's versatility extends to medical applications. Liu, Zhao et al. engineered a biofilm-degrading system by fusing MagR to the C-terminus of Dispersin B (DspB) (Liu *et al.* 2022). The recombinant protein was immobilized on Fe_3O_4@SiO_2 nanoparticles, significantly enhancing the enzyme's stability and shifting its optimal activity to 37°C. This system effectively degraded bacterial biofilms, removing up to 60% of those formed by *Staphylococcus aureus* and *Bacillus cereus*, demonstrating its potential for medical and industrial applications.

Additionally, Kang et al. developed a rapid and highly sensitive diagnostic method using MagR-MazE fusion proteins for viral nucleic acid detection (Kang *et al.* 2021). The MagR-MazE fusion was conjugated to silica-coated Fe_3O_4 magnetic

nanoparticles and used in nucleic acid detection assays, demonstrating high specificity and sensitivity while underscoring MagR's value in diagnostic applications.

In summary, MagR offers a versatile platform for protein purification and immobilization. Its magnetic properties enable rapid, cost-effective separation using magnetic nanoparticles, eliminating the need for centrifugation or filtration. MagR fusion proteins demonstrate compatibility across diverse pH levels, salt concentrations, and temperatures, ensuring robust performance in various environments. Furthermore, recombinant MagR expression in systems such as *E. coli* makes it scalable and economically viable.

1.5.4 The controversies and unresolved questions surrounding MagR.

Although several independent research groups have successfully utilized Fe_3O_4-SiO_2 magnetic beads to purify and immobilize catalytically active enzymes expressed as MagR fusion proteins, the functionality and practical applications of the MagR protein have sparked scientific debate, as evidenced by conflicting findings in recent studies.

In the 2016 paper Physical limits to magnetogenetics (Meister 2016), Markus Meister critically examined claims about the magnetic properties of certain protein complexes and their proposed applications in magnetogenetics. He highlighted that the theoretical magnetic forces generated by these complexes are vastly insufficient to influence biological systems at physiological temperatures. Meister calculated that approximately 10^6 closely packed iron (Fe) atoms per complex would be necessary to achieve a detectable permanent magnetic moment. This estimate far exceeds the actual number of iron atoms present in studied protein assemblies, such as MagR. Consequently, Meister concluded that the observed phenomena in such studies were unlikely to stem from genuine magnetic interactions and suggested alternative mechanisms to explain the reported effects, thereby challenging the feasibility of magnetogenetics under current assumptions.

Winklhofer and Mouritsen further argued that the proposed magnetic properties of the MagR complex, as suggested by Xie et al. (2016), are fundamentally flawed (Winklhofer and Mouritsen 2016). They calculated that, for a protein complex to achieve a permanent magnetic moment capable of aligning with Earth's magnetic field, a significantly greater number of iron atoms would be necessary. Specifically, they estimated that approximately 10^6 closely packed iron atoms per complex would be necessary, far exceeding the 40 iron atoms present in the MagR complex. They argued that the magnetic moment of the MagR/Cry4 complex would need to be 10^7

times larger than the values measured by Xie et al. (2016) to account for the reported orientation behavior.

Although Wang et al.'s study demonstrated the feasibility of immobilizing the quorum-sensing signal hydrolase AiiA using the MagR fusion approach, it also raised questions about the true nature of MagR's magnetic properties (Wang et al. 2019). The findings suggested that the observed binding to silica-coated Fe_3O_4 beads may result from ionic interactions rather than inherent magnetism. Similarly, a study showed that, although Drosophila melanogaster MagR (dmMagR) bound to silica-coated Fe_3O_4 magnetic beads, the process lacked specificity, with significant nonspecific adsorption of host-cell proteins (Pekarsky et al. 2021). Binding studies indicated that dmMagR adhered strongly to beads across a wide pH range (5–11) and salt conditions (up to 2 M NaCl), though binding was disrupted at pH 12. These observations suggest that ionic interactions, rather than magnetic properties, might be the driving factor.

To investigate the origin of MagR's magnetic effects, two independent research groups have developed electrochemical magnetic sensors utilizing a layer of pigeon MagR/Cry4 protein complex immobilized on an electrode (Xue *et al.* 2020, Cheng *et al.* 2023). These sensors demonstrated sensitivity to magnetic fields as low as ~1 mT, attributed to a magnetic field-induced alignment of MagR/Cry4 molecules on the electrode surface, which reduced charge carrier scattering and enhanced current output. Notably, the magnetic response was absent when either MagR or Cry4 was used alone. Furthermore, the response required light to be effective, and the MagR/Cry4 complex was found to lack a measurable permanent magnetic moment.

Further exploration by Li *et al.* transfected pigeon MagR/Cry4 genes into *E. coli* cells and cultured eukaryotic mesenchymal stem cells in the presence of exogenous iron ions (Fe^{3+}) (Li *et al.* 2023). These cells exhibited enhanced T2 contrast in magnetic resonance imaging (MRI); however, no similar effect was observed when only the MagR gene was transfected or when exogenous Fe^{3+} was not supplied. This suggests that the MagR/Cry4 complex may facilitate the formation of intracellular paramagnetic iron oxide granules, accelerating transverse relaxation in MRI and enhancing T2 signal contrast. However, multiple laboratories have failed to confirm whether MagR/Cry4 possesses a permanent magnetic moment. It is possible that MagR/Cry4 participates in the biosynthesis of magnetic nanoparticles (e.g., Fe_3O_4 or Fe_2O_3) or that observed effects results from contamination by pre-existing magnetic nanoparticles.

In response to these controversies, Xie's team has published several papers discussing MagR's structural and functional properties. One study (Zhou *et al.* 2023) highlighted

the synergistic roles of iron and iron-sulfur cluster binding in conferring magnetic properties to MagR, suggesting a sophisticated mechanism essential for optimal function. Further investigations into the mitochondrial targeting sequence (MTS) of MagR have revealed its role in protein stability and functionality within mitochondria, suggesting its involvement in magnetoreception and cellular iron homeostasis (Zhang *et al.* 2024). Comparative analyses between robin and pigeon MagR proteins uncovered species-specific adaptations that influence iron and iron-sulfur binding capacities, highlighting MagR's functional plasticity in response to distinct ecological niches (Wang *et al.* 2024). Additionally, evolutionary studies have demonstrated that while the core function of MagR in iron-sulfur cluster assembly is conserved, variations have emerged to tailor its role to the specific magnetoreceptive needs of different organisms (Zhang *et al.* 2024).

In conclusion, the existence and function of the MagR/Cry4 protein complex *in vivo* remain subjects of considerable debate. While co-expression, functional studies, and in vitro experiments support the hypothesis, definitive in vivo validation and consistent observations of magnetic properties are lacking. Further research using advanced imaging and proteomic techniques is necessary to determine whether this complex genuinely forms and functions within living organisms. The exact origin of MagR/Cry4's magnetic effects—whether intrinsic or linked to biosynthetic processes—remains an open question in the field.

1.6 Conclusion and project introduction

β-Amino acids are structurally distinguished by the separation of their amino and carboxyl groups by two carbon atoms, introducing multiple possibilities for stereochemical configurations at both the Cα and Cβ positions. This structural flexibility allows the existence of up to four diastereomers for a single side chain and permits di-substitution, thereby greatly enriching their chemical diversity. Such diversity has made β-amino acids highly attractive building blocks for tailored molecular design. In particular, they serve as indispensable components in the development of peptidomimetics—molecules with potent biological activity and exceptional resistance to proteolysis—and as chiral scaffolds in pharmaceutical synthesis, where they can be used in the production of bioactive compounds and therapeutic agents.

Despite these advantages, the production of optically pure β-amino acids continues to present considerable challenges. Conventional chemical methods often require

multiple protection and deprotection steps, operate under harsh conditions, and suffer from poor atom economy and stereoselectivity. These limitations restrict scalability and raise environmental concerns, making chemical synthesis an unsustainable option for large-scale production. There is a critical research gap which is the urgent need for efficient, selective, and environmentally responsible alternatives for β-amino acid manufacturing.

Biocatalysis has emerged as a promising solution. Enzymes such as aspartase (AspA and AspB) and methylaspartate ammonia lyase (MAL) have demonstrated considerable potential due to their catalytic precision, broad substrate tolerance, and amenability to protein engineering. Engineered aspartase variants, for example, have been shown to catalyze the conversion of crotonic acid into β-aminobutyric acid (BABA), a non-proteinogenic amino acid with notable applications in agriculture as a stress-resistance inducer and in biotechnology as a versatile building block. MAL complements these capabilities by catalyzing the asymmetric synthesis of β-substituted aspartates and other unnatural amino acids. These case studies illustrate the catalytic versatility of ammonia lyases and underscore their promise as biocatalytic tools for sustainable amino acid synthesis.

This project builds on these foundations with two main innovations. The first lies in the application of advanced protein engineering strategies to improve the activity, stability, and substrate range of AspA, AspB, and MAL, thereby expanding their potential as biocatalysts for β-amino acid and ohter unnatural amino acid synthesis. The second innovation is the exploration of the magnetoreceptor protein MagR as a tool for one-step purification and immobilization of engineered aspartases. By enabling magnetic recovery and reuse, this strategy addresses longstanding bottlenecks in enzyme purification and recycling, improving both the economic and environmental feasibility of large-scale enzymatic processes.

On top of that, this research is the focus on thermophilic variants of AspA and MAL. Thermophilic enzymes are naturally more stable and active at elevated temperatures, qualities that make them particularly attractive for industrial applications. Using recombinant expression, this work successfully produced thermophilic enzyme variants and validated their activity through both nuclear magnetic resonance (NMR) spectroscopy and spectrophotometric assays. These findings provide a strong foundation for expanding the enzymatic toolbox toward industrially relevant conditions.

The overarching aim of this study is to establish a robust enzymatic platform for the synthesis of β-amino acids and unnatural amino acids in a manner that is both sustainable and scalable. Within this aim, several objectives are pursued. First,

engineered AspB variants are developed to broaden substrate specificity and enhance catalytic efficiency in β-amino acid production. Second, thermophilic AspA and MAL variants are explored for their potential to provide greater stability and activity under industrially relevant conditions. Third, the fusion of engineered aspartases with MagR is investigated as a strategy for simultaneous enzyme purification and immobilization, thereby streamlining downstream processing and improving enzyme reusability. Fourth, enzymatic activity and product formation are systematically evaluated using spectrophotometric and NMR-based assays to establish robust methods of analysis. Finally, current bottlenecks in enzymatic β-amino acid synthesis are identified, with strategies proposed for greener and more cost-effective solutions.

This project is guided by several key hypotheses. It is anticipated that rational and computational protein design can expand the substrate scope of AspA, AspB, and MAL without compromising stereoselectivity, and that thermophilic homologues will display superior performance under industrial conditions compared to mesophilic counterparts. Moreover, it is hypothesized that fusing engineered aspartases with MagR will enable efficient magnetic purification and immobilization, providing a scalable method for enzyme reuse and recovery. Together, these strategies are expected to overcome the key challenges of instability, narrow substrate tolerance, and costly downstream processing that currently limit the industrial application of β-amino acid biocatalysts.

The structure of this thesis is outlined as follows. Chapter 1 introduces the background and significance of β-amino acids and unnatural amino acids, highlights synthetic methods, and establishes the rationale for focusing on AspA, AspB, and MAL. Chapter 2 details the materials and methods employed, including DNA construction, protein expression, enzymatic assays, and analytical approaches. Chapter 3 examines the engineering of AspB for β-amino acid synthesis. Chapter 4 investigates *Pasteurella multocida* AspA (PmAspA) as a platform for unnatural amino acid production while Chapter 5 focuses on the engineering of MAL for asymmetric synthesis. Chapter 6 explores the novel application of MagR for purification and immobilization of aspartases. Finally, Chapter 7 summarizes the key findings, discusses their industrial relevance, and proposes future directions.

In conclusion, this project is aiming to address the challenges of β-amino acid synthesis through the development of engineered enzymes with expanded capabilities, integrated with innovative immobilization and purification strategies. By combining protein engineering, thermophilic enzyme exploration, and MagR-based purification, this study advances the field of enzymatic amino acid production and provides a sustainable, scalable pathway for future pharmaceutical and industrial applications.

2 Materials and Methods

2.1 Bacterial strains and growth conditions

2.1.1 Bacterial strains.

Escherichia coli DH5α (provided by Prof Tuck Seng Wong) was used for genetic manipulation and plasmids propagation. *E. coli* BL21(DE3) and C41(DE3) (provided by Prof Tuck Seng Wong) were used for protein expression experiments.

2.1.2 Cell growth media and conditions.

E. coli DH5α and BL21(DE3) cells were cultured in 2xTY medium (2x Yeast Extract Tryptone medium). TYE agar plates supplemented with 50 μg/mL kanamycin were used for the selection of transformants and recombinants. All cell cultures were incubated at 37°C with shaking at 250 rpm, unless specified otherwise.

2.2 Plasmid DNA preparation

Plasmid DNA vectors were utilized throughout this project for the expression of engineered enzymes and accessory genes required for enzymatic synthesis studies. These plasmids were integral to facilitating the expression of enzyme variants and fusion proteins in *Escherichia* coli strains, enabling both transient and stable enzyme expression.

A summary of the plasmids utilized in the project is provided in Table 4. These plasmids were constructed and used for various experimental purposes, including the molecular cloning and expression of wild-type and mutant enzymes. Each plasmid contained specific genes of interest, alongside appropriate selection markers and promoters to ensure efficient expression in the designated host organisms.

The table provides a systematic summary of the plasmid names, key features, and respective applications, offering a comprehensive overview of their roles in the study.

Table 4 The plasmids utilized in this study.

Plasmid name	Key features	Applications	Source
pET24a-HLTev-	T7 promoter, His-tag for	Plasmid backbone	(Provided by Prof

VsLegH	purification, HLTev-VsLegH fusion gene	vector	Tuck Seng Wong)
pET28a-B19	T7 promoter, kanamycin resistance, AspB gene with B19 mutation	AspB expression for substrate conversion studies	(Li, Wijma et al. 2018)
pET28a-N5	T7 promoter, kanamycin resistance, AspB gene with N5 mutation	AspB expression for substrate conversion studies	(Li, Wijma et al. 2018)
pET28a-P1	T7 promoter, kanamycin resistance, AspB gene with P1 mutation	AspB expression for substrate conversion studies	(Li, Wijma et al. 2018)
pET28a-F29	T7 promoter, kanamycin resistance, AspB gene with F29 mutation	AspB expression for substrate conversion studies	(Li, Wijma et al. 2018)
pET28b-aspB-M1	T7 promoter, kanamycin resistance, AspB gene with M1 mutation	AspB expression for substrate conversion studies	(Zhao 2021)
pET28b-aspB-M2	T7 promoter, kanamycin resistance, AspB gene with M2 mutation	AspB expression for substrate conversion studies	(Zhao 2021)
pUC-GW-Kan-AspB-AA15	pUC-GW vector, kanamycin resistance, aspB gene with AA15 mutations	Construction of AA15 mutants insert for substrate-specific enzyme activity studies	(Cui *et al.* 2021)
pUC-GW-Kan-AspB-PA15	pUC-GW vector, kanamycin resistance, aspB gene with PA15 mutations	Construction of PA15 mutants insert for substrate-specific enzyme activity studies	(Cui *et al.* 2021)
pUC-GW-Kan-AspB-BA15-M13	pUC-GW vector, kanamycin resistance, aspB gene with BA15-M13 mutations	Construction of BA15-M13 mutants insert for substrate-specific enzyme activity studies	(Cui *et al.* 2021, Wang *et al.* 2020)
pUC-GW-Kan-Enz2-M20	pUC-GW vector, kanamycin resistance, aspB gene with Enz2-M20 mutations	Construction of Enz2-M20 mutants insert for substrate-specific enzyme activity studies	(Tian 2019, Wang *et al.* 2020)

pUC-GW-Kan-PmAspA	pUC-GW vector, kanamycin resistance, PmAspA gene from *Pasteurella multocida*	Expression and analysis the substrate scope of novel AspA enzyme from *Pasteurella multocida*	Novel constructed
pUC-GW-Kan-DtMA	pUC-GW vector, kanamycin resistance, DtMAL gene from *Dictyoglomus thermophilum*	Expression and analysis the substrate scope of novel MAL enzymes from *Dictyoglomus thermophilum*	Novel constructed
pUC-GW-Kan-6H-PmAspA-QM	pUC-GW vector, His-tag for purification, kanamycin resistance, PmAspA gene with T189C, M323I, K326M and N328C mutations	Expression and analysis the substrate scope of mutant aspartase enzyme from *Dictyoglomus thermophilum*	Novel constructed
pUC-GW-Kan-6H-DtMAL -SM	pUC-GW vector, His-tag for purification, kanamycin resistance, DtMAL gene with L384A mutation	Expression and analysis the substrate scope of mutant MALenzyme from *Dictyoglomus thermophilum*	Novel constructed
pUC-GW-Kan-ClMagR	pUC-GW vector, kanamycin resistance, ClMagR gene from *Columba livia*	Construction of universal vectors harboring MagR for one-step immobilization and purification	(Jiang *et al.* 2017)
pUC-GW-Kan-dmMagR	pUC-GW vector, kanamycin resistance, dmMagR gene from *Drosophila melanogaster*	Construction of universal vectors harboring MagR for one-step immobilization and purification	(Jiang *et al.* 2017)

2.2.1 Plasmids DNA design.

Plasmid pET24a-HLTev-VsLegH was used as the primary protein expression vector and was provided by Prof. Tuck Seng Wong. The pET-24a vector was specifically engineered for high-level protein expression in E. coli, driven by the T7 promoter. This vector offered significant flexibility for recombinant protein production with minimal modifications. Its design allowed for the insertion of genes into a multiple cloning site (MCS) and provided the option for a C-terminal His-tag, which facilitated purification via affinity chromatography while avoiding potential interference with protein function by N-terminal tags. The vector contained a kanamycin resistance gene for selection and incorporated optimized translation signals to ensure efficient protein synthesis. These features made pET-24a an excellent choice for applications in structural biology, enzymology, and industrial protein production. The pET24a-HLTev-VsLegH plasmid used in this project is shown in Figure 2-1.

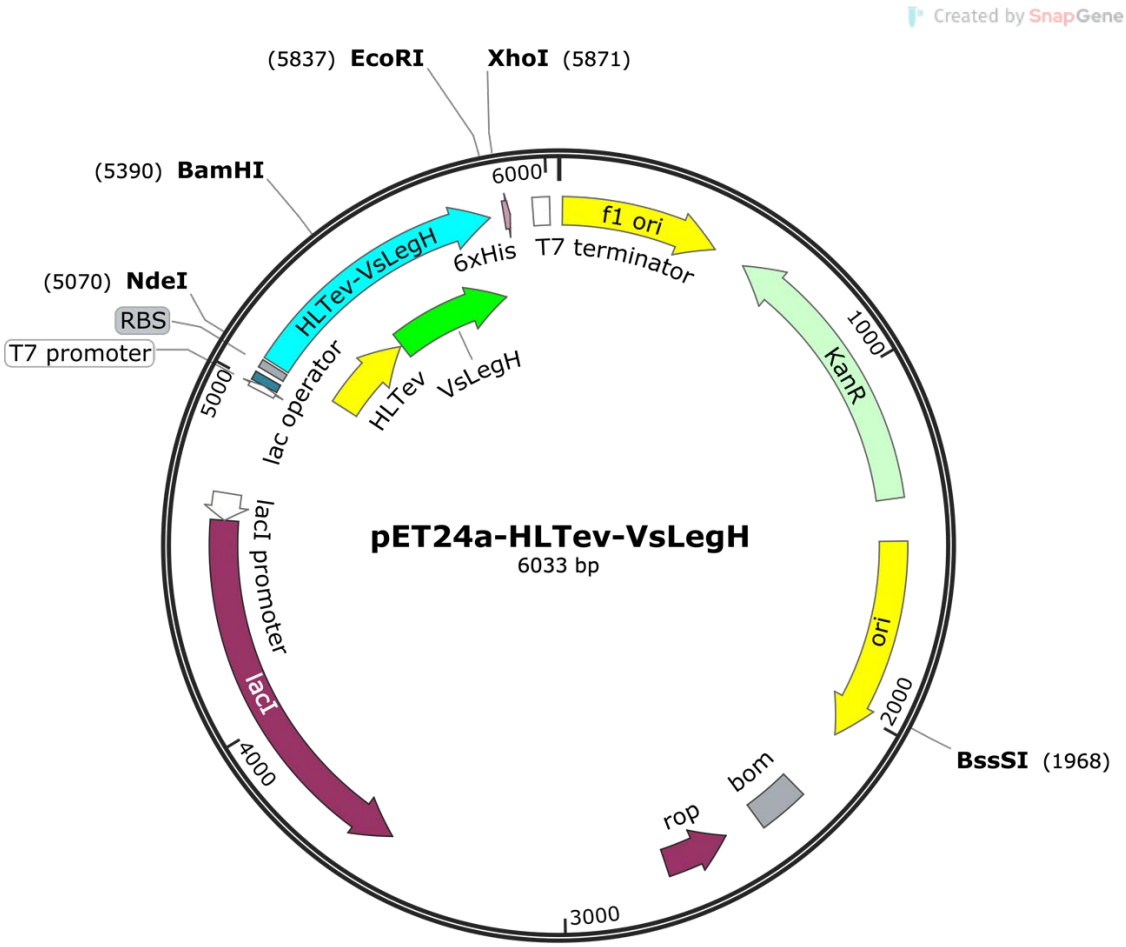

Figure 2-1 The plasmid map of pET24a-HLTev-VsLegH as backbone vector pET24a- used in this project.

The plasmid map shows the backbone plasmid used during this project. This plasmid contains the T7 promoter for inducible, high-level expression of the target gene in host strains such as BL21(DE3), which provide T7 RNA polymerase. Unlike pET-28a (+), pET-24a provides an option for a C-terminal His tag but does not include a default N-terminal His tag. However, the tag can be added by cloning. This plasmid vector Includes a kanamycin resistance gene for selection in bacterial cultures. The T7 terminator ensures proper termination of transcription.

All engineered genes and their wild-type counterparts in this study were expressed using the pET24a, pET28a, and pET28b vectors. The plasmids pET28a-B19, pET28a-N5, pET28a-P1, pET28a-F29, pET28b-aspB-M1, and pET28b-aspB-M2, each harboring genes encoding AspB mutants, were employed for both gene amplification and protein expression. Additionally, plasmids pUC-GW-Kan-AspB-AA15, pUC-GW-Kan-AspB-PA15, pUC-GW-Kan-AspB-BA15-M13, and pUC-GW-Kan-Enz2-M20, which also contained aspartase mutant genes, were used for plasmid construction. The AspB gene utilized in this project originated from Bacillus sp. YM55-1 but included specific mutations summarized in Table 5. Among these, the AspB-B19, AspB-M1, and AspB-M2 variants were designed as biocatalysts to synthesize (R)-β-aminobutanoic acid from crotonic acid.

Table 5 The amino acid substitutions of AspB mutants compared to wildtype AspB for producing β-amino acids.

Enzyme	Mutations	Substrate	Source
B19, M1	T187C, M321I, K324L, N326A	Crotonic acid	(Li *et al.* 2018)
M2 (patent)	T187C, M321I, K324M, N326C	Crotonic acid	(Zhao 2021)
P1	T187C, M321I, K324L, N326C	2-Pentenoic acid	(Li *et al.* 2018)
N5	M321I, K324N, N326C	Fumaric acid monoamide	(Li *et al.* 2018)

F29	T187C, M321V, K324I, N326C	Cinnamic acid	(Li *et al.* 2018)
Enz2 (patent)	T187C, M321V, K324T, N326S	(E)-4-(2 ,4 ,5-trifluorophenyl)-2-butenoic acid	(Tian 2019)
M13	K19E, N125D, S133D, T187C, M321I, K324L, N326A	Crotonic acid	(Wang *et al.* 2020)
M20	N87E, N125D, S133D, T187C, Q262E, M321I, K324L, N326A,N451E	Crotonic acid	(Wang *et al.* 2020)
BA15	A99G, N142S, T187C, M321I, K324L, N326A, L358V, E362M	Unsaturated acid electrophiles with amine nucleophiles	(Cui *et al.* 2021)
AA15	A99G, N142S, L358V, E362M	Unsaturated acid electrophiles with amine nucleophiles	(Cui *et al.* 2021)
PA15	A99G, N142S, T187C, M321, IK324L, N326C, L358V, E362M	Unsaturated acid electrophiles with amine nucleophiles	(Cui *et al.* 2021)

Plasmids pUC-GW-Kan-PmAspA and pUC-GW-Kan-DtMAL, harboring genes encoding novel aspartaseA and methylaspartate ammonia-lyase, respectively, were used for plasmid construction. The PmAspA gene (GenBank Accession No. Q9CLV0), used in this project, originated from Pasteurella multocida, and the

methylaspartate ammonia-lyase DtMAL gene (GenBank Accession No. WP_012547215.1) originated from Dictyoglomus thermophilum. The MagR genes used in this project were: clMagR (GenBank Accession No. XP_005508102.1) and dmMagR (GenBank Accession No. NP_573062). The gene clMagR (GenBank Accession XP_005508102.1) originated from Columba livia, and dmMagR (GenBank Accession NP_573062) originated from Drosophila melanogaster. All these genes were synthesized and purchased from GENEWIZ (South Plainfield, New Jersey).

To allow engineered enzyme immobilization and purification, the clMagR and dmMagR gene fragments were cloned into the N-terminus of engineered aspartase genes, respectively, creating fusion proteins for expression. The design of universal vectors for the fusion expression of engineered aspartase and MagR is shown in Figure 2-2.

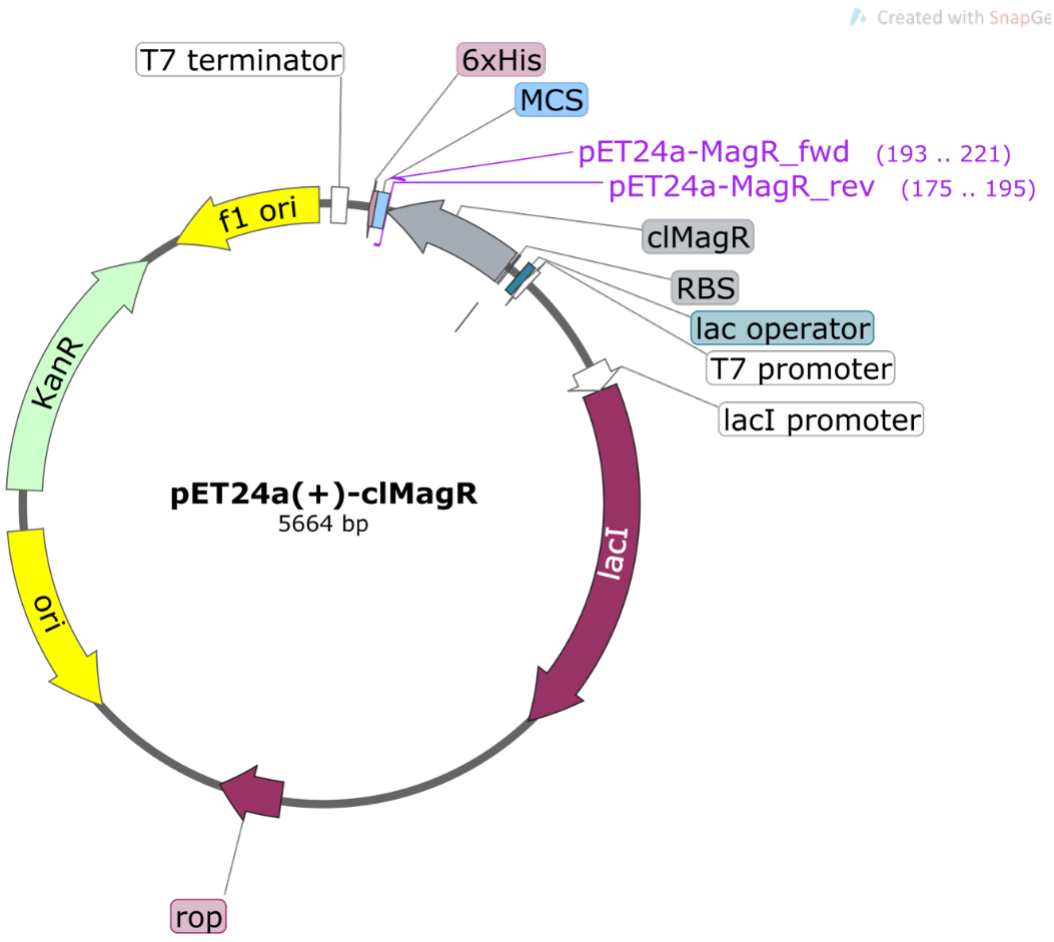

Figure 2-2 The plasmid map of designed universal vectors for fusion expression of engineered aspartase and MagR.

2.2.2 Site-directed mutagenesis of DNA plasmid.

Site-directed mutagenesis (SDM) was employed to introduce precise genetic modifications—such as point mutations or multiple substitutions—into plasmids encoding engineered enzyme variants. The method relied on mutagenic primers containing the desired base changes and high-fidelity PCR amplification. Following amplification, the parental template DNA was digested with DpnI, leaving only the newly synthesized mutant plasmids, which were transformed into *E. coli* and verified by sequencing.

In this study, SDM was used to construct several aspartase variants. For example, the Enz2 variant was generated by introducing the C326S mutation into plasmid pET28a-F29 using a two-stage PCR strategy (Figure 2-3). The design and setup were performed with the publicly available OneClick tool (Warburton *et al.* 2015). Unlike conventional one-step mutagenesis, this two-stage approach involved independent reactions with each mutagenic primer for 10 cycles, followed by combining the reactions and running 20 additional cycles to amplify the full-length product. The PCR components and cycling conditions are shown in Tables 6 and 7.

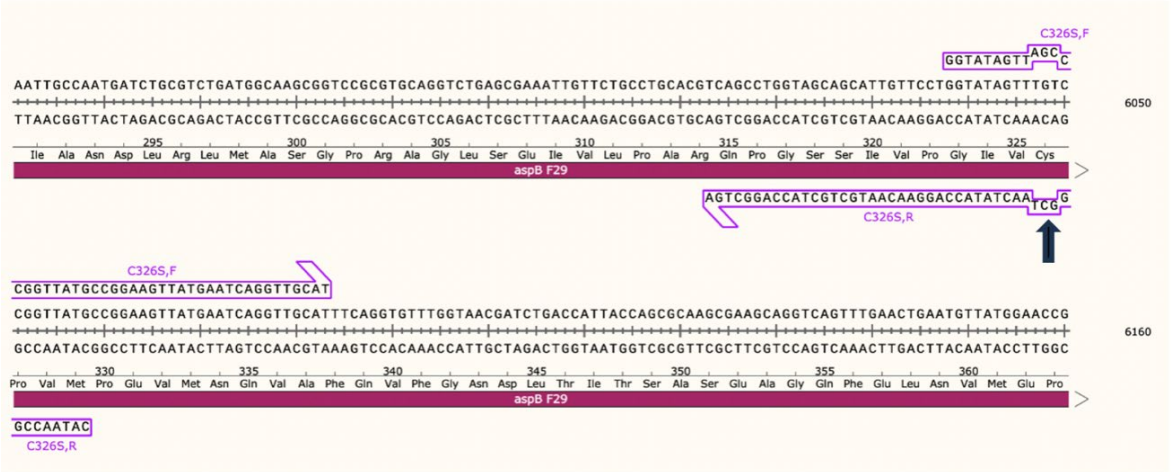

Figure 2-3 The designing of SDM for creating C326S mutation.

Partially overlapping primers C326S, F/C326S designed by OneClick, for introducing C362S mutation on pET28a-aspB-F29. The residue 326 mutation site is indicated by black arrow.

Table 6 The details of PCR components for SDM.

Component	Stock Concentration	Volume per Tube(μL)	
		TubeF	TubeR
Water		37	37
Q5 buffer (NEB)	5x	10	10
dNTPs	10 mM	1	1
DNA template	100 ng/μL	0.5	0.5
Forward Primer	20 μM	1	0
Reverse Primer	20 μM	0	1
Q5 High-Fidelity DNA polymerase (NEB)	2 U/μL	0.5	0.5
Total Reaction Volume		**50**	**50**

Table 7 The details of PCR conditions for SDM.

Stage	Temperature (°C)	Duration (min)	Repeat
1: Denaturation	98	00:30	1
2: Amplification (for each DNA strand)	98	00:08	9
	55	00:20	
	72	02:50	
3: Pause, mix TubeF and TubeR, redistribute equally before continuing			
4: Amplification (for both DNA strand)	98	00:08	19
	55	00:20	
	72	02:50	
4: Extension	72	02:00	1
5: Hold	8		1

Additional variants were produced using SDM, including the M13 variant (mutations K19E, N125D, and S133D introduced into B19) and the BA15 variant (mutations A99G, N142S, L358V, and E362M introduced into B19). The primers used are listed in Table 8. For constructs requiring multiple complex mutations, synthetic DNA fragments encoding the desired *aspB* gene variants were purchased directly from GENEWIZ to streamline the process.

Table 8 Primers used in this project.

Variant	Primer sequence (5'→3')
BamHI-AspB-F	TATAGGATCCATGAATACCGATGTGCGCATCG
AspB-EcoRI-R	TATAGAATTCTTATTTACGACCTGCAATACCCGGATG
K19E, F	GAAATCCCGGAAGATGCCTATTATGGTGTTCAGACCATTCGTGCAA
K19E, R	ATAGGCATCTTCCGGGATTTCTTTTTCGCCCAGAAAATCTTTTTCG
S133D, F	AGCCCGAATGATCATGTTAATATGAGCCAGAGCACCAATGATGCAT
S133D, R	ATTAACATGATCATTCGGGCTGATTTTGCTATAG TTA
N125D, F	GAAAAAGGTGATTATAGCAAAATCAGCCCGAATGAT CATGTTAATA
N125D, R	TTTGCTATAATCACCTTTTTCTTCACCCATCAGTTCCA GTGCACGG
I324T, F	GTTCCTGGTACCGTTAGCCCGGTTATGCCGGAAGTTA TGAATCAGG
I324T, R	CGGGCTAACGGTACCAGGAACAATGCTGCTACCAGG CTGACGTGCA
C326S, F	GGTATAGTTAGCCCGGTTATGCCGGAAGTTATGAATC AGGTTGCAT
C326S, R	CATAACCGGGCTAACTATACCAGGAACAATGCTGCT ACCAGGCTGA
A99G, F	CAAGGTGGTGGCGGCACCAGCATTAATATGAATGCA AATGAAGTTA
A99G, R	GCTGGTGCCGCCACCACCTTGAATCGGGTCCACAATA AACTGATCA
N142S, F	CAGAGCACCAGCGATGCATTTCCGACCGCAACACAT ATTGCAGTTC
N142S, R	AAATGCATCGCTGGTGCTCTGGCTCATATTAACATGG CTATTCGGG

L358V, F	CAGTTTGAAGTGAATGTTATGGAACCGGTGCTGTTTT TCAATCTGA
L358V, R	CATAACATTCACTTCAAACTGACCTGCTTCGCTTGCG CTGGTAATG
E362M, F	AATGTTATGATGCCGGTGCTGTTTTTCAATCTGATTC AGAGCATTA
E362M, R	CAGCACCGGCATCATAACATTCACTTCAAACTGACCT GCTTCGCTT
cldmVec_fwd	TCACCACTAACGAGCTCCGTCGACAAGC
clM1and2Vec_rev	TATTGCCATAATTCTTAGGATCCAATGTTGAAGCTTTC
M1and2Insert_fwd	CCTAAGAATTATGGGCAATACCGATGTG
PmAspA ins_fwd	CACCACCATCACCATCACACCGTTACTCGCAAAGAG
AspAMALvet_rev	CATATGTATATCTCCTTCTTAAAGTTAAAC
dtMAL ins_fwd	CACCACCATCACCATCACATCAAAGACGCGTTC

2.2.3 High-fidelity (HiFi) DNA assembly for preparing DNA plasmid.

High-fidelity (HiFi) DNA assembly is a seamless and highly efficient molecular cloning technique used to join multiple DNA fragments based on overlapping homologous sequences. This method employs a mix of enzymes—exonuclease, polymerase, and ligase—to ensure accurate alignment and ligation of DNA fragments without introducing scars or unwanted sequences. Known for its rapidity and high efficiency, HiFi DNA assembly is particularly advantageous for constructing complex constructs, such as multi-fragment recombinant plasmids, gene circuits, or genome-editing tools like CRISPR/Cas9.

In this study, HiFi DNA assembly, facilitated by the NEBuilder HiFi DNA Assembly Master Mix, was used to construct plasmids pET24a-clMagR-M1, pET24a-clMagR-M2, pET24a-dmMagR-M1, and pET24a-dmMagR-M2. As illustrated in Figure 2-4, the fragments containing the aspB-M1 and aspB-M2 genes were amplified via PCR using primers M1and2_Insert_fwd and M1andM2_Insert_rev (detailed in Table 8). Concurrently, the universal vectors pET24a-clMagR and pET24a-dmMagR were amplified using primers cldmVec_fwd/clM1and2Vec_rev and cldmVec_fwd/dmM1and2Vec_rev, respectively (Table 8).

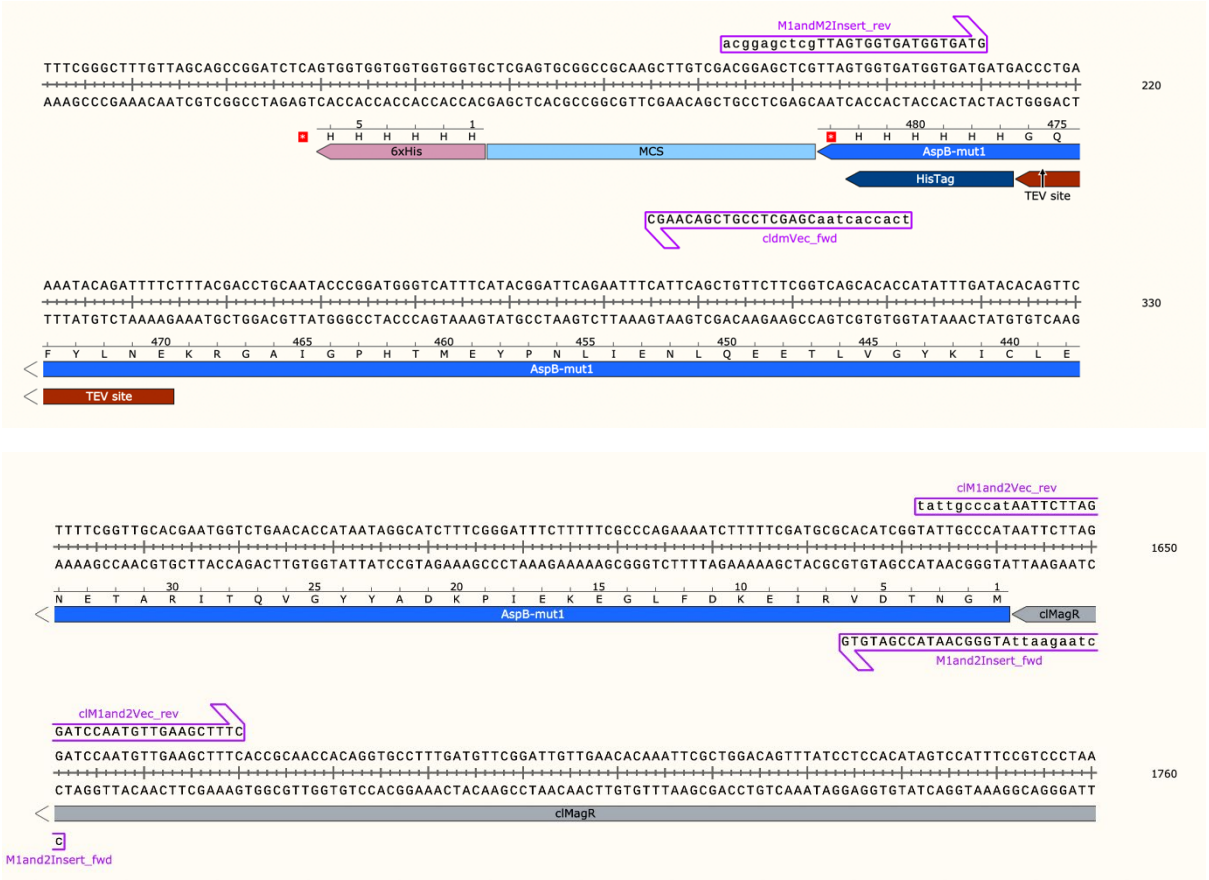

Figure 2-4 High-fidelity (HiFi) DNA assembly to clone AspB mutant into universal vector.

The four primers designed by the NEBuilder for the amplification of AspB-mut1 insert and plasmid backbone pET24a-clMagR. *Top:* Primer M1andM2 Insert_rev overlaps with primer cldmVec_fwd. *Bottom*: Primer clM1and2Vec_rev overlaps with primer M1and2 Insert_fwd.

The PCR products were purified using a PCR purification kit or gel extraction kit to remove impurities. Equimolar amounts of purified PCR products were mixed in a single tube, and NEBuilder HiFi DNA Assembly Master Mix was added. The reaction was incubated at 50°C for 15 minutes to facilitate assembly (Table 9).

The assembled products were then transformed into transformation-competent *E. coli* DH5α cells using CaCl2 method (section 2.3.2). Recombinant plasmids were screened and verified through restriction digestion analysis (section 2.3.6). Successfully transformed *E. coli* DH5α cells were preserved in 25% glycerol stock and stored at -80°C for future use.

Table 9 HiFi assembly component make up.

Component	Volume (µL)
Water	0
NEBuilder HiFi DNA Assembly Master Mix	10
Vector: pET24a-dmMagR and pET24a-clMagR (from gel extraction)	1
Insert: M1 and M2 for dmMagR and clMagR (from gel extraction)	9
Total	20

2.2.4 PCR for preparing DNA plasmids with 6-Histidine tag.

PCR was used to amplify and modify DNA sequences for plasmid construction. The reaction proceeds through the standard denaturation, annealing, and extension steps, with Q5 DNA polymerase (New England Biolabs, NEB) employed for its high fidelity and efficiency. Reaction components and cycling conditions are summarized in Tables 10 and 11.

Table 10 Standard PCR reaction mixture using Q5 DNA polymerase.

Component	Stock Concentration	Final Concentration	Volume(µL)
Water	-	-	36
Q5 buffer (NEB)	5x	1x	10
dNTPs	10 mM	0.2 mM	1
DNA template	Measured by Versa Wave	-	0.5
Forward Primer	20 µM	0.4 µM	1
Reverse Primer	20 µM	0.4 µM	1
Q5 High-Fidelity	2 U/µL	1 U/50 µL	0.5

DNA polymerase (NEB)			
Total Reaction Volume	-	-	50

Table 11 Standard PCR programme set-up using Q5 DNA polymerase.

Stage	Temperature (°C)	Duration (min)	Repeat
1: Denaturation	98	00:30	1
2: Amplification	98	00:08	29
	X (Use NEB Tm Calculator)	00:20	
	72	Y sec (Use 25 sec/kb)	
3: Extension	72	02:00	1
4: Hold	8		1

To enable protein purification, a 6xHis tag (~0.8 kDa) was introduced at the N-terminus of PmAspA and DtMAL using PCR with two primer sets: PmAspAins_fwd/AspAMALvet_rev and dtMALins_fwd/AspAMALvet_rev (Table 8). The His-tag facilitates affinity purification by binding immobilized nickel or cobalt ions in IMAC and can be cleaved post-purification if required.

Following PCR, the amplified DNA fragments were prepared for transformation using a Kinase-Ligase-DpnI (KLD) reaction (Tables 12 and 13). This single-step process phosphorylates, ligates, and digests parental DNA templates, improving cloning efficiency and ensuring only newly synthesized plasmids are retained.

Table 12 KLD reaction component.

Component	Volume (µL)
Water	19.5 - X

T4 ligase buffer (NEB)	2.5
Purified PCR product	X (with final volume of 150 ng)
DpnI (NEB)	1
T4 polynucleotide kinase	1
T4 Ligase	1
Total	25

Table 13 Temperature cycling using PCR machine for KLD reaction.

Stage	Temperature (°C)	Duration (min)
1: Recommended temperature for DpnI and PNK	37	30:00
2: Recommended temperature for T4 ligase	16	-
3: Hold	16	-

2.3 Plasmid DNA amplification

Plasmid DNA amplification is a critical step for obtaining high-quality plasmid DNA required for various downstream applications, such as cloning, sequencing, and transfection. In this study, *E. coli* DH5α cells (provided by Prof. Tuck Seng Wong) were transformed with the desired plasmid constructs. The transformed cells were cultured in liquid media supplemented with Kanamycin to ensure the propagation of plasmid-bearing bacteria. Following bacterial growth, plasmid DNA was extracted and purified using commercial plasmid miniprep kits, following the manufacturer's protocols.

Quantification of the plasmid DNA was carried out using the EzDrop 1000 UV spectrophotometer (Blue-Ray Biotech). The DNA concentration was determined based on absorbance measurements at 260 nm (A260), while the purity was evaluated using the A260/A280 ratio. Baseline correction was performed at 340 nm to ensure the accuracy of the results.

2.3.1 Bacterial growth media.

For plasmid amplification, E. coli strains were cultured under the same conditions described in Section 2.1.2, using 2xTY broth or TYE agar supplemented with 50 µg/mL kanamycin as the selection marker. Media preparation followed standard protocols, and cultures were incubated at 37 °C with shaking at 250 rpm.

2.3.2 Transformation of *E. coli* with plasmid DNA.

Bacterial transformation is a technique used to introduce foreign DNA, such as plasmids, into bacterial cells, enabling the expression of genetic material. In this project, the $CaCl_2$ method was used for bacterial transformation.

To begin, an overnight culture of *E. coli* was prepared by inoculating 5 mL of 2×TY medium and incubating the culture at 37°C with shaking at 250 rpm. The next day, 50 µL of the overnight culture was used to inoculate 5 mL of fresh 2×TY medium in a 50 mL Falcon tube. The culture was incubated under the same conditions, and the optical density at 600 nm (OD_{600}) was monitored (Eppendorf BioPhotometer Plus). Once the OD_{600} reached approximately 0.5–0.6, indicating exponential growth, 1 mL aliquots of the culture were transferred into sterile 1.5 mL microcentrifuge tubes.

The cells were centrifuged at 2800 rpm for 2 minutes at room temperature, and the supernatant was discarded. The pellet was gently resuspended in 1 mL of pre-chilled 50 mM $CaCl_2$ solution, followed by another round of centrifugation under the same conditions. The supernatant was removed, and the cells were resuspended in 500 µL of pre-chilled 50 mM $CaCl_2$ solution. All $CaCl_2$ solutions were autoclaved and stored at 4°C to maintain sterility and functionality. The resuspended cells were incubated on ice for 30 minutes to enhance competency; this incubation time could be reduced to 10 minutes when working with intact plasmids.

For transformation, 1 µg of plasmid DNA (~1 µL) was added to the competent cells, mixed gently, and incubated on ice for an additional 30 minutes. To facilitate DNA uptake, a heat shock at 42°C for 1 minute was performed, followed by immediate cooling on ice for 2 minutes. Recovery was initiated by adding 800 µL of pre-warmed (37°C) 2×TY medium to the cells, which were then incubated at 37°C with shaking at 250 rpm for 60 minutes**.** This step allowed the cells to recover and express antibiotic resistance encoded by the plasmid.

TYE agar plates supplemented with the appropriate antibiotic (50 mM kanamycin) were pre-warmed at 37°C. After the recovery phase, the cells were centrifuged at 2800 rpm for 2 minutes, and 1000–1100 µL of the supernatant was discarded. The pellet was gently resuspended in the remaining 200–300 µL of the medium. The cell suspension was plated onto the pre-warmed agar plates. For intact plasmid

transformations, the centrifugation and resuspension steps could be skipped, and 100 µL of the recovery culture was directly plated.

The plates were incubated upside-down overnight at 37°C, allowing individual bacterial colonies to form. Colonies were selected for restriction digestion analysis to verify the presence of the plasmid and used to inoculate shaken cultures for further experimental applications.

2.3.3 Amplification of transformed *E. coli*.

To amplify transformed *E. coli*, a single colony was selected from the transformation plate and inoculated into 5 mL of sterile 2×TY medium containing 50 µg/mL kanamycin to ensure plasmid maintenance. The culture was incubated at 37°C with shaking at 250 rpm for approximately 16 hours, allowing sufficient time for the cells to reach a high density (overnight growth).

For large-scale amplification, the overnight culture was diluted at a 1:200 ratio into a larger volume of 2×TY medium supplemented with 50 µg/mL kanamycin in a sterile flask. The culture was incubated under the same conditions (37°C and 250 rpm shaking) until the desired optical density was reached, typically measured at 600 nm (OD_{600}) using the Eppendorf BioPhotometer Plus (see Section 2.3.2).

Once the bacterial cells reached the optimal growth phase, they were harvested by centrifugation for use in downstream applications, such as plasmid DNA extraction or protein expression studies. This amplification method ensured robust bacterial growth while maintaining plasmid stability, providing sufficient material for subsequent experimental procedures.

2.3.4 Miniprep of amplified plasmid DNA.

Plasmid DNA was isolated and purified from 5 mL of overnight *E. coli* culture using the E.Z.N.A.® Plasmid DNA Mini Kit I, supplied by Omega BIO-TEK (Germany). The protocol followed a standard alkaline lysis procedure using specific reagents provided in the kit. To begin, 5 mL of the transformed *E. coli* overnight culture was harvested by centrifugation at 12,000 × g for 1 minute to pellet the bacterial cells. The supernatant was discarded, and the cell pellet was carefully resuspended in 250 µL of Solution I contain RNase A, ensuring complete dispersion of the cells.

Following resuspension, 250 µL of Solution II was added to lyse the cells, with the mixture gently inverted 4–6 times to avoid shearing of DNA. Solution II was pre-warmed to 37°C to ensure that any precipitates in the bottle were fully dissolved prior to use. After lysis, 350 µL of Solution III was immediately added to the mixture to neutralize the alkaline lysate. The sample was inverted 4–6 times to precipitate

cellular debris, proteins, and genomic DNA. The neutralized lysate was then centrifuged at 12,000 × g for 10 minutes, and the cleared lysate was carefully transferred to a HiBind DNA Mini Column fitted into a collection tube, ensuring no precipitate was carried over.

To remove contaminants, the column was washed sequentially with 500 µL of HBC Buffer, which had been diluted with isopropanol, followed by centrifugation at 10,000 × g for 1 minute. A second wash was performed using 700 µL of DNA Wash Buffer, diluted with ethanol, to further ensure the removal of impurities. After washing, the column was dried by centrifuging for an additional 1 minute to remove residual ethanol, which is critical for preventing interference during the elution process.

To elute the plasmid DNA, 50 µL of Elution Buffer was added directly to the center of the column membrane. The column was incubated at room temperature for 1–2 minutes to enhance the recovery of larger plasmids. Following incubation, the DNA was collected by centrifuging at 10,000 × g for 1 minute. The eluted DNA was immediately stored at 4°C for downstream applications, including sequencing, cloning, or protein expression. The quality and concentration of the purified plasmid DNA were confirmed using spectrophotometric analysis, and its integrity was verified through agarose gel electrophoresis.

The solutions used during the miniprep played essential roles in the purification process. Solution I, the resuspension buffer, contained Tris-HCl (pH 8.0), EDTA, and RNase A. This buffer maintained a stable pH and ensured RNA degradation to enhance plasmid DNA purity. Solution II, the lysis buffer, comprised sodium hydroxide (NaOH) and sodium dodecyl sulfate (SDS). This alkaline solution lysed the bacterial cells by breaking the cell membrane and denaturing proteins. Solution III, the neutralization buffer, contained potassium acetate and acetic acid, which precipitated cellular debris, genomic DNA, and SDS-protein complexes while neutralizing the lysate. HBC Buffer diluted with isopropanol facilitates the binding of plasmid DNA to the silica membrane by increasing ionic strength and reducing DNA solubility, ensuring efficient purification.

2.3.5 Purify PCR product using PCR purification Kit and Gel Extraction Kit.

PCR product purification was carried out to remove unwanted components such as primers, enzymes, and nucleotides, ensuring high-purity DNA for downstream applications. Two methods were employed: the PCR Purification Kit for direct purification from reaction mixtures and the Gel Extraction Kit for isolating specific DNA fragments from agarose gels. The NucleoSpin® Gel and PCR Clean-up Kit

(supplied by Omega BIO-TEK, Germany) was used according to the manufacturer's protocol.

For direct purification of amplified DNA, the PCR product was mixed with Buffer NT1 in a 1:2 (sample: buffer) ratio to facilitate binding of the DNA to the silica membrane of the column. This solution was then loaded onto the NucleoSpin® Clean-up Column, centrifuged at 12,200 rpm for 30 seconds, and the flow-through was discarded. The column was washed twice with Buffer NT3, which contains ethanol to remove salts and other impurities, ensuring optimal A260/A230 ratios for high-quality DNA. Following washing, the column was centrifuged for 2 minutes at 12,200 rpm to remove residual ethanol and dried thoroughly. Elution was carried out using Buffer NE, which is a low-salt elution buffer, ensuring efficient recovery of purified DNA for subsequent applications.

For gel-based DNA purification, specific DNA fragments were excised from an agarose gel using a clean scalpel, ensuring minimal contamination. Approximately 0.8 g of gel containing the desired DNA fragment was transferred into a microcentrifuge tube. Buffer NT1 (200 µL per 100 mg of gel) was added, and the mixture was incubated at 50°C until the gel was completely dissolved. This step ensured that the DNA was released into the solution and could bind to the silica membrane.

The dissolved gel solution was loaded onto the NucleoSpin® Gel and PCR Clean-up Column placed in a 2 mL collection tube, with a maximum of 700 µL processed per spin. The column was centrifuged at 12,200 rpm for 30 seconds, and the flow-through was discarded. This step was repeated for the remaining solution until the entire sample was processed.

The silica membrane was washed twice with 700 µL of Buffer NT3, which is an ethanol-based wash buffer designed to remove residual salts and impurities that could inhibit downstream applications. After washing, the column was centrifuged for an additional 2 minutes at 12,200 rpm to ensure complete removal of ethanol and thorough drying of the membrane.

Finally, to recover purified DNA, the column was placed into a new 1.5 mL microcentrifuge tube, and 30 µL of Buffer NE (a Tris buffer with pH ~8.5) was added directly to the membrane. The mixture was incubated at room temperature for 1 minute to maximize DNA recovery and then centrifuged for 1 minute at 12,400 rpm. The eluted DNA was immediately ready for downstream applications, including cloning, sequencing, or PCR amplification.

2.3.6 Measurement of DNA concentration and purity.

To determine DNA concentration and purity, the EzDrop 1000 UV-Vis spectrophotometer (Blue-Ray Biotech, Taiwan) has been used. This device utilizes

ultraviolet (UV) absorbance to quantify nucleic acids based on their absorbance at 260 nm (A260). Prior to measurement, the instrument was blanked using the elution buffer used during DNA purification to eliminate background absorbance. For each sample, a 2 µL aliquot of the eluted DNA was carefully pipetted onto the pedestal, and measurements were automatically recorded by the software, which calculated DNA concentrations in ng/µL using Beer's Law.

Purity was assessed using the A260/A280 and A260/A230 absorbance ratios. The A260/A280 ratio provided insight into protein contamination, as proteins absorb UV light at 280 nm. A ratio of approximately 1.8 indicated high-purity DNA, while deviations below this value suggested protein contamination, and values exceeding 2.0 implied potential RNA contamination. Similarly, the A260/A230 ratio assessed the presence of organic or chemical contaminants, such as phenol, guanidine, or residual salts. Pure DNA typically exhibited an A260/A230 ratio in the range of 2.0–2.2. Values below this range indicated contamination, which could compromise downstream applications.

2.3.7 Restriction digestion of plasmid DNA for checking plasmid constructions.

Restriction digestion was performed to validate the accuracy of plasmid constructions by using sequence-specific restriction enzymes to excise and analyze DNA fragments. This method ensures the correct insertion and orientation of target genes within plasmids. Each digestion reaction typically contained 1–2 µg of plasmid DNA, one or two selected restriction enzymes, the corresponding reaction buffer, and nuclease-free water, adjusted to a final volume of 20-100 µL. Reactions were incubated at the recommended temperature for the chosen enzymes, usually 37°C, for 2 hours to allow complete digestion of the DNA.

After digestion, the reaction products were analyzed via agarose gel electrophoresis. The digested fragments were visualized under UV light after staining with a DNA-intercalating dye, and their sizes were compared to a GeneRuler 1 kb DNA Ladder (Thermo Scientific, UK), which served as a molecular weight reference. This allowed confirmation of the expected fragment sizes and verification of the plasmid construction. The integrity of the plasmid, insertion of the target gene, and the orientation of DNA fragments were assessed based on the observed banding pattern.

For a typical 100 µL reaction, the components are outlined in Table 14**,** the mixture includes 10 µL of a 10× buffer (e.g., CutSmart or Buffer 4), 1 µL each of restriction enzymes (e.g., BamHI-HF, EcoRI-HF, NdeI, or XhoI, at 20 U/µL), nuclease-free water to make up the final volume, and the desired amount of plasmid or PCR product.

The digestion mixture was thoroughly mixed and incubated at the appropriate temperature for the restriction enzymes, as specified by the manufacturer. To maintain precise temperature control, an incubator was used instead of a thermocycler, which is less optimal for prolonged incubations. The digestion reaction was terminated by heat inactivation of the enzymes (if compatible) or direct purification of the DNA.

Post-digestion, the DNA fragments were cleaned using a PCR Purification Kit or a Gel Extraction Kit, especially when the digestion products were intended for downstream cloning or sequencing. Care was taken to ensure that buffers and enzyme concentrations were appropriate for each reaction, as deviations could compromise the efficiency of digestion. Any uncut plasmid or incomplete digestion products were interpreted as an indication of suboptimal reaction conditions or errors in enzyme selection, necessitating troubleshooting and optimization.

Table 14 The component of plasmid DNA restriction digestion.

Component	Stock Concentration	Final Concentration	Volume(μL)
Distilled Water	-	-	88-x
CutSmart (NEB)	10x	1x	10
Plasmid DNA	Measureed by versa Wave	-	X
Restriction Enzymes	Various conc’	20 U/100 μL	
Total	-	-	**100**

2.3.8 DNA Electrophoresis for plasmid analysis.

DNA electrophoresis was employed to analyze DNA fragments for size and integrity. A 0.7% agarose gel was prepared by dissolving 0.35 g of agarose in 50 mL of 1× TBE buffer, followed by heating until the agarose was fully dissolved. The 5× TBE stock buffer solution was prepared with the following components: 445 mM Tris (54.03 g/L), 445 mM boric acid (27.51 g/L), and 10 mM EDTA (0.29 g/L), adjusted to pH 8.0 at 25°C. The working 1× TBE buffer was obtained by diluting the stock solution with deionized water.

Once the agarose solution had cooled to approximately 50°C, 2 μL of ethidium bromide was added as a DNA-staining agent to enable visualization of DNA bands

under UV light. The agarose solution was poured into a gel tray equipped with a comb to form wells and allowed to solidify at room temperature. After solidification, the gel was placed in an electrophoresis tank containing 1× TBE buffer.

For analysis, DNA samples were mixed with a 6× loading dye (NEB, UK) to facilitate loading and tracking of the migration during electrophoresis. Typically, 5 µL of DNA sample was combined with 1 µL of 6× loading dye before being loaded into the gel wells. A DNA ladder was included as a molecular weight reference to determine the size of the DNA fragments. For PCR product verification, undigested plasmid DNA was often included as a control to assess the quality and integrity of the DNA sample.

Electrophoresis was conducted at a constant voltage of 100 V for 60 minutes. The DNA fragments migrated through the gel matrix based on size, with smaller fragments traveling faster than larger ones. Following electrophoresis, DNA bands were visualized under UV light using a gel documentation system (VWR, part of Avantor, USA). To minimize UV-induced DNA damage, particularly for cloning applications, imaging was performed as quickly as possible. When DNA fragments were intended for gel extraction and downstream applications, all steps involving UV exposure were executed swiftly and carefully to preserve DNA integrity.

2.3.9 Ligation of DNA fragments.

Ligation is used to covalently join DNA fragments, enabling the construction of recombinant plasmids for downstream applications. This process is catalyzed by T4 DNA Ligase (NEB, UK), which forms phosphodiester bonds between the 3'-hydroxyl and 5'-phosphate ends of DNA fragments. In this study, DNA fragments prepared by restriction digestion or PCR amplification were ligated into linearized plasmid vectors to generate constructs for protein expression and functional studies. Ligation reactions were carried out in a total volume of 20 µL, containing 1× T4 DNA Ligase Buffer, a 3:1 molar ratio of insert to vector, 1 µL T4 DNA Ligase, and nuclease-free water. The reactions were incubated at 16°C overnight or for 1 hour at room temperature for time-sensitive experiments.

Post-ligation, 5 µL of the ligation product was transformed into *E. coli* DH5α cells and plated on selective agar containing the appropriate antibiotic. Colony screening was performed by restriction digestion and sequencing to confirm the presence of the desired recombinant plasmid. Control ligation reactions without insert DNA were included to assess background religation of the vector. The efficiency of ligation was influenced by DNA purity, concentration, and the insert-to-vector ratio, with sticky-end ligations yielding higher transformation efficiencies compared to blunt-end ligations.

2.4 Protein expression and analysis

Protein expression involves synthesizing target proteins in a host organism, typically *E. coli*, by cloning the desired gene into an expression vector, transforming it into a host strain, and inducing protein production using agents such as isopropyl β-D-1-thiogalactopyranoside (IPTG). Following induction, proteins are extracted by lysing the host cells and subsequently analyzed using techniques like sodium dodecyl sulfate-polyacrylamide gel electrophoresis (SDS-PAGE) to confirm protein size, expression levels, and integrity. Quantification of protein concentration is performed spectrophotometrically, while purification is commonly achieved using affinity chromatography, such as Ni-NTA (nickel-nitrilotriacetic acid) for His-tagged proteins, providing high purity and yield.

2.4.1 Transformation and culture growth for protein expression.

Recombinant plasmids were transformed into *E. coli* BL21(DE3) or C41(DE3) strains, which served as the expression hosts. The transformation procedure was described in detail in Section 2.3.2. For protein expression, transformed colonies were first cultured in 5 mL of 2×TY medium supplemented with 50 μg/mL kanamycin as a starter culture. The cultures were incubated at 37°C with shaking at 250 rpm for 16 hours to reach stationary phase. Subsequently, the overnight culture was inoculated into 50 mL of fresh 2×TY medium at a 5% (v/v) ratio to ensure sufficient cell density for protein production. The culture volume was adjusted according to the downstream application, including large-scale or small-scale expression setups.

The optical density at 600 nm (OD_{600}) was used to monitor cell growth and ensure optimal cell density before induction, typically targeting an OD_{600} of ~0.5–0.6. This range corresponds to the mid-logarithmic growth phase, where cells are metabolically active and highly receptive to induction. Accurate OD measurements were performed using a spectrophotometer calibrated with sterile medium as the blank control. The setup ensured reproducible growth conditions and protein expression for subsequent analysis.

2.4.2 Induction of protein expression.

The host strains *E. coli* BL21(DE3) and *E. coli* C41(DE3) harbor the T7 RNA polymerase gene under the control of a lac operon, enabling tightly regulated protein expression. When the optical density at 600 nm (OD_{600}) of the culture reached 0.5–0.6, corresponding to the mid-logarithmic growth phase, protein expression was induced by adding isopropyl β-D-1-thiogalactopyranoside (IPTG). IPTG concentrations ranging from 0.1 mM to 1.0 mM were used in this project, depending on the specific

protein being expressed. IPTG acts as a molecular mimic of lactose, binding to the lac repressor and inducing the T7 RNA polymerase to transcribe the target gene from the T7 promoter. Following IPTG induction, the cultures were incubated at 30°C with shaking at 250 rpm for 8–20 hours, depending on the stability and solubility of the target protein. These conditions were optimized to maximize protein yield while minimizing the formation of insoluble aggregates.

2.4.3 Cell culture harvesting and storage.

After the expression period, cells were harvested by centrifugation at 8000 × g for 10 minutes at 8°C to ensure efficient recovery of biomass. The resulting cell pellet was collected and immediately processed or stored depending on the downstream requirements. For immediate use, the pellet was kept on ice to preserve protein integrity. For short-term storage, the pellet was transferred to -20°C, while for long-term storage, it was stored at -80°C to ensure maximal stability and prevent degradation. To maintain sample quality, freeze-thaw cycles were minimized, as repeated freezing and thawing can lead to protein denaturation and reduced activity. Proper storage and handling ensured the integrity of the expressed proteins for subsequent purification and analysis.

2.4.4 Protein purification.

Protein purification was performed using a HisTrap™ High Performance column on an ÄKTA pure™ chromatography system. The process involved harvesting cell pellets from *E. coli* BL21(DE3) cultures induced for protein expression, followed by storage at -80°C to preserve protein integrity prior to purification. The purification workflow included cell lysis, affinity chromatography, and protein elution, with each step carefully optimized to ensure high yield and purity of the recombinant proteins.

2.4.4.1. Buffer preparation

Buffer formulations were tailored based on the isoelectric point (pI) of the target protein and the requirements of immobilized metal affinity chromatography (IMAC). To maintain protein solubility and binding efficiency during purification, buffer pH was adjusted to at least 1 unit away from the protein's pI. For His-tagged proteins, the preferred pH range was 7.0–8.0, which ensures effective interaction between histidine residues and the nickel or cobalt resin. In this study, the lysis and elution buffers were set to pH 8.0 to optimize the purification of His-tagged PmAspA and DtMAL, whose pI values are 5.29 and 6.31, respectively.

The lysis, equilibration, and column washing buffer (Buffer A) was prepared with 50 mM NaH_2PO_4, 300 mM NaCl, and 10 mM imidazole, adjusted to pH 8.0 using NaOH. To protect the target protein from degradation during lysis, one tablet of a protease inhibitor cocktail was added to 50 mL of Buffer A, along with 10 µg/mL DNase (from a 10 mg/mL stock solution) and 10 µg/mL RNase (from a 10 mg/mL stock solution). The elution buffer (Buffer B) was prepared with 50 mM NaH_2PO_4, 300 mM NaCl, and 250 mM imidazole, adjusted to pH 8.0 using NaOH. Both buffers were filtered through a 0.2 µm vacuum membrane filter and sterilized by autoclaving to ensure sterility. Additionally, a 20% ethanol solution was prepared as a storage and sterilization buffer by diluting ethanol with Type 2 water, followed by filtration through a 0.2 µm vacuum membrane filter. These steps ensured the purity and stability of the reagents, critical for reproducible protein purification.

2.4.4.2. Cell lysis

Cell lysis was performed to release recombinant proteins from *E. coli* BL21(DE3) cells. Frozen cell pellets were thawed on ice and resuspended in 25 mL of lysis buffer prepared as described in Section 2.4.4.1. The resuspended cells were subjected to sonication using a 130 W, 20 kHz sonicator set at 40% amplitude. The sonication process consisted of alternating pulses of 15 seconds on and 45 seconds off for a total duration of 5 minutes, with the sample maintained on ice throughout to prevent overheating and denaturation of the proteins. If adequate protein release was not observed, the sonication amplitude was increased to 50%, or the total sonication time was extended in subsequent trials.

Following sonication, the lysate was clarified by centrifugation at 10,000 rpm for 15 minutes at 4°C to separate insoluble cell debris from the soluble protein fraction. The resulting supernatant was carefully transferred to a clean tube, avoiding contamination with the pellet. To ensure removal of residual debris and particulates, the supernatant was filtered sequentially through 0.45 µm and 0.2 µm membrane filters. The filtered lysate was then used for downstream protein purification steps.

2.4.4.3. Chromatography setup

Protein purification was conducted using the ÄKTA pure™ chromatography system equipped with a HisTrap™ High Performance column pre-filled with 20% ethanol as a storage solution. To ensure a contamination-free environment and prevent precipitation, the chromatography system and column were flushed thoroughly with type 2 water prior to use. The system was prepared by connecting the chromatography lines (A1, A2, B1, and B2) to the respective buffers. The column was equilibrated with 5 column volumes (CV) of Buffer A (binding buffer) at a flow rate of 5 mL/min. For the 5 mL HisTrap™ column used, a total of 25 mL of Buffer A was required for the equilibration step.

The filtered lysate, containing His-tagged recombinant proteins, was loaded onto the column at a flow rate of 5 mL/min to facilitate binding of the target proteins to the nickel-charged resin. Unbound proteins and contaminants were removed by washing the column with 10 CV (100 mL) of Buffer A, followed by an additional wash with a mixture of 95% Buffer A and 5% Buffer B to ensure removal of loosely bound impurities. Elution of the His-tagged proteins was achieved using a linear gradient of Buffer B (elution buffer containing 250 mM imidazole) over 20 CV at a reduced flow rate of 1 mL/min. Eluted fractions were collected using a fraction collector, and UV absorbance at 280 nm was monitored in real time to detect protein elution peaks.

Post-purification, the column was regenerated with 5 CV of 100% Buffer B, followed by 5 CV of 100% Buffer A to restore the binding capacity of the resin. The system and column were flushed with water and reconditioned with 20% ethanol to maintain sterility and prevent microbial growth, ensuring readiness for subsequent use.

2.4.4.4. Purified protein storage

Following protein purification, the eluted fractions were analyzed by monitoring UV absorbance at 280 nm to identify peaks corresponding to the target protein. Fractions with prominent protein peaks were selected for further analysis. These selected fractions were assessed for purity and molecular integrity using SDS-PAGE to confirm the presence of the desired protein and exclude potential contaminants. To ensure stability during storage and compatibility with downstream applications, the eluted proteins were subjected to buffer exchange, which removed imidazole and replaced it with a suitable storage buffer optimized for the protein's stability.

Buffer exchange was conducted using a PD-10 desalting column and size exclusion chromatography, following a gravity-based protocol. This method separates proteins from small molecules such as salts and imidazole, ensuring the proteins are in a buffer suitable for long-term storage or experimental use. The column was prepared by removing the top cap and draining the storage solution, followed by flushing the resin with 10 mL of water to remove residual ethanol. The column was equilibrated with approximately 25 mL of the new storage buffer, added in four consecutive 5–10 mL steps to saturate the resin bed fully, and the flow-through was discarded after each step. Subsequently, up to 2.5 mL of protein sample was loaded onto the column, ensuring complete penetration into the packed resin bed, with any flow-through being discarded. Finally, 3.5 mL of storage buffer was used to elute the protein, and the eluted sample was collected in a clean test tube.

The purified proteins were aliquoted to minimize freeze-thaw cycles and stored at -20°C for short-term applications or at -80°C for long-term preservation. This systematic approach ensures the integrity, functionality, and stability of the purified protein for subsequent experimental procedures.

2.4.5 Analyzing of expressed and purified proteins.

The analysis of expressed and purified proteins involved both qualitative and quantitative approaches to ensure accurate assessment of protein size, purity, and concentration. SDS-PAGE (sodium dodecyl sulfate-polyacrylamide gel electrophoresis) was employed as a robust method to separate proteins based on molecular weight, with visualization achieved using Coomassie Brilliant Blue staining. For quantitative evaluation, UV-Vis spectrophotometry at 280 nm was used to estimate protein concentration, and purity was assessed by determining the A260/A280 ratio, where a value of ~1.8 indicated minimal contamination with nucleic acids.

In SDS-PAGE, 10% resolving gels were routinely used, while 15% resolving gels were prepared for analyzing proteins smaller than 30 kDa. The component of protein gel used in SDS-PAGE is shown in Table 15. The resolving gel consisted of acrylamide/bis-acrylamide, Tris-HCl (pH 8.8), SDS, and ammonium persulfate (APS), with TEMED used to initiate polymerization. Once poured, the resolving gel was overlaid with water to prevent drying and allowed to polymerize for 45–60 minutes. A 4% stacking gel, composed of acrylamide/bis-acrylamide, Tris-HCl (pH 6.8), SDS, APS, and TEMED, was then poured above the resolving gel, with a comb inserted to create sample wells. Protein samples for SDS-PAGE were prepared by resuspending cell pellets in 50 mM phosphate buffer (pH 7.5 at 25°C), supplemented with 4× SDS reducing buffer and β-mercaptoethanol, followed by incubation at 94°C for 20 minutes. After centrifugation, 5 µL of supernatant was loaded for crude protein samples. For analyzing purified protein sample, 30 µL of purified protein together with 10 µL of 4× SDS reducing buffer (supplemented with β-mercaptoethanol) was added.

Electrophoresis was carried out at a constant voltage of 200 V for approximately 35 minutes, stopping when the dye front reached near the gel edge. The gel was washed to remove residual SDS, stained with Dark SDS-PAGE Stain for 15–20 minutes, and destained by repeated rinsing with water and overnight soaking. Protein bands were visualized using a gel documentation system and compared with the PageRuler Unstained Broad Range Protein Ladder to estimate molecular weights. Negative control samples were run to identify specific bands corresponding to induced protein expression. The appearance of a distinct band at the expected molecular weight confirmed successful protein expression, while additional bands in purified samples indicated contamination or degradation. Single bands in purified protein lanes confirmed high purity, whereas multiple bands necessitated further optimization of the purification process.

Table 15 The component of resolving gel and stacking gel for SDS-PAGE.

Component (resolving gel)	For 10% gel	For 15% gel
DDI water	2.05 mL	1.65 mL
30% Acrylamide/Bis	1.65 mL	2.05 mL
1.5 M Tris-HCl, pH 8.8	1.25 mL	1.25 mL
10% w/v SDS	0.05 mL	0.05 mL
TIMED	2.5 µL	2.5 µL
10% APS	25 µL	25 µL
Component (staking gel)		
DDI water	3.05 mL	
30% Acrylamide/Bis	0.65 mL	
0.5 M Tris-HCl, pH 6.8	1.25 mL	
10% w/v SDS	0.05 mL	
TIMED	5 µL	
10% APS	25 µL	

2.5 Enzymatic activity assay for expressed proteins.

The enzymatic activity assay evaluates the functional efficacy of expressed proteins by measuring their ability to catalyze specific reactions. These assays typically involve the conversion of a substrate into a product in an optimized reaction buffer that provides appropriate pH, ionic strength, and cofactors, such as Mg^{2+}. The reaction is incubated at the optimal temperature for the enzyme, and the extent of substrate depletion or product formation is monitored using analytical techniques such as spectrophotometry and nuclear magnetic resonance (NMR) spectroscopy. To ensure reliability and reproducibility, the assay includes negative controls (reactions without the enzyme to measure background signals).

2.5.1 The enzymatic activity assay using aspB mutants as enzymes.

The enzymatic activity assay for AspB mutants was performed following the workflow illustrated in Figure 2-5. First, a 50 mL culture of transformed *E. coli* cells expressing AspB mutants was centrifuged at 8000 rpm for 10 minutes to harvest the cell pellet. The pellet (with OD600=10) was resuspended in 10 mL of Solution A (100 mM sodium phosphate buffer, pH 8) to prepare a uniform cell suspension. This suspension served as the enzyme source. A 0.5 mL aliquot of the cell suspension (OD600= 0.5) was added to a 2-mL centrifuge tube. To initiate the enzymatic reaction, 1.5 mL of Solution B (300 g/L crotonic acid solution adjusted to pH 9.0 with 35% ammonia solution) was added to the tube.

The reaction mixture was incubated at 37°C with shaking at 500 rpm in a Ther-mix Heated Laboratory Thermal Mixer (Vitl Life Science Solutions, UK), with the lid temperature maintained at 42°C to prevent condensation. The enzymatic conversion of crotonic acid was monitored by measuring the decrease in absorbance at 235 nm (OD235) using a SpectraMax M2e Multilabel Microplate Reader (Marshall Scientific, US) and Hellma Analytics high-precision quartz cuvettes (10 × 4 mm light path). To identify the optimal operating temperature for each AspB mutant, the assay was repeated across various incubation temperatures.

The absorbance at OD235 was measured at intervals of 30 minutes initially, which were later extended to 3 hours for a total reaction duration of 24 hours due to the slow reaction kinetics. Additionally, purified AspB mutant enzymes were extracted and reacted with Solution B under the same conditions to evaluate enzymatic activity and verify substrate conversion efficiency. Measurements were also taken every 3 hours over a 24-hour period.

In addition to crotonic acid, other substrates, such as fumaric acid and (E)-2-pentenoic acid, were evaluated for specific AspB mutants. The assays used 130 g/L fumaric acid and 80 g/L (E)-2-pentenoic acid, both adjusted to pH 9.0 with 35% ammonia solution, as substrates. These

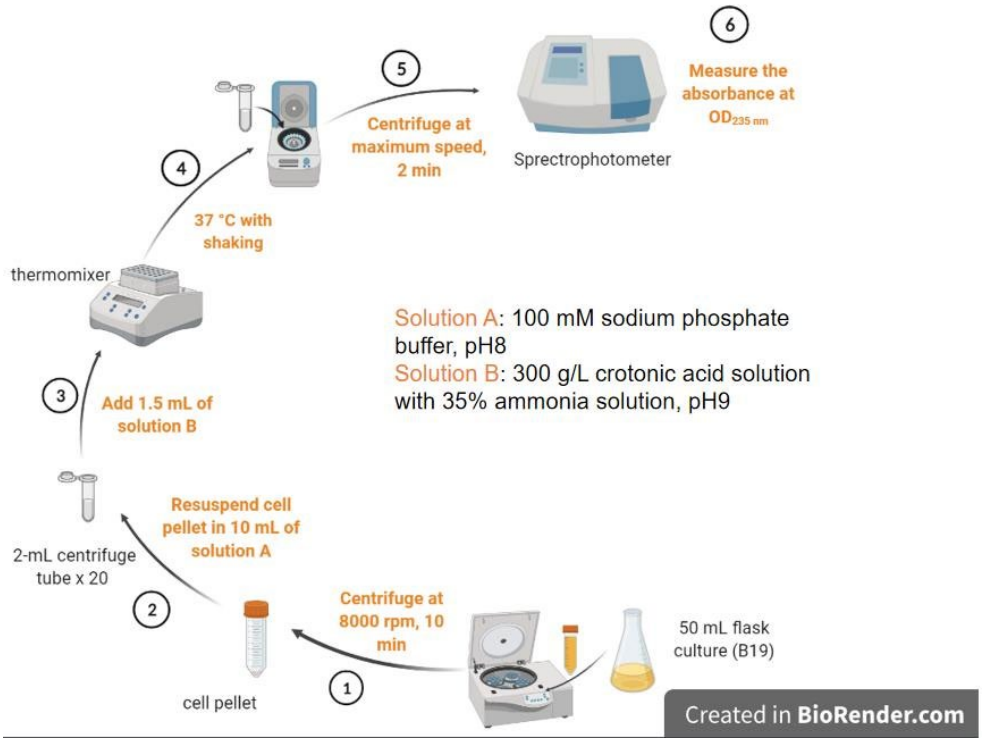

Figure 2-5 Workflow for enzymatic activity assay of AspB mutants.

The step-by-step workflow for conducting an enzymatic activity assay using *E. coli* cultures expressing AspB mutants. (1) A 50 mL flask culture is centrifuged at 8000 rpm for 10 minutes to pellet the cells. (2) The cell pellet is resuspended in 10 mL of Solution A (100 mM sodium phosphate buffer, pH 8). (3) A 0.5 mL aliquot of the resuspended cells is mixed with 1.5 mL of Solution B (300 g/L crotonic acid solution adjusted to pH 9.0 with 35% ammonia solution) in a 2 mL centrifuge tube. (4) The reaction mixture is incubated at 37°C with shaking at 500 rpm in a thermomixer, with the lid temperature maintained at 42°C. (5) After incubation, the reaction mixture is centrifuged at maximum speed for 2 minutes. (6) The decrease in crotonic acid absorbance at 235 nm (OD235) is measured using a spectrophotometer, enabling the determination of enzymatic activity. Solution A and Solution B are specifically optimized for the assay conditions.

2.5.2 The enzymatic activity assay for using PmAspA and DtMAL as enzymes.

Enzymatic activity assays for PmAspA and DtMAL were performed using a workflow similar to that described in Section 2.5.1. Cell pellets (with OD_{600}=10) derived from 50 mL flask cultures were harvested by centrifugation at 8000 rpm for

10 minutes and subsequently resuspended in 10 mL of 100 mM sodium phosphate buffer (Solution A, pH 8). For the activity assays, 0.5 mL of the resuspended cell suspension (OD_{600}= 0.5) was combined with 1.5 mL of substrate solution in 2 mL centrifuge tubes. In addition to crotonic acid, 130 g/L fumaric acid and 10 mM caffeic acid, both prepared in 35% ammonia solution (pH 9.0) with 2% (v/v) DMSO, were used as substrates. For reactions involving DtMAL, 20 mM $MgCl_2$ was included in the reaction mixture as the enzyme requires divalent metal ions for activity. The reaction mixtures were incubated under varying temperatures in a thermomixer set to 500 rpm. After incubation, the reaction samples were centrifuged at maximum speed for 2 minutes, and the supernatant was analyzed spectrophotometrically. Substrate conversion rates were determined by monitoring changes in absorbance specific to each substrate.

The enzymatic activity assays for purified PmAspA and DtMAL involved a slightly modified workflow compared to assays using crude cell suspensions. The reactions were carried out in a 20 mL system, divided into ten separate 2 mL centrifuge tubes. Each tube contained 0.5 mL of 40 mM substrate acid solution with 2% (v/v) DMSO, ensuring a final substrate concentration of 10 mM in each tube. Substrate concentrations were adjusted based on the specific requirements of each tested substrate. The reaction mixture was prepared with a final composition of 20 mM $MgCl_2$, 200 mM Tris-HCl buffer (pH 8.5), 500 mM NH_4Cl, and approximately 200 mg/L of purified enzyme. The reactions were incubated under various temperatures to identify the optimal conditions for enzymatic activity.

In all cases, the enzymatic reactions were monitored over time to assess substrate conversion rates and to determine the enzymes' catalytic efficiency under varying conditions. By comparing the activity profiles of purified enzymes to those in crude cell suspensions, these assays provided insights into the effects of purification on enzyme activity and stability.

2.5.3 NMR spectroscopy to calculate enzymatic activity.

^1H NMR spectroscopy was employed as a precise and indirect method to evaluate enzymatic activity by monitoring changes in substrate and product concentrations during enzyme-catalyzed reactions. Enzymatic activity assays were conducted using enzyme-containing cell suspensions. Harvested cell pellets were resuspended in 5 mL of solution A (100 mM sodium phosphate buffer, pH 8.0). The reactions were initiated by combining 0.4 g of an unsaturated acid solution (pH adjusted to 9.0 with 35% ammonia solution) with 0.135 g of the prepared cell suspension and 0.06 g of deuterium oxide (D_2O) in NMR tubes. The inclusion of D_2O was critical for obtaining accurate ^1H NMR spectra. As a non-hydrogen solvent, D_2O eliminates interference from solvent hydrogen signals, ensuring clear spectral resolution. Additionally, D_2O

provides a stable lock signal for the NMR spectrometer and minimizes proton exchange between the solvent and exchangeable protons in the sample, thereby improving spectral clarity. Enzymatic activity was measured over a 24-hour period, with spectra recorded at 2-hour intervals to monitor substrate conversion and product formation. Reactions were carried out at optimized temperatures for each enzyme.

The enzymatic activity of purified wild-type DtMAL and PmAspA, along with their mutant variants, was also evaluated using ^{1}H NMR spectroscopy, focusing on their ability to catalyze the addition of ammonia to various electrophilic substrates. The reaction mixtures were prepared in NMR tubes containing 500 µL of a 1 M NH_4Cl solution (pH 9.0, with 20 mM $MgCl_2$), 50 µL of D_2O, and 100 µL of a 500 mM electrophile stock solution (also pH 9.0, with 20 mM $MgCl_2$). Reactions were initiated by the addition of 200 µg of freshly purified enzyme and incubated at optimized temperatures. ^{1}H NMR spectra were collected at multiple time points (24 hours, 3 days, and 7 days post-initiation) to monitor the enzymatic conversion. Product formation was quantified by integrating the corresponding product signals in the NMR spectra, enabling precise calculations of enzymatic efficiency and catalytic rates.

2.6 Measurement and calculation of enzymatic activity

The measurement and calculation of enzymatic activity are critical for understanding enzyme kinetics, catalytic efficiency, and enzyme-substrate interactions. In this project, two complementary methods were employed to evaluate enzymatic activity: absorbance-based spectroscopy and nuclear magnetic resonance (NMR) spectroscopy. These methods provided both rapid quantitative assessments and molecular-level insights into the enzymatic processes.

Absorbance-based methods were used to monitor real-time changes in substrate concentration during enzymatic reactions. For this project, the decrease in absorbance at 235 nm was measured for reactions involving unsaturated substrate acids. The specific wavelength corresponded to the characteristic absorbance spectra of the substrate, enabling accurate tracking of reaction progress. Substrate conversion rates were calculated from the absorbance data, which were used to determine enzymatic activity.

NMR spectroscopy, on the other hand, provided a detailed and versatile platform for analyzing enzymatic activity. By detecting the unique chemical environments of nuclei in substrate and product molecules, NMR enabled the quantification of relative concentrations over time. This approach was especially advantageous for reactions where absorbance changes were minimal or for systems involving complex mixtures

of substrates and products. NMR data allowed for precise calculations of enzymatic activity while also revealing structural and dynamic aspects of the enzymatic reactions.

2.7 Statistical analysis techniques

The data obtained in this study was curated and analyzed using Microsoft® Excel for Mac (version 16.80, build 23121017) for initial data manipulation, while graphical plotting and advanced statistical analyses were performed using GraphPad Prism 10 for macOS (version 10.3.1, released August 21, 2024). These tools ensured a comprehensive and systematic approach to data processing and presentation.

Statistical analyses were conducted using the mean and standard deviation (SD) as key metrics to summarize and interpret the data. The mean,calculated as the total sum of all observed values divided by the number of observations, provided a central tendency representation for each dataset.. The SD was used to quantify the variability or dispersion of the data points relative to mean, offering insight into data's distribution and consistency. Both biological and technical replicates were included into the analysis to enhance reliability and minimize experimental bias. The SD was determined using the formula: $SD = \sqrt{\frac{\Sigma(x-\bar{x})^2}{n-1}}$, where x represents individual values, the $\overline{X}$ represents the mean of each sample, and n is the sample size. All calculations were conducted using Prism software, providing a consistent approach for statistical analysis of the experimental data.

Inferential statistics were applied using unpaired two-tailed Student's t-tests to compare experimental groups. For multi-group comparisons, one-way ANOVA followed by Tukey's post hoc test was performed to account for multiple testing and to identify significant differences between specific group pairs. This test determined whether observed differences between groups were statistically significant, with a significance threshold set at $p < 0.05$.

3 Engineering of *Bacillus* sp. YM55-1 Aspartase (AspB) for Catalyzing Asymmetric Addition to Ammonia to Produce β-Amino Acids.

3.1 Introduction of engineering AspB for β-amino acids manufacturing

The engineering of enzymes for industrial applications has gained significant traction in recent years due to the growing demand for efficient, sustainable, and highly specific biocatalysts. AspB from *Bacillus* sp. YM55-1 plays an important role in microbial nitrogen metabolism and is widely utilized in the industrial production of L-aspartate, a precursor for food additives and sweeteners. AspB is a member of the aspartase enzyme family, catalyzing the reversible deamination of L-aspartic acid to yield fumaric acid and ammonia. Its catalytic efficiency, substrate specificity, and stability make it a promising candidate for bioengineering efforts aimed at expanding its industrial applications.

Structural studies of AspB in both unliganded and L-aspartate-bound states reveal a substrate-induced conformational change in the SS loop, which transitions from an open to a closed state to seal the active site. This conformational shift positions Ser318, a conserved residue in the SS loop, as a catalytic base that initiates the reaction by abstracting a proton from L-aspartate's Cβ position. This mechanism has been corroborated by mutagenesis studies. Additionally, the enzyme stabilizes a high-energy enediolate-like intermediate through extensive hydrogen bonding with active-site residues such as Thr101, Ser140, Thr141, and Ser319. The SS loop is crucial not only for substrate binding but also for catalysis, with disruptions significantly impairing enzymatic activity. Moreover, AspB's thermostability and broad nucleophile specificity enhance its utility as a biocatalyst for the industrial-scale production of N-substituted aspartic acids and enantiopure amino acid derivatives.

Recent advancements have expanded AspB's utility even further. Computational redesign of AspB using Rosetta Enzyme Design has enabled the development of regio- and enantioselective biocatalysts for hydroamination reactions, facilitating the production of β-amino acids with exceptional specificity. These modifications have enabled the enzyme to process unsaturated carboxylic acids at substrate concentrations of up to 300 g/L, achieving 99% conversion, regioselectivity above 99%, and enantiomeric excess exceeding 99%. Such engineering efforts have enabled the synthesis of high-value β-amino acids, including β-aminobutanoic acid, β-aminopentanoic acid, and β-asparagine, with applications spanning agriculture, pharmaceuticals, and bioactive compound development.

On top of that, computationally redesigned AspB has been transformed into a versatile C–N lyase capable of catalyzing asymmetric hydroamination reactions to produce non-canonical amino acids (ncAAs). Through molecular dynamics simulations and Rosetta Enzyme Design, the enzyme's active site was tailored to accommodate diverse nucleophiles and electrophiles, yielding conversion rates up to 99% and enantiomeric excess exceeding 99%. These redesigned enzymes are compatible with a broad spectrum of substrates, enabling kilogram-scale synthesis of ncAAs with high yields and stereoselectivity. Additionally, they can be integrated into chemoenzymatic cascades to produce β-lactam compounds and pharmaceutical precursors.

β-Amino acids hold significant value in the pharmaceutical, agrochemical, and material science industries due to their incorporation into bioactive molecules, such as β-lactam antibiotics, peptides, and small-molecule drugs. Their unique structural properties, including the presence of a β-amino group, confer enhanced stability against enzymatic degradation, making them desirable building blocks for therapeutic and industrial applications. The use of AspB for producing β-amino acids is particularly advantageous due to its high catalytic efficiency, regioselectivity, and enantioselectivity. Unlike traditional chemical synthesis methods, which often require harsh conditions, multiple steps, and result in racemic mixtures, AspB-catalyzed processes are environmentally friendly, operate under mild conditions, and produce enantiomerically pure products. Furthermore, AspB's broad nucleophile specificity and its ability to accommodate diverse substrates through computational redesign make it a versatile biocatalyst. These properties position AspB as a highly effective enzyme for manufacturing β-amino acids, addressing the growing demand for sustainable and efficient biocatalytic solutions in various industrial sectors. This chapter explores the expression of selected AspB mutants and the validation of their enzymatic activity, focusing on their potential applications in β-amino acid manufacturing.

3.2 Engineering of AspB for unnatural amino acids manufacturing

3.2.1 Selection of AspB mutants.

To engineer AspB for the efficient production of unnatural β-amino acids, a variety of mutants were selected based on prior literature and computational design approaches (summarized in Table 5). These mutants—including B19 (M1), P1, N5, F29, M2, BA15-M13, and others—were tailored to specific substrates and reaction conditions to improve catalytic efficiency, substrate specificity, and enantioselectivity. Selection

criteria included substrate type (e.g., crotonic acid, 2-pentenoic acid, cinnamic acid), amine donor compatibility, and reaction conditions such as pH and temperature, ensuring relevance to industrial applications. Advanced designs, such as Enz2-M20 and BA15-M13, incorporated both active site and surface mutations to expand substrate scope and enhance reaction rates under optimized conditions, highlighting their potential for high-value compound synthesis.

Key mutants identified from previous studies demonstrate how structural insights guided rational engineering. For example, AspB-B19 carries mutations T187C, M321I, K324L, and N326A, which were introduced near the active site to optimize substrate binding and product release. In particular, mutations around residues 321–326 reshape the binding pocket, improving accommodation of short-chain α,β-unsaturated acids such as crotonic acid. As a result, AspB-B19 achieved >99% conversion of crotonic acid to (R)-β-aminobutyric acid with excellent enantioselectivity under alkaline conditions (pH 9.0) at 55 °C.

Similarly, AspB-P1, N5, and F29 were designed to broaden substrate scope beyond crotonic acid. The rationale for these variants was to test different structural modifications of the binding site that could accommodate sterically or electronically distinct substrates. AspB-P1 was optimized for 2-pentenoic acid, a bulkier unsaturated acid, by incorporating mutations that enlarged the pocket while preserving stereoselectivity. AspB-N5 was tailored to process fumaric acid monoamide, where mutations increased hydrogen bonding interactions to stabilize the amide group. AspB-F29 was designed to act on cinnamic acid, requiring mutations that introduced hydrophobic interactions to accommodate the aromatic ring. Each of these mutants achieved high conversion rates and enantioselectivity, validating the strategy of tuning AspB's pocket for different substrate classes.

The design of second-generation mutants further illustrates the logic of combining active site and surface modifications. For example, Enz2-M20 integrates active site mutations (T187C, M321V, K324T, N326S) that reshape the catalytic pocket with surface mutations (N87E, N125D, S133D) intended to improve stability and modulate enzyme dynamics. This combination enhanced activity under neutral to slightly alkaline pH and broadened substrate tolerance. Similarly, BA15-M13 represents a hybrid strategy, incorporating active site mutations from BA15 (A99G, N142S, T187C) that fine-tune stereoselectivity with surface mutations from M13 (K19E, N125D, S133D) that increase flexibility and stability. These changes allow the enzyme to accommodate sterically demanding amine donors, such as allylamine and cyclopropylamine, while maintaining high stereoselectivity.

Collectively, these rationally designed AspB mutants highlight the underlying principles of enzyme engineering: active site mutations modulate binding pocket geometry and catalytic interactions, while surface mutations improve stability and dynamics. Together, they demonstrate how AspB can be systematically tailored for the efficient and sustainable production of diverse unnatural β-amino acids under conditions relevant to industrial biocatalysis.

3.2.2 Plasmid construction for preparing AspB mutants' expression.

The preparation of plasmids harboring AspB mutants B19, P1, N5, and F29 was carried out by Dr. Joseph Webb, and the constructs were subsequently verified by DNA sequencing to confirm the presence of the intended mutations. These mutants were cloned into pET28a vectors, as illustrated in Figure 3-1. The plasmid pET28a-aspB B19 contains the AspB B19 mutant sequence with the mutations T187C, M321I, K324L, and N326A, optimized for reactions involving crotonic acid. The plasmid pET28a-aspB P1, which includes mutations T187C, M321I, K324L, and N326C, was designed for catalytic activity with 2-pentenoic acid. Similarly, pET28a-aspB N5, carrying the mutations M321I, K324N, and N326C, targets fumaric acid monoamide, while pET28a-aspB F29, with mutations T187C, M321V, K324I, and N326C, is tailored for cinnamic acid as a substrate. Notably, none of these plasmids included a His-tag, reflecting their specialized design for substrate-specific catalysis.

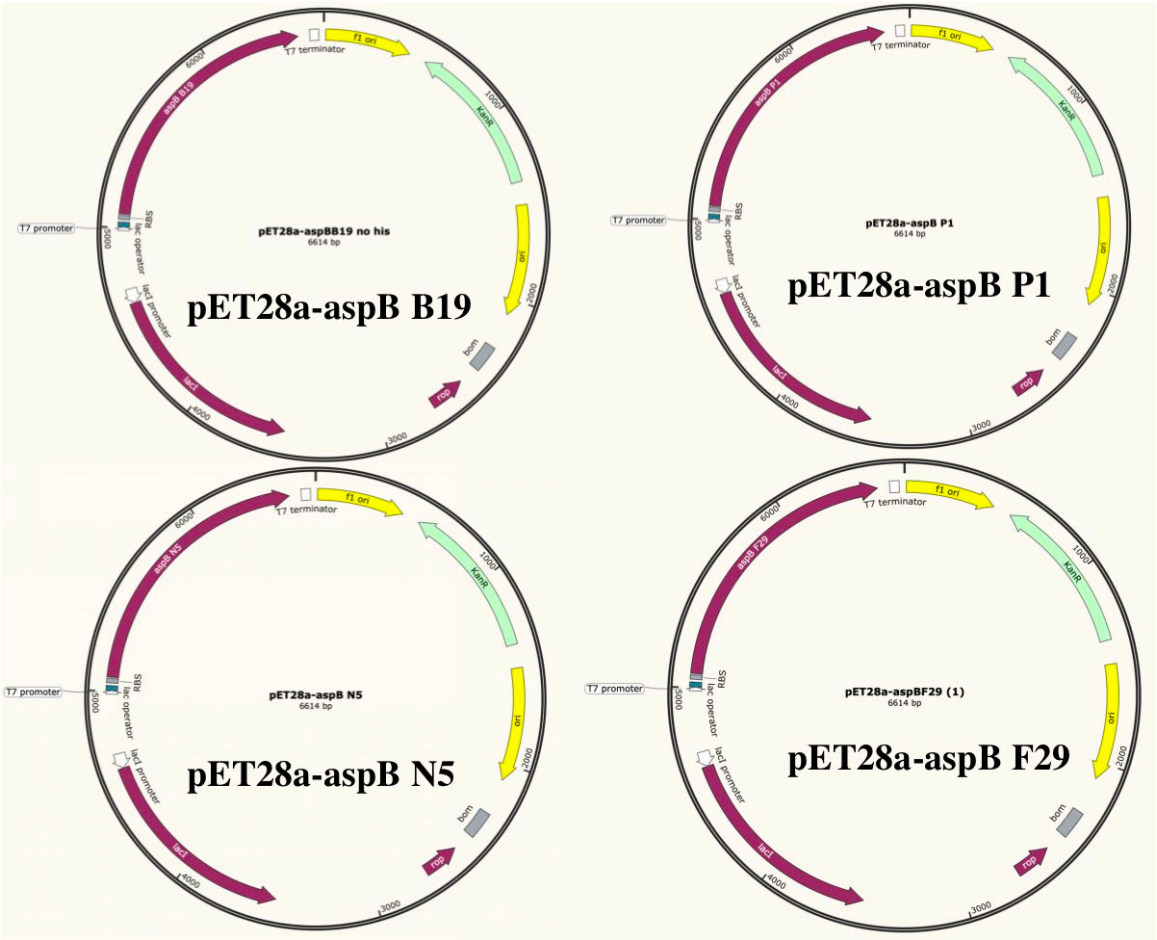

Figure 3-1 Plasmid maps of engineered Aspartase B (AspB) mutants cloned into the pET28a expression vector.

All constructs utilize the T7 promoter for high-level expression in compatible host strains, with other vector components including a kanR gene and origin of replication (ori).

The AspB genes encoding AA15, PA15, BA15-M13, and Enz2-M20 mutants were synthesized by GENEWIZ and cloned into *E. coli* DH5α cells using the $CaCl_2$ transformation method. As depicted in Figure 3-2, transformation plates for all mutants demonstrated robust colony growth, while the negative control plate, lacking plasmid DNA, showed no colonies, confirming the success of the transformation procedure. Plasmid DNA was extracted from transformed colonies using a Plasmid Mini Kit. To confirm the presence of AspB mutant inserts, the purified plasmids were digested with NdeI and EcoRI restriction enzymes, and the digestion products were analyzed via gel electrophoresis. The electrophoresis results, shown in Figure 3-3, revealed clear bands corresponding to the expected insert sizes (~1450 bp), indicating successful digestion and isolation of the AspB mutant genes for subsequent cloning steps.

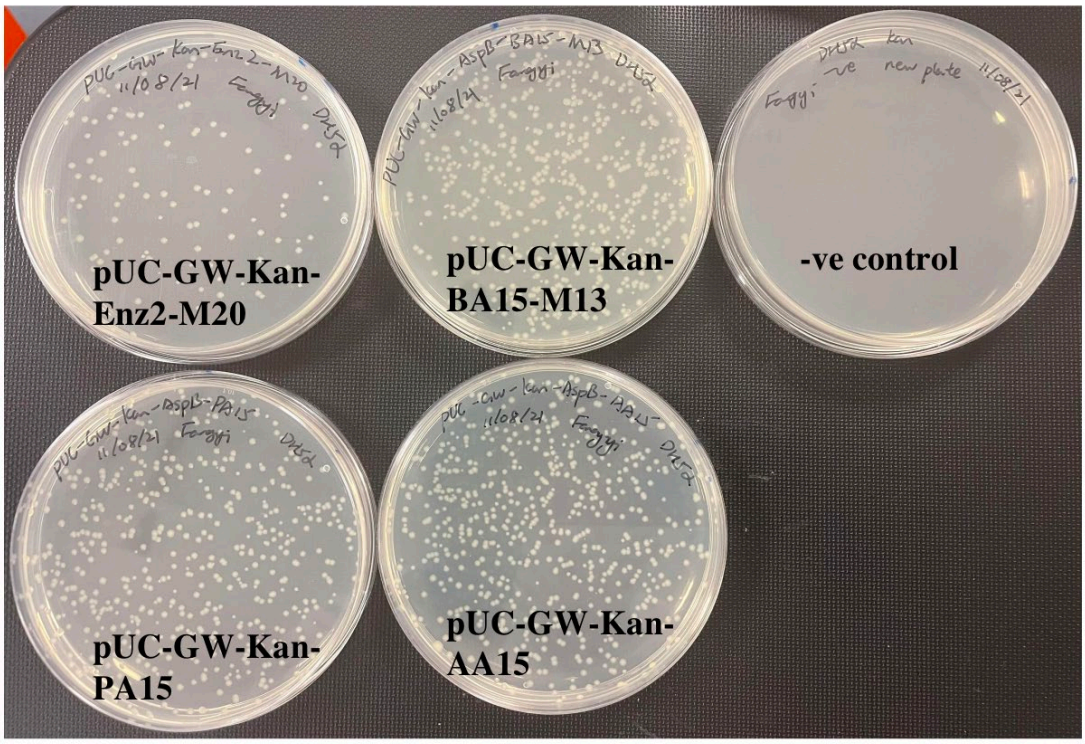

Figure 3-2 Bacterial transformation of AspB mutants into *E. coli* DH5α cells.

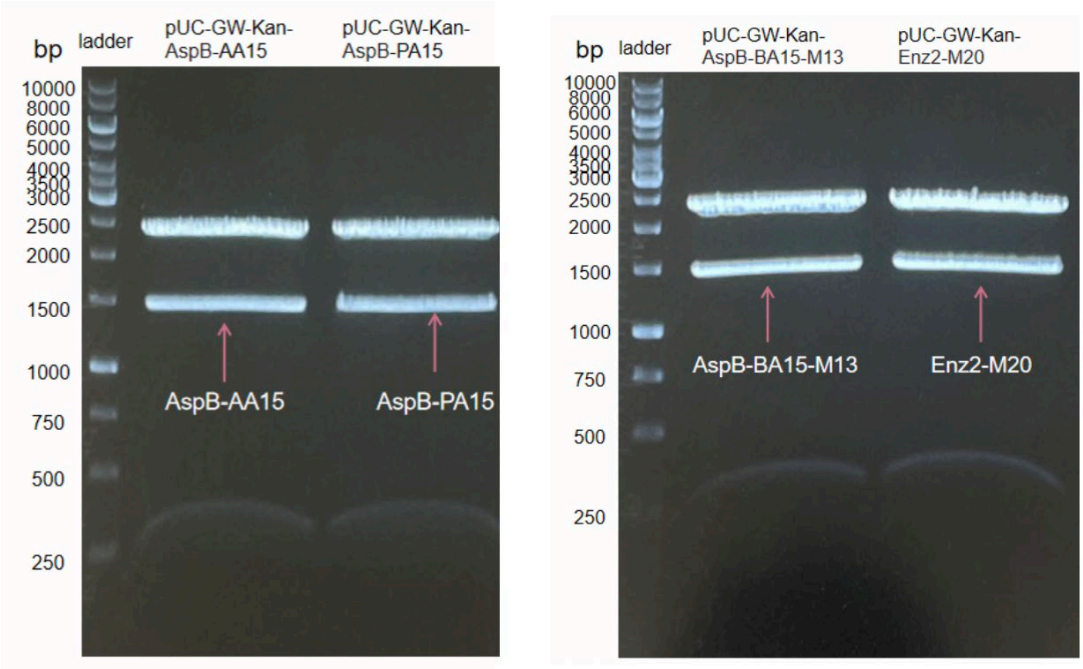

Figure 3-3 Restriction digestion and gel electrophoresis analysis of plasmids containing AspB mutant genes.

Plasmids pUC-GW-Kan-AspB-AA15, pUC-GW-Kan-AspB-PA15, pUC-GW-Kan-AspB-BA15-M13, and pUC-GW-Kan-Enz2-M20 were digested with *NdeI* and *EcoRI* restriction enzymes. The resulting digested products were separated on an agarose gel, and bands corresponding to the AspB mutant inserts (~1450 bp) were observed, confirming successful restriction digestion. The DNA ladder (leftmost lanes) provides size markers for reference.

Plates display colony growth for plasmids carrying four AspB mutants: pUC-GW-Kan-Enz2-M20, pUC-GW-Kan-BA15-M13, pUC-GW-Kan-PA15, and pUC-GW-Kan-AA15, indicating successful transformation and expression of kanamycin resistance. The negative control (-ve control) plate, lacking plasmid DNA, shows no colony formation, confirming the absence of contamination and validating the experiment. The robust colony growth on the mutant plates demonstrates effective uptake of the AspB-mutant plasmids, which were subsequently prepared for downstream applications such as plasmid purification and restriction digestion.

The isolated AspB mutant genes were ligated into pET24a expression vectors to facilitate downstream protein expression. The ligated plasmids were transformed into *E. coli* DH5α cells for propagation, and their construction was validated through plasmid mini-prep, restriction digestion, and gel electrophoresis. As shown in Figure 3-4, digestion of the recombinant plasmids with NdeI and EcoRI released the AspB mutant inserts (~1450 bp) and the pET24a vector backbone (~5300 bp), confirming successful insertion of the AspB mutant genes into the expression vectors. This validated the readiness of the recombinant plasmids for protein expression experiments.

Additionally, plasmids pET28b-AspB-M1 and pET28b-AspB-M2, prepared by Mark J. Thompson, were verified by DNA sequencing with the plasmid maps shown in Figure 3-5. These plasmids were transformed into *E. coli* DH5α cells to generate glycerol stocks, ensuring availability for future protein expression and enzymatic activity analyses. These steps collectively ensured the preparation of AspB mutants for their respective biochemical and catalytic studies.

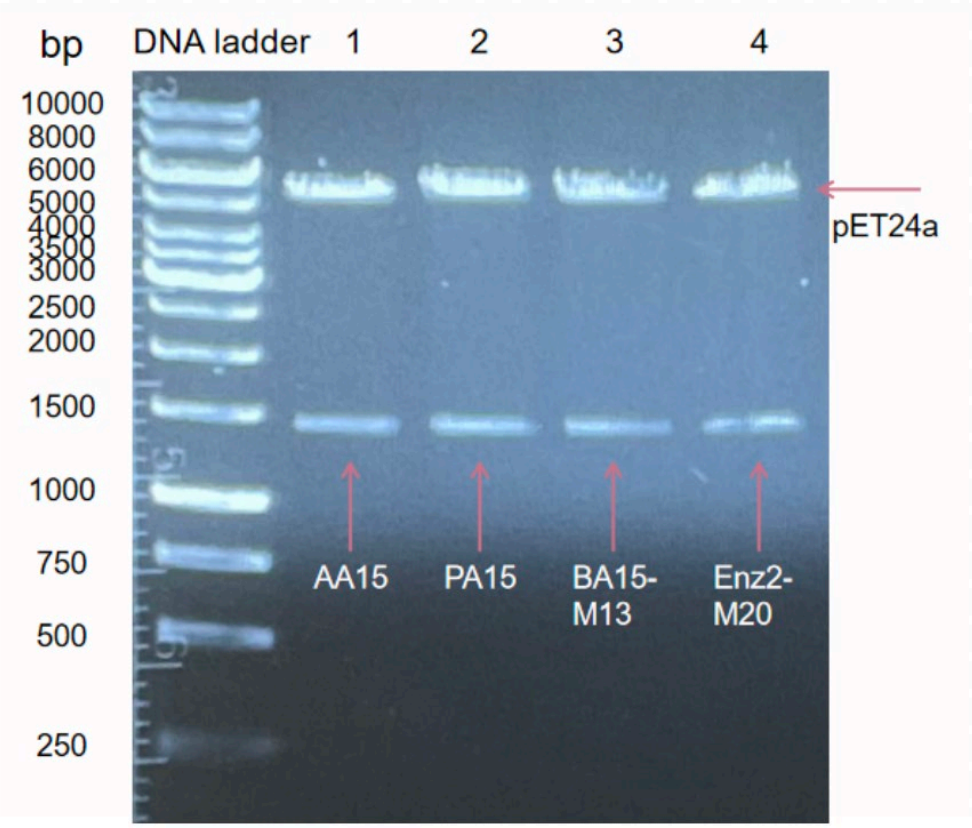

Figure 3-4 Gel electrophoresis of NdeI and EcoRI digested pET24a-AspB mutant plasmids.

The DNA ladder (leftmost lane) serves as a size reference. Lanes 1–4 display the digested plasmids for pET24a-AspB-AA15, pET24a-AspB-PA15, pET24a-AspB-BA15-M13, and pET24a-AspB-Enz2-M20, respectively. Each lane shows two distinct bands: the AspB mutant insert (~1450 bp, lower band) and the pET24a vector backbone (~5300 bp, upper band), confirming the presence and correct size of the AspB mutant gene inserts in the constructed plasmids.

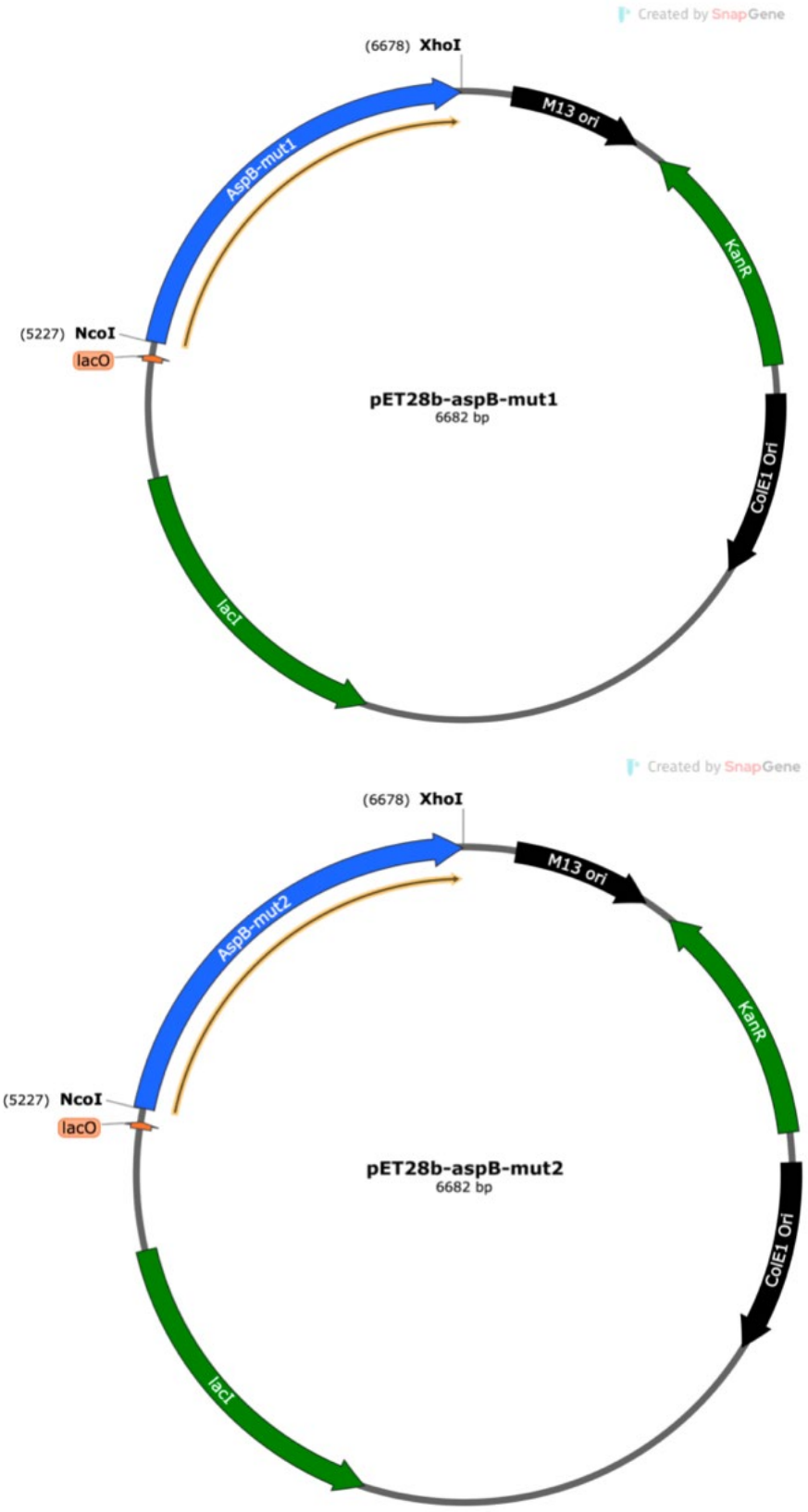

Figure 3-5 Plasmid maps of pET28b-aspB-mut1 and pET28b-aspB-mut2.

Both plasmids are constructed in the pET28b backbone (6682 bp), with the respective AspB mutant genes (mut1 and mut2) inserted between the *NcoI* (5227 bp) and *XhoI* (6678 bp) restriction sites. Key features of the plasmids include the lac operator (*lacO*) for IPTG-inducible expression, a kanamycin resistance gene (*KanR*) for selection, and an origin of replication (*ColE1 ori*) for plasmid propagation in *E. coli*.

3.3 Expression of engineered AspB mutants

Engineered AspB mutants were expressed in *Escherichia coli* (*E. coli*) using the procedures described in Section 2.4 (Protein expression and analysis). *E. coli* is a widely employed expression host due to its rapid growth, well-characterized genetics, cost-effectiveness, and capacity for high protein yields. Recombinant expression vectors from the pET series (Section 2.2.1) were used, providing strong T7 promoters, ribosome binding sites, and antibiotic selection markers to ensure robust protein synthesis. Protein expression was induced with IPTG as described in Section 2.4.2, allowing temporal control over production and minimizing metabolic stress. SDS-PAGE analysis (Section 2.4.5) was used to confirm expression and evaluate protein levels.

As shown in Figure 3-6 (a), AspB mutants B19, M1, and M2 were expressed in *E. coli* BL21(DE3) cells following IPTG induction. Cultures were induced at an OD600 of 0.5–0.6 using 1 mM IPTG, and 10% SDS-PAGE analysis revealed clear bands at approximately 51 kDa, corresponding to the expected molecular weight of the expressed mutants. The negative control lane (BL21(DE3) cells without plasmid) showed no bands, confirming the specificity of expression. Among the mutants, AspB-B19 exhibited the highest expression level, while M1 and M2 also demonstrated robust production. Figure 3-6(b) shows the expression of additional mutants—AA15, PA15, Enz2-M20, and BA15-M13—in BL21(DE3). Clear protein bands were observed for AA15, Enz2-M20, and BA15-M13, confirming their successful expression. However, the band for AspB-PA15 was faint, indicating poor expression in this system.

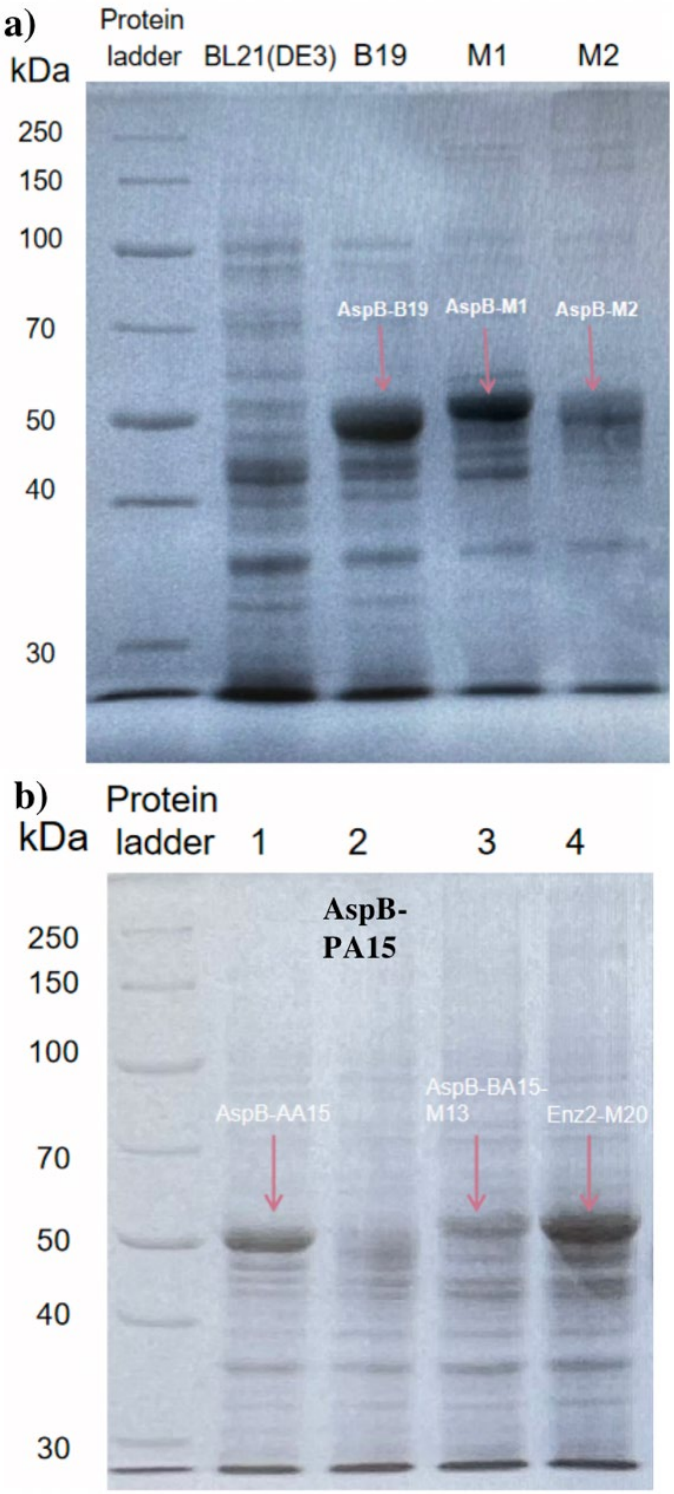

Figure 3-6 SDS-PAGE analysis of AspB mutant protein expression in *E. coli* BL21(DE3) cells.

(a) Protein expression of AspB mutants M1 and M2 compared to the AspB-B19 in *E. coli* BL21(DE3) cells. Lane 1 shows the negative control (BL21(DE3) without plasmid), confirming no non-specific protein bands. Lane 2 presents the positive control for pET28a-AspB-B19, showing the expected protein band at

approximately 51 kDa. Lanes 3 and 4 show expression of pET28b-AspB-M1 and pET28b-AspB-M2, respectively, with bands at ~51 kDa, confirming successful protein expression for both mutants.

(b) Expression of additional AspB mutants in *E. coli* BL21(DE3) cells using pET24a vectors. Lane 1 shows expression of pET24a-AspB-AA15, Lane 2 shows pET24a-AspB-PA15, Lane 3 shows pET24a-AspB-BA15-M13, and Lane 4 shows pET24a-Enz2-M20, with expecting bands at ~51 kDa.

The protein ladder is indicated in the leftmost lane of both images, serving as a molecular weight reference. These results confirmed the successful expression of the AspB mutants at the expected molecular weight for all tested constructs, excepted AspB-PA15.

To improve expression of poorly performing variants, plasmids were also transformed into *E. coli* C41(DE3), a strain optimized for toxic or difficult-to-express proteins (see Section 2.4.1). As shown in Figure 3-7, clear protein bands at approximately 51 kDa were detected for AA15, BA15-M13, and Enz2-M20, confirming their expression in this host strain. However, no detectable bands were observed for AspB-B19 or AspB-PA15, suggesting limited compatibility of these constructs with the C41(DE3) system. The absence of detectable AspB-PA15 in both BL21(DE3) and C41(DE3) strains may result from issues such as protein instability, misfolding, or aggregation. Meanwhile, the failure of AspB-B19 to express in C41(DE3) suggests that BL21(DE3) may be more suitable for its production. BL21(DE3) is a common strain for protein expression because it has the T7 RNA polymerase under an inducible promoter. But sometimes, proteins that are toxic or form inclusion bodies don't express well. C41(DE3) is a derivative of BL21, designed to handle toxic proteins better by having lower T7 RNA polymerase activity, which reduces the rate of protein synthesis and might help with proper folding. While beneficial for challenging proteins (e.g., membrane proteins), this lower activity may insufficiently drive transcription of AspB-B19, leading to undetectable expression. Additionally, AspB-B19 may inherently impose a higher metabolic burden due to its mutations (e.g., T187C, M321I, K324L, N326A). BL21(DE3)'s robust translational machinery tolerates this burden, whereas C41(DE3)'s reduced transcription rate may fail to meet the threshold for detectable expression.

While the observed molecular weights of most AspB mutants matched the expected size, the possibility of post-expression modifications or structural changes due to mutations cannot be ruled out. These factors could affect protein performance,

underscoring the importance of conducting enzymatic activity and stability assays to comprehensively evaluate their functionality.

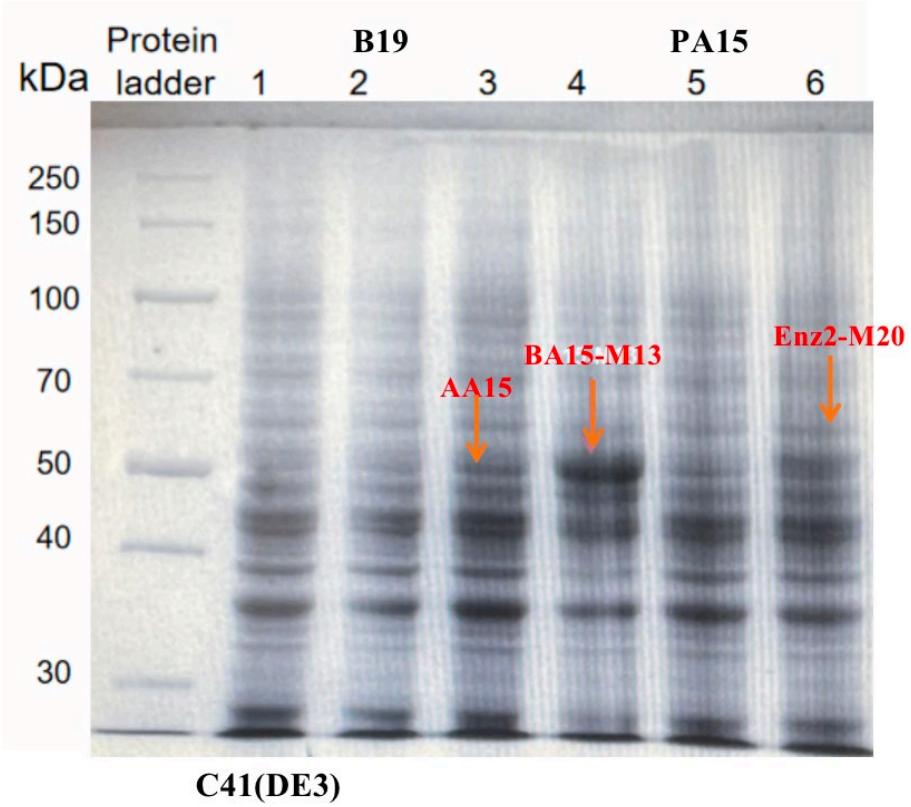

Figure 3-7 SDS-PAGE analysis of AspB mutant protein expression in *E. coli* C41(DE3) cells.

Protein samples were analyzed after induction with IPTG (1 mM) at an OD600 of 0.5–0.6. Lane 1 represents the negative control (C41(DE3) cells without plasmid), showing protein bands represent AspB. Lane 2 is pET28a-AspB-B19, with expected clear band at ~51 kDa. Lanes 3, 4, 5, and 6 show the expression of AspB mutants pET24a-AspB-AA15, pET24a-AspB-BA15-M13, pET24a-AspB-PA15, and pET24a-Enz2-M20, respectively, with bands corresponding to the expected molecular weight (~51 kDa) for the AspB mutants. The protein ladder in Lane 1 provides molecular weight references, confirming the correct size of the expressed proteins.

3.4 Testing enzymatic activity of AspB mutants for producing β-amino acids

In this chapter, the ability of AspB mutants to catalyze the production of β-aminobutyric acid (BABA), a compound with applications in pharmaceuticals and agriculture, is examined. Targeted amino acid substitutions in the active site and surface of AspB mutants aim to improve enzyme stability, activity, and pH tolerance. Additionally, the substrate scope of the AspB mutants was tested using crotonic acid, 2-pentenoic acid, fumaric acid, and cinnamic acid under varied conditions. Protein expression was induced using IPTG, and enzymatic activity was analyzed using spectrophotometric and NMR methods to monitor substrate conversion.

3.4.1 Enzymatic activity analysis using AspB-B19, AspB-M1 and AspB-M2 as enzymes to convert crotonic acid.

AspB-B19, AspB-M1, and AspB-M2 were initially assessed for their ability to convert crotonic acid to R-BABA under alkaline conditions (pH 9.0) at 37°C, using a 35% ammonia solution as the amine source. Enzymatic assays were conducted using both cell suspensions and extracted enzymes, as detailed in Sections 2.5 and 2.6. Initially, a reaction mixture (Solution B) containing 100 mM sodium phosphate buffer, 400 mM NH_4OH, and 400 mM crotonic acid was tested. Despite a 24-hour incubation period, no significant substrate conversion was detected. To address this, the reaction conditions were adjusted based on literature recommendations (Li *et al.* 2018), reformulating Solution B with 300 g/L (3.48 M) crotonic acid at pH 9.0 using 35% ammonia solution. However, no measurable substrate conversion was observed, leading to an increase in cell density for subsequent assays. Cell pellets were harvested from 800 mL cultures, achieving higher OD600 values of 43.4, 42.5, and 34.4 for AspB-B19, AspB-M1, and AspB-M2, respectively.

As illustrated in Figure 3-8, substrate conversion in the original Solution B (400 mM crotonic acid) remained negligible for AspB-B19, regardless of using cell suspensions or extracted enzymes. Conversely, the reformulated Solution B (300 g/L crotonic acid) significantly improved conversion rates, particularly with AspB-M2, which exhibited the highest efficiency among the tested mutants. Extracted enzymes are typically concentrated during purification, increasing the effective catalytic load compared to diluted intracellular pools in whole cells. Additionally, extracted enzymes generally outperformed cell suspensions due to the absence of barriers like incomplete lysis or substrate diffusion limitations. Extracted enzymes also minimized the risks associated with endogenous protease activity. Whole cells contain proteases that degrade target

enzymes over time. Extraction often includes protease inhibitors or partial purification, minimizing this risk. Statistical analysis was conducted using unpaired two-tailed Student's t-tests in GraphPad Prism. Significant differences between old and new formulations of solution B were observed for AspB-M1 (* $p < 0.05$) and AspB-M2 (** $p < 0.01$), whereas AspB-B19 showed no significant improvement under any condition. Extracted enzymes consistently outperformed cell suspensions, supporting the role of purification in minimizing diffusion barriers and protease activity.

While extracted enzymes offer advantages for controlled assays, they also present several limitations that can impact their practicality and efficiency. One major drawback is the increased cost and time associated with their preparation. The extraction process involves multiple steps, which require additional labor, reagents, and processing time compared to whole-cell systems. Moreover, extracted enzymes often exhibit reduced stability since they lack the protective cellular components, such as chaperones and osmolytes, that help maintain enzyme integrity. This stability issue is particularly significant in industrial applications where enzymes must remain active over extended periods. Scalability also poses a challenge, as large-scale enzyme extraction is resource-intensive and less feasible than using whole-cell biocatalysts, which can be continuously reused. Another concern is the potential loss of activity during the extraction process itself. Harsh purification techniques, such as sonication or high-speed centrifugation, can cause enzyme denaturation or structural damage, further reducing efficiency. Lastly, contamination risks must be considered, as incomplete purification may leave behind unwanted enzymes, such as hydrolases, that could interfere with assays or undesirably alter reaction outcomes.

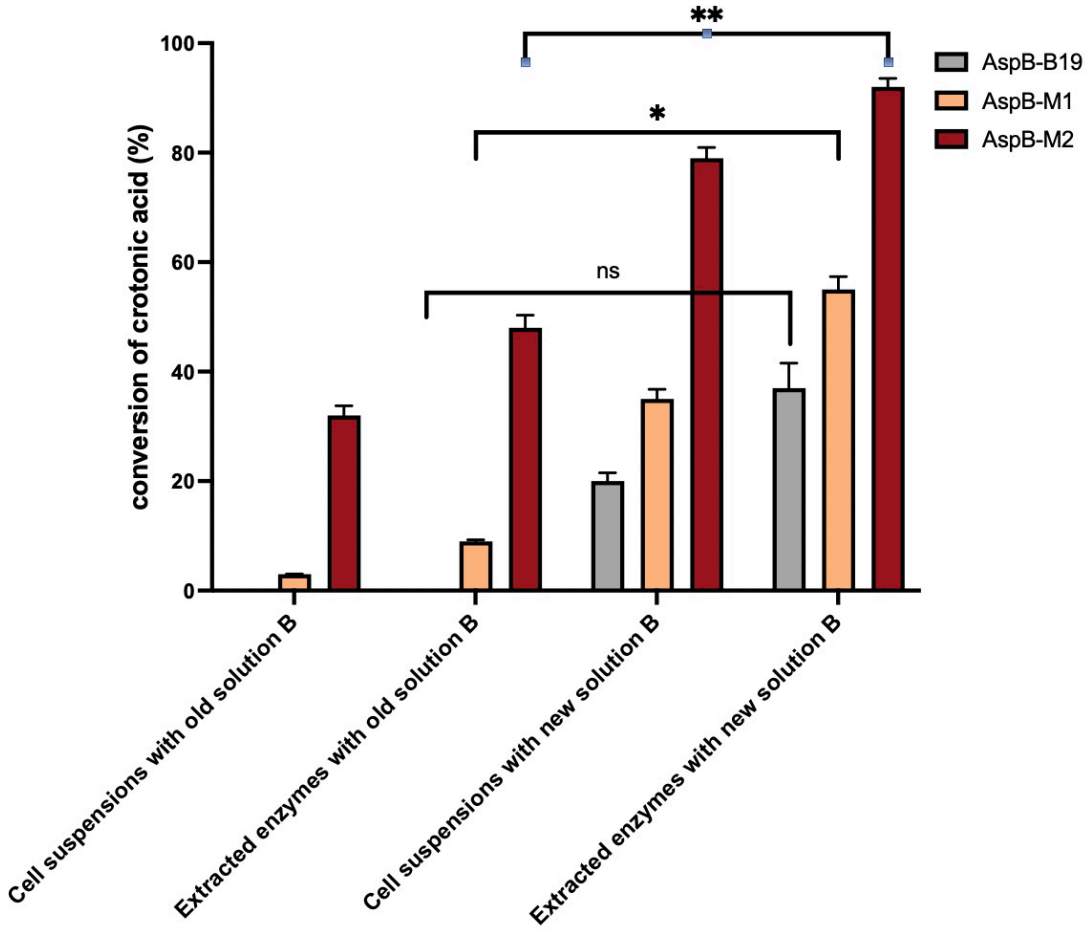

Figure 3-8 Conversion of crotonic acid by AspB mutants using different conditions and solutions.

The percentage conversion of crotonic acid at 37 °C after 24 hours for three AspB mutants (AspB-B19, AspB-M1, and AspB-M2) under various conditions is shown. Experiments were performed with both extracted enzymes and cell suspensions, using either the original formulation of solution B (400 mM crotonic acid) or the reformulated solution B (300 g/L crotonic acid). Data represent mean values ± standard deviation from biological replicates (n = 3). Statistical analysis was conducted using unpaired two-tailed Student's t-tests in GraphPad Prism.

Given AspB-M2's superior performance, it was selected as the primary enzyme for producing R-BABA. To provide a more practical and scalable alternative to enzyme extraction, cell suspensions were employed for activity optimization. The conversion of crotonic acid by AspB-M2 cell suspensions was evaluated at a range of temperatures (37–50 °C). As shown in Figure 3-9, conversion rates increased with temperature, reaching their highest efficiency at 45 °C and 48 °C, where substantial substrate depletion occurred within the first 12 h. Statistical analysis at this timepoint

confirmed significant differences between conditions (one-way ANOVA, $F(4,10) = 1739.3$, $p < 0.0001$). Tukey's post hoc test revealed that both 45 °C and 48 °C achieved significantly greater conversion compared with 40 °C and 43 °C ($p < 0.001$), while activity at 50 °C was significantly reduced relative to 45 °C and 48 °C ($p < 0.05$), consistent with thermal inactivation at elevated temperatures. In contrast, lower temperatures (37 °C and 40 °C) resulted in markedly slower conversion, with substantial amounts of substrate persisting after 24 h. To optimize production, activity was assessed across temperatures from 37 °C to 50 °C, using cell suspensions normalized to $OD_{600} = 0.5$. Initial specific rates (0–3 h) revealed a clear temperature dependence: activity increased from 0.197 $\Delta OD_{235} \cdot h^{-1} \cdot OD^{-1}$ at 37 °C to a maximum of 1.03 $\Delta OD_{235} \cdot h^{-1} \cdot OD^{-1}$ at 48 °C, corresponding to a 5.2-fold enhancement. Intermediate temperatures showed graded increases (43 °C ≈2.2-fold, 45 °C ≈3.8-fold), whereas activity at 40 °C was slightly lower than at 37 °C. At 50 °C, activity declined to 0.38 $\Delta OD_{235} \cdot h^{-1} \cdot OD^{-1}$ (≈1.9-fold vs 37 °C), consistent with partial thermal inactivation. These findings suggest the temperature-dependent activity of AspB-M2, with 45–48 °C representing the optimal range for efficient bioconversion.

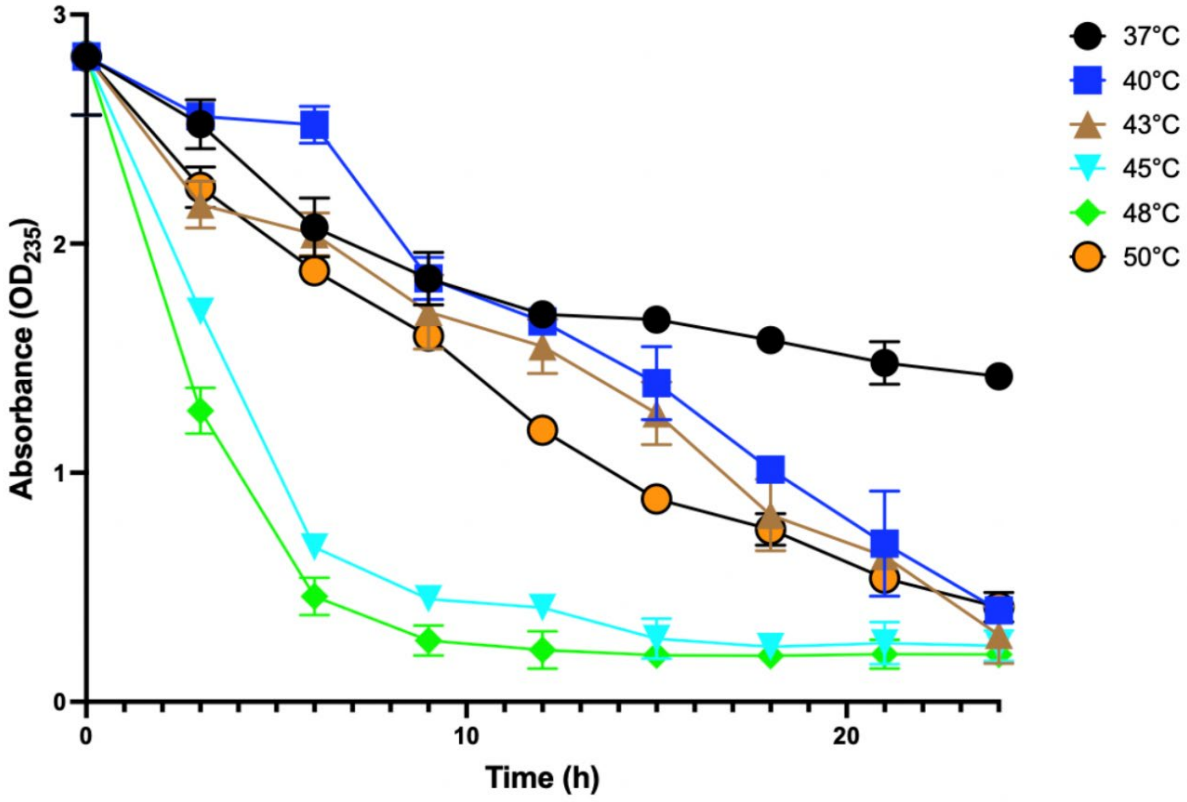

Figure 3-9 Temperature-dependent conversion of crotonic acid by AspB-M2 cell suspensions over 24 hours.

The conversion of crotonic acid into R-BABA by AspB-M2 cell suspensions was monitored at different temperatures (37, 40, 43, 45, 48, and 50 °C) for 24 h. Conversion was quantified by the decrease in crotonic acid absorbance at OD_{235}. Data represent mean ± SD (n = 3 biological replicates). Statistical analysis was performed at the 12 h timepoint using one-way ANOVA ($F(4,10) = 1739.3$, $p < 0.0001$), followed by Tukey's post hoc test. Conversion at 45 °C and 48 °C was significantly greater than at 40 °C and 43 °C ($p < 0.001$), while activity at 50 °C was significantly lower than at 45 °C and 48 °C ($p < 0.05$), consistent with partial thermal inactivation.

The enzymatic conversion of crotonic acid by AspB-M2 was further validated using ^{1}H NMR spectroscopy. As shown in Figure 3-10, the pre-reaction spectrum displayed characteristic peaks for crotonic acid, including signals at δ6.46 ppm and δ5.68 ppm. After enzymatic treatment, these peaks disappeared, replaced by signals at δ3.36 ppm, δ2.26 ppm, and δ1.10 ppm, indicative of BABA formation. These spectral changes confirmed the enzymatic reduction of crotonic acid's C=C double bond, further validating AspB-M2's catalytic activity in producing R-BABA under optimized conditions.

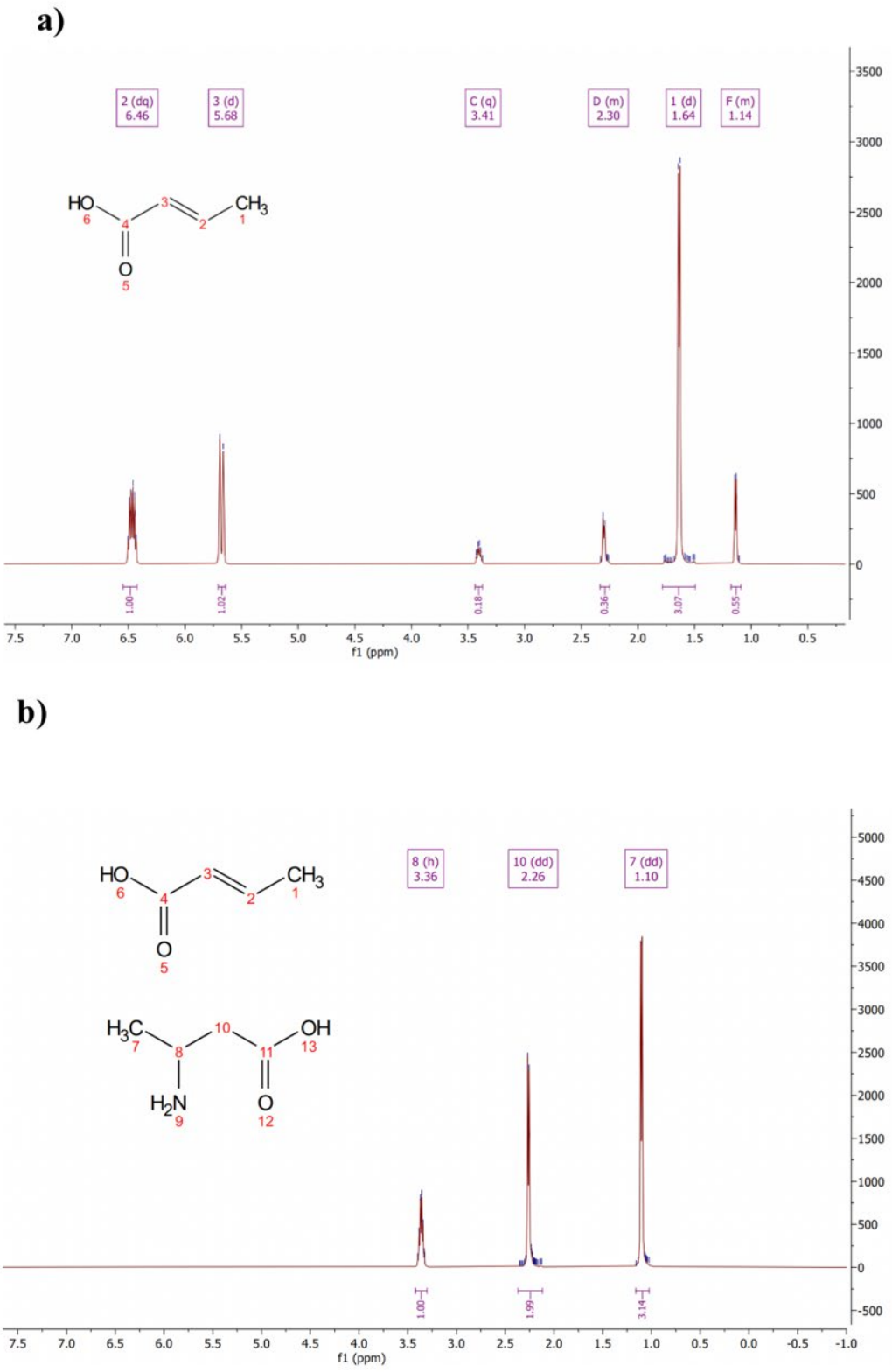

Figure 3-10 ^{1}H NMR spectra of 300 g/L crotonic acid converted to R-BABA by AspB-M2.

(a) before adding cell suspension containing AspB-M2, and (B) after adding crude lysate containing AspB-M2 for 5 hours at 48°C.

3.4.2 Enzymatic activity analysis by using P1, N5 and F29 as enzymes to convert 2-pentenoic acidm, fumaric acid and cinnamic acid .

AspB-P1, which features mutations T187C, M321I, K324L, and N326C, is engineered to catalyze the addition of ammonia to 2-pentenoic acid, facilitating the production of β-amino acids with extended carbon chains under optimal conditions of pH 9.0 and 50°C (Figure 3-11). The enzymatic reaction, illustrated below, involves the hydroamination of 2-pentenoic acid, a process critical for synthesizing specialized β-amino acids. As shown in Figure 3-12, the conversion of 80 g/L 2-pentenoic acid was measured spectrophotometrically at 235 nm under various temperatures (37°C, 42°C, 46°C, and 50°C) over a 24-hour period. Minimal conversion was observed at 37°C and 42°C, indicating limited enzymatic activity under these conditions. However, at 46°C and 50°C, substrate conversion significantly improved, suggesting enhanced catalytic efficiency at elevated temperatures, with 50°C likely representing the optimal temperature for AspB-P1 activity.

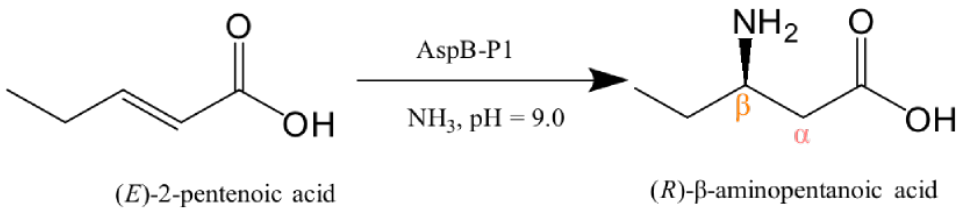

Figure 3-11 Enzymatic Conversion of 2-Pentenoic Acid by AspB-P1.

The enzymatic reaction catalyzed by AspB-P1, an engineered aspartase variant, which facilitates the addition of ammonia to 2-pentenoic acid, leading to the production of β-amino acids with extended carbon chains. This reaction occurs optimally at pH 9.0.

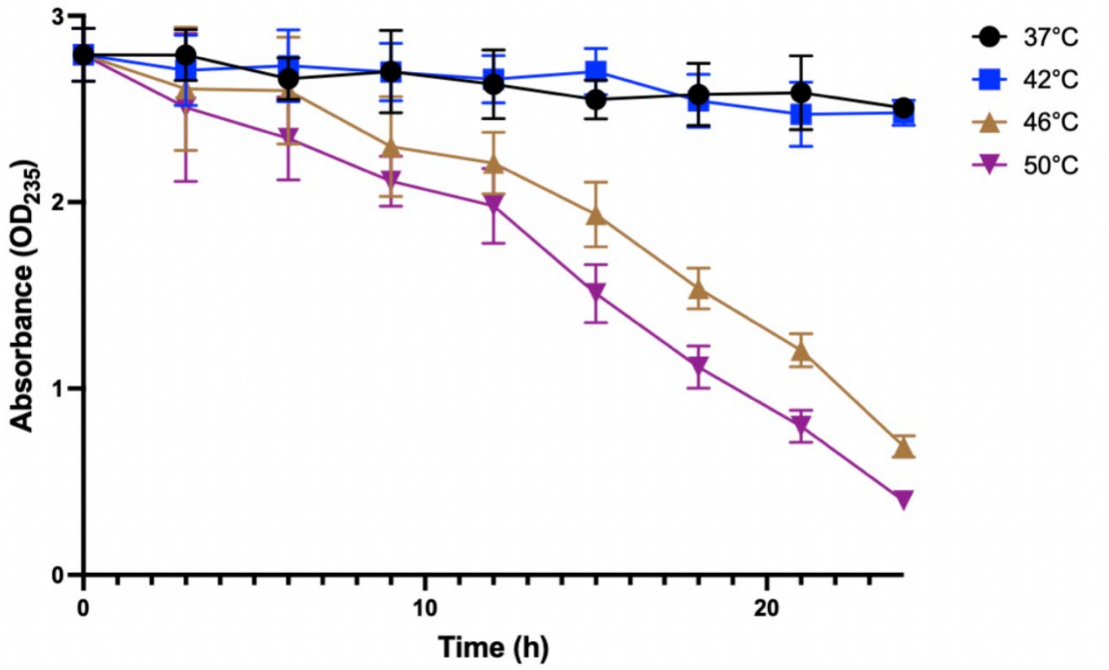

Figure 3-12 Temperature-dependent conversion curves of 2-pentenoic acid by AspB-P1 enzyme over 24 hours.

The graph shows the absorbance OD_{235} of 80 g/L 2-pentenoic acid over 24 hours during its conversion by the enzyme AspB-P1 at four different temperatures: 37°C (black circles), 42°C (blue squares), 46°C (brown triangles), and 50°C (purple inverted triangles). Data represent mean values ± standard deviation (error bars) from three independent biological replicates (n = 3).

The ^1H NMR results for AspB-P1-mediated conversion of 2-pentenoic acid are unclear due to interference from the water peak. The NMR results will be included in the appendix. The H_2O peak typically appears around 4.8 ppm in ^1H NMR, though this can vary with temperature and pH. It's usually broad and can be quite intense due to the high concentration of water in biological samples. 2-pentenoic acid and its β-amino acid product likely have proton signals in the 3-5 ppm region as the α-proton of the β-amino acid product would appear here. The disappearance of alkene protons and appearance of new CH-NH signals would be key indicators of successful conversion. AspB-P1-mediated conversion of 2-pentenoic acid. The D_2O has already been used in ^1H NMR to minimize the effect of water. To overcome the effect of water, water suppression techniques can be employed, including presaturation of the water signal, WATERGATE (Water suppression by gradient-tailored excitation), or excitation sculpting methods in the future. Additionally, the NMR experiment can be conducted at slightly modified temperatures to shift the water peak away from regions of interest. As an alternative strategy, 13C NMR spectroscopy can be utilized as a

complementary technique, as it is not affected by the water signal and can clearly show the disappearance of alkene carbons (around 130-150 ppm) and the appearance of new sp^3 carbons (approximately 30-50 ppm) that would indicate successful conversion of the substrate.

AspB-N5, which carries the mutations M321I, K324N, and N326C, is optimized for smaller, more polar substrates such as fumaric acid monoamide. This substrate, derived from fumaric acid with one carboxylic group replaced by an amide group (-$CONH_2$), is not commercially available, necessitating its synthesis for enzymatic assays. While fumaric acid can theoretically be converted by aspartase, its evaluation using spectrophotometric measurements poses challenges due to native *E. coli* BL21(DE3) metabolism. Fumaric acid is an intermediate in the tricarboxylic acid (TCA) cycle, where host cell enzymes like fumarase can convert fumaric acid to malate independently of AspB-N5 activity (Figure 3-13). Consequently, decreases in fumaric acid absorbance may reflect native metabolic processes rather than AspB-N5-mediated catalysis.

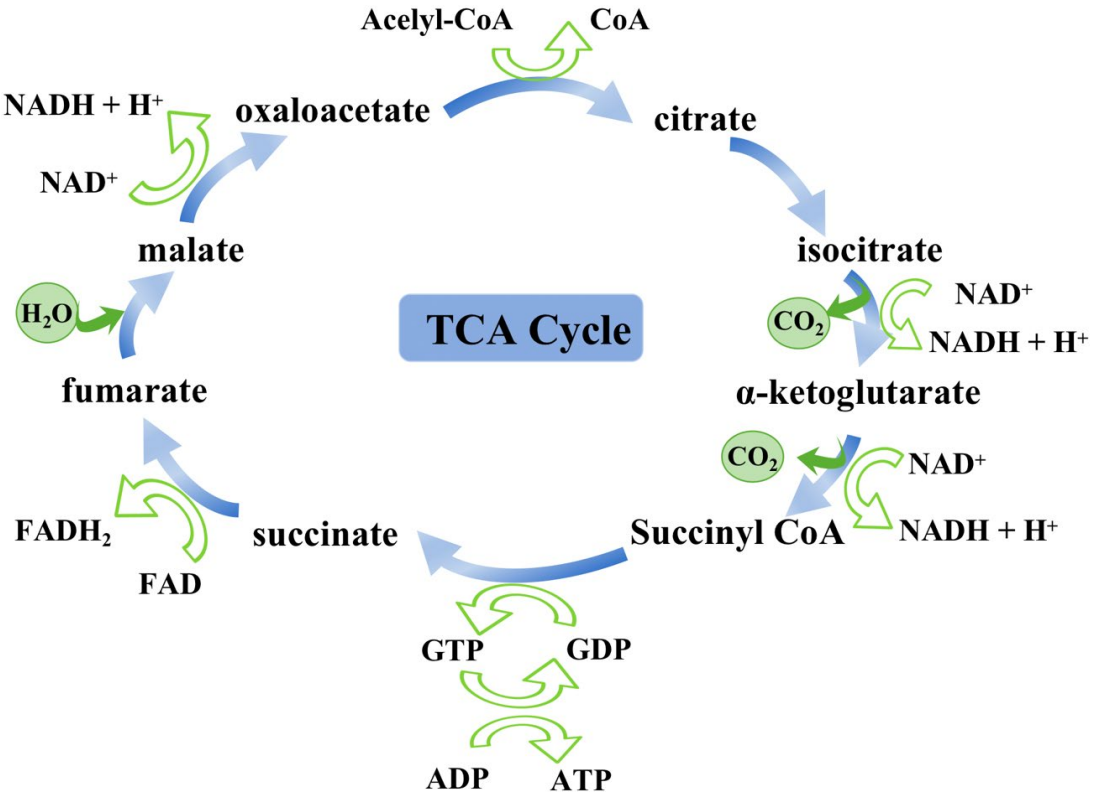

Figure 3-13 Tricarboxylic acid (TCA) cycle: central pathway of cellular metabolism.

The TCA cycle, also known as the Krebs cycle or citric acid cycle, is a crucial metabolic pathway occurring in the mitochondria that plays a central role in energy production and biosynthesis. The cycle begins with the condensation of acetyl-CoA

and oxaloacetate to form citrate, followed by a series of enzymatic reactions that regenerate oxaloacetate while producing reduced cofactors NADH and $FADH_2$, as well as GTP/ATP. These reduced cofactors are essential for oxidative phosphorylation and ATP synthesis. Key intermediates such as α-ketoglutarate and succinyl-CoA serve as precursors for various biosynthetic pathways. The green arrows indicate the conversion of cofactors and release of products such as CO_2 and water during the cycle.

AspB-F29, which incorporates the mutations T187C, M321V, K324I, and N326C, was designed to target cinnamic acid, an aromatic substrate, for the production of β-phenyl-β-amino acids with high enantioselectivity under optimal conditions of pH 8.8 and 30°C. Cell suspensions expressing AspB-F29 were tested for substrate conversion at various temperatures, including room temperature, 30°C, 37°C, and 45°C, over a 24-hour period. However, no significant changes in cinnamic acid absorbance were observed under any of these conditions. The lack of activity in AspB-F29 with cinnamic acid can be attributed to several key factors. The primary challenges likely stem from substrate-related issues, including cinnamic acid's distinct aromatic structure, which differs significantly from the natural substrate, potential solubility limitations in aqueous solutions, and possible steric hindrance from the phenyl group affecting binding. Additionally, enzyme structural and functional issues may play a crucial role, as the current mutations (T187C, M321V, K324I, N326C) might not create sufficient space for accommodating the bulky phenyl group, or the active site architecture may not facilitate proper substrate orientation.

To address these challenges, several optimization strategies can be implemented. These include fine-tuning reaction conditions through systematic pH adjustment (7.5-9.5), testing various buffer systems (phosphate, HEPES, Tris), and incorporating organic co-solvents (DMSO, methanol) at low concentrations (1-5%) to enhance substrate solubility. Enzyme engineering approaches could involve introducing mutations to expand the active site cavity, improving substrate binding without compromising catalytic activity, and conducting directed evolution focusing on residues near the active site. Process optimization strategies such as exploring different cell lysis methods, adding stabilizing agents (glycerol, BSA), implementing two-phase systems for better substrate delivery, and considering enzyme immobilization could also enhance performance. Furthermore, employing more sensitive detection methods (HPLC, LC-MS) and monitoring reaction progress using multiple analytical techniques could provide better insights into the enzyme's activity and guide further optimization efforts.

3.4.3 Enzymatic activity analysis by using other AspB mutants as enzymes to convert crotonic acid.

As discussed in Section 3.3, the expression of AspB-AA15, AspB-BA15-M13, and Enz2-M20 was confirmed by SDS-PAGE analysis, whereas AspB-PA15 expression could not be detected. Therefore, the enzymatic activity of the expressed mutants (AspB-AA15, AspB-BA15-M13, and Enz2-M20) was evaluated for the conversion of crotonic acid (300 g/L, pH 9.0, adjusted with 35% NH_4OH) at 42°C and 48°C. Spectrophotometric measurements at OD235 were taken over a 24-hour reaction period to monitor substrate depletion. However, no significant decreases in OD235 was observed, indicating minimal or no enzymatic activity under these conditions.

Further investigation using ^1H NMR spectroscopy provided detailed insights into the reaction. For Enz2-M20, chemical shifts in the NMR spectra, collected every two hours at 48°C, revealed partial conversion of crotonic acid. A reduction in the vinyl proton signals at δ6.46 ppm and δ5.68 ppm was detected, along with the appearance of new product peaks at δ3.41 ppm, δ2.31 ppm, and δ1.65 ppm, indicating the formation of R-BABA. Similar spectral trends were observed for AspB-BA15-M13 and AspB-AA15, suggesting these mutants exhibit some catalytic activity under the tested conditions. The NMR results for Enz2-M20, AspB-BA15-M13, and AspB-AA15 will be included in the appendix to provide a comprehensive record of the spectral data and support the findings discussed in the main text.

In conclusion, while spectrophotometric analysis at OD235 showed no significant changes in absorbance, ^1H NMR spectroscopy confirmed partial conversion of crotonic acid to R-BABA using AspB mutants as biocatalysts. These results highlight the importance of employing complementary analytical techniques to assess enzymatic activity accurately, especially in complex reaction systems.

3.5 Discussion and conclusions

The engineering of *Bacillus* sp. YM55-1 AspB mutants for β-amino acid production showcases the potential of enzyme engineering for industrial biocatalysis. While several AspB mutants exhibited activity and selectivity toward specific substrates, significant discrepancies between the current results and reported literature highlight the challenges of optimizing enzyme performance under practical conditions. These discrepancies include inconsistencies in enzymatic activity, limitations in substrate scope, and poor solubility or stability of certain mutants. Addressing these issues

through targeted experimental approaches and advanced engineering strategies could pave the way for more effective biocatalysts for β-amino acid production.

3.5.1 Selection of substrates for production of β-amino acids.

The selection of substrates such as crotonic acid, 2-pentenoic acid, fumaric acid monoamide, and cinnamic acid was guided by the reported substrate scope of AspB mutants in the literature. Crotonic acid, a simple unsaturated acid, served as a model substrate. Its conversion to R-β-aminobutyric acid (R-BABA) by AspB-B19, M1, and M2 was consistent with previous studies demonstrating their activity under alkaline conditions (pH 9.0) and elevated temperatures (45–50°C). However, although these mutants demonstrated partial conversion of crotonic acid, their efficiency was significantly lower than the >99% conversion rates reported in the literature (Li, Wijma et al. 2018). This discrepancy may result from several reasons. The primary considerations include variations in enzyme expression and quality, such as differences in protein expression levels, folding stability, and potential activity loss during preparation or storage. Reaction condition variations also play a crucial role, including subtle differences in pH control, buffer composition, temperature maintenance, substrate concentration, and enzyme-to-substrate ratios. Analytical method differences could also contribute, encompassing variations in conversion rate measurements, sample preparation, handling procedures, and calibration standards. Environmental factors such as local atmospheric conditions, mixing methods, and reaction vessel materials may impact the results. Additionally, reagent quality variations, including different sources of crotonic acid, buffer component quality, and potential presence of inhibitory compounds, could affect conversion rates. To improve results, careful attention should be paid to matching literature conditions exactly, optimizing protein expression and purification protocols, implementing precise temperature and pH control, validating analytical methods, and ensuring proper reagent quality and storage conditions.

Similarly, AspB-P1 showed promising activity with 2-pentenoic acid, achieving enhanced conversion rates at higher temperatures (46–50°C). However, the absence of significant enzymatic activity for AspB-F29 with cinnamic acid contrasts with literature reports that this mutant efficiently produces β-phenyl-β-amino acids under similar conditions. This suggests potential issues with protein folding, substrate binding, or catalytic turnover that were not addressed in the current experimental setup. Protein folding and stability could be enhanced by incorporating stabilizing agents such as glycerol (5-10%) or BSA into the reaction mixture, while substrate binding might be improved through optimization of reaction conditions, including testing various buffer systems, and adding small amounts of organic co-solvents to

enhance cinnamic acid solubility. A step-wise temperature adaptation protocol could also help maintain proper protein folding at the required reaction temperature.

Furthermore, the AspB-N5's specificity for fumaric acid monoamide cannot be identified due to lack of fumaric acid monoamide. on top of that, the challenges of distinguishing its activity in converting fumaric acid from native *E. coli* metabolism emphasize the need for specialized assays or alternative host strains to eliminate confounding factors. The first challenge of substrate availability can be addressed through chemical synthesis of fumaric acid monoamide using established protocols, exploring commercial sources, or establishing collaborations with chemical synthesis laboratories. The second challenge of distinguishing enzymatic activity from native *E. coli* metabolism requires more sophisticated approaches, such as utilizing *E. coli* knockout strains lacking fumarase genes, implementing cell-free protein expression systems, or developing in *vitro* assays with purified enzyme. Additionally, selective analytical methods like chiral HPLC or the use of isotope-labeled substrates could help track enzyme-specific conversion.

The limited activity observed for AspB mutants with certain substrates highlights a need to further optimize substrate binding and catalytic efficiency. Structural insights from molecular dynamics simulations or crystallography could guide the rational redesign of the active site to improve substrate accommodation and reaction kinetics. Additionally, the poor solubility and aggregation of AspB mutants, particularly AspB-BA15-M13, Aspb-AA15 and AspB-PA15, suggest issues with protein folding and stability. Exploring alternative expression systems, such as Pichia pastoris or chaperone co-expression in *E. coli*, could enhance protein solubility and activity. The reliance on spectrophotometric methods for activity measurements under high substrate concentrations was insufficient to detect subtle enzymatic changes. Advanced techniques such as kinetic modeling and real-time NMR spectroscopy should be routinely employed to capture low-activity mutants' performance and identify intermediate reaction products. A practical first step would be to increase assay sensitivity through higher enzyme loading, longer incubation times, or by concentrating substrate–enzyme mixtures prior to analysis. More powerful analytical techniques, such as HPLC or LC–MS, could be employed to directly quantify substrate depletion and product formation with much greater precision than UV-based methods. Complementary coupled assays that convert the product into a chromogenic or fluorogenic readout would also allow weak activity to be detected in a high-throughput format. Additionally, refining reaction conditions — for example, testing a range of pH values, cofactor supplementation, or using stabilizing additives — could enhance catalytic turnover and improve detectability. Together, these strategies would help ensure that low-activity mutants are not overlooked and provide a more reliable assessment of enzymatic potential.

3.5.2 Identifying the optimized conversion conditions for β-Amino acids production.

The optimization of reaction conditions revealed that temperature and pH are critical determinants of enzymatic activity. AspB-M2 demonstrated the highest activity with crotonic acid at temperatures between 45°C and 48°C, while AspB-P1 achieved optimal performance with 2-pentenoic acid at 50°C. These findings align with the literature, which highlight the importance of elevated temperatures for AspB activity (Li *et al.* 2018). However, at 50°C, a decline in activity was observed in some mutants, suggesting a threshold beyond which thermal denaturation occurs.

Future studies should investigate the thermal stability of AspB mutants to identify and address factors contributing to protein denaturation. Detailed thermal denaturation studies could be conducted using differential scanning calorimetry (DSC) and circular dichroism (CD) spectroscopy to precisely determine the melting temperatures (Tm) and unfolding patterns of each mutant. These techniques would provide quantitative data about the protein's structural stability at different temperatures and help identify the exact temperature thresholds where denaturation begins. Temperature-dependent kinetic studies would form another crucial aspect of the investigation. This would involve measuring enzyme kinetics (Km and kcat) across a range of temperatures (30-60°C) at smaller intervals (e.g., every 2-3°C) to create detailed temperature-activity profiles. Additionally, time-course stability studies at different temperatures could help understand the rate of activity loss and determine the enzyme's half-life at each temperature. This information would be valuable for optimizing reaction conditions and predicting enzyme performance over extended periods.

Protein engineering approaches could also be implemented to enhance thermal stability. This might include computational design to identify stabilizing mutations, particularly focusing on regions that show high flexibility at elevated temperatures. Structure-guided engineering could be used to introduce additional salt bridges, disulfide bonds, or optimize surface charge distribution to enhance stability. Furthermore, directed evolution experiments specifically targeting thermostability could be performed, possibly using error-prone PCR or DNA shuffling followed by screening at elevated temperatures.

The role of stabilizing agents and reaction conditions in preventing thermal denaturation could also be explored. This would involve testing various additives (such as glycerol, sorbitol, or specific ions), different buffer systems, and protein

concentrations to identify conditions that enhance thermal stability. The interaction between pH and temperature stability could be investigated to find optimal combinations that maximize both activity and stability. Additionally, exploring protein immobilization techniques or enzyme formulation strategies might provide ways to enhance the operational stability of these enzymes at elevated temperatures.

3.5.3 Identifying the optimized substrates and amine donors for β-Amino acids production.

The roles of amine donors and substrate concentration also proved critical. While 35% ammonium hydroxide provided an optimal nucleophile for hydroamination reactions, further studies should explore alternative amine donors, such as substituted amines, to enhance reaction scope and efficiency. In addition to this, high substrate concentrations (300 g/L crotonic acid) tested the tolerance of AspB mutants under industrially relevant conditions; however, significant activity loss was observed. Future experiments should evaluate the impact of substrate inhibition and explore strategies to reduce it, such as stepwise substrate addition or enzyme immobilization.

The investigation of alternative amine donors and substrate concentration effects could be approached through several key studies. For amine donor optimization, a systematic screening of different amine sources could be conducted, including primary amines (methylamine, ethylamine), diamines (ethylenediamine, putrescine), and amino alcohols (ethanolamine, propanolamine). Structure-activity relationship studies would help understand how amine donor properties (size, electronic effects, pH) influence reaction rates and product formation. Additionally, kinetic studies comparing the reaction rates and binding affinities of different amine donors would provide insights into the enzyme's nucleophile preference.

Addressing the substrate concentration challenges would require a multi-faceted approach. First, detailed kinetic studies should be performed to characterize substrate inhibition, including determining Ki values, and establishing inhibition patterns. The impact of high substrate concentrations on enzyme stability could be investigated using protein stability assays (DSC, CD spectroscopy) in the presence of varying substrate concentrations. Process engineering solutions, such as fed-batch substrate addition strategies, could be developed and optimized to maintain substrate concentrations below inhibitory levels while achieving high total conversion.

Various enzyme stabilization strategies could be explored to enhance tolerance to high substrate concentrations. This might include enzyme immobilization on different support materials (resins, nanoparticles, or membranes) to provide physical protection and potentially reduce local substrate concentration effects. The use of two-phase systems or organic co-solvents could be investigated to modulate substrate availability.

Additionally, protein engineering approaches could be employed to develop variants with improved substrate tolerance, either through rational design focusing on substrate-binding regions or directed evolution with screening under high substrate conditions.

Finally, the relationship between reaction conditions and substrate inhibition should also be examined. This would involve studying how factors such as temperature, pH, ionic strength, and buffer composition influence substrate inhibition patterns. The potential use of stabilizing additives (osmolytes, surfactants) could be investigated to mitigate substrate inhibition effects. Furthermore, the development of in situ product removal strategies could help maintain favorable reaction equilibria and reduce product inhibition effects that might compound substrate inhibition challenges.

In conclusion, this chapter underscores the potential of AspB mutants for the enzymatic production of β-amino acids while highlighting the challenges associated with optimizing their activity, solubility, and substrate scope. While AspB-B19 (AspB-M1) and AspB-M2 demonstrated promising activity with crotonic acid, other mutants exhibited limited or no conversion, highlighting discrepancies between experimental results and reported literature. Advanced protein engineering strategies, coupled with rigorous reaction condition optimization and analytical techniques, are essential for bridging these gaps and fully realizing the industrial potential of AspB mutants. Future work should focus on improving enzyme stability, broadening substrate compatibility, and scaling up reactions to industrially relevant conditions, thereby paving the way for the efficient and sustainable production of β-amino acids.

4 Engineering of Pasteurella Multocida Aspartase (PmAspA) for Expanding the Commercial Production of Unnatural Amino Acids

4.1 Introduction of AspA.

In the previous chapters, the focus was placed on engineering AspB (aspartase B) from Bacillus sp. YM55-1 for the efficient synthesis of β-amino acids, alongside the exploration of novel strategies such as enzyme immobilization with MagR to improve purification and reusability. These studies demonstrated how mutagenesis, computational redesign, and immobilization could collectively enhance AspB's catalytic performance, broaden its substrate scope, and increase its applicability in industrial biotechnology. However, while AspB served as a valuable model for demonstrating proof-of-concept in β-amino acid production, its utility is restricted by limitations in substrate range, stability under certain process conditions, and incomplete mechanistic understanding.

To address these challenges, attention has turned to Aspartase A (AspA), also known as L-aspartate ammonia-lyase (EC 4.3.1.1), catalyzes the reversible deamination of L-aspartate into fumarate and ammonia. AspA has been extensively studied as a model enzyme for understanding lyase mechanisms and facilitating protein engineering. Structurally, AspA is a homotetramer, with each subunit consisting of approximately 478 amino acids, which together form a sophisticated molecular architecture. In industrial biotechnology, AspA has gained significant attention for its pivotal role in producing L-aspartic acid, a valuable precursor for numerous commercial products, including the artificial sweetener aspartame and various pharmaceutical compounds. Its natural properties, such as high substrate specificity and reasonable stability, make AspA an attractive candidate for protein engineering efforts.

Despite its industrial relevance, the precise catalytic mechanism of AspA remains elusive. Unlike other enzymes, AspA has not been found to have a catalytically essential acidic residue in its active site through mutagenesis studies, leaving significant gaps in understanding its catalytic function. Moreover, structural studies are limited, as no crystal structure of AspA complexed with its substrate or product has been resolved. This limitation has hindered detailed mechanistic insights into AspA's enzymatic activity. These unresolved questions present challenges to advancing AspA's application and optimization for industrial processes.

Recently, using approaches such as directed evolution, rational design, and computational methods, researchers have successfully enhanced the catalytic

efficiency, thermostability, and operational stability of AspB, a structurally and functionally similar aspartase. Additionally, immobilization strategies have been developed to improve aspartase reusability and stability in industrial processes, further broadening its practical applications. Given the structural and functional similarities between AspA and AspB, applying similar protein engineering techniques for AspA offers a promising avenue for expanding the enzymatic toolbox for the commercial production of unnatural amino acids. By leveraging advances in protein engineering, AspA could serve as a versatile biocatalyst in industrial biotechnology.

4.2 Selection of target AspA for engineering

The selection of Aspartase A (AspA) for protein engineering requires a systematic and rational approach to align its properties with specific functional and industrial application goals. The engineering of Aspartase B (AspB) to enhance its catalytic efficiency for non-canonical substrates, such as crotonic acid, provides a strategic blueprint for optimizing Aspartase A (AspA). AspB and AspA share evolutionary and structural homology, including a conserved TIM barrel fold, active-site architecture, and reliance on the MIO cofactor. Mutations in AspB (e.g., T189C, M323I, K326M, N328C) that improved substrate binding, steric accommodation, and intermediate stabilization offer a validated framework for AspA engineering. By aligning the sequences and structures of AspA and AspB, homologous residues can be identified—for instance, if AspB's T189 corresponds to T187 in AspA, analogous substitutions (e.g., T187C) could be introduced to replicate functional enhancements. These mutations likely modulate flexibility, hydrophobicity, or electrostatic interactions in regions critical for substrate recognition, enabling AspA to adopt similar catalytic improvements for target reactions, such as β-aminobutyric acid (BABA) synthesis.

To translate these insights into practice, a systematic approach is required. First, sequence alignment tools (e.g., Clustal Omega) and structural modeling (via PyMOL or SWISS-MODEL) should identify conserved active-site residues and their AspB-equivalent positions. For example, substituting AspA's M321I (analogous to AspB's M323I) could reduce steric hindrance for bulkier substrates, while N326C (matching AspB's N328C) might enhance nucleophilic attack during β-amino acid formation. However, AspA's unique substrate preferences—such as a natural affinity for fumarate over aspartate—necessitate adjustments. Computational tools like Rosetta or molecular dynamics (MD) simulations can predict how transplanted mutations interact with AspA's distinct electrostatic environment, ensuring compatibility. Subsequent cloning of mutants into expression vectors (e.g., tag-free pET24a) and

activity assays (e.g., HPLC for conversion rates, kinetic profiling) would validate their performance.

In this project, sequence and structural analyses form the foundation for identifying promising AspA candidates. Gene sequences of AspA variants were retrieved from the NCBI database, and sequence homology was assessed using BLAST to identify conserved regions and potential functional residues. Figure 4-1 illustrates the sequence alignment between AspA from *Pasteurella multocida* and AspB from *Bacillus sp. YM55-1*, highlighting both conserved motifs and differences that may influence enzymatic activity and stability. *Pasteurella multocida* is a Gram-negative, facultatively anaerobic bacterium known for its role as a pathogen in both animals and humans, thriving at moderate (mesophilic) temperatures of approximately 37°C. In contrast, *Bacillus sp. YM55-1* is a thermophilic bacterium isolated from hot springs, thriving at temperatures ranging from 45°C to 70°C. This organism's enzymes, such as AspB, exhibit high thermostability, making them ideal for industrial applications requiring elevated temperatures. These contrasting environmental adaptations of AspA and AspB provide valuable insights into how structural modifications can expand the applicability of AspA.

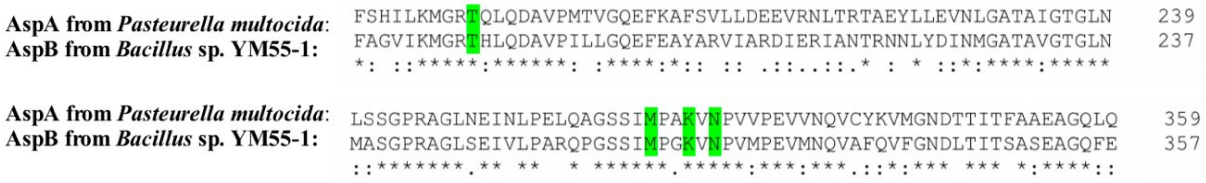

Figure 4-1 Sequence alignment of AspA from Pasteurella multocida and AspB from Bacillus sp. YM55-1.

Conserved residues between the two sequences are indicated by asterisks (*), and conserved substitutions are marked with colons (:). Specific residues highlighted in green represent targets for mutagenesis or protein engineering to investigate or enhance enzyme functionality.

To identify effective mutation sites for AspA, structural modeling tools like AlphaFold were employed to predict key functional residues and their spatial arrangement. The experimentally validated mutation points from AspB-M2—T189C, M323I, K326M, and N328C—were selected as targets for AspA engineering based on their demonstrated role in improving activity, substrate specificity, and stability in AspB. Figure 4-2 illustrates the predicted structural model of AspA with the proposed mutation sites, providing a roadmap for subsequent experimental validation.

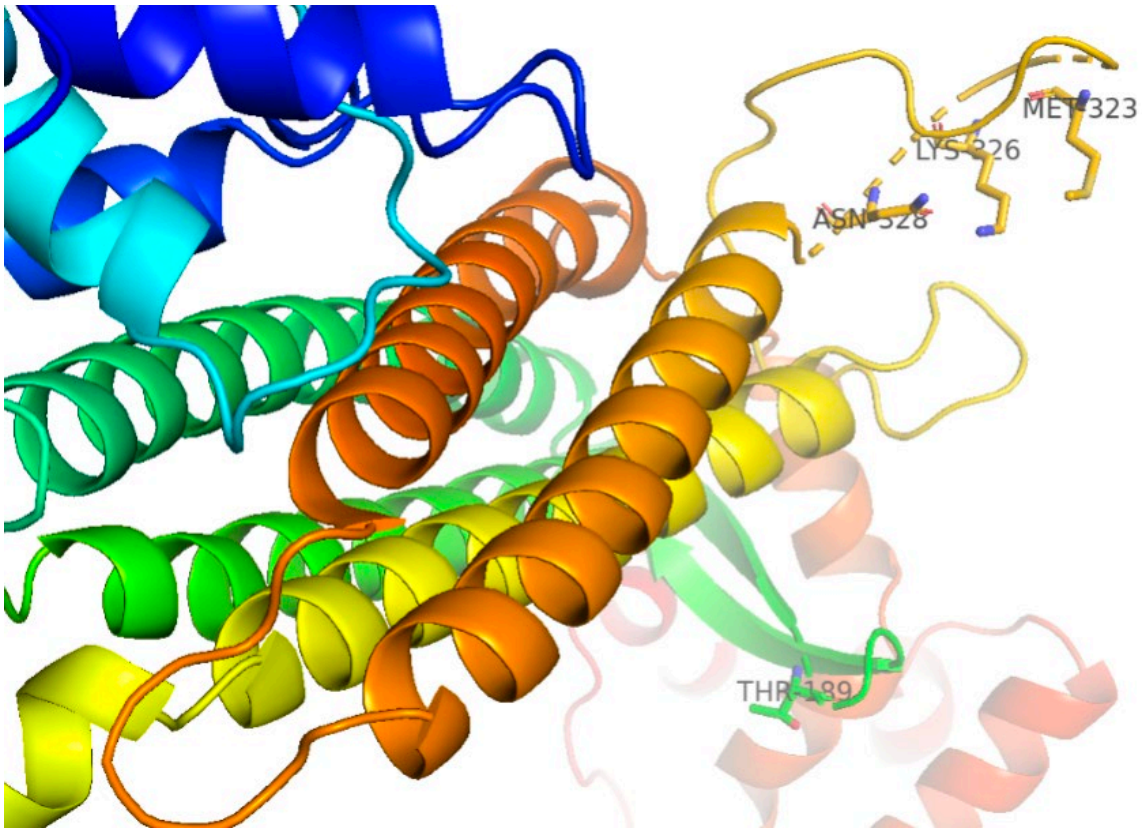

Figure 4-2 Structural prediction of Pasteurella multocida AspA (PmAspA) generated using AlphaFold predictions and visualized in PyMOL.

The structure highlights specific residues identified as potential mutation targets: Thr189, Met323, Lys326, and Asn328. These residues are labeled and shown in stick representation within the protein's secondary structure, which is depicted in a color-coded ribbon format. The positions of these residues suggest their potential importance for catalytic activity or structural integrity, making them key targets for mutagenesis and protein engineering.

4.3 Expression of selected PmAspA.

4.3.1 DNA Plasmid construction for PmAspA expression.

The gene fragment encoding PmAspA was first cloned into a pUC vector. To initiate the expression of Pasteurella multocida Aspartase A (PmAspA), plasmid construction and subsequent subcloning into an expression vector were required. The PmAspA insert (~1400 bp) was excised using NdeI and EcoRI restriction enzymes, and the

digested samples were subjected to agarose gel electrophoresis (Figure 4-3(a)). The target band corresponding to the PmAspA fragment was identified and excised. The fragment was subsequently purified using the NucleoSpin® Gel and PCR Clean-up Kit, ensuring high purity and integrity for downstream cloning and expression.

The purified PmAspA fragment was ligated into the pET24a vector, generating the pET24a-PmAspA plasmid. Following ligation, the plasmid was transformed into *E. coli* DH5α cells using the $CaCl_2$ transformation method. Colonies were selected on kanamycin-supplemented agar plates. Plasmids were extracted from selected colonies using a mini-prep kit, and successful construction of the pET24a-PmAspA plasmid was confirmed by restriction digestion with NdeI and EcoRI. Gel electrophoresis of the digested products revealed the expected band sizes of ~1400 bp for the PmAspA insert and ~5250 bp for the vector backbone (Figure 4-3(b)).

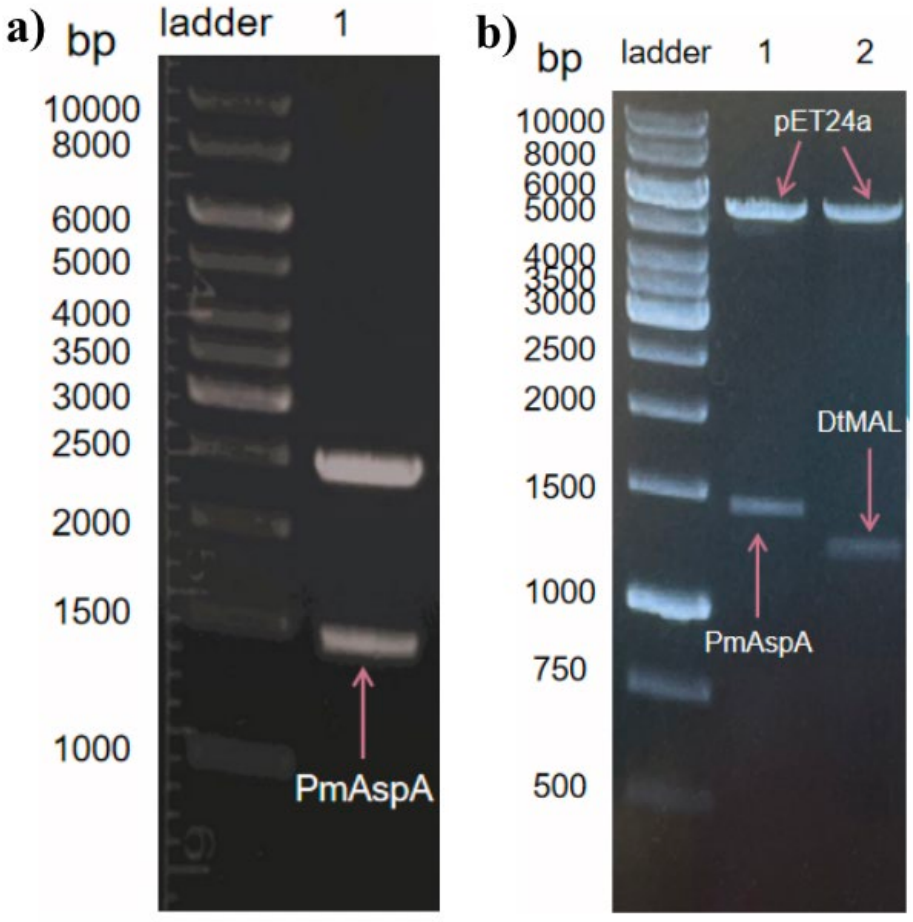

Figure 4-3 Construction of pET24a-PmAspA analysed by DNA agarose gel.

(a) Agarose gel electrophoresis of Nde I/EcoR I-digested pUC-GW-Kan-PmAspA. The single band at ~1400 bp indicates the successful excision of the PmAspA insert. Ladder: 1 kb gene ruler.

(b) Agarose gel electrophoresis of digested plasmids. Lane 1**:** *Nde I/EcoR I*-digested pET24a-PmAspA showing the ~1400 bp PmAspA insert. Lane 2: *Nde I/EcoR I*-digested pET24a-DtMAL showing the ~1250 bp DtMAL insert. Ladder: 1 kb gene ruler.

To enable downstream purification, a 6×His tag was added to the N-terminus of PmAspA using a PCR-based approach Primers PmAspA_ins_fwd and AspAMAL vet_rev were used to incorporate the His-tag sequence into the amplified product. The PCR products were treated with DpnI to digest the parental plasmid and then transformed into *E. coli* DH5α cells for selection. Successful incorporation of the His-tag was verified by gel electrophoresis, which showed the expected band sizes (Figure 4-4). This newly constructed plasmid was designated as pET24a-PmAspA-6H.

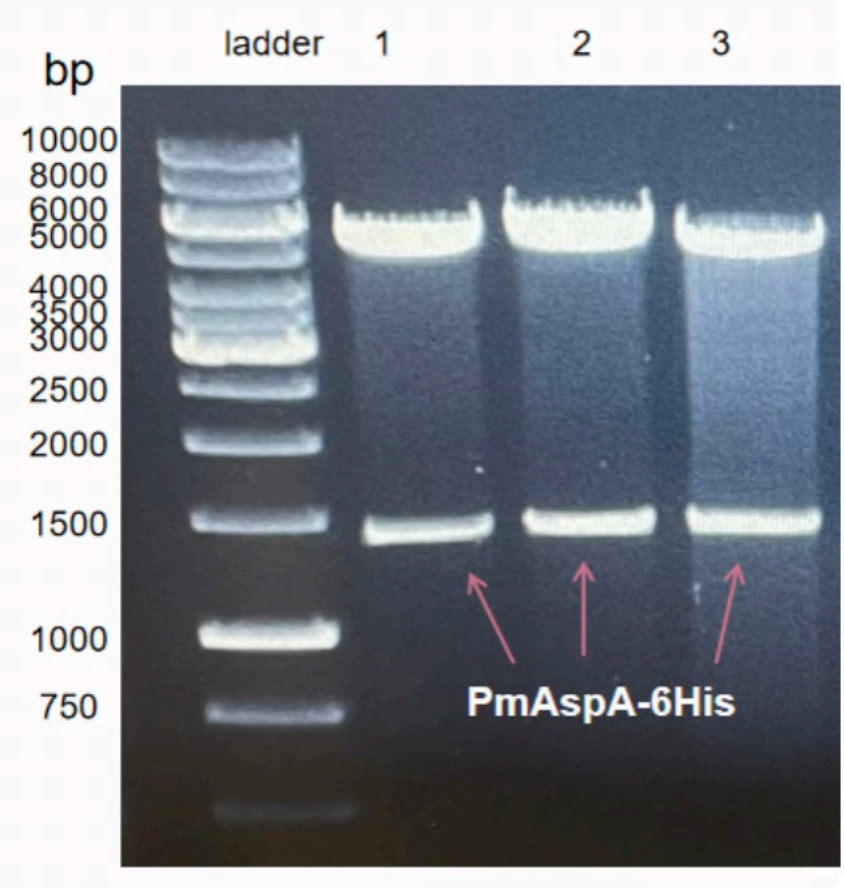

Figure 4-4 Agarose gel electrophoresis confirming the presence of the 6His-tag in pET24a-PmAspA.

Lanes 1-3: DpnI-digested PCR products transformed into *E. coli* DH5α and isolated from selected colonies. The band at ~1400 bp corresponds to the PmAspA-6His insert, confirming successful incorporation of the 6His-tag.

In parallel, a mutant version of PmAspA incorporating four targeted mutations (T189C, M323I, K326M, and N328C) and an N-terminal His-tag, was constructed. This mutant, referred to as 6H-PmAspA-QM, was excised from the pUC vector and ligated into the pET24a vector backbone. Additionally, a separate plasmid encoding DtMAL with the L384A mutation and an N-terminal His-tag (6H-DtMAL-SM) was constructed. The 6H-PmAspA-QM (~1446 bp) and 6H-DtMAL-SM (~1281 bp) inserts were ligated into the pET24a vector, producing pET24a-6H-PmAspA-QM and pET24a-6H-DtMAL-SM plasmids, respectively (Figure 4-5). The details of 6H-DtMAL-SM will be discussed in chapter 6. The ligated products were transformed into *E. coli* DH5α cells for selection.

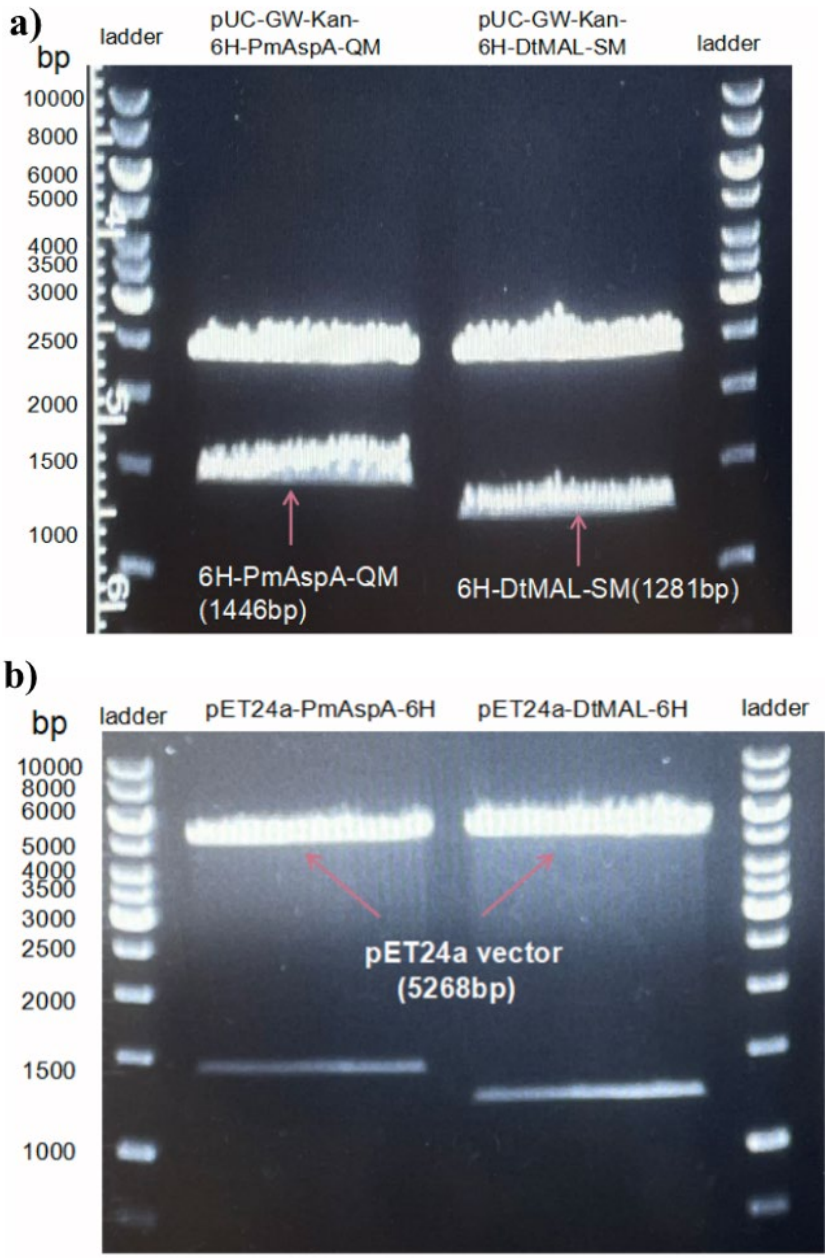

Figure 4-5 Construction of pET24a-6H-PmAspA-QM and pET24a-6H-DtMAL-SM, analysed by DNA agarose gel.

(a) Agarose gel electrophoresis showing the digested 6H-PmAspA-QM insert (~1446 bp) and 6H-DtMAL-SM insert (~1281 bp) excised from the pUC-GW-Kan plasmid using NdeI and EcoRI-HF. Lanes are labeled with the respective plasmids and band sizes.

(b) Agarose gel electrophoresis showing the digested pET24a vector (~5268 bp) prepared for ligation with the 6H-PmAspA-QM and 6H-DtMAL-SM inserts.

Plasmids from selected colonies were extracted and confirmed via restriction digestion and gel electrophoresis. As shown in Figure 4-6, distinct bands corresponding to the pET24a backbone (~5268 bp), the 6H-PmAspA-QM insert (~1446 bp, lane 1), and the 6H-DtMAL-SM insert (~1281 bp, lane 2) comfirmed the successful construction of the pET24a-6H-PmAspA-QM and pET24a-6H-DtMAL-SM plasmids. These results confirm the readiness of the plasmids for subsequent protein expression and functional analysis.

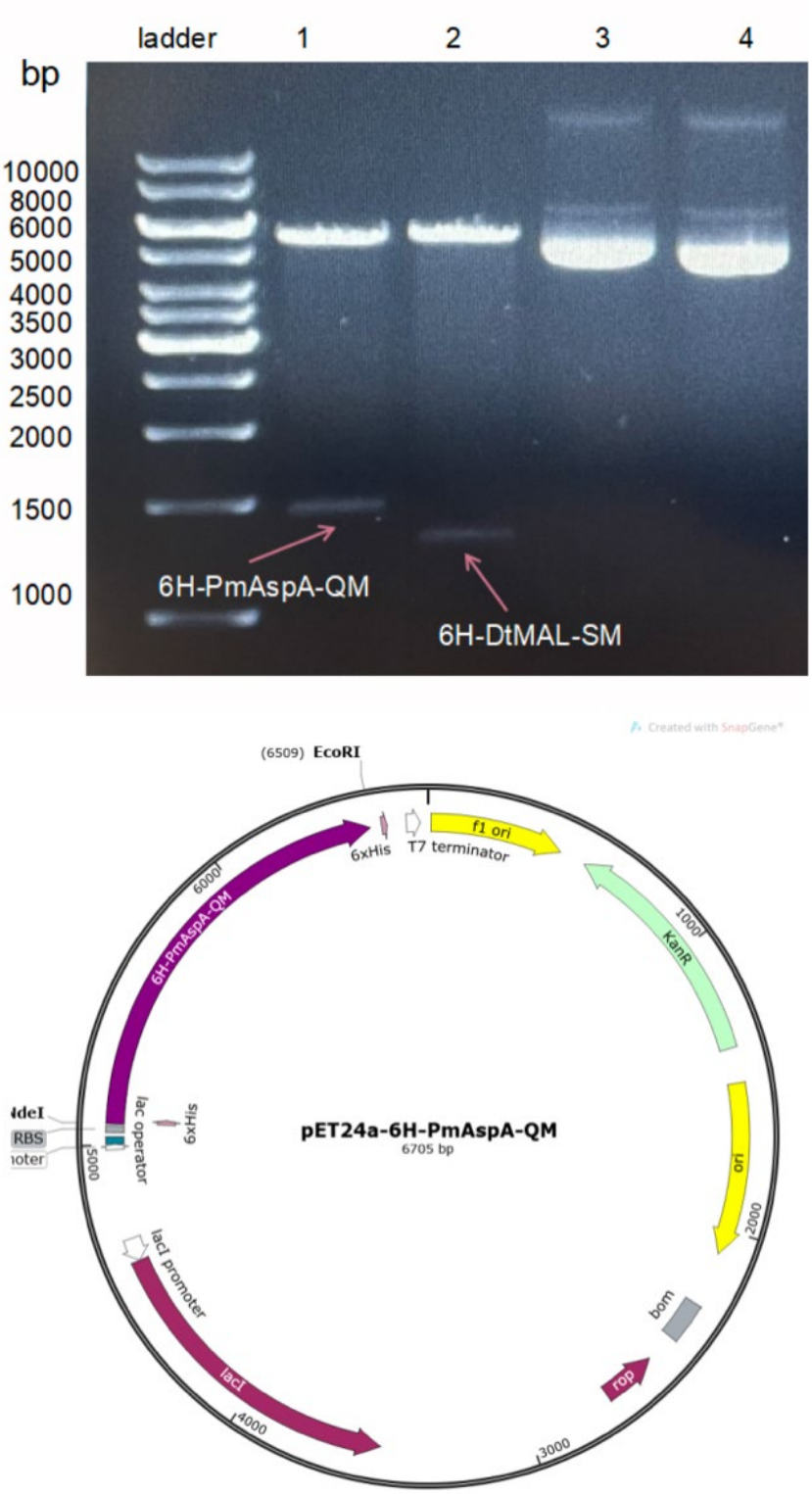

Figure 4-6 Confirmation of the pET24a-6H-PmAspA-QM and pET24a-6H-DtMAL-SM plasmids through agarose gel electrophoresis.

***Top**:* Gel electrophoresis results of digested and undigested plasmids. Lane 1: Digested pET24a-6H-PmAspA-QM showing the insert (~1446 bp) and vector backbone (~5268 bp). Lane 2: Digested pET24a-6H-DtMAL-SM showing the insert (~1281 bp) and vector backbone (~5268 bp). Lane 3: Undigested pET24a-6H-

PmAspA-QM (-ve control). Lane 4: Undigested pET24a-6H-DtMAL-SM (-ve control). ***Bottom***: Map of the pET24a-6H-PmAspA-QM plasmid showing key features, including the 6His-tag, T7 promoter, and restriction enzyme sites (NdeI and EcoRI) used for cloning and verification.

4.3.2 Expression of PmAspA and PmAspA mutant.

The expression of Pasteurella multocida Aspartase A (PmAspA) was performed in *E. coli* BL21(DE3) cells under IPTG induction. Protein expression was initiated by adding IPTG to a final concentration of either 1 mM or 0.1 mM when the bacterial culture reached an OD600 of 0.5–0.6. Following induction, the cells were harvested, and protein expression was analyzed using 10% denaturing SDS-PAGE (Figure 4.7(a)). The SDS-PAGE analysis revealed a prominent protein band at approximately 51 kDa, corresponding to the calculated molecular weight of PmAspA, thereby confirming the successful expression of PmAspA from the pET24a vector in *E. coli* BL21(DE3). Additionally, PmAspA expression was also evaluated in *E. coli* C41(DE3) cells to compare expression efficiency across strains (Figure 4.7(b)).

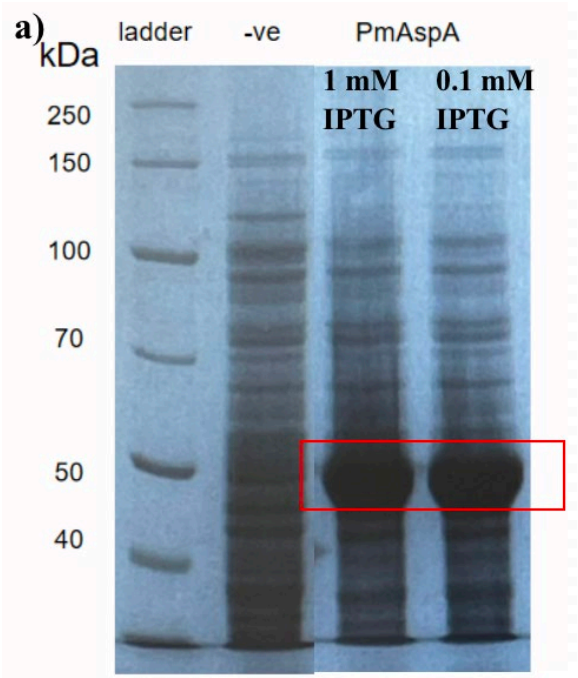

Figure 4-7 SDS-PAGE analysis of PmAspA expression under different conditions.

(a) Expression of PmAspA in *E. coli* BL21(DE3) cells induced with 1 mM and 0.1 mM IPTG. Prominent protein bands at ~51 kDa, indicated by red boxes, confirm successful expression of PmAspA under both induction conditions. (b) Expression of PmAspA in *E. coli* C41(DE3) cells induced with 1 mM IPTG. The distinct band at

~51 kDa, highlighted by the red box, shows successful expression of PmAspA in this host strain. The results demonstrate effective PmAspA expression in both BL21(DE3) and C41(DE3) strains with IPTG induction.

Furthermore, the plasmids pET24a-6H-PmAspA-QM and pET24a-6H-DtMAL-SM were transformed into *E. coli* BL21(DE3) cells using the $CaCl_2$ transformation method. SDS-PAGE analysis of the induced cultures revealed distinct protein bands for both constructs (Figure 4-8). Lane 1, representing the negative control (*E. coli* BL21(DE3) without a plasmid), showed no protein bands, confirming the specificity of the expression system. Lane 2 displayed a strong band at ~52 kDa, corresponding to the expressed 6H-PmAspA-QM protein, while Lane 3 exhibited a band at ~48 kDa, representing the expressed 6H-DtMAL-SM protein.

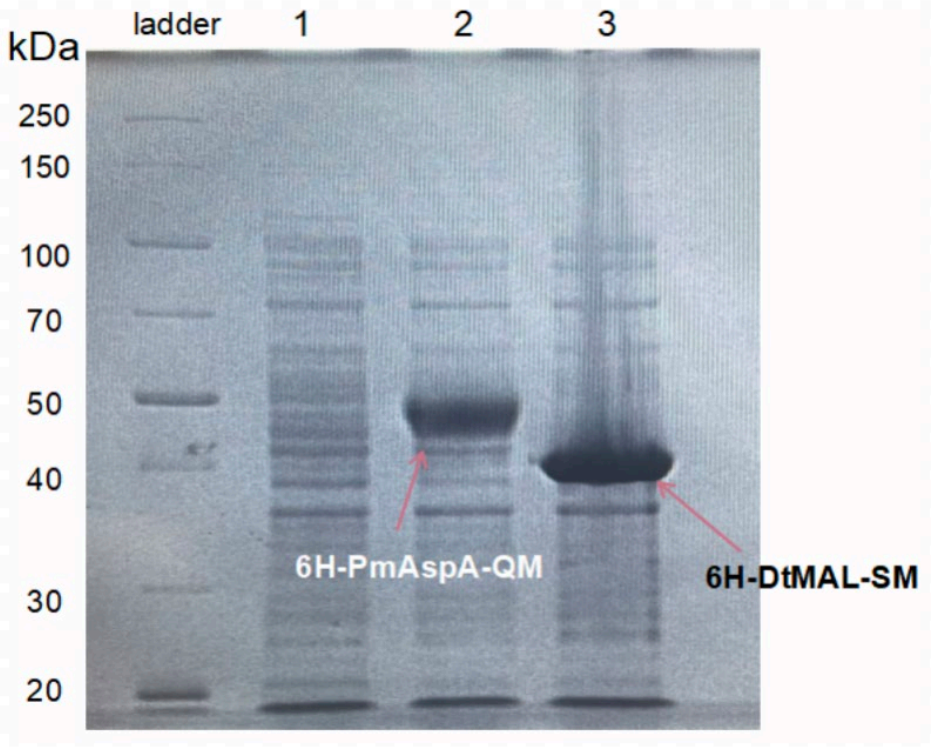

Figure 4-8 SDS-PAGE analysis of 6H-PmAspA-QM and 6H-DtMAL-SM protein expression.

From left to right, Lane 1: Negative control (*E. coli* BL21(DE3) without plasmid), showing no specific protein bands, Lane 2: Expression of 6H-PmAspA-QM, with a distinct band at ~52 kDa corresponding to its calculated molecular weight, Lane 3: Expression of 6H-DtMAL-SM, with a distinct band at ~48 kDa matching its calculated molecular weight. The PageRuler Unstained Broad Range Protein Ladder is used to estimate the molecular weights of the expressed proteins. These results

confirm the successful expression of both 6H-PmAspA-QM and 6H-DtMAL-SM in *E. coli* BL21(DE3) cells.

To summarize, this results demonstrated the successful expression of PmAspA and its mutant (6H-PmAspA-QM) in *E. coli* BL21(DE3) cells, with a clear protein yield confirmed by SDS-PAGE. The distinct molecular weights of 6H-PmAspA-QM and 6H-DtMAL-SM were consistent with their calculated values, confirming the constructs and their expression for subsequent functional and enzymatic analyses.

4.3.3 Analyzing purified PmAspA and PmAspA mutant.

The purification and analysis of 6H-PmAspA and its mutant (6H-PmAspA-QM) were performed as described in Section 2.4.4. The results confirmed the successful purification of 6H-PmAspA from an 800 mL flask culture. Chromatographic absorbance profiles showed peaks corresponding to specific fractions, with fractions 4, 8, 9, and 10 selected for further analysis (Figure 4.9(a)). These fractions were subjected to SDS-PAGE analysis, which revealed a distinct band at approximately 51 kDa, consistent with the calculated molecular weight of 6H-PmAspA. The purification effectively removed non-specific proteins, as shown by the reduction of extraneous bands in the purified fractions.

Control samples, including the unpurified protein extract and the flow-through during protein loading, were also analyzed. The unpurified sample showed a clear band corresponding to 6H-PmAspA, whereas the flow-through lacked any detectable 6H-PmAspA, indicating efficient binding of the target protein to the chromatography column (Figure 4.9(b)). These findings confirm that the selected fractions contained highly purified 6H-PmAspA, indicating the successful separation of the target protein from cellular components during purification. Following purification, the fractions underwent buffer exchange to remove imidazole and replace it with a suitable storage buffer, ensuring protein stability for downstream applications.

In addition to purifying the His-tagged wild-type PmAspA, the 6×His-tagged PmAspA mutant (6H-PmAspA-QM) was also purified and analyzed using the same protocol. Detailed data on the purification and analysis of 6H-PmAspA-QM are included in the appendix.

In summary, the successful purification of 6H-PmAspA is evidenced by multiple complementary analytical results. The chromatographic data shows distinct peaks in specific fractions (4, 8, 9, and 10), indicating controlled protein elution, while the absence of significant non-specific peaks suggests effective separation. The lack of target protein in the flow-through confirms efficient column binding. SDS-PAGE analysis further validates the purification success, showing a single distinct band at 51 kDa that matches the expected molecular weight of 6H-PmAspA. The clear contrast between the multiple bands in unpurified samples and the single band in purified fractions, along with the absence of the target protein in the flow-through, provides strong evidence for successful protein isolation.

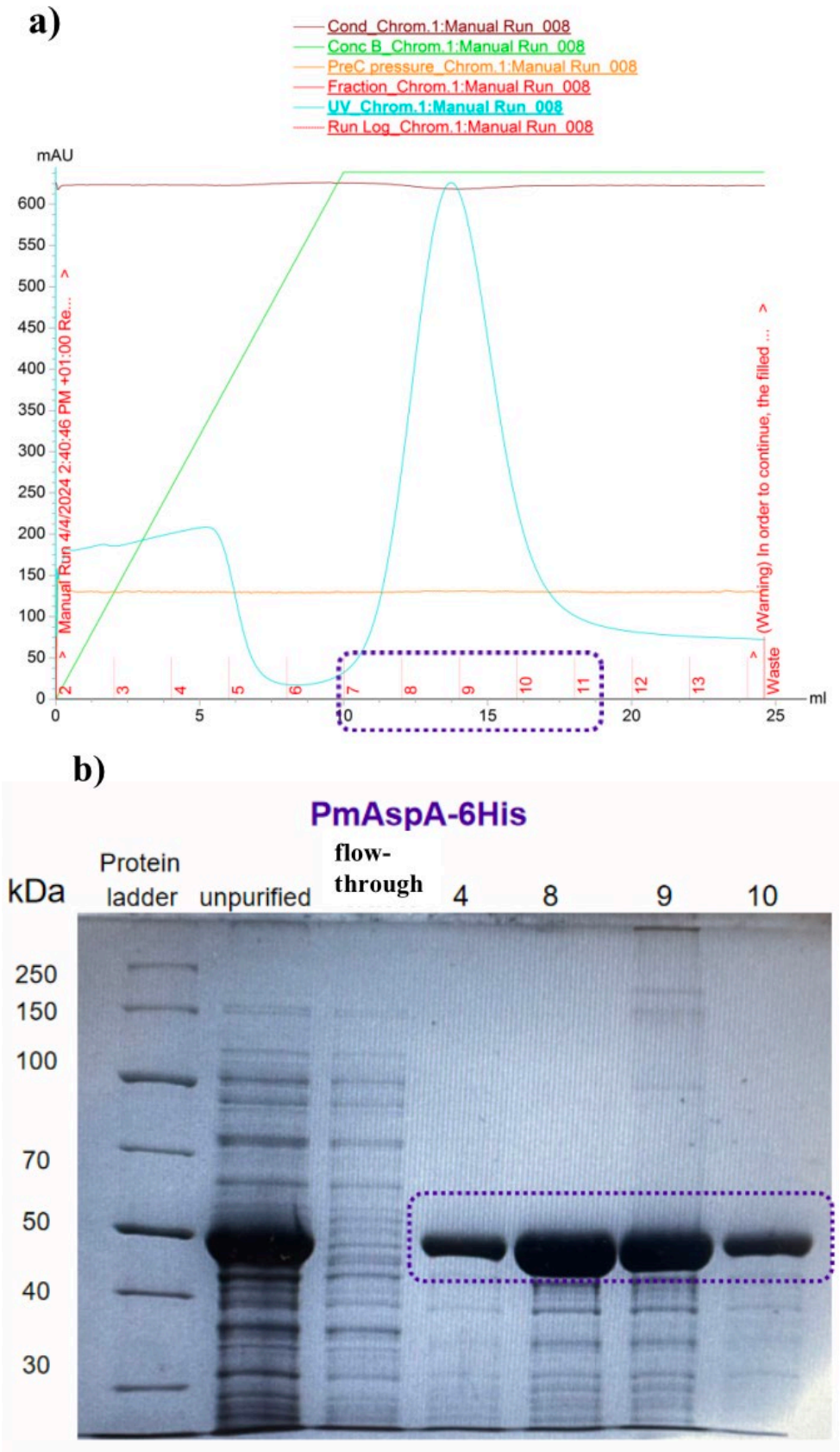

Figure 4-9 Purification and Analysis of PmAspA-6His Using HisTrap Chromatography.

(a) Chromatogram of PmAspA-6His purification using the HisTrap column on the ÄKTA Pure chromatography system. The elution profile shows peak at fractions 8–10 corresponding to the elution of PmAspA-6His under optimal conditions.

(b) SDS-PAGE analysis of fractions collected during purification. Lane 1: Protein ladder; Lane 2: Unpurified PmAspA; Lane 3: Flow-through. Lanes 4, 8, 9, and 10: Eluted fractions corresponding to the peak in the chromatogram. A clear band at ~51 kDa confirms the successful purification of PmAspA-6His.

The results validate the expression and purification of PmAspA-6His, with the calculated molecular weight aligning with the observed protein band.

4.4 The enzymatic activity assay of purified PmAspA and PmAspA-QM

The enzymatic activity of the purified wild-type PmAspA-6His and the mutant 6H-PmAspA-QM was assessed using fumaric acid, crotonic acid, and caffeic acid as substrates (final concentration: 10 mM) at 30°C over 24 hours. Substrate conversion was monitored spectrophotometrically by measuring the decrease in absorbance at 235 nm (Figure 4-10). For PmAspA-6His, significant enzymatic activity was observed with fumaric acid, resulting in near-complete conversion. In contrast, no measurable activity was observed for crotonic acid, as indicated by a stable OD235, while moderate conversion was detected for caffeic acid. For PmAspA, the initial specific activity (0–3 h, OD_{600}= 0.5) was 0.148 $\Delta OD_{235} \cdot h^{-1}$ for fumaric acid, 0.009 $\Delta OD_{235} \cdot h^{-1}$ for crotonic acid, and 0.028 $\Delta OD_{235} \cdot h^{-1}$ for caffeic acid. In contrast, 6H-PmAspA-QM displayed markedly altered substrate preferences, with fumaric acid activity reduced to 0.019 $\Delta OD_{235} \cdot h^{-1}$ (≈8-fold decrease), crotonic acid activity increased to 0.024 $\Delta OD_{235} \cdot h^{-1}$ (≈2.7-fold enhancement), and caffeic acid activity remaining comparable at 0.031 $\Delta OD_{235} \cdot h^{-1}$ (≈1.1-fold change). These results indicate that the 6H-PmAspA-QM mutations substantially reprogrammed enzyme specificity, shifting catalytic efficiency away from fumaric acid and toward crotonic acid, while maintaining baseline activity toward caffeic acid.

These results indicate that PmAspA-6His exhibits high specificity for fumaric acid, with lower catalytic efficiency for caffeic acid and no activity for crotonic acid under the tested conditions, reflects the enzyme's structural and mechanistic specialization.

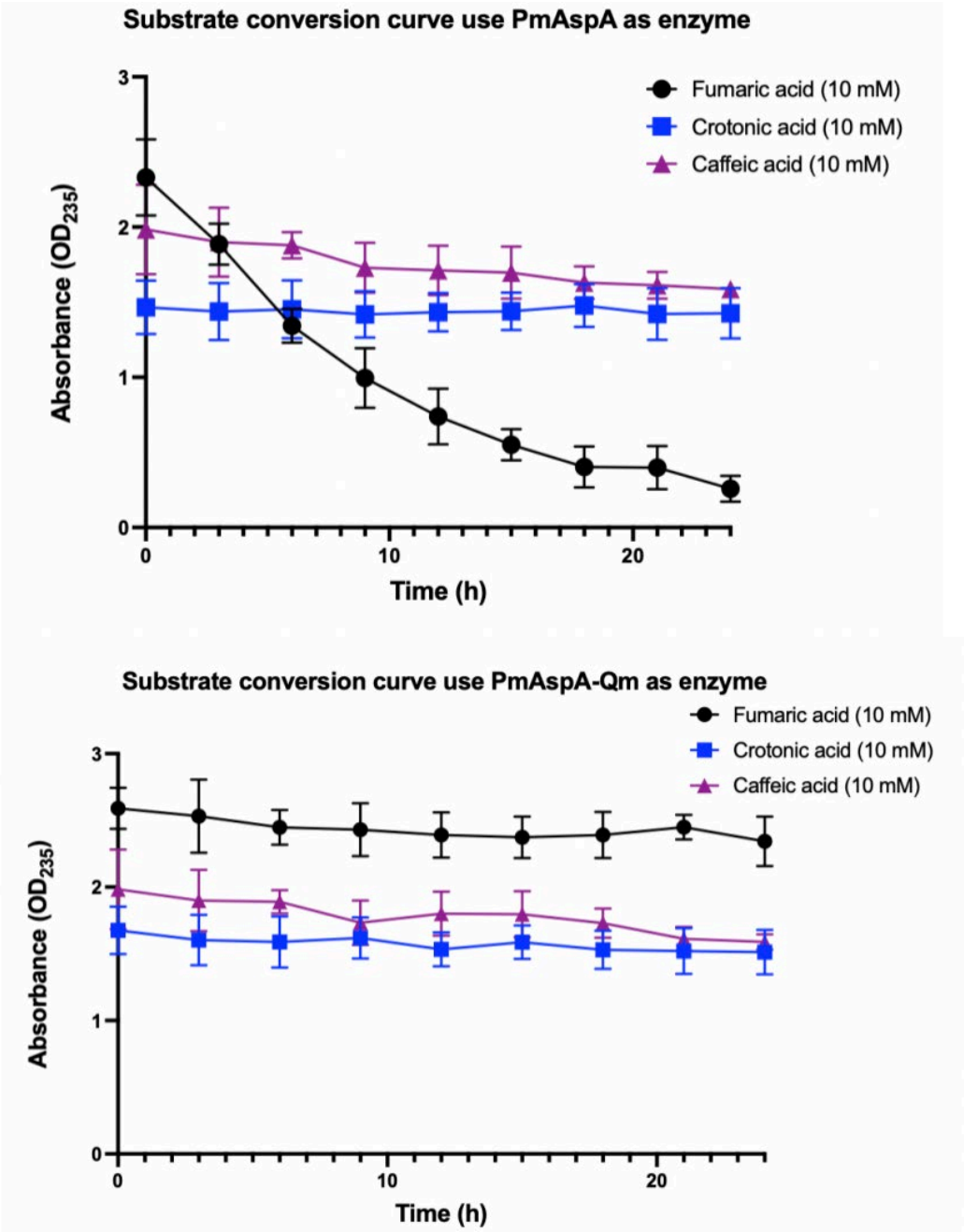

Figure 4-10 Substrate conversion curves of fumaric acid, crotonic acid, and caffeic acid using PmAspA and PmAspA-Qm as enzymes.

Conversion was monitored at OD_{235} (mean ± SD, n = 3). Top: PmAspA shows near-complete conversion of fumaric acid, while crotonic and caffeic acids remain largely unchanged. Bottom: PmAspA-Qm exhibits reduced conversion of fumaric acid but increased activity toward crotonic acid; caffeic acid remains mostly unchanged.

Fumaric acid, a natural α,β-unsaturated dicarboxylic acid, aligns precisely with the active-site architecture of aspartases like PmAspA. The enzyme's catalytic machinery—including conserved residues and the MIO (4-methylideneimidazole-5-

one) cofactor—evolved to stabilize substrates with two carboxyl groups, enabling optimal positioning for β-elimination reactions. The dual carboxyl moieties of fumaric acid likely engage in hydrogen bonding with key active-site residues (e.g., arginine or lysine side chains), while its planar trans-configuration fits snugly within the hydrophobic pocket, facilitating efficient deamination or related transformations. This structural complementarity explains the near-complete conversion observed with fumaric acid under the tested conditions.

In contrast, caffeic acid—which retains the α,β-unsaturated carboxylate motif but incorporates a bulky phenolic hydroxyl group—experiences steric and electronic mismatches within the active site. The hydroxyl group may clash with residues lining the substrate-binding pocket, displacing the molecule from its ideal catalytic orientation. Additionally, the electron-donating nature of the hydroxyl group could alter the electronic environment of the double bond, reducing its susceptibility to nucleophilic attack by the MIO cofactor. These factors collectively diminish catalytic efficiency, resulting in partial but measurable conversion.

The complete lack of activity with crotonic acid underscores the enzyme's stringent requirement for dicarboxylic substrates. As a monocarboxylic acid with a shorter carbon chain, crotonic acid cannot form the critical electrostatic interactions necessary for substrate anchoring. The absence of a second carboxyl group prevents engagement with residues that typically stabilize the transition state, leaving the α,β-unsaturated bond improperly aligned for catalysis. Furthermore, the shorter chain length may position the reactive double bond too far from the MIO cofactor, rendering the enzyme incapable of initiating the reaction.

The mutant 6H-PmAspA-QM exhibited distinct substrate specificity compared to the wild type. While fumaric acid conversion was greatly reduced, as evidenced by a minimal decrease in OD235, crotonic acid showed a reduction in OD235, indicating enhanced enzymatic activity toward this substrate. Caffeic acid activity remained negligible, similar to that of the wild type. These observations suggest that the engineered PmAspA-QM displays altered substrate preferences, shifting its activity away from fumaric acid toward crotonic acid. Fumaric acid, the wild-type enzyme's natural substrate, is a dicarboxylic acid with a rigid, planar structure. The mutations in 6H-PmAspA-QM likely disrupted key interactions critical for binding dicarboxylic acids and the mutant's active site may have reduced flexibility, impairing its ability to accommodate fumaric acid's rigid geometry. On the other hand, crotonic acid, a monocarboxylic acid with a shorter carbon chain, benefits from structural adjustments in the mutant. Mutations (e.g., replacing polar residues with nonpolar ones like valine or isoleucine) may have created a more hydrophobic environment, favoring crotonic acid's aliphatic chain. Additionally, the active site might have been reshaped to better accommodate monocarboxylic acids by removing residues that previously required a

second carboxyl group for binding. However, caffeic acid's phenolic hydroxyl group remains incompatible with both wild-type and mutant enzymes may due to the bulky hydroxyl group cannot fit within the active site, even after mutations and the electron-rich hydroxyl group may disrupt charge complementarity or interfere with MIO-mediated catalysis.

Complementary insights were provided by ^{1}H NMR spectroscopy. For PmAspA-6His, the conversion of 100 mM fumaric acid to aspartic acid at 30°C was rapid and complete (Figure 4-11). Before enzyme addition, the spectrum displayed characteristic peaks of fumaric acid at δ6.6 ppm. Within 5 minutes of adding the enzyme, these peaks diminished significantly, with new peaks at δ3.4 ppm and δ2.8 ppm corresponding to aspartic acid. By 30 minutes, the fumaric acid peaks had disappeared entirely, confirming complete conversion. In contrast, for 6H-PmAspA-QM, fumaric acid conversion was slower (Figure 4-12). After 12 hours, a reduction in fumaric acid peaks was observed, accompanied by emerging aspartic acid peaks at δ3.4 ppm and δ2.8 ppm. By 24 hours, substantial conversion was evident, though not complete.

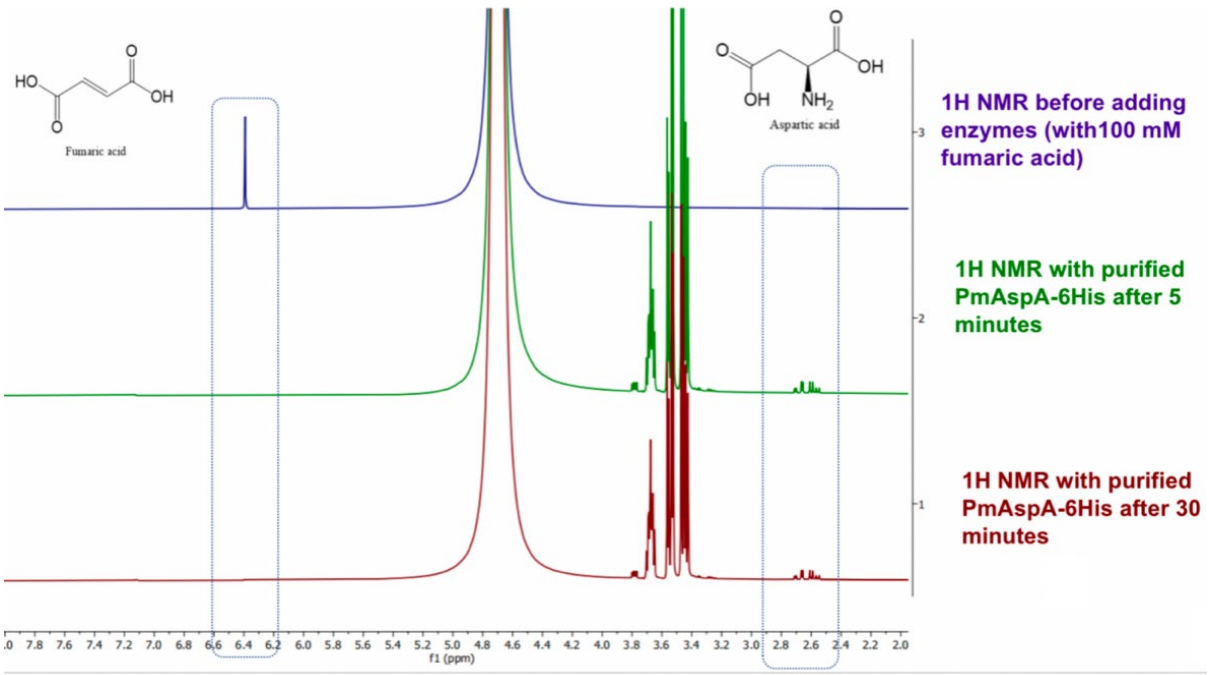

Figure 4-11 Rapid conversion of fumaric acid to aspartic acid by purified PmAspA-6His monitored via 1H NMR at 30°C.

The ^{1}H NMR spectra illustrate the enzymatic conversion of 100 mM fumaric acid to aspartic acid by purified PmAspA-6His at 30°C. The purple spectrum represents the initial fumaric acid solution, showing characteristic peaks at δ6.6 ppm. Green spectrum represents the conversion reaction started after 5 minutes. Red spectrum

represents the conversion reaction started after 30 minutes, confirming complete substrate conversion.

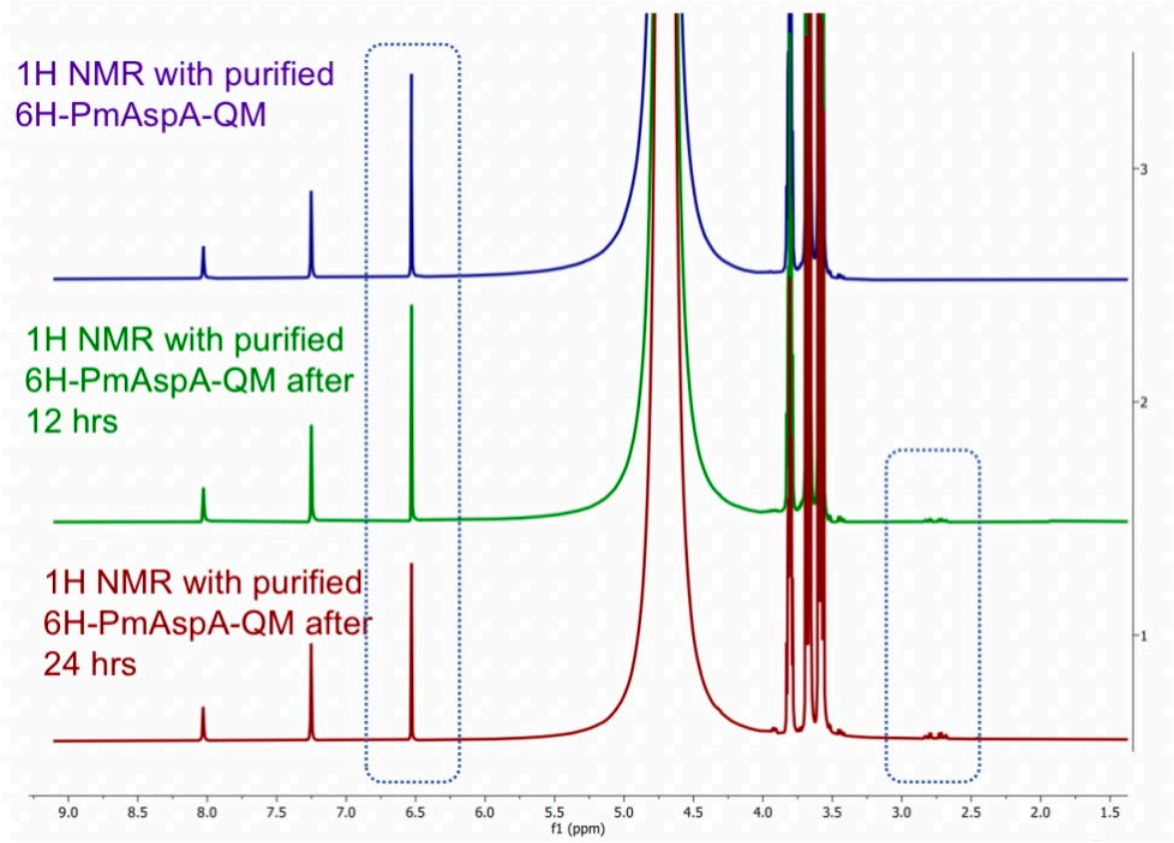

Figure 4-12 Conversion of fumaric acid to aspartic acid by purified 6H-PmAspA-QM monitored via 1H NMR at 30°C.

The blue spectrum represents the initial reaction containing fumaric acid, showing characteristic peaks at δ6.6 ppm. After 12 hours (green spectrum), a reduction in fumaric acid peaks is observed, along with the emergence of new peaks at δ3.4 ppm and δ2.8 ppm, corresponding to aspartic acid. By 24 hours (red spectrum), the fumaric acid peaks have degreased, with increased aspartic acid peaks confirming substrate conversion.

The enzymatic activity of 6H-PmAspA-QM with crotonic acid and caffeic acid was also evaluated using ^{1}H NMR (Figure 4-13 and Figure 4-14). The spectra revealed structural changes in the substrates over time, indicating enzymatic conversion. These results further highlight the shift in substrate specificity introduced by the engineered mutations in PmAspA-QM. Together, the spectrophotometric and NMR analyses

demonstrate the potential for utilizing PmAspA-QM in reactions requiring activity toward crotonic acid, complementing the wild type's strong activity for fumaric acid.

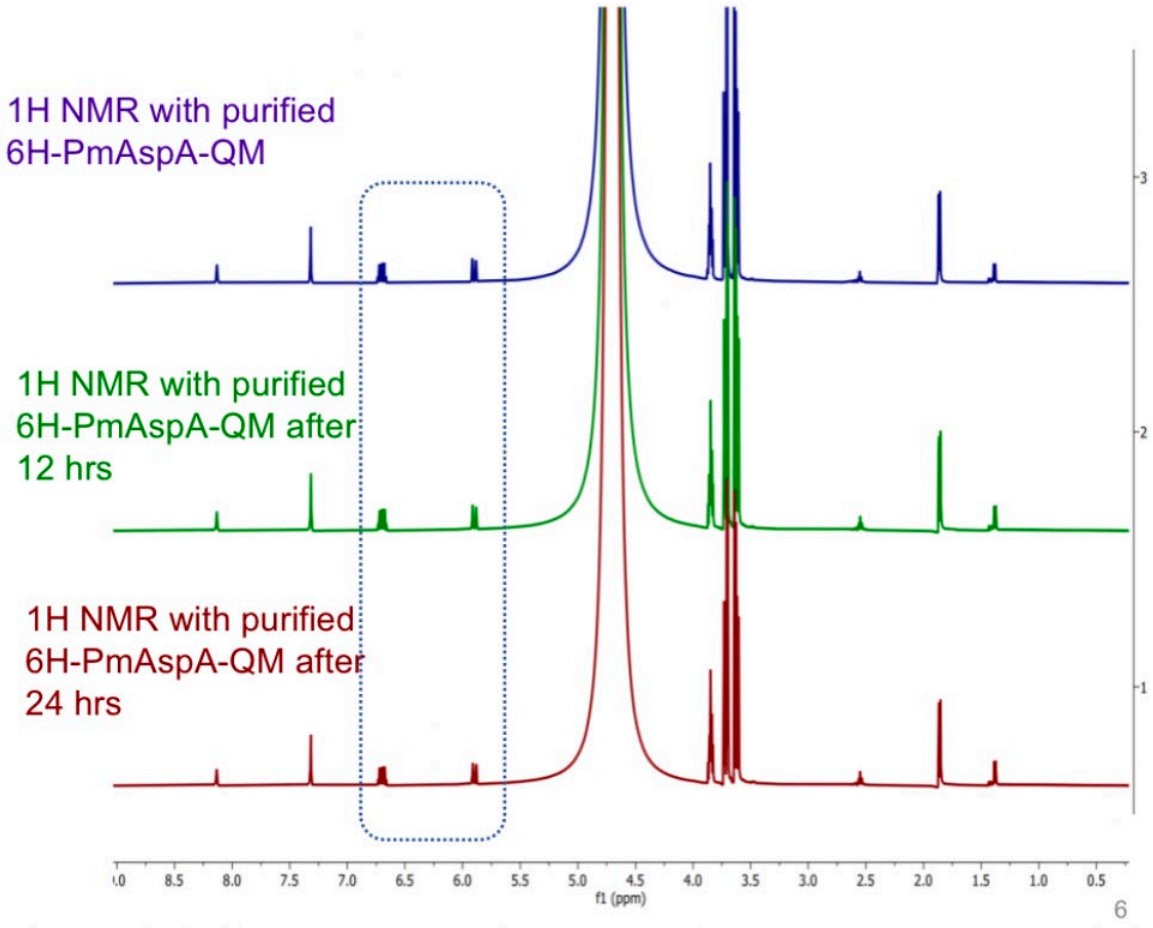

Figure 4-13 Conversion of crotonic acid to R-BABA by purified 6H-PmAspA-QM monitored via 1H NMR at 30°C.

Blue spectrum: The initial reaction containing crotonic acid. Green spectrum: The reaction after 12 hours. Green spectrum: The reaction after 24 hours. The peaks highlighted represent the present of crotonic acid.

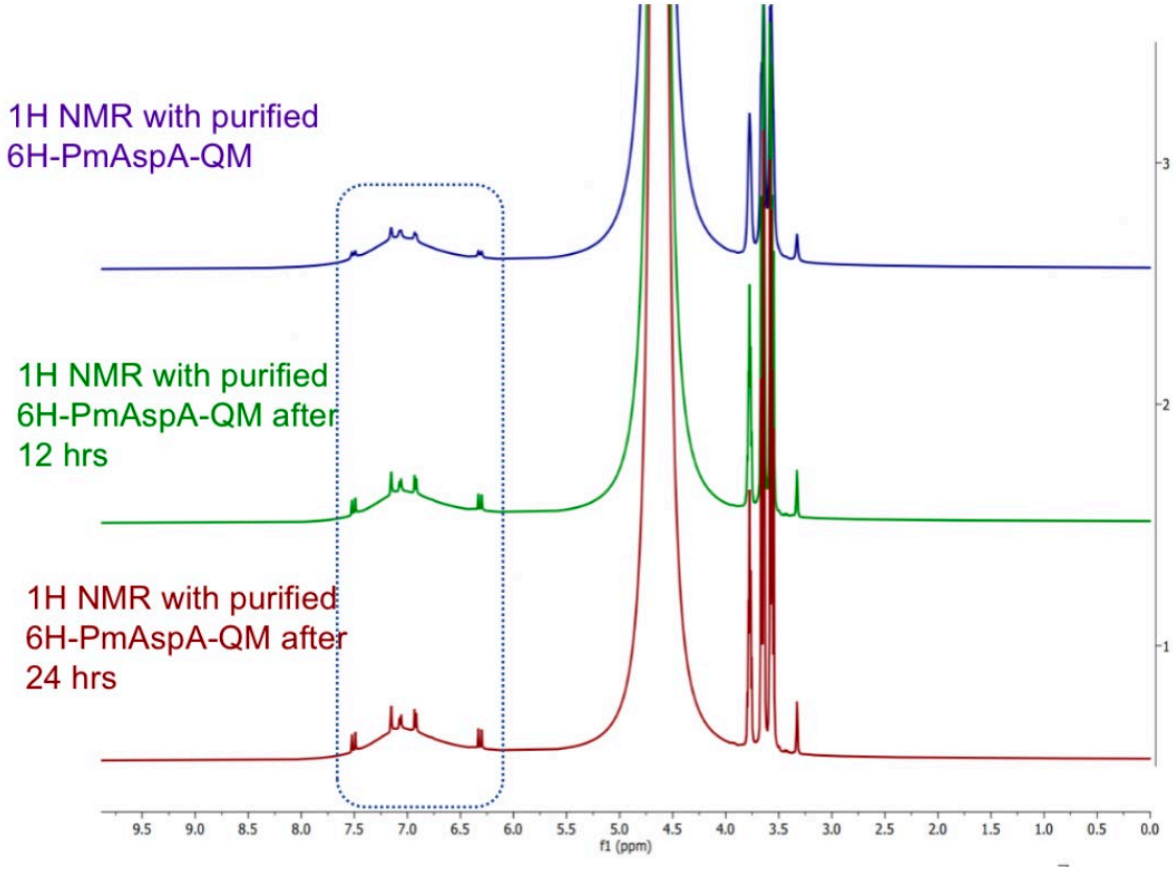

Figure 4-14 Conversion of caffeic acid by purified 6H-PmAspA-QM monitored via 1H NMR at 30°C.

Blue spectrum: The initial reaction containing crotonic acid. Green spectrum: The reaction after 12 hours. Green spectrum: The reaction after 24 hours. The peaks highlighted represent the present of caffeic acid.

4.5 Discussion and conclusion

4.5.1 Engineering of PmAspA for Enhanced Catalysis.

In this study, targeted mutations were introduced into the PmAspA active site and surface regions, inspired by analogous engineering efforts on AspB from *Bacillus sp.* YM55-1. The wild-type PmAspA-6His exhibited high catalytic efficiency and substrate specificity for fumaric acid, consistent with its natural role in nitrogen metabolism. However, the engineered mutant 6H-PmAspA-QM exhibited altered substrate preferences, shifting its catalytic activity toward crotonic acid, a substrate relevant to β-amino acid synthesis. This shift highlights the potential of rational design to tailor enzyme specificity, a critical factor in expanding the enzymatic repertoire for industrial applications.

Despite these advances, the reduced activity of PmAspA-QM toward fumaric acid raises questions about the balance between catalytic efficiency and substrate specificity when multiple mutations are introduced. Therefore, compensatory mutations could be introduced to restore critical interactions with fumaric acid without sacrificing gains in crotonic acid activity. For example, reintroducing polar residues (e.g., arginine or lysine) near the active site could stabilize the second carboxyl group of fumaric acid, while retaining hydrophobic substitutions that favor crotonic acid binding. Computational tools like Rosetta or FoldX could predict mutations that broaden substrate tolerance, enabling the design of bifunctional variants capable of processing both substrates. Concurrently, pH- or temperature-sensitive mutations might allow dynamic control over substrate preference, tailoring enzyme activity to specific industrial conditions.

Additionally, the limited activity toward caffeic acid underscores the need for further optimization to enhance compatibility with structurally diverse substrates. Expanding activity toward caffeic acid requires remodeling the active site to accommodate its bulky phenolic hydroxyl group. Saturation mutagenesis targeting flexible loops near the substrate entrance could create space for the hydroxyl moiety, while introducing polar residues (e.g., serine or aspartate) might hydrogen-bond with the group, improving alignment with the MIO cofactor. Additionally, chemical protection of the hydroxyl group (e.g., methyl ether derivatives) could bypass steric clashes, enabling preliminary catalysis assays to guide further enzyme engineering. Co-optimizing the MIO cofactor environment—through mutations to adjacent histidine or tyrosine residues—might further stabilize intermediates derived from caffeic acid, enhancing catalytic efficiency.

Structural and computational approaches are critical to overcome these limitations. Resolving the crystal or cryo-EM structures of PmAspA-QM bound to fumaric and crotonic acid would reveal how mutations distort substrate binding or cofactor positioning. Molecular dynamics simulations could identify residues causing steric hindrance or poor transition-state stabilization, informing targeted redesigns. Machine learning models trained on aspartase mutation libraries might predict "silent" mutations that mitigate destabilizing effects, balancing specificity and activity. In addition to this, high-throughput screening methods, such as directed evolution coupled with microfluidic droplet assays, could accelerate the discovery of variants with enhanced multi-substrate activity. Error-prone PCR or DNA shuffling followed by selection under dual-substrate conditions (fumaric + crotonic acid) might yield enzymes that retain broad specificity. For industrial scalability, immobilizing PmAspA-QM on magnetic nanoparticles or mesoporous silica could enhance stability and reusability, while fed-batch fermentation strategies could optimize enzyme yield under large-scale production.

Finally, collaboration with AI-driven platforms (e.g., Ginkgo Bioworks) or enzyme engineering consortia could expedite the design-test-build cycle, leveraging synthetic biology tools to prototype and validate multi-functional variants. By integrating these strategies, PmAspA-QM could evolve into a versatile biocatalyst, bridging natural and non-canonical substrate conversion while aligning with industrial demands for sustainable, high-efficiency processes.

4.5.2 Implications and future directions.

To summarize, this chapter underscores the feasibility and challenges of engineering PmAspA as a versatile biocatalyst for producing unnatural amino acids. This study successfully demonstrated the expression, purification, and characterization of both wild-type and mutant PmAspA enzymes. While the wild-type enzyme exhibited high specificity for fumaric acid, the engineered PmAspA-QM mutant displayed enhanced activity toward crotonic acid, indicating the potential of rational design to alter enzymatic properties. Nevertheless, the limited activity toward structurally complex substrates and the reduced efficiency of the mutant for fumaric acid highlight areas for further improvement. By integrating structural insights, directed evolution, and process engineering, future studies can unlock the full potential of PmAspA.

To address the gaps identified in this study, several future research directions are proposed. Solving high-resolution crystal structures of PmAspA mutants with bound substrates or transition-state analogs could provide critical insights into the molecular basis of their altered catalytic activity. These structural studies, complemented by molecular dynamics simulations, would enhance our understanding of enzyme flexibility and active-site dynamics, paving the way for more targeted engineering strategies. Additionally, combining rational design with directed evolution presents a promising approach to identifying beneficial mutations that extend beyond those tested in this study. Screening diverse libraries of PmAspA variants under varied conditions could uncover mutations that enhance both catalytic activity and stability across a broader range of substrates. To effectively screen PmAspA variant libraries, a comprehensive approach combining multiple library generation methods is essential. The libraries can be created through site-saturation mutagenesis targeting active site residues, error-prone PCR for random mutagenesis, DNA shuffling with homologous AspA genes, and combinatorial incorporation of beneficial mutations. These diverse approaches ensure broad coverage of possible beneficial variants. The screening process should utilize high-throughput methods including colorimetric assays measuring fumarate production, pH-sensitive indicators for ammonia release, growth complementation in AspA-deficient strains, and fluorescence-based activity sensors. These methods enable rapid evaluation of large variant populations under different conditions, maximizing the chances of identifying improved variants. A systematic

screening matrix should be implemented varying key parameters such as temperature (25-60°C), pH (5.0-9.0), substrate concentrations, ionic strengths, and the presence of organic solvents. Stability assessment should include thermal denaturation monitoring, long-term storage stability testing, resistance to chemical denaturants, and activity retention after multiple cycles. The substrate scope testing should encompass various amino acids beyond aspartate, structural analogs of fumarate, non-natural amino acids, and β-substituted aspartate derivatives. This broad substrate testing would help identify variants with expanded catalytic capabilities while maintaining stability, ultimately leading to enzymes with improved industrial applicability.

To improve the operational stability and reusability of PmAspA mutants, immobilization strategies should be explored. For example, covalent binding to functionalized supports, entrapment in matrices, formation of cross-linked enzyme aggregates, physical adsorption on porous materials, and magnetic nanoparticle conjugation all offer distinct advantages for enzyme stabilization and recovery. These immobilization methods can be optimized based on the specific reaction conditions and substrate requirements. On top of that, integration into continuous-flow processes represents a crucial step toward industrial scalability. This can be accomplished through packed-bed reactors with immobilized enzyme columns, membrane reactors with enzyme-functionalized surfaces, and microfluidic systems. In-line monitoring systems can track product formation and substrate conversion in real-time, while process parameters can be continuously optimized to maintain peak efficiency and reduce production costs.

Furthermore, synergistic mutations require a sophisticated approach combining multiple strategies. Combinatorial libraries incorporating beneficial mutations from both crotonic and caffeic acid-active variants can be created, supported by machine learning-guided prediction of effective combinations. Structure-guided design focusing on substrate binding pocket flexibility, coupled with stability engineering, ensures maintained activity across multiple substrates under industrial conditions.

Expansion of substrate scope focuses on industrially relevant compounds can also be explored. This includes various unsaturated carboxylic acids like acrylic acid and cinnamic acid derivatives, phenolic compounds such as p-coumaric and ferulic acid, and halogenated derivatives of existing substrates. Testing branched-chain α,β-unsaturated acids and novel β-amino acid precursors provides valuable insights into enzyme versatility and potential industrial applications, while deepening our understanding of structure-activity relationships.

Additionally, more comprehensive protein characterization could be implemented in the future, including Western blot analysis to confirm His-tag presence, mass spectrometry for precise molecular weight determination, size exclusion chromatography to assess protein oligomerization state, and dynamic light scattering

to verify protein homogeneity. The purification process itself could be optimized by fine-tuning the imidazole concentration gradient, testing different column materials and binding conditions, adding complementary purification steps such as ion exchange chromatography, and evaluating various buffer compositions for improved stability.

Quality assessment could be strengthened through multiple approaches. This includes measuring the specific activity of the purified enzyme, determining protein concentration using multiple methods (Bradford, BCA, A280), assessing long-term stability under different storage conditions, and conducting thermal stability analysis. Process documentation could be enhanced by calculating purification yield and recovery percentages, including detailed protein purity analysis, documenting batch-to-batch variability, and performing comprehensive stability studies during buffer exchange.

Alternative approaches could also be explored, such as testing different protein tags (Strep-tag, FLAG-tag). Strep-tag II offers high specificity with mild elution conditions using biotin, while FLAG-tag utilizes calcium-dependent binding with EDTA elution. The traditional His6-tag remains valuable for IMAC purification, though placement must be optimized to prevent activity interference. Twin-Strep-tag provides enhanced binding affinity for challenging proteins, and split-tag systems combining His-tag with Strep-tag can achieve superior purity levels through tandem purification.

Finally, evaluating various expression systems may achieving a higher yield, exploring different cell lysis methods, and considering automated purification systems for better reproducibility. Automated purification systems, particularly ÄKTA platforms, can significantly improve reproducibility through standardized protocols. The system setup includes programmed methods with defined gradient profiles, automated sample loading, and comprehensive monitoring of UV, conductivity, and pressure parameters. Method development focuses on establishing cleaning protocols, creating reusable templates for different tags, and implementing automated column regeneration procedures. Quality control in automated purification relies on real-time monitoring systems and automated peak detection with fraction collection. Integration with analytical tools enables continuous assessment of purification quality, while digital data recording facilitates trend analysis. Process optimization incorporates standardized buffer preparation, regular column performance monitoring, and automated method optimization routines to maintain consistency across purification runs. Documentation plays a crucial role in maintaining reproducibility, with electronic batch records and automated report generation providing detailed process tracking. Trend analysis helps identify potential issues early, while equipment maintenance logs ensure system reliability. This comprehensive approach to

automated purification ensures consistent protein quality and yield across multiple purification runs.

5 Engineering of Methylaspartate Ammonia Lyase (MAL) for Asymmetric Synthesis of Unnatural Amino Acids.

5.1 Introduction of MAL.

The preceding chapters demonstrated how AspB (aspartase B) and AspA (aspartase A) can be engineered to expand their substrate scope, enabling the sustainable synthesis of β-amino acids and other non-natural amino acids. These studies suggested the value of leveraging natural enzyme promiscuity and applying targeted mutagenesis, computational design, and immobilization strategies to improve enzyme stability, activity, and industrial applicability. Building on this foundation, the focus of this chapter shifts to Methylaspartate Ammonia Lyase (MAL), another member of the ammonia lyase family with complementary catalytic potential.

Methylaspartate Ammonia Lyase (MAL) is an enzyme that facilitates the reversible addition of ammonia to mesaconate, producing L-threo-(2S,3S)-3-methylaspartate. As a member of the lyase family, specifically the ammonia lyases, MAL catalyzes the elimination of ammonia from substrates and plays a critical role in the glutamate fermentation pathways of certain bacteria, particularly *Clostridium tetanomorphum*. This enzyme has garnered significant interest in biocatalysis, particularly due to its engineered variants, which exhibit an expanded substrate scope for the asymmetric synthesis of β-substituted aspartic acids.

The natural substrate promiscuity of wild-type MAL provides a foundation for engineering efforts that further enhance its versatility. Structure-guided engineering has pinpointed several active-site residues crucial for substrate specificity, with mutations at position Q73 demonstrating notable effects on enzyme activity (Raj, Szymański et al. 2012). For example, the Q73A variant has exhibited increased activity toward various structurally diverse linear and cyclic alkylamines, with distinct substituents at the C2 position. Another impactful mutation, L384A, expands the active site to accommodate bulkier substrates, including various fumarate derivatives while preserving the enzyme's stereoselectivity. Combining mutations, such as the H194A/L384A double mutant, has further extended the enzyme's capabilities, enabling it to process substrates with aromatic β-position substituents that wild-type MAL cannot efficiently handle.

These engineered MAL variants, particularly from *Clostridium tetanomorphum*, demonstrate the ability to accept a wide range of substrates to produce non-natural amino acids, a feature that holds considerable promise for synthesizing pharmaceutical intermediates. These variants maintain high stereoselectivity while

accommodating novel substrates, thereby enhancing their utility in asymmetric synthesis. This expanded substrate scope, coupled with retained stereoselectivity, positions engineered MAL variants as indispensable biocatalysts for the production of diverse β-substituted aspartic acid derivatives. In this chapter, efforts to engineer MAL sourced from a novel thermophilic bacterium, *Dictyoglomus thermophilum*, were undertaken to broaden the enzymatic toolbox for producing unnatural amino acids.

5.2 Selection of MAL to engineer for unnatural amino acids production.

MAL has been identified and characterized in various thermophilic bacteria, such as *Carboxydothermus hydrogenoformans*, a thermophile that grows optimally at 70–72°C, and *Chloroflexus aurantiacus*, a thermophilic green nonsulfur bacterium. The selection process for MAL engineering followed a methodology similar to that used for AspA, as described in Section 5.2.

Figure 5-1 illustrates a comparative sequence alignment of MAL from *Clostridium tetanomorphum* and *Dictyoglomus thermophilum*, highlighting conserved regions and potential mutation sites. *Dictyoglomus thermophilum* is a Gram-negative, strictly anaerobic bacterium isolated from geothermal hot springs. Its extreme thermophilic nature enables it to thrive at elevated temperatures, with an optimal growth range of 73–78°C and a maximum growth threshold of approximately 80°C. The bacterium is adapted to a slightly acidic to neutral environment, preferring a pH range of 6.5–7.5, which makes it a robust candidate for industrial applications requiring thermostable enzymes.

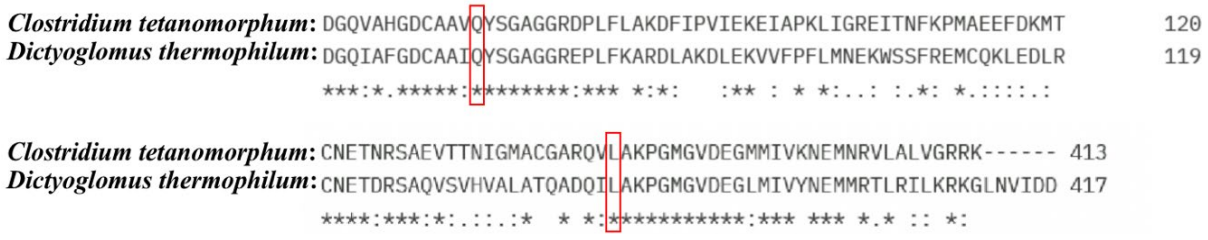

Figure 5-1 Sequence alignment of MAL from Clostridium tetanomorphum and *Dictyoglomus thermophilum.*

Conserved residues between the two sequences are indicated by asterisks (*), and conserved substitutions are marked with colons (:). Red boxes highlight target residues for mutagenesis or protein engineering to investigate their enzymatic activity.

To identify effective mutation sites, structural predictions for *Dictyoglomus thermophilum* MAL were generated using AlphaFold (Figure 5-2). As a deep learning-based tool, AlphaFold generates highly accurate 3D structural models, even for enzymes lacking experimentally resolved structures. This capability proved critical for dtMAL, whose active-site architecture and substrate-binding pockets had not been fully characterized. By providing a reliable structural model, AlphaFold enabled precise visualization of residues such as Leu382, located near the catalytic center, which were hypothesized to influence substrate accommodation. Previous studies, including work by (Raj, Szymański et al. 2012), suggested that reducing steric bulk in analogous residues could broaden substrate specificity while retaining stereoselectivity. AlphaFold's predictions validated this hypothesis, confirming Leu382's position within a region critical for substrate access and positioning. The decision to engineer the Leu382Ala mutation was directly informed by AlphaFold's structural insights. Leucine, with its bulky hydrophobic side chain, was predicted to obstruct the binding of larger or non-canonical substrates. Substituting it with alanine—a smaller, less sterically demanding residue—was anticipated to expand the active-site volume, facilitating accommodation of structurally diverse substrates like unnatural amino acids. AlphaFold's model further revealed that this mutation would minimally disrupt the enzyme's overall fold or catalytic geometry, preserving essential interactions (e.g., hydrogen bonding networks, MIO cofactor alignment) required for stereoselective catalysis. This balance between flexibility and precision underscores the advantage of combining computational predictions with literature-driven hypotheses, avoiding the inefficiencies of purely trial-and-error approaches. This mutation is expected to expand the active site and enhance substrate accommodation while preserving the enzyme's high stereoselectivity. The rationale for selecting this mutation lies in its potential to improve MAL's catalytic performance in synthesizing unnatural amino acids, particularly those with larger or more structurally diverse substrates.

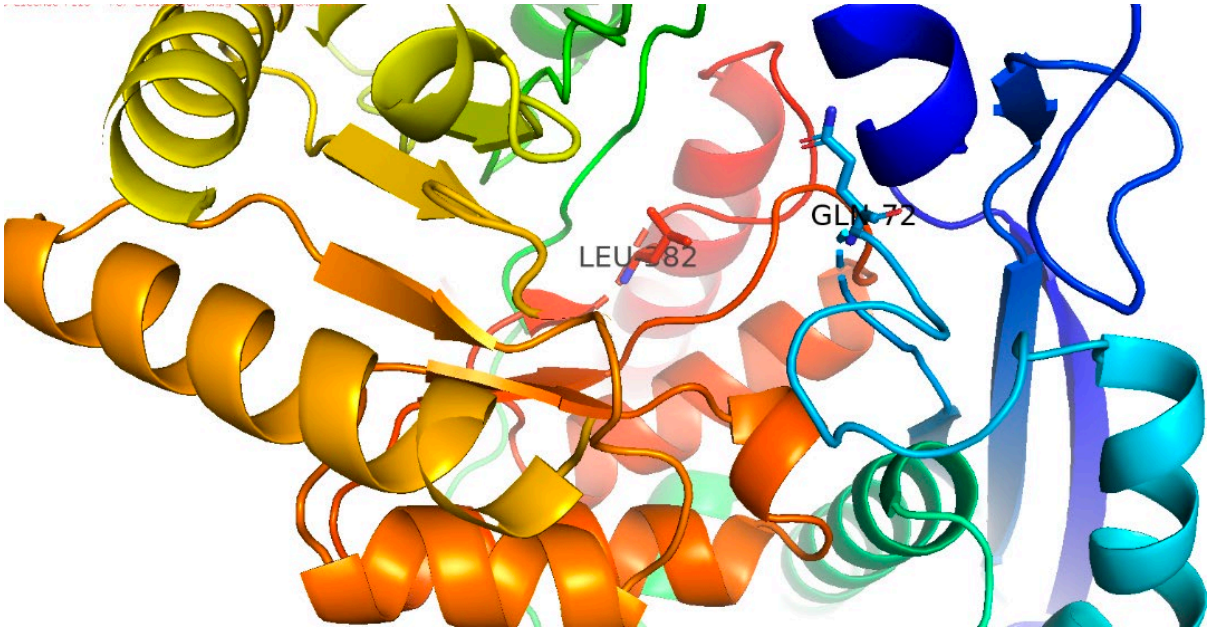

Figure 5-2 Structural prediction of Dictyoglomus thermophilum Methylaspartate Ammonia-Lyase (DtMAL) based on AlphaFold predictions and visualized using PyMOL

The structure highlights key residues identified for mutagenesis: Leu382 and Gln72, labeled and shown in stick representation. These residues were selected for their potential to enhance the enzyme's regio- and enantioselectivity or broaden its substrate scope. The protein's secondary structure is depicted in a color-coded ribbon format, emphasizing the spatial positioning of the mutation sites within the enzyme's active or functional regions.

5.3 Expression of selected DtMAL.

5.3.1 DNA Plasmid construction for protein expression.

The construction of the expression plasmid carrying the Dictyoglomus thermophilum MAL (DtMAL) gene followed a classical restriction–ligation strategy, optimized to ensure correct cloning and efficient downstream protein expression. Initially, the DtMAL gene was maintained in the shuttle vector pUC-GW-Kan, which served as a convenient platform for gene storage and amplification. For subcloning into the high expression pET24a vector, restriction sites for NdeI and EcoRI were chosen, as these sites flank the multiple cloning site of pET24a and are compatible with the orientation and reading frame required for efficient transcription under the control of the strong T7 promoter.

Restriction digestion of pUC-GW-Kan-DtMAL with NdeI/EcoRI successfully released the ~1250 bp DtMAL fragment, as shown inFigure 5-3 (a). The excised band was clearly distinguishable from the vector backbone when compared against the 1 kb DNA ladder, confirming the expected size of the gene insert. The fragment was carefully excised and purified using the NucleoSpin® Gel and PCR Clean-up Kit to remove contaminants such as nucleases, buffer salts, and agarose residues. High-purity DNA at this stage was critical to maximize ligation efficiency and reduce the risk of vector self-ligation or non-specific recombination.

The purified DtMAL fragment was ligated into the linearized pET24a backbone using T4 DNA ligase, generating the recombinant construct pET24a-DtMAL. The pET24a vector was chosen due to its established efficiency for high-level expression in *E. coli* BL21(DE3), facilitated by the T7 promoter and optimized ribosome binding sites.

The ligated plasmid was transformed into *E. coli* DH5α cells using the $CaCl_2$ transformation method, resulting in abundant colony formation on selective TYE agar plates, whereas the negative control plate (no plasmid) showed no colony growth. Plasmids were extracted from positive colonies using a mini-prep kit, and DNA concentration and purity were analyzed. To confirm correct assembly, the plasmids underwent a second digestion with NdeI and EcoRI, followed by electrophoresis (Figure 5-3(b)). Digestion of pET24a-DtMAL yielded two distinct bands: the ~1250 bp DtMAL insert and the ~5250 bp vector backbone, consistent with the expected construct design. Parallel digestion of pET24a-PmAspA (~1400 bp insert) was used as a positive control. The presence of clearly resolved insert and backbone bands confirmed the successful cloning of DtMAL into the pET24a vector.

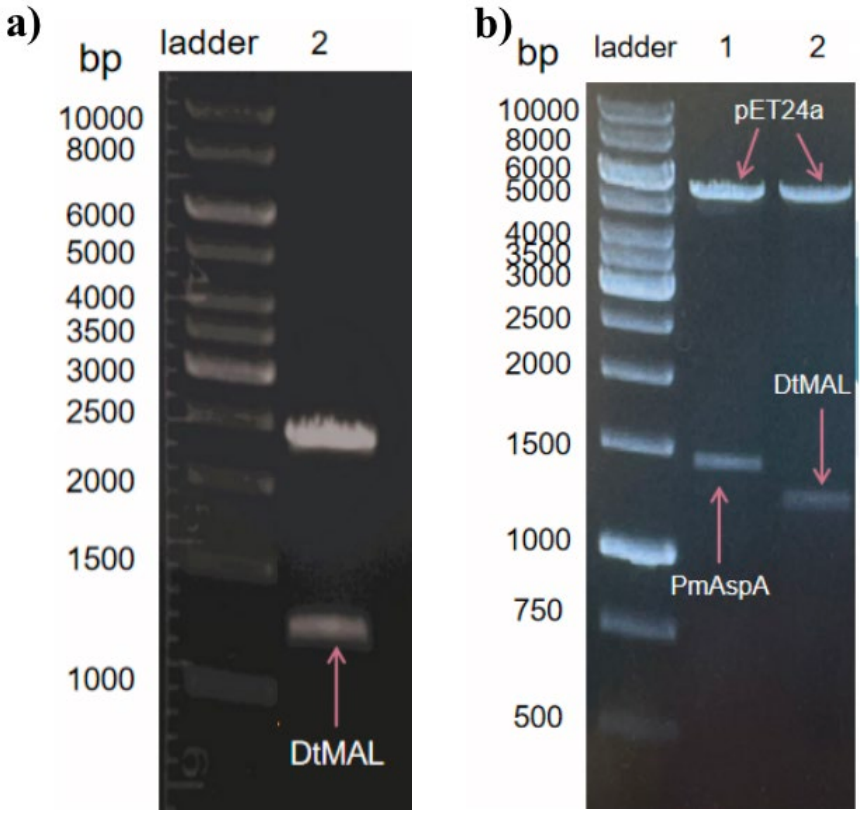

Figure 5-3 Construction of pET24a-DtMAL analysed by DNA agarose gel.

(a) Agarose gel electrophoresis of Nde I/EcoR I-digested pUC-GW-Kan-DtMAL. The single band at ~1250 bp indicates the successful excision of the PmAspA insert. Ladder: 1 kb gene ruler.

(b) Agarose gel electrophoresis of digested plasmids. Lane 1**:** *Nde I/EcoR I*-digested pET24a-PmAspA showing the ~1400 bp PmAspA insert. Lane 2: *Nde I/EcoR I*-digested pET24a-DtMAL showing the ~1250 bp DtMAL insert. Ladder: 1 kb gene ruler.

To facilitate downstream purification and biochemical characterization, a PCR-based cloning strategy was employed to introduce a 6×His-tag into the *Dictyoglomus thermophilum* MAL (DtMAL) construct. Unlike restriction–ligation approaches, PCR-based tagging allows for the precise incorporation of short peptide sequences directly at the desired terminus without the need for additional cloning steps. Custom-designed primers, dtMAL_ins_fwd and AspAMAL_vet_rev, were synthesized to amplify the DtMAL open reading frame (ORF) while simultaneously incorporating the 6×His sequence at the N-terminus. This approach ensured that the His-tag was fused in-frame with the DtMAL coding sequence, preserving structural and functional integrity of the protein. The use of high-fidelity polymerase minimized the risk of

introducing unwanted mutations during amplification, an essential requirement when generating constructs for protein engineering.

Following PCR amplification, the reaction products contained both newly synthesized plasmid DNA and residual methylated parental template. To eliminate background from template carryover, the PCR mixture was treated with DpnI, a restriction enzyme that selectively digests methylated and hemimethylated DNA. This step ensured that only the amplified, His-tagged plasmid construct was available for transformation, increasing cloning efficiency and reducing false positives during colony screening.

The digested PCR products were transformed into *E. coli* DH5α competent cells using the $CaCl_2$ heat-shock method. Colonies grew robustly on kanamycin-selective agar plates, consistent with the presence of the kanamycin resistance marker encoded by the pET24a backbone. Several colonies were randomly selected for verification, and plasmids were purified using mini-prep protocols.

Verification of successful His-tag incorporation was carried out by agarose gel electrophoresis. As shown in Figure 5-4, digestion and analysis of plasmid DNA from positive colonies consistently revealed a band of ~1250 bp, corresponding to the expected size of the DtMAL-6His insert. The presence of this distinct band, aligned with the 1 kb DNA ladder, confirmed the correct amplification and incorporation of the His-tag into the plasmid construct. Multiple independent colonies showed identical banding patterns, supporting the reproducibility of the cloning procedure.

Additionally, the detailed construction of pET24a-6H-DtMAL-SM, which introduces specific mutations to the DtMAL sequence, is described in Section 4.3.1. Together, these constructs serve as robust tools for evaluating the enzymatic potential of DtMAL and its engineered variants in subsequent experiments.

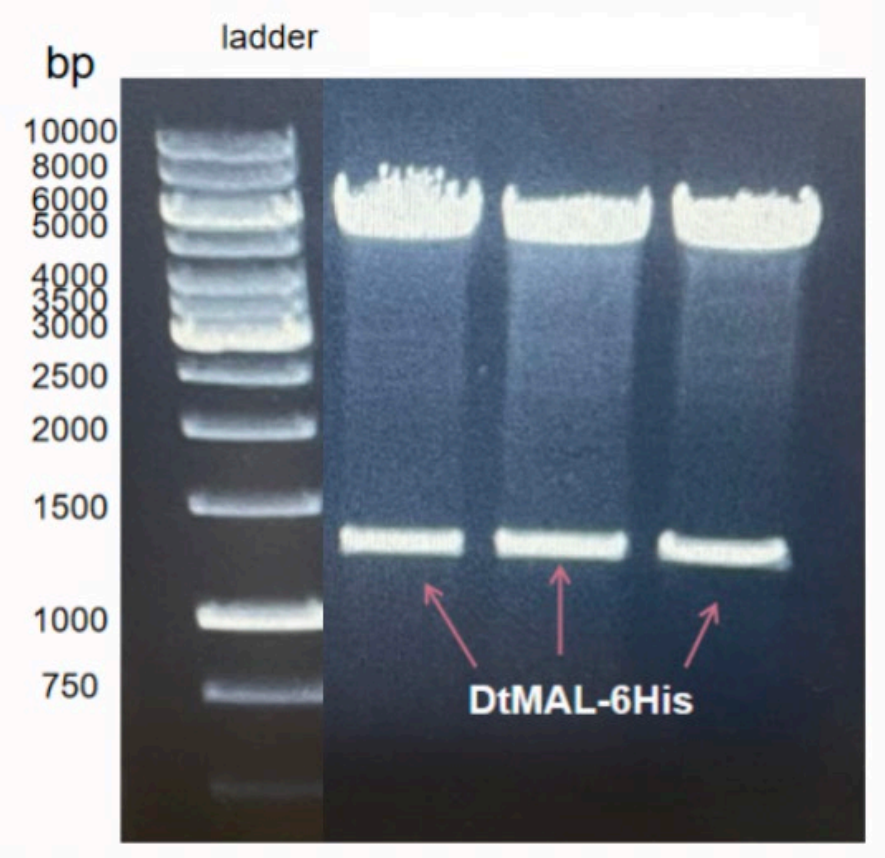

Figure 5-4 Agarose gel electrophoresis confirming the presence of the 6His-tag in pET24a-DtMAL.

Lanes from left to right are 1 kb gene ruler and DpnI-digested PCR products transformed into *E. coli* DH5α and isolated from selected colonies. The band at ~1250 bp corresponds to the DtMAL-6His insert, verifying the successful incorporation of the 6His-tag into the plasmid.

5.3.2 Expression of DtMAL and DtMAL mutant.

Expression of DtMAL was evaluated in *E. coli* BL21(DE3) cells under two different induction conditions to assess the effect of IPTG concentration on protein yield. Cultures were grown to mid-log phase (OD_{600} = 0.5–0.6), ensuring that cells were metabolically active at the time of induction, and then treated with either 1 mM or 0.1 mM IPTG. This dual-concentration approach allowed comparison between high-level induction (1 mM IPTG), which often maximizes protein yield but can increase the risk of inclusion body formation, and lower induction (0.1 mM IPTG), which can favor soluble protein expression by reducing the metabolic stress imposed on host cells.

SDS-PAGE analysis of total cell lysates revealed a distinct protein band at approximately 47 kDa in both IPTG-induced samples, corresponding closely to the theoretical molecular weight of DtMAL (Figure 5.5 (a)). This band was absent in the uninduced control (-ve lane), confirming that expression was IPTG-dependent and attributable to the DtMAL construct. The intensity of the bands was notably strong under both induction conditions, suggesting that DtMAL was efficiently expressed regardless of IPTG concentration. Interestingly, the gel pattern showed that expression levels at 0.1 mM IPTG were comparable to those at 1 mM IPTG, indicating that high IPTG concentrations were not required for robust DtMAL expression in BL21(DE3).

IPTG concentration plays a crucial role in regulating protein expression levels and quality. At high concentrations (1 mM), IPTG completely derepresses the lac operon, leading to maximum protein expression. However, this can create significant metabolic burden on cells, potentially resulting in inclusion body formation and increased cellular stress response. Lower IPTG concentrations (0.1 mM) offer more controlled expression through partial derepression. This reduced metabolic load often results in better protein folding and improved soluble protein yield. The decreased cellular stress can lead to healthier cultures and more stable protein production, though at potentially lower total yields than high-concentration induction.

To complement the BL21(DE3) expression trials, DtMAL was also expressed in *E. coli* C41(DE3), a derivative strain specifically engineered to better tolerate the expression of toxic or aggregation-prone proteins. Induction was performed at OD_{600} = 0.5–0.6 with 1 mM IPTG, and protein production was analyzed by SDS-PAGE. As shown in Figure 5-5(b), a strong band at ~47 kDa was observed, corresponding to the predicted molecular weight of DtMAL, thereby confirming successful expression in this alternative host.

The expression profile in C41(DE3) was generally similar in intensity to that observed in BL21(DE3), suggesting that DtMAL is not inherently toxic or prone to complete translational arrest in *E. coli.* However, the advantage of using C41(DE3) lies in its ability to reduce basal toxicity and mitigate inclusion body formation by moderating transcriptional activity from the T7 RNA polymerase. In practice, this can improve the solubility and stability of heterologous proteins, particularly at higher IPTG concentrations, where BL21(DE3) often drives excessive, non-functional overexpression.

Notably, the observed molecular weight of DtMAL on SDS-PAGE (~47 kDa), which is slightly lower than the calculated value, may be attributed to several factors. Signal peptide cleavage during secretion, post-translational removal of terminal residues, or proteolytic processing could all result in a smaller final protein product than theoretically calculated from the amino acid sequence. The *E. coli* expression system

itself may contribute to size differences through several mechanisms. Differences in codon usage between the native organism and *E. coli* could affect translation efficiency and completeness. Premature termination of protein synthesis might occur due to rare codons or other translation constraints, resulting in truncated products. Additionally, variations in protein folding or charge-to-mass ratio—potentially caused by non-uniform SDS binding—may alter the migration pattern during electrophoresis. Furthermore, post-translational modifications also play a significant role in determining the final protein size. While *E. coli* generally performs fewer modifications than eukaryotic systems, unexpected modifications by bacterial machinery or the absence of native modifications could affect protein mobility during SDS-PAGE analysis. The expression and analysis of 6H-DtMAL-SM, previously described in Sectionn 4.3.2, demonstrated a similar trend. The protein band corresponding to 6H-DtMAL-SM also migrated slightly below its calculated molecular weight (~48 kDa). The consistency of these findings between DtMAL and 6H-DtMAL-SM strongly suggests these size differences are inherent to the proteins' expression and processing in *E. coli* rather than experimental artifacts. This understanding provides valuable insight into the behavior of these proteins in the *E. coli* expression system and emphasizes the importance of considering multiple factors when interpreting molecular weight data from SDS-PAGE analysis.

In addition to SDS-PAGE, western blot analysis can be used in the future to provide a more specific confirmation method. Using antibodies against DtMAL or its fusion tags enables definitive identification of the target protein while also revealing any post-translational modifications or processing events that might explain the size difference. Mass spectrometry can also be used to provide precise molecular characterization through peptide mass fingerprinting and sequence coverage analysis. This technique can determine the exact mass of the expressed protein, identify any modifications or truncations, and validate the complete sequence, providing comprehensive evidence of successful expression despite SDS-PAGE size variations.

Figure 5-5 SDS-PAGE analysis of DtMAL expression under different conditions.

(a) Expression of DtMAL in *E. coli* BL21(DE3) cells induced with 1 mM and 0.1 mM IPTG. The red boxes highlighted protein bands at ~47 kDa, indicated by confirm successful expression of DtMAL under both induction conditions.

(b) Expression of DtMAL in *E. coli* C41(DE3) cells induced with 1 mM IPTG. A prominent band at ~47 kDa, highlighted by the red box, demonstrates successful expression of DtMAL in this host strain.

These results confirm effective DtMAL expression in both BL21(DE3) and C41(DE3) strains with IPTG induction.

5.3.3 Analyzing purified MAL and DtMAL mutant.

DtMAL-6His was purified using the ÄKTA Pure chromatography system and analyzed via SDS-PAGE. The ÄKTA Pure system offers automated, high-precision chromatography which enables precise control over critical purification parameters such as flow rate, buffer composition, and elution conditions. The system's real-time monitoring capabilities allow tracking of protein elution through UV absorbance, ensuring optimal fraction collection and helping identify potential issues during the purification process. Furthermore, the automated nature of the system reduces human error and increases throughput compared to manual chromatography methods. As shown in Figure 5.6 (a), the chromatography elution profile exhibited a prominent peak between fractions 7 and 11, indicating the successful collection of purified DtMAL-6His. SDS-PAGE analysis further validated the purification process, revealing a distinct protein band at approximately 48 kDa, consistent with the calculated molecular weight of DtMAL-6His (Figure 5.6 (b)).

Control experiments were included to assess the efficiency of the purification process. The unpurified DtMAL extract, representing the crude protein before purification, showed a clear band at ~47 kDa, along with multiple additional bands. In contrast, the flow-through, collected during protein loading, lacked significant bands at this molecular weight, confirming that the target protein had efficiently bound to the affinity resin. These results underscore the effectiveness of the purification protocol, yielding highly pure DtMAL-6His with the expected molecular weight. 6H-DtMAL-SM was also purified using the ÄKTA Pure chromatography system and analyzed via SDS-PAGE. Detailed results of this analysis will be included in the appendix.

The SDS-PAGE analysis showed a distinct single band at 48 kDa in the purified fractions, with the absence of contaminating proteins that were present in the crude extract. This purity is essential because contaminant proteins could interfere with both enzymatic assays and structural studies. In enzymatic studies, contaminants might have their own catalytic activities or interact with substrates, leading to confounding results. For structural studies, protein heterogeneity from contaminants can prevent crystal formation or lead to poor-quality diffraction data. The consistent molecular

weight observed (48 kDa) matches the calculated value, suggesting the protein is intact and properly expressed. This integrity is crucial because truncated or degraded proteins might lack important catalytic or structural elements. The matching molecular weight indicates that the protein likely maintains its complete primary structure, including important domains necessary for enzymatic activity and proper folding. Additionally, the efficient binding to the affinity resin (demonstrated by the absence of the target protein in the flow-through) and subsequent elution in a distinct peak suggests the His-tag is accessible and functional. This not only validates the protein's correct expression but also provides a method for additional purification if needed for more demanding applications like crystallography. The accessibility of the His-tag also indicates proper protein folding, as buried tags might suggest misfolding issues. Finally, the successful purification through a standardized chromatography system (ÄKTA Pure) demonstrates that the protein is stable enough to withstand typical purification conditions and can be produced in sufficient quantities for extensive characterization. This stability and yield are essential prerequisites for downstream enzymatic and structural studies.

Figure 5-6 Purification and Analysis of DtMAL-6His Using HisTrap Chromatography.

(a) Chromatogram of DtMAL-6His purification using the HisTrap column on the ÄKTA Pure chromatography system. The elution profile shows a significant peak

between fractions 7–12 corresponding to the elution of DtMAL-6His under optimized conditions.

(b) SDS-PAGE analysis of fractions collected during purification. Lane 1: Protein ladder; Lane 2: Unpurified DtMAL; Lane 3: Flow-through; Lanes 7, 10, 8, 9, and 11: Eluted fractions. A clear band at ~47 kDa, highlighted in purple, confirms the successful purification of DtMAL-6His.

The results validate the expression and purification of DtMAL-6His, with the calculated molecular weight aligning with the observed protein bands.

5.4 Testing enzymatic activity of purified MAL on producing unnatural amino acids.

The enzymatic activity of wild-type DtMAL and its mutant DtMAL-SM was evaluated for substrate conversion using fumaric acid, crotonic acid, and caffeic acid, each at a final concentration of 10 mM, at 30°C. Since DtMAL is being expressed in *E. coli* (as mentioned in the previous text), 30°C aligns well with temperatures that *E. coli* proteins typically function at. This suggests the protein should be stable and properly folded at this temperature, even though it's not the native organism's temperature. Substrate conversion was monitored by measuring absorbance at 235 nm over 24 hours. As illustrated in Figure 5-7, wild-type DtMAL effectively catalyzed the conversion of fumaric acid, as indicated by a continuous and substantial decrease in OD235 values. In contrast, minimal changes in OD235 were observed for crotonic acid and caffeic acid, suggesting limited or negligible enzymatic activity toward these substrates under the tested conditions. For the mutant DtMAL-SM, no detectable activity was observed for any of the three substrates.

Specific activity (0–3 h) was normalized to the experimental OD_{600} of 0.5, yielding an initial rate of 0.253 $\Delta OD_{235} \cdot h^{-1}$ for fumaric acid, 0.035 $\Delta OD_{235} \cdot h^{-1}$ for crotonic acid, and 0.018 $\Delta OD_{235} \cdot h^{-1}$ for caffeic acid. Thus, fumaric acid conversion by DtMAL was ~7.3-fold higher than crotonic acid and ~14-fold higher than caffeic acid, confirming fumarate as the preferred substrate. While crotonic acid showed limited turnover, caffeic acid conversion was negligible under the tested conditions. These data demonstrate that wild-type DtMAL exhibits strong substrate preference for fumarate, with much lower activity toward structurally distinct unsaturated acids. Furthermore, DtMAL-SM formed visible precipitates during the reaction at 30°C, suggesting protein stability issues.

Figure 5-7 Substrate conversion curves using DtMAL as enzyme.

The graph illustrates the substrate conversion curves for fumaric acid (10 mM, black circles), crotonic acid (10 mM, blue squares), and caffeic acid (10 mM, purple triangles) catalyzed by DtMAL. Substrate conversion was monitored by measuring absorbance at 235 nm over 24 hours at 30°C (n = 3 biological replicates per condition). Fumaric acid showed a significant and continuous decrease in OD235, indicating high enzymatic activity and complete conversion within 24 hours. In contrast, crotonic acid exhibited a moderate decrease in OD235, suggesting lower enzymatic activity. Caffeic acid showed minimal change in OD235, indicating negligible enzymatic activity for this substrate.

These results reveal distinct differences between wild-type DtMAL and its mutant DtMAL-SM, alongside clear substrate preferences. The wild-type enzyme demonstrated significant activity specifically toward fumaric acid, evidenced by decreasing OD235 values over time. However, its minimal activity with crotonic acid and caffeic acid suggests a highly specific active site architecture optimized for fumaric acid's structure and chemical properties. In contrast, DtMAL-SM showed no detectable activity with any of the tested substrates and exhibited stability issues through visible precipitation, indicating that the introduced mutations likely disrupted both catalytic function and protein folding stability. These findings suggest several potential avenues for optimization. For wild-type DtMAL, a comprehensive

temperature optimization study could help identify the ideal operating conditions. Additionally, exploring different substrate concentrations beyond the initial 10 mM, along with varying pH conditions and the addition of stabilizing agents like glycerol or specific ions, could further enhance enzyme performance. General optimization strategies could also be employed for both enzyme variants. These include testing different buffer systems and concentrations, examining the effects of ionic strength, and exploring various cofactors or additives that might enhance activity. The analytical approach could be expanded beyond OD235 measurements to include alternative activity assays, while ensuring proper controls for spontaneous substrate degradation.

In addition to spectroscopy analysis, Figure 5-8 presents the ^{1}H NMR analysis of 100 mM fumaric acid before and after enzymatic treatment with purified DtMAL-6His, confirming its efficient conversion to aspartic acid. Before the reaction, characteristic vinyl proton peaks of fumaric acid were observed at δ6.6 ppm. Within 5 minutes of adding DtMAL-6His, these peaks decreased significantly, accompanied by the emergence of new peaks at δ2.8 ppm and δ3.4 ppm, corresponding to aspartic acid. After five hours, fumaric acid peaks were nearly undetectable, and aspartic acid signals dominated the spectrum, confirming near-complete substrate conversion. The rapid response observed within the first 5 minutes, shown by the significant decrease in fumaric acid's vinyl proton peaks (δ6.6 ppm), indicates that DtMAL-6His is highly active and begins catalyzing the reaction immediately. This quick initial rate suggests the enzyme efficiently binds and converts its substrate under the tested conditions. The disappearance of these peaks represents the loss of the double bond in fumaric acid as it's converted. The simultaneous appearance of new peaks at δ2.8 ppm and δ3.4 ppm, characteristic of aspartic acid's protons, provides direct evidence of product formation. These chemical shifts are consistent with the aliphatic protons of aspartic acid, confirming that the enzyme is specifically catalyzing the conversion of fumaric acid to aspartic acid rather than to other potential products. The near-complete disappearance of fumaric acid peaks after five hours, coupled with the dominance of aspartic acid signals, demonstrates that the enzyme maintains its activity over an extended period and can achieve almost complete substrate conversion. This suggests both good enzyme stability under the reaction conditions and efficient catalysis to near completion. The NMR data complements the earlier spectroscopic analysis by providing detailed structural information about both substrate consumption and product formation. While spectroscopy showed decreasing absorption at 235 nm (indicating loss of the double bond), NMR provides direct evidence of the chemical transformation by tracking specific proton signals. Together, these techniques provide comprehensive validation of DtMAL-6His's catalytic activity and specificity.

Figure 5-8 Conversion of fumaric acid to aspartic acid by purified DtMAL monitored via 1H NMR.

The ^{1}H NMR illustrate the enzymatic conversion of 100 mM fumaric acid to aspartic acid by purified DtMAL-6His at 30°C. The purple spectrum represents the sample before enzyme addition, showing characteristic fumaric acid peaks at δ6.6 ppm, corresponding to its vinyl protons. The green spectrum, taken 5 minutes after adding DtMAL-6His, shows a significant reduction in fumaric acid peaks and the shows peaks at δ2.8 ppm and δ3.4 ppm, corresponding to aspartic acid. The red spectrum, recorded after 5 hours, shows the near-complete disappearance of fumaric acid peaks and formation of aspartic acid peaks, indicating nearly total conversion.

For 6H-DtMAL-SM, enzymatic activity toward fumaric acid was assessed using ^{1}H NMR at 22 °C, as higher incubation temperatures (30 °C) caused rapid enzyme precipitation, precluding activity measurements. As shown in Figure 5-9, the initial spectrum (purple) displayed characteristic fumaric acid peaks at δ 6.6 ppm, corresponding to the vinyl protons of fumaric acid. After 24 hours (teal spectrum), negligible change in these peaks was observed, indicating minimal activity. By day 3 (green spectrum), a slight reduction in fumaric acid signals was accompanied by the emergence of weak new peaks at δ 2.8 ppm, consistent with aspartic acid formation, suggesting slow substrate conversion. After 7 days (red spectrum), fumaric acid peaks were substantially diminished, while aspartic acid resonances at δ 2.8 and δ 3.4 ppm became more prominent, confirming enzymatic turnover. These data validate that 6H-DtMAL-SM retains catalytic activity, but only at very low rates under the tested conditions.

In the ^{1}H NMR analysis of crotonic acid using 6H-DtMAL-SM, no significant spectral changes were observed after seven days, indicating no enzymatic conversion. Additionally, the low solubility of caffeic acid at 22°C prevented its analysis in liquid-phase ^{1}H NMR. The poor solubility of caffeic acid at this temperature can be attributed to its hydrophobic nature, a tendency to crystallize at lower temperatures, and strong intermolecular hydrogen bonding. These factors, coupled with the temperature- and pH-dependent solubility profile of caffeic acid, further limit its dissolution in neutral or acidic conditions at lower temperatures. Several strategies could be employed to enhance caffeic acid solubility, including the use of NMR-compatible co-solvents like DMSO-d6, exploring different pH conditions where caffeic acid shows better solubility, or implementing cyclodextrins or surfactant-based systems. Alternative analytical approaches could also be considered, such as solid-state NMR techniques or HPLC analysis, which might be less affected by solubility limitations. Using lower substrate concentrations combined with more sensitive detection methods might also prove beneficial.

Figure 5-9 Conversion of fumaric acid to aspartic acid by purified 6H-DtMAL-SM monitored via 1H NMR.

The ^{1}H NMR spectra illustrate the enzymatic conversion of 100 mM fumaric acid to aspartic acid by 6H-DtMAL-SM at 22°C, following the observation of precipitate formation at higher reaction temperatures. The purple spectrum represents the initial fumaric acid solution, showing characteristic peaks at δ6.6 ppm corresponding to the vinyl protons of fumaric acid. After 24 hours (teal spectrum), no significant change in

fumaric acid peaks was observed, indicating minimal enzymatic activity. By 3 days (green spectrum), slight reductions in fumaric acid peaks were accompanied by minor new peaks at δ2.8 ppm, suggesting slow conversion. After 7 days (red spectrum), a greater decrease in fumaric acid peaks and new peaks at δ2.8 ppm and δ3.4 ppm, corresponding to aspartic acid. These results indicate slow enzymatic activity of 6H-DtMAL-SM under the tested conditions.

The complete lack of activity toward crotonic acid, even after extended incubation periods, suggests fundamental issues with substrate recognition or binding in the modified active site. This could be addressed through substrate engineering approaches, such as testing crotonic acid derivatives that might better fit the active site, exploring different substrate concentrations, or investigating potential co-substrate effects. Additionally, reaction condition optimization specifically for crotonic acid could be valuable, including exploring various temperature ranges below the precipitation point, optimizing pH and ionic conditions, and testing different additives that might facilitate substrate binding or catalysis. These comprehensive optimization efforts could potentially improve the enzyme's performance across all substrates while maintaining its stability.

5.5 Discussion and conclusion.

In this chapter, the engineering and enzymatic characterization of Methylaspartate Ammonia Lyase (MAL) sourced from *Dictyoglomus thermophilum* (DtMAL) and its mutant variant (6H-DtMAL-SM) for producing unnatural amino acids were explored. This study focused on expanding the substrate scope of DtMAL by introducing targeted mutations, leveraging its thermophilic properties, and assessing its functionality through biochemical assays and structural analyses.

The selection of DtMAL was guided by insights from the literature. The mutation Leu382Ala was introduced into the DtMAL structure to expand its active site and accommodate bulkier or structurally diverse substrates. Structural modeling using AlphaFold highlighted the spatial implications of this mutation, supporting the hypothesis that this change would improve substrate flexibility while retaining stereoselectivity. However, the experimental results showed that while the wild-type DtMAL retained significant activity toward fumaric acid, the engineered DtMAL-SM exhibited compromised functionality, with no activity observed for crotonic acid or caffeic acid and limited activity for fumaric acid. Control assays prepared without enzyme showed no significant changes in fumaric acid peaks over the same period, confirming that substrate conversion was enzyme-dependent and not due to spontaneous degradation or non-enzymatic hydrolysis.

The reduced catalytic activity of the Leu382Ala mutant (DtMAL-SM), particularly its loss of activity toward crotonic and caffeic acid and diminished efficiency for fumaric acid, likely stems from unintended structural and functional disruptions caused by the mutation. Although the Leu382Ala substitution was designed to expand the active site and accommodate bulkier substrates, this alteration may have destabilized critical interactions essential for catalysis. In the wild-type enzyme, the hydrophobic side chain of Leu382 likely contributes to substrate positioning via van der Waals interactions, ensuring proper alignment of fumaric acid with the catalytic MIO cofactor. Replacing leucine with alanine—a smaller, less hydrophobic residue—could reduce these stabilizing forces, misaligning the substrate and cofactor. This misalignment would impair the enzyme's ability to stabilize the transition state, leading to the observed decline in fumaric acid conversion. Furthermore, the mutation may have introduced excessive flexibility into the rigid thermophilic scaffold of DtMAL, compromising its structural integrity under assay conditions and resulting in partial unfolding or conformational heterogeneity.

The complete lack of activity toward crotonic and caffeic acid suggests that expanding the active site alone is insufficient to accommodate non-native substrates. Crotonic acid, a monocarboxylic acid, lacks the second carboxyl group required for electrostatic anchoring in aspartases, while caffeic acid's phenolic hydroxyl group likely clashes with unmodified residues in the binding pocket. The Leu382Ala mutation may have enlarged the active site without introducing complementary functional groups (e.g., polar residues to hydrogen-bond with the hydroxyl group of caffeic acid or hydrophobic patches to stabilize crotonic acid's aliphatic chain). Additionally, the MIO cofactor's precise positioning—critical for ammonia elimination/addition—might have been perturbed by the mutation, disrupting proton transfer or intermediate stabilization. AlphaFold's static structural model, while invaluable for predicting spatial changes, cannot fully capture dynamic shifts in cofactor coordination or conformational flexibility during catalysis, which are vital for enzymatic activity.

The retained but reduced activity toward fumaric acid hints at residual substrate binding, albeit in suboptimal orientations. Weak interactions with conserved residues (e.g., backbone hydrogen bonds) may allow limited catalysis, but the mutation's destabilizing effects likely slow turnover. This underscores a fundamental challenge in enzyme engineering: mutations aimed at broadening substrate scope often destabilize the native catalytic machinery. For thermophilic enzymes like DtMAL, which rely on compact, rigid structures for high-temperature stability, even minor perturbations can disproportionately impact function at moderate temperatures. The Leu382Ala mutation exemplifies this trade-off, where gains in substrate flexibility are offset by losses in thermostability and catalytic precision.

To address these limitations, future efforts could adopt a multi-faceted approach. Combinatorial mutagenesis—pairing Leu382Ala with secondary mutations (e.g., Gly381Asp to restore electrostatic interactions)—might reconcile substrate accommodation with catalytic efficiency. By integrating computational predictions, high-throughput screening, and iterative optimization, the engineered enzyme could evolve into a robust biocatalyst, balancing substrate promiscuity with industrial-grade performance.

Wild-type DtMAL and 6H-DtMAL-SM were successfully expressed in *E. coli* systems, with molecular weight confirmed through SDS-PAGE and purification achieved using the ÄKTA Pure chromatography system. However, challenges arose with the stability of DtMAL-SM, as evidenced by protein precipitation during enzymatic activity assays at higher temperatures (30°C). In wild-type DtMAL, the bulky hydrophobic side chain of Leu382 contributes to tight packing within the protein's core, minimizing solvent exposure of nonpolar regions and maintaining structural rigidity. Replacing leucine with alanine—a smaller, less hydrophobic residue—reduces these stabilizing van der Waals interactions, destabilizing the tertiary structure. This destabilization exposes hydrophobic patches that are typically buried, promoting aggregation and precipitation, particularly under the moderate temperatures (30°C) used in enzymatic assays. Such behavior contrasts with the wild-type enzyme, which evolved in the thermophilic *Dictyoglomus thermophilum* and retains stability even at higher temperatures due to its densely packed, rigid architecture.

The mutation may also impair oligomerization, a common feature of thermostable enzymes. Leu382 could reside at an intersubunit interface, where its side chain stabilizes quaternary interactions between monomeric units. Substituting it with alanine likely weakens these interactions, disrupting the assembly of functional oligomers. Misfolded or monomeric DtMAL-SM would lack the structural reinforcement provided by oligomerization, rendering it more prone to denaturation and aggregation. This hypothesis aligns with observations of precipitation during assays, as improperly assembled subunits fail to adopt stable conformations under stress. Additionally, the Leu382Ala mutation may interfere with the enzyme's folding pathway. Thermophilic proteins often require precise folding kinetics, and heterologous expression in *E. coli* can strain the host's chaperone systems. The mutation might destabilize folding intermediates, leading to misfolded aggregates that overwhelm cellular quality-control mechanisms. Even if partially folded, these aggregates lack catalytic activity and are susceptible to precipitation during purification or thermal stress. This folding defect could explain why DtMAL-SM, despite being expressed at levels comparable to the wild type, fails to retain functionality under assay conditions.

AlphaFold predictions suggest Leu382 occupies a critical position near the active site, potentially within a loop or secondary structure essential for maintaining catalytic geometry. Replacing it with alanine may distort hydrogen-bonding networks or introduce strain in adjacent regions, destabilizing the active-site architecture. These perturbations could propagate globally, reducing the enzyme's overall rigidity and accelerating denaturation. Moreover, the loss of solvent-shielded interactions might expose polar or charged residues to the aqueous environment, triggering electrostatic repulsion or unfavorable solvation effects that further destabilize the folded state. For thermophilic enzymes, even minor alterations to hydrophobic cores or oligomeric interfaces can disproportionately impact function.

The enzymatic assays revealed contrasts between the wild-type and mutant enzymes. DtMAL demonstrated robust catalytic efficiency for fumaric acid, achieving nearly complete conversion within hours, as confirmed by ^{1}H NMR. However, its activity for crotonic acid and caffeic acid was negligible, indicating limited substrate promiscuity in its native form. In contrast, DtMAL-SM showed no activity for all tested substrates under standard conditions, with slow conversion of fumaric acid detectable only over extended durations and at lower temperatures. The lack of observable activity for crotonic acid and caffeic acid highlights a potential misalignment between the theoretical predictions of the mutations and their practical effects on substrate accommodation.

The contrasting success of engineering CtMAL (from *Clostridium tetanomorphum*) compared to DtMAL-SM (from *Dictyoglomus thermophilum*) underscores the profound influence of evolutionary history and structural context on enzyme engineering outcomes. CtMAL's mesophilic origin likely endowed it with inherent flexibility, allowing mutations to broaden substrate promiscuity without destabilizing its core architecture. In contrast, DtMAL evolved under the extreme thermal pressures of a thermophilic environment, favoring a rigid, densely packed structure optimized for stability over versatility. Mutations like Leu382Ala, which expand the active site to accommodate non-native substrates, disrupt critical hydrophobic interactions and oligomeric interfaces in DtMAL, destabilizing its thermophilic scaffold. This rigidity-stability trade-off highlights how evolutionary priorities shape an enzyme's tolerance to engineering: CtMAL's ancestral adaptability facilitates functional redesign, while DtMAL's thermostability imposes stringent constraints on structural perturbations.

Species-specific structural nuances further complicate direct comparisons. Residues targeted in CtMAL may occupy distinct functional or spatial contexts in DtMAL, even if sequence alignments suggest positional equivalence. For instance, a mutation that enlarges CtMAL's active site without destabilization might lie near a critical cofactor-binding loop in DtMAL, inadvertently misaligning the MIO group or disrupting proton transfer networks. Additionally, epistatic interactions—where

mutations synergize with neighboring residues in CtMAL—may lack counterparts in DtMAL, rendering analogous substitutions ineffective or deleterious. These differences emphasize that homology-based engineering strategies must account for higher-order structural and dynamic features, not just sequence conservation.

The limitations of computational tools like AlphaFold also contribute to the gap between theoretical predictions and experimental results. While AlphaFold provides high-accuracy static models, it cannot fully capture the dynamic motions or cofactor-substrate interplay critical for catalysis. For DtMAL-SM, the Leu382Ala mutation's impact on transient conformational states (e.g., substrate-binding loop flexibility or MIO repositioning) may explain its experimental instability, which static models overlook. Similarly, assay conditions optimized for mesophilic CtMAL (e.g., moderate temperatures) may misalign with DtMAL's thermophilic adaptations, exacerbating destabilization. These factors underscore the need for empirical validation to complement in silico predictions. To overcome these limitations, comprehensive structural and functional studies are essential. High-resolution techniques like cryo-EM or X-ray crystallography could resolve substrate-bound states of DtMAL-SM, identifying steric clashes or electronic mismatches invisible to predictive models. Molecular dynamics simulations might reveal how mutations alter conformational landscapes, while thermal shift assays could quantify destabilization effects. Directed evolution campaigns, guided by dual selection pressures (e.g., thermostability and substrate conversion), could uncover compensatory mutations that restore stability without sacrificing activity.

In conclusion, this chapter demonstrated the feasibility of engineering MAL from *Dictyoglomus thermophilum* for biotechnological applications, particularly in producing unnatural amino acids. The wild-type DtMAL exhibited high efficiency for fumaric acid conversion, confirming its potential as a robust biocatalyst for traditional substrates. However, the engineered DtMAL-SM variant showed significant limitations, including reduced enzymatic activity and substrate specificity, as well as issues with protein stability. These results underscore the challenges in engineering thermophilic enzymes for expanded substrate scopes and highlight the necessity for a deeper understanding of the structural and functional implications of targeted mutations.

6 Application of MagR for Purification and Immobilization of Aspartase.

6.1 Introduction.

Enzymes, as nature's biocatalysts, have emerged as indispensable tools in industrial processes, biomedical applications, and sustainable chemistry due to their unparalleled specificity, efficiency, and eco-compatibility. However, the use of enzymes presents several limitations, including susceptibility to denaturation under operational conditions, difficulty in recovery for reuse, and the laborious, multi-step purification processes required to isolate active enzymes. To address these challenges, enzyme immobilization has been employed, offering enhanced stability, simplified recovery, and improved operational performance. Traditional immobilization techniques—such as physical adsorption, covalent coupling, and entrapment in polymeric matrices—have been extensively employed, yet they frequently suffer from drawbacks including low enzyme-loading efficiency, leaching, and high material costs. Similar challenges persist in enzyme purification, where conventional chromatographic methods (e.g., affinity, ion exchange) require specialized infrastructure, costly resins, and time-consuming optimization.

In recent years, the integration of biomolecular engineering with nanotechnology has opened new frontiers for streamlining biocatalyst preparation. Magnetic nanoparticle (MNP)-based systems have gained traction for their ability to combine purification and immobilization into a single platform, leveraging magnetic susceptibility for rapid separation and reuse. However, existing approaches often rely on non-specific adsorption or chemical crosslinking, which may compromise enzyme activity or necessitate additional functionalization steps. Against this backdrop, the magnetoreceptor protein (MagR) presents a groundbreaking opportunity. MagR is a naturally occurring protein capable of forming stable complexes with MNPs through iron-sulfur cluster interactions. By fusing MagR to target enzymes, its innate magnetic affinity can be exploited for simultaneous purification and immobilization, bypassing the need for chemical modifiers or complex conjugation protocols.

This chapter explores the innovative application of MagR to revolutionize the purification and immobilization of aspartase enzymes, with a focus on engineered variants of Aspartase B (AspB), a lyase critical in the synthesis of β-amino acids. AspB mutants, optimized for enhanced activity toward non-canonical substrates, highlight the need for efficient, scalable biocatalyst preparation methods to unlock their industrial potential. Here, we hypothesize that MagR-mediated magnetic immobilization can overcome the limitations of traditional methods by enabling a one-step process. *E. coli*-expressed MagR-tagged AspB mutants bind directly to

MNPs, allowing magnetic separation to concurrently purify and immobilize the enzyme. This approach leverages MagR's unique bioaffinity for MNPs while preserving enzyme activity through oriented, non-destructive immobilization. By eliminating chromatographic purification and chemical immobilization, this protocol reduces production costs, environmentally friendly, and enhances scalability—key considerations for industrial biocatalysis. Furthermore, the enzyme immobilized via magnetic adsorption can be easily recovered and reused. This chapter details the development, optimization, and validation of the MagR-based platform, utilizing a combination of biochemical assays, structural analyses, and functional studies to evaluate immobilization efficiency, catalytic performance, and operational stability. Through this work, we aim to establish a versatile and sustainable paradigm for biocatalyst engineering.

6.2 Fusion expression of MagR with aspartaseB mutants.

Fusion protein expression is a versatile technique in molecular biology and biotechnology, enabling the integration of distinct protein domains into a single polypeptide chain to enhance stability, functionality, or introduce new capabilities. By combining the complementary properties of different proteins, fusion expression simplifies purification workflows, enhances enzymatic performance, and facilitates the development of innovative biosensors and biocatalysts.

In this chapter, the fusion of MagR—a magnetoreceptor protein—with Aspartase B, an enzyme that catalyzes the reversible conversion of aspartate to fumarate, was explored. Aspartase B mutants were incorporated into the fusion constructs to investigate their synergistic effects on substrate specificity, catalytic efficiency, and magnetic-responsive properties.

6.2.1 Creating universal vectors harboring MagR gene fragments.

The construction of universal vectors began with the preparation of the pET24a vector and the *clMagR*/*dmMagR* gene fragments. Plasmids harboring the desired genes—pUC-GW-Kan-clMagR, pUC-GW-Kan-dmMagR, and pET24a-HLTev-VsLegH—were extracted from *E. coli* DH5α cultures grown in 2×TY medium supplemented with kanamycin. Plasmid purification was performed using the E.Z.N.A.® Plasmid DNA Mini Kit I, and their concentrations were recorded (Table 16). Restriction digestion of the purified plasmids using NdeI and EcoRI produced DNA fragments of the expected sizes: 5268 bp for the pET24a vector backbone, 756 bp for HLTev-VsLegH, and ~400 bp for both *clMagR* and *dmMagR* gene fragments. The success of

restriction digestion was confirmed by comparing the DNA bands to a molecular weight ladder during agarose gel electrophoresis (Figure 6-1).

Table 16 Purity and concentration of purified plasmids pUC-GW-Kan-clMagR, pUC-GW-Kan-dmMagR, and pET24a-HLTev-VsLegH.

Plasmid	Concentration (ng/µl)	A260/A280	A260/A230
pUC-GW-Kan-clMagR	367	1.782	1.739
pUC-GW-Kan-dmMagR	364	1.783	1.991
pET24a-HLTev-VsLegH	81	1.706	1.159

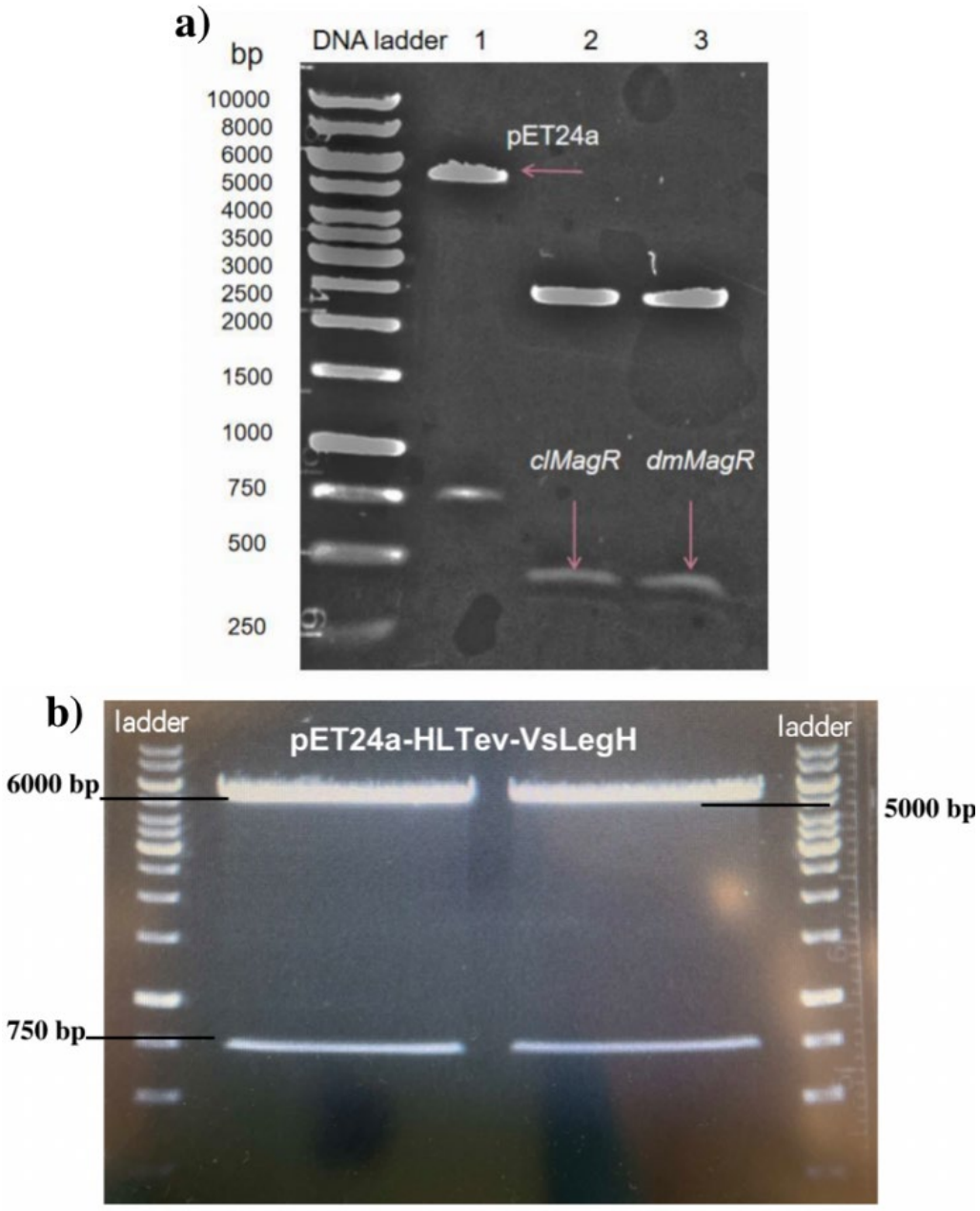

Figure 6-1 Agarose gel electrophoresis of digested pUC-GW-Kan-clMagR, pUC-GW-Kan-dmMagR, and pET24a-HLTev-VsLegH vectors.

(a) Gel showing restriction digestion products of pET24a-HLTev-VsLegH, pUC-GW-Kan-clMagR and pUC-GW-Kan-dmMagR plasmids. Lane 1: DNA ladder with molecular weight markers (in bp). Lane 2: Digested pET24a vector (~5300 bp). Lanes 3 and 4: Digested clMagR and dmMagR inserts (~400 bp), isolated from their respective plasmids using restriction digestion. (b) Gel showing separation of digested pET24a-HLTev-VsLegH. The digested plasmid DNA (Lanes 2 and 3) migrated as two distinct bands: ~5000 bp corresponding to the pET24a backbone and ~750 bp representing the insert HLTev-VsLegH. Lanes 1 and 4: DNA ladder.

Following gel electrophoresis, the desired DNA fragments were extracted using the NucleoSpin® Gel and PCR Clean-up Kit. Approximately 2000 ng of plasmid DNA was used for restriction digestion, and subsequent gel extraction yielded pET24a at a concentration of 17 ng/µL, with an A260/A280 ratio of 1.563, indicating DNA suitable for downstream applications. Similarly, *clMagR* and *dmMagR* gene fragments were recovered with concentrations of 4 ng/µL and A260/A280 ratios of 1.750 and 2.173, respectively. Although the A260/A230 ratios were low (0.387 for *clMagR* and 0.330 for *dmMagR*), the manufacturer's protocol indicated that this could be disregarded for subsequent steps.

The extracted DNA fragments were ligated into the pET24a vector using a standard ligation protocol, and the ligation products were transformed into *E. coli* DH5α cells via the $CaCl_2$ transformation method. Transformed cells were plated onto kanamycin-supplemented agar plates, resulting in abundant single colonies for pET24a-*clMagR* and pET24a-*dmMagR* constructs, with no colonies observed on the negative control plates. To verify succesful ligation, plasmids extracted from selected colonies were analyzed using restriction digestion with BamHI. Agarose gel electrophoresis revealed linearized plasmid bands of approximately 5600 bp, matching the expected sizes (Figure 6-2). The uncut plasmids, included as controls, migrated as supercoiled forms. These results confirmed the successful assembly of pET24a-clMagR and pET24a-dmMagR plasmids, which were subsequently used for downstream experiments.

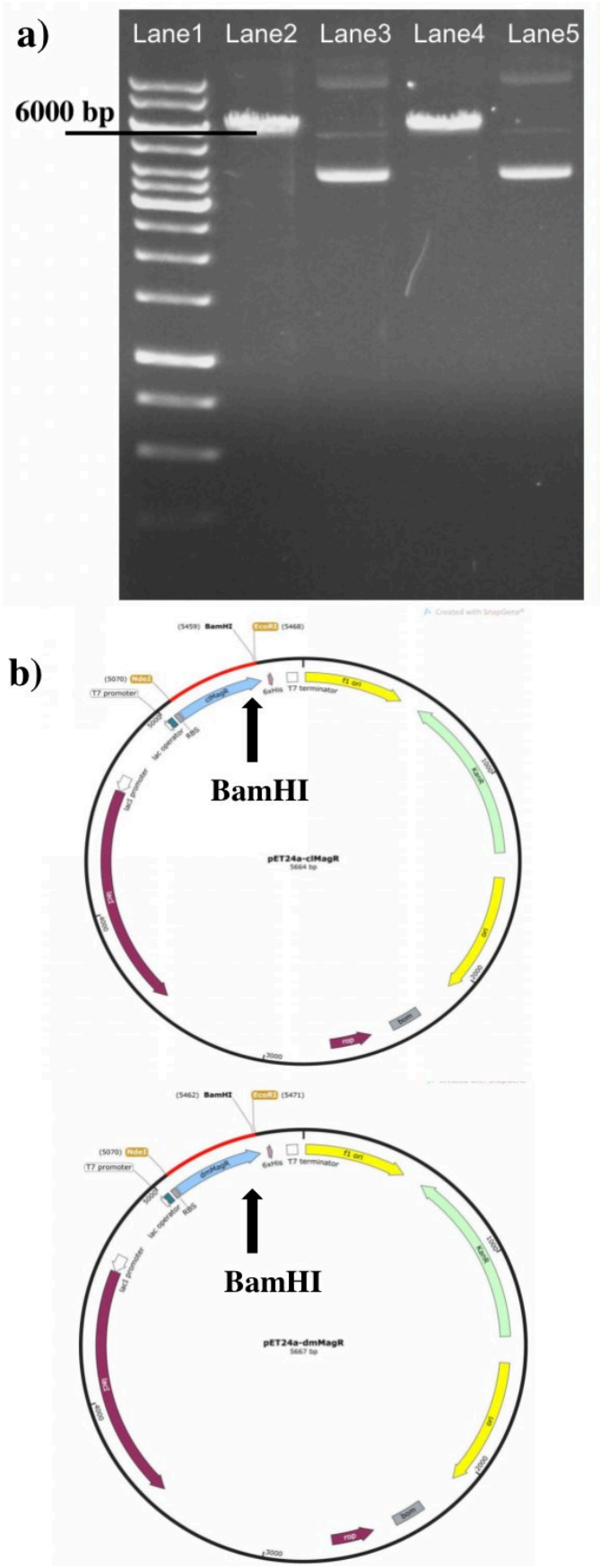

Figure 6-2 Restriction digestion analysis of MagR gene-inserted universal vectors.

(a) Gel electrophoresis analysis of BamHI digested pET24a-clMagR and pET24a-dmMagR. Lane 1: 1kb DNA ladder (molecular weight marker); Lane 2: pET24a-clMagR (digested by BamHI); Lane 3: pET24a-clMagR (uncut) ; Lane 4: pET24a-dmMagR (digested by BamHI); Lane 5: pET24a-dmMagR (uncut). The linearized plasmids migrated at the expected size (~5600 bp), confirming successful digestion. (b) Vector maps of pET24a-clMagR and pET24a-dmMagR showing the insertion sites of the MagR genes, flanked by the Nde I and EcoR I restriction sites, as well as the BamHI sites used for confirmation. These maps illustrate the structural design of the universal vector.

6.2.2 Cloning of aspB-B19 into universal vectors.

Following the successful construction of the universal vectors, the next step involved cloning the *aspB*-B19 gene into the C-terminus of the *clMagR* and *dmMagR* constructs. Aspartase B (AspB) is a catalytically active enzyme requiring proper folding of its TIM barrel domain and active-site residues. By fusing aspB-B19 to the C-terminus of MagR, the enzyme is positioned distal to MagR's functional N-terminal domains, reducing the likelihood of misfolding or steric clashes that might impair AspB-B19's catalytic activity. This spatial separation ensures that both MagR (for immobilization) and AspB-B19 (for catalysis) retain independent functionality. Additionally, C-terminal fusions often exhibit superior stability compared to N-terminal fusions, as the N-terminus of proteins is typically more sensitive to proteolytic degradation.

To achieve this, the aspB-B19 gene fragment was amplified from the plasmid pET28a-B19 using Q5 DNA Polymerase (NEB) with primers BamHI-AspB-F (forward) and AspB-EcoRI-R (reverse). The expected PCR product size of 1407 bp was confirmed by agarose gel electrophoresis, with a prominent band observed alongside faint side bands located above the primary product (Figure 6-3). To ensure the purity of the PCR product, the amplified *aspB*-B19 fragment was excised and purified using the NucleoSpin® Gel and PCR Clean-up Kit. The purified product had a quantified concentration of 121 ng/μL and an A260/A280 ratio of 1.727, indicating high purity. The *aspB*-B19 gene fragment was subsequently digested with BamHI and EcoRI to generate compatible ends for ligation. Post-digestion, the fragment underwent an additional purification step to eliminate residual restriction fragments, yielding a clean product for downstream cloning.

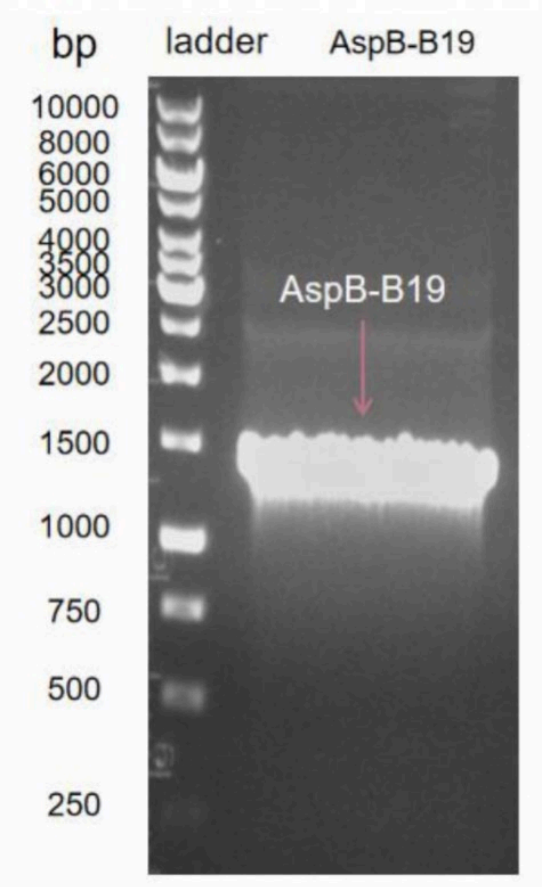

Figure 6-3 DNA agarose gel image of the BamHI/EcoRI-digested AspB-B19 gene fragment.

The gel confirms the presence of the expected AspB-B19 band at approximately 1407 bp. Lane 1: DNA ladder with molecular weight markers, and Lane 2: BamHI/EcoRI-digested AspB-B19 fragment. This purified fragment was used for subsequent cloning into pET24a-based MagR vectors.

Ligation of the digested aspB-B19 fragment into the linearized pET24a-clMagR and pET24a-dmMagR vectors was performed using T4 DNA ligase. The pET24a-MagR vectors were linearized by digestion with the same restriction enzymes (BamHI and EcoRI) to ensure compatibility with the prepared aspB-B19 insert. The ligation reaction products were transformed into *E. coli* DH5α competent cells and plated on kanamycin-supplemented agar for selection.

To confirm the successful construction of pET24a-clMagR-aspB-B19 and pET24a-dmMagR-aspB-B19, plasmids were extracted via miniprep and analyzed for concentration and purity. The plasmid maps of pET24a-clMagR-aspB-B19 and pET24a-dmMagR-aspB-B19 is shown in Figure 6-4. The isolated plasmids exhibited A260/A280 ratios of 1.775–1.798 and A260/A230 ratios ranging from 1.273–1.477,

indicating suitability for downstream applications. Restriction digestion analysis was conducted using NdeI and EcoRI to validate the presence of the aspB-B19 insert. As shown in Figure 6-5, the digestion of the plasmids yielded fragments of 1073 bp, 799 bp, and 5266 bp, consistent with the expected sizes. Additional control digestions with BamHI and negative controls with undigested plasmids confirmed the structural integrity of the constructs.

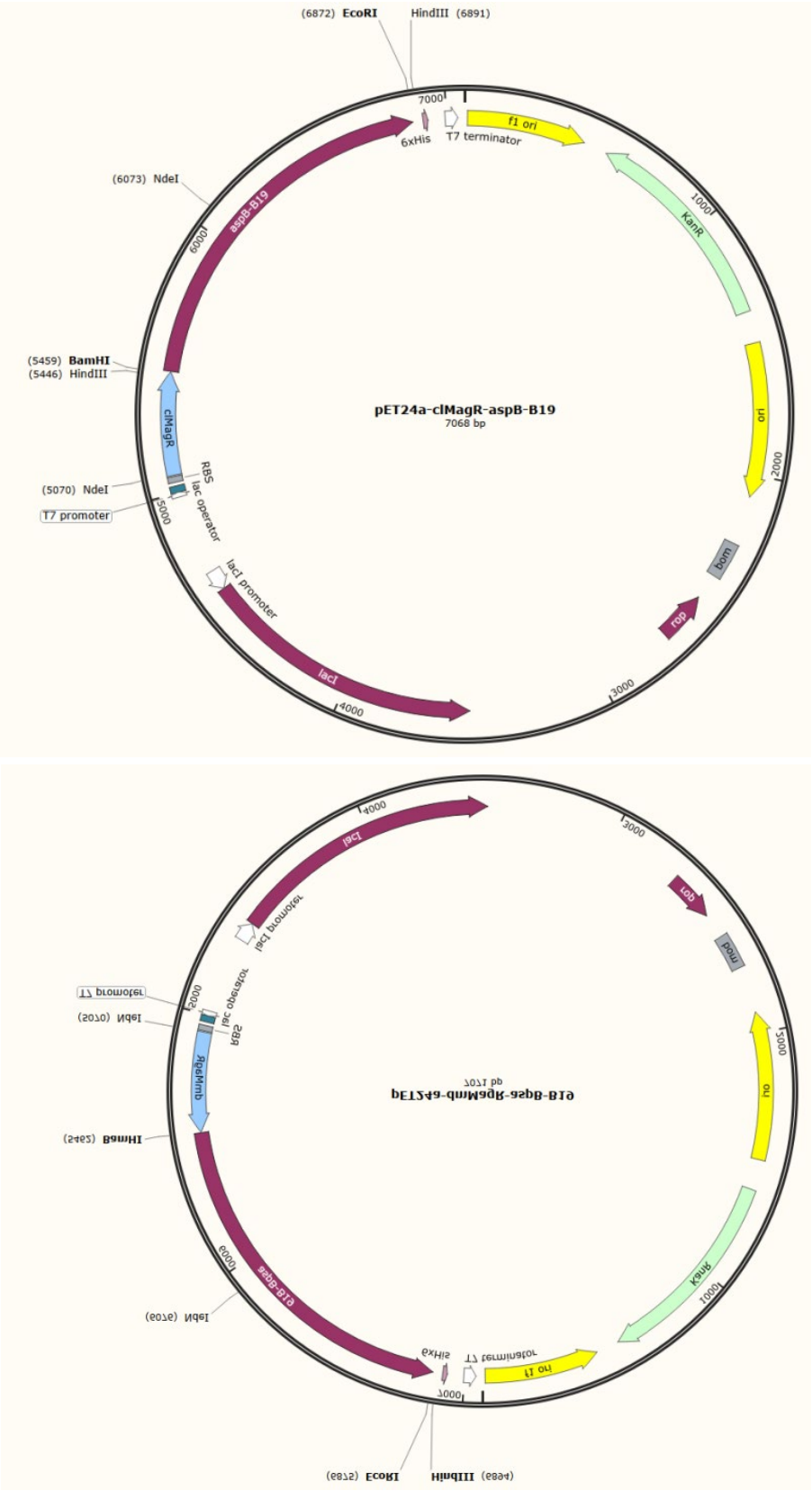

Figure 6-4 Plasmid maps of pET24a-clMagR-aspB-B19 (*top*) and pET24a-dmMagR-aspB-B19 (*bottom*).

The plasmids were constructed by ligating the *aspB-B19* gene into the pET24a-clMagR and pET24a-dmMagR backbones. The maps display the key features of the plasmids, including the T7 promoter for protein expression, the 6× His tag for purification, and the aspB-B19 insert flanked by the restriction enzyme sites BamHI and EcoRI. This recombinant plasmid was used for protein fusion expression.

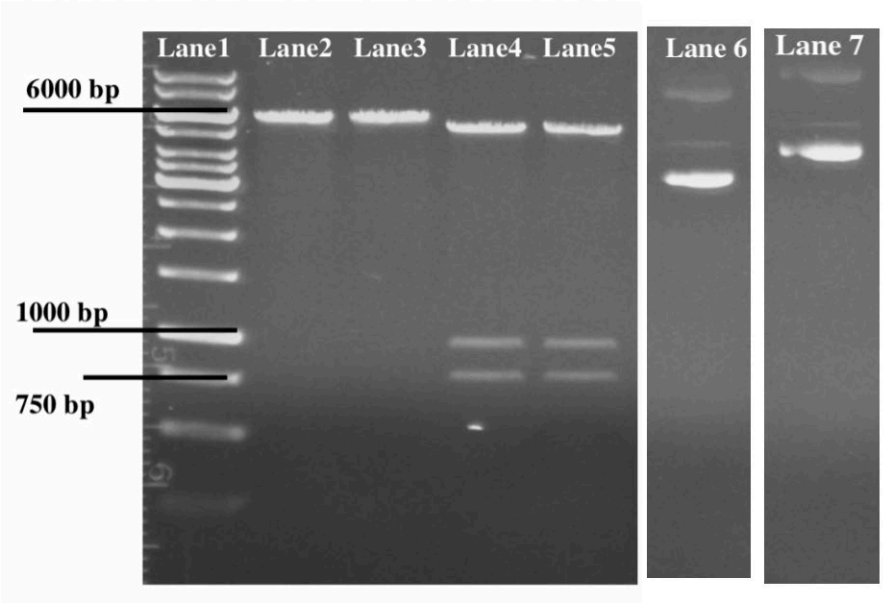

Figure 6-5 Validation of recombinant plasmids by DNA gel electrophoresis.

Gel electrophoresis analysis of BamHI-digested pET24a-MagR plasmids and NdeI/ EcoRI-digested pET24a-MagR-aspB-B19 plasmids. Lane 1: 1kb DNA ladder; Lane 2**:** pET24a-clMagR (BamHI-digested); Lane 3**:** pET24a-dmMagR (BamHI-digested); **Lane 4:** pET24a-clMagR-aspB-B19 (NdeI/ EcoRI-digested); Lane 5: pET24a-dmMagR-aspB-B19 (NdeI/ EcoRI-digested); Lane 6: undigested pET24a-clMagR-aspB-B19 (-ve control); Lane 7: undigested pET24a-dmMagR-aspB-B19 (-ve control). The observed bands match the expected sizes for the vector and insert fragments, confirming successful cloning of aspB-B19 into the respective plasmids.

The successfully verified plasmids pET24a-clMagR-aspB-B19 and pET24a-dmMagR-aspB-B19 were used to create glycerol stocks for long-term storage and subsequent use in downstream applications. This completed the preparation of fusion constructs, enabling their use in further experiments to evaluate expression, purification, and functionality.

6.2.3 Analysis of fusion expressed MagR and AspB-B19.

To evaluate the fusion expression of MagR and AspB-B19, the recombinant plasmids pET24a-clMagR, pET24a-dmMagR, pET24a-clMagR-aspB-B19, and pET24a-dmMagR-aspB-B19 were transformed into *E. coli* BL21(DE3) cells using the $CaCl_2$ transformation method. As a positive control, the plasmid pET28a-B19 was transformed, while a negative control (no plasmid) was included to ensure the absence of contamination. After overnight incubation at 37°C, successful transformations were confirmed by the appearance of numerous single colonies on all experimental plates (Figure 6-6). The positive control plate exhibited several distinct colonies, indicating that the transformation conditions were optimized, while the negative control plate remained devoid of colonies, validating the sterility of the experiment. Plates transformed with recombinant plasmids (pET24a-clMagR, pET24a-dmMagR, pET24a-clMagR-aspB-B19, and pET24a-dmMagR-aspB-B19) displayed abundant colony formation, confirming the successful uptake of the respective plasmids.

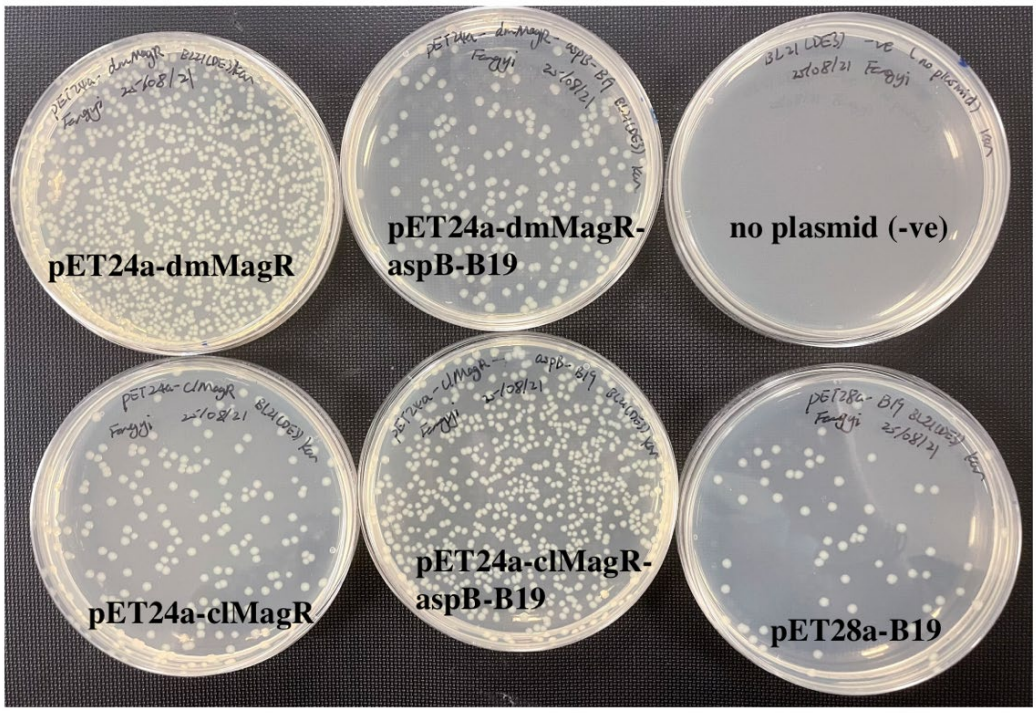

Figure 6-6 Transformation of recombinant plasmids into BL21(DE3) cells.

Transformation results for various recombinant plasmids using the $CaCl_2$ transformation method. Plates include the following: pET24a-dmMagR, pET24a-dmMagR-aspB-B19, pET24a-clMagR, pET24a-clMagR-aspB-B19, and pET28a-B19 (positive control). A negative control plate without plasmid is also shown.

Fusion protein expression in *E. coli* BL21(DE3) cells was induced by adding 1 mM IPTG, followed by incubation at 30°C for 16–24 hours. Protein expression was analyzed using SDS-PAGE under denaturing conditions with both 10% (Figure 6-7(a)) and 15% (Figure 6.7(b)) polyacrylamide gels. The results demonstrated successful expression of AspB-B19, which appeared as a prominent band at the expected molecular weight of approximately 51 kDa (Figure 6.7(a), lane 2; Figure 6.7(b), lanes 2–4). This confirmed the proper expression of the AspB-B19 enzyme. This robust expression can be attributed to several key factors. The use of the pET24a vector, which contains a strong T7 promoter, enables high transcription levels under IPTG induction. Additionally, AspB-B19's coding sequence likely exhibits good compatibility with E. coli's tRNA pool, facilitating efficient translation of the protein. The protein's stability in E. coli suggests proper folding, which helps it avoid cellular degradation pathways. The clear visualization of AspB-B19 on SDS-PAGE is also aided by its relatively large size of 51 kDa. Proteins of this size are generally easier to resolve and visualize on SDS-PAGE compared to smaller proteins, such as MagR at approximately 14 kDa. Smaller proteins can present detection challenges as they may migrate close to the dye front or be difficult to distinguish from background noise in the gel.

In contrast, the individual MagR proteins (dmMagR and clMagR), which have calculated molecular weights of approximately 14 kDa, were not clearly visible under these conditions. In Figure 6.7(b), lane 5, a faint band at approximately 14 kDa suggests low-level expression of clMagR under the tested experimental conditions. However, the expression of dmMagR remained undetectable (Figure 6.7(b), lane 6). The low or undetectable expression of MagR variants (dmMagR and clMagR) may be due to the small size of protein. This detection limitation is exemplified by the faint band observed for clMagR in Figure 6.7(b), lane 5, suggesting expression levels that barely reach the detection threshold. Small proteins like MagR are inherently more vulnerable to proteolytic degradation in *E. coli*, potentially leading to rapid protein turnover. Additionally, the coding sequence of MagR might contain rare codons or form secondary mRNA structures that impede efficient translation. A particularly crucial factor could be MagR's requirement for iron-sulfur clusters, which are essential for its function. Under standard *E. coli* expression conditions, these clusters may not be efficiently assembled, potentially resulting in protein instability or misfolding. Unlike AspB-B19, which appears to possess inherent solubility, MagR's expression might be hampered by solubility issues. The absence of solubility-enhancing fusion partners, such as SUMO or MBP tags, could contribute to its poor expression or stability. These structural and functional requirements suggest that successful expression of MagR might require more specialized conditions or molecular engineering approaches to overcome these limitations.

Furthermore, aggregated proteins were observed as prominent bands at the top of the gel in Figure 6.7(a), lane 4, and Figure 6.7(b), lanes 6 and 8, indicating potential issues with protein solubility, improper folding, or formation of insoluble aggregates. These results highlight possible challenges in expressing and isolating soluble dmMagR and the MagR-AspB-B19 fusion protein, necessitating further optimization of expression and purification conditions. This instability commonly occurs in fusion proteins where steric clashes or incompatible domain interactions can compromise proper protein folding. The specific arrangement of the fusion, with MagR at the C-terminal end of AspB-B19, appears to create particular challenges. This configuration might interfere with MagR's ability to properly assemble its iron-sulfur clusters, leading to misfolding and subsequent aggregation. Additionally, AspB-B19's TIM barrel domain could physically obstruct MagR's interaction with MNPs, potentially contributing to the overall instability of the fusion protein. The expression conditions themselves may also play a crucial role in the observed aggregation. The extended induction period at 30°C (16-24 hours) could overwhelm *E. coli*'s chaperone systems, which are essential for proper protein folding. Additionally, the high IPTG concentration (1 mM) used for induction might result in overly rapid protein production, exceeding the cell's capacity for proper protein folding and processing. These conditions collectively contribute to the formation of inclusion bodies rather than properly folded, soluble fusion proteins.

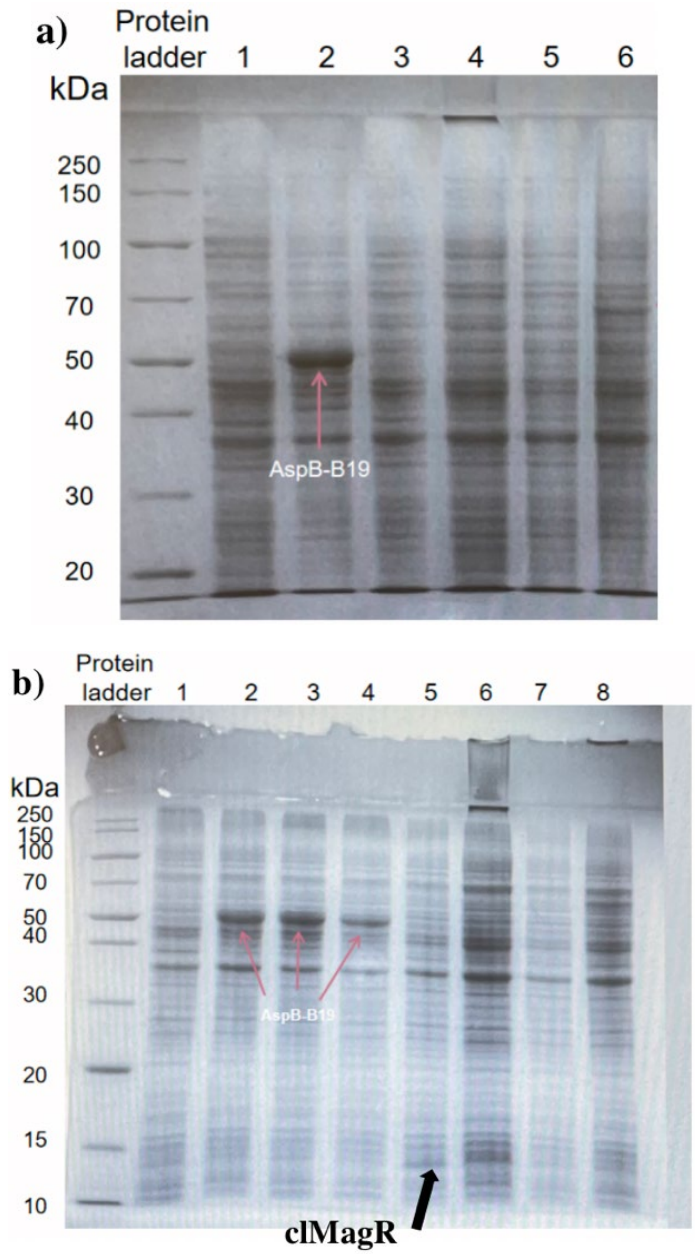

Figure 6-7 Analysis of protein expression in BL21(DE3) cells by denaturing SDS-PAGE gel.

(a) 10% denaturing SDS-PAGE gel. Lane descriptions: Ladder - PageRuler Unstained Broad Range Protein Ladder; Lane 1: BL21(DE3) negative control; Lane 2: pET28a-AspB-B19 positive control; Lane 3: pET24a-clMagR; Lane 4: pET24a-dmMagR; Lane 5: pET24a-clMagR-aspB-B19; Lane 6: pET24a-dmMagR-aspB-B19. The AspB-B19 protein band (~51 kDa) is indicated with an arrow in Lane 2.

(b) 15% denaturing SDS-PAGE gel. Lane descriptions: Ladder - PageRuler Unstained Broad Range Protein Ladder; Lane 1: BL21(DE3) negative control; Lanes 2-4: pET28a-AspB-B19 positive control; Lane 5: pET24a-clMagR; Lane 6: pET24a-dmMagR; Lane 7: pET24a-clMagR-aspB-B19; Lane 8: pET24a-dmMagR-aspB-

B19. The clMagR band (~14 kDa) is marked with an arrow, and the AspB-B19 band (~51 kDa) is highlighted in Lanes 2-4.

The differential expression observed between clMagR and dmMagR can be attributed to sequence-specific characteristics and protein stability factors. The *Drosophila melanogaster* MagR (dmMagR) may face expression challenges due to its eukaryotic codon bias and structural elements, such as disulfide bonds, which are not well-suited to the reducing environment of *E. coli*'s cytoplasm. In contrast, the *Columba livia* MagR (clMagR) appears to have a sequence that is more compatible with prokaryotic expression systems, resulting in detectable protein production. The stability of these proteins in *E. coli* also appears to play a crucial role in their expression outcomes. The undetectable expression of dmMagR suggests it may be particularly susceptible to degradation or misfolding in the bacterial host system compared to clMagR. This difference in protein stability could reflect evolutionary adaptations specific to their original host organisms, with clMagR's sequence potentially being more robust to expression in heterologous systems.

6.2.4 Cloning aspB-M1 and aspB-M2 to the universal vectors.

In addition to aspB mutant B19, the aspB mutant M1 and M2 was also cloned onto the C-terminus of C-terminus of clMagR and dmMagR, respectively. The process began with the amplification of aspB-M1 and aspB-M2 fragments via PCR using Q5 DNA Polymerase (NEB), with plasmids pET28b-aspB-M1 and pET28b-aspB-M2 serving as templates. The primers M1and2Insert_fwd and M1andM2Insert_rev were used for amplification, resulting in the expected band size of 1449 bp for both fragments. PCR products were visualized on a 7% agarose gel Figure 6-8 (a)). Following gel electrophoresis, the PCR-amplified aspB-M1 and aspB-M2 fragments were excised from the gel and purified using a gel extraction kit to ensure the removal of any contaminants or unwanted products.

In parallel, the universal vectors pET24a-clMagR and pET24a-dmMagR were amplified by PCR using the primer sets cldmVec_fwd/clM1and2Vec_rev and cldmVec_fwd/dmM1and2Vec_rev, respectively. The PCR amplification yielded products of the expected sizes of 5664 bp for pET24a-clMagR and 5667 bp for pET24a-dmMagR, as shown in Figure 6-8(b). These amplified vector fragments were

purified using gel extraction to remove non-specific PCR products, primer dimers, and potential contaminants, ensuring the success of downstream DNA assembly.

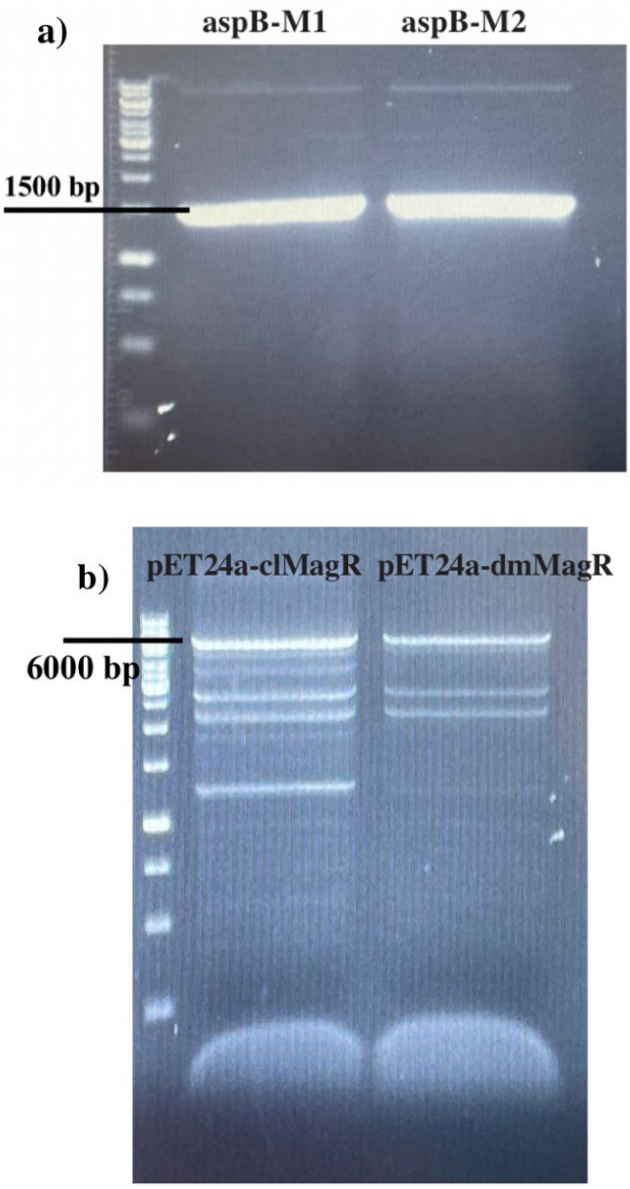

Figure 6-8 PCR Amplification of aspB-M1, aspB-M2, pET24a-clMagR, and pET24a-dmMagR for HiFi DNA Assembly.

(a) PCR amplification of aspB-M1 and aspB-M2. From left to right: Lane 1: 1 kb gene ruler; Lane 2: PCR product of aspB-M1; Lane 3: PCR product of aspB-M2. The expected band size for both PCR products is 1449 bp, which is clearly visible. Gel extraction is required to purify the amplified fragments.

(b) PCR amplification of pET24a-clMagR and pET24a-dmMagR. From left to right: Lane 1: 1 kb gene ruler; Lane 2: PCR product of pET24a-clMagR (expected size: 5664 bp); Lane 3: PCR product of pET24a-dmMagR (expected size: 5667 bp). Gel extraction is necessary to isolate the fragments due to the appearance of side bands.

The amplified pET24a-MagR vectors and aspB-M1/M2 inserts were subsequently assembled using the NEBuilder HiFi DNA Assembly Master Mix. The resulting constructs, pET24a-clMagR-M1, pET24a-clMagR-M2, pET24a-dmMagR-M1, and pET24a-dmMagR-M2, were validated by restriction digestion analysis. The plasmid maps of pET24a-clMagR-M1 and pET24a-dmMagR-M2 are shown in Figure 6-9. To confirm successful plasmid assembly, the constructs were subjected to digestion with NdeI, followed by agarose gel electrophoresis.

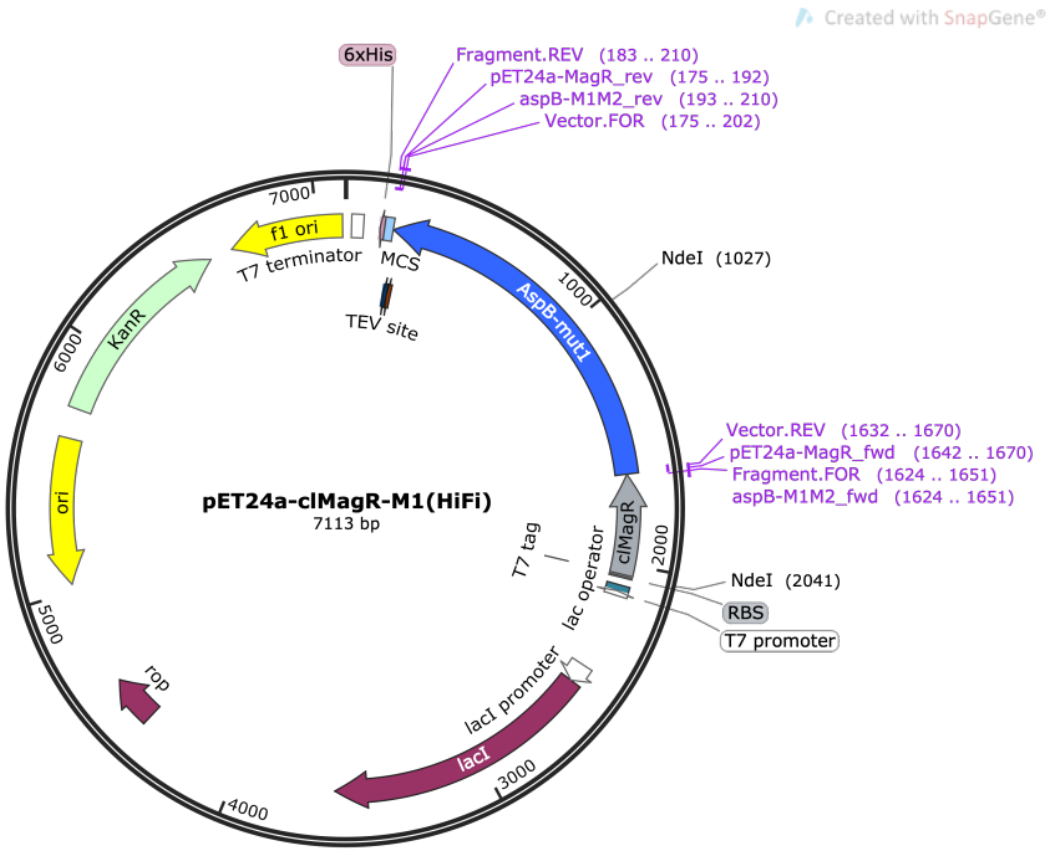
Created with SnapGene®
6xHis
Fragment.REV (183 .. 210)
pET24a-MagR_rev (175 .. 192)
aspB-M1M2_rev (193 .. 210)
Vector.FOR (175 .. 202)
7000
f1 ori
T7 terminator
MCS
TEV site
NdeI (1027)
1000
AspB-mut1
6000
KanR
Vector.REV (1632 .. 1670)
pET24a-MagR_fwd (1642 .. 1670)
Fragment.FOR (1624 .. 1651)
aspB-M1M2_fwd (1624 .. 1651)
ori
pET24a-clMagR-M1(HiFi)
7113 bp
T7 tag
clMagR
lac operator
2000
NdeI (2041)
RBS
T7 promoter
5000
rop
lacI promoter
lacI
3000
4000

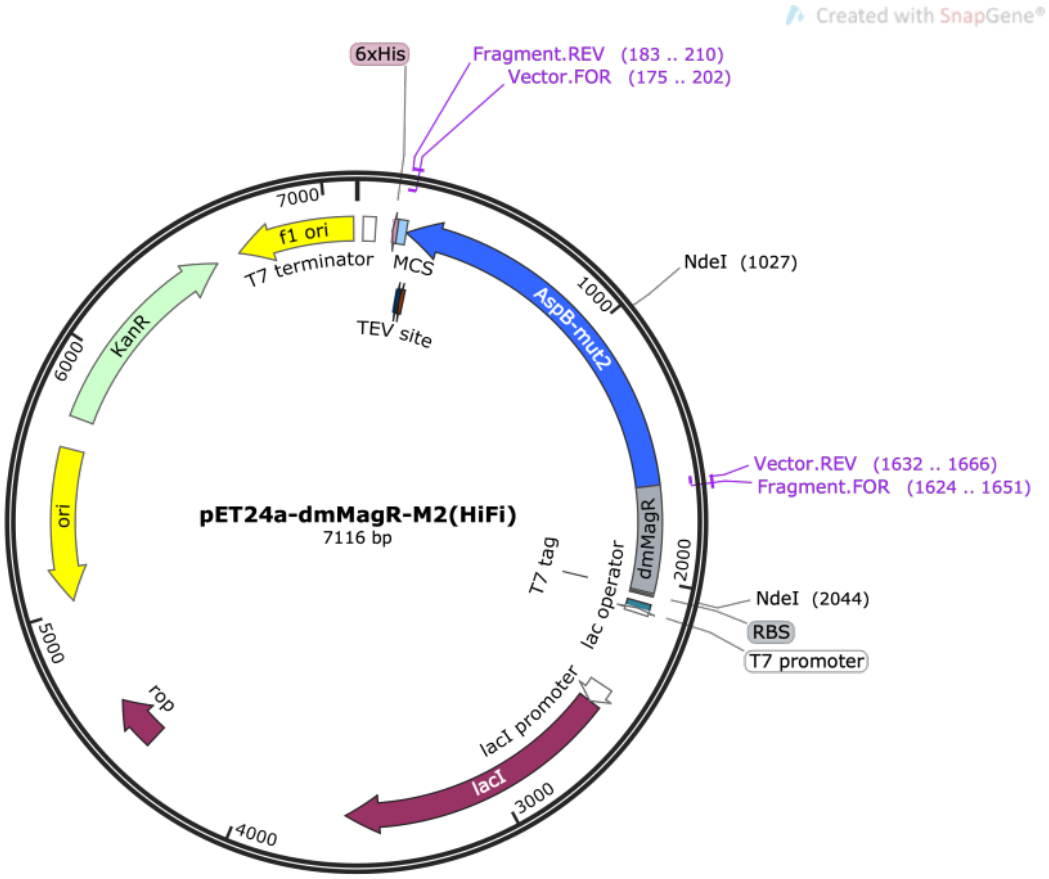
Created with SnapGene®
6xHis
Fragment.REV (183 .. 210)
Vector.FOR (175 .. 202)
7000
f1 ori
T7 terminator
MCS
TEV site
NdeI (1027)
1000
AspB-mut2
6000
KanR
Vector.REV (1632 .. 1666)
Fragment.FOR (1624 .. 1651)
ori
pET24a-dmMagR-M2(HiFi)
7116 bp
T7 tag
dmMagR
lac operator
2000
NdeI (2044)
RBS
T7 promoter
5000
rop
lacI promoter
lacI
3000
4000

Figure 6-9 Plasmid Maps of pET24a-clMagR-M1 (*top*) and pET24a-dmMagR-M2 (*bottomt*).

The plasmid maps represent the construction of *(left)* pET24a-clMagR-M1 and (*right*) pET24a-dmMagR-M2 using HiFi DNA assembly. The vectors contain the MagR gene (clMagR or dmMagR) fused with the AspB-M1 or AspB-M2 insert, driven by the T7 promoter for high-level expression in *E. coli* cells. The NdeI restriction sites was used for verification of successful assembly. The plasmids also include a 6xHis tag for protein purification, KanR for kanamycin resistance, and other essential vector components, including the lacI promoter, lac operator, and f1 ori for plasmid replication.

For pET24a-clMagR-M1 and pET24a-dmMagR-M1 (Figure 6-10 (a)), digestion resulted in distinct bands corresponding to the vector backbone (~6000 bp) and the M1 insert (~1000 bp), confirming successful ligation and assembly. Similarly, for pET24a-clMagR-M2 and pET24a-dmMagR-M2 (Figure 6-10 (b)), digestion analysis revealed the correct assembly of the M2 insert, with highlighted lanes showing the expected vector backbone and insert sizes. Colonies harboring plasmids with the correct constructs were identified, and glycerol stocks were prepared and stored for future use.

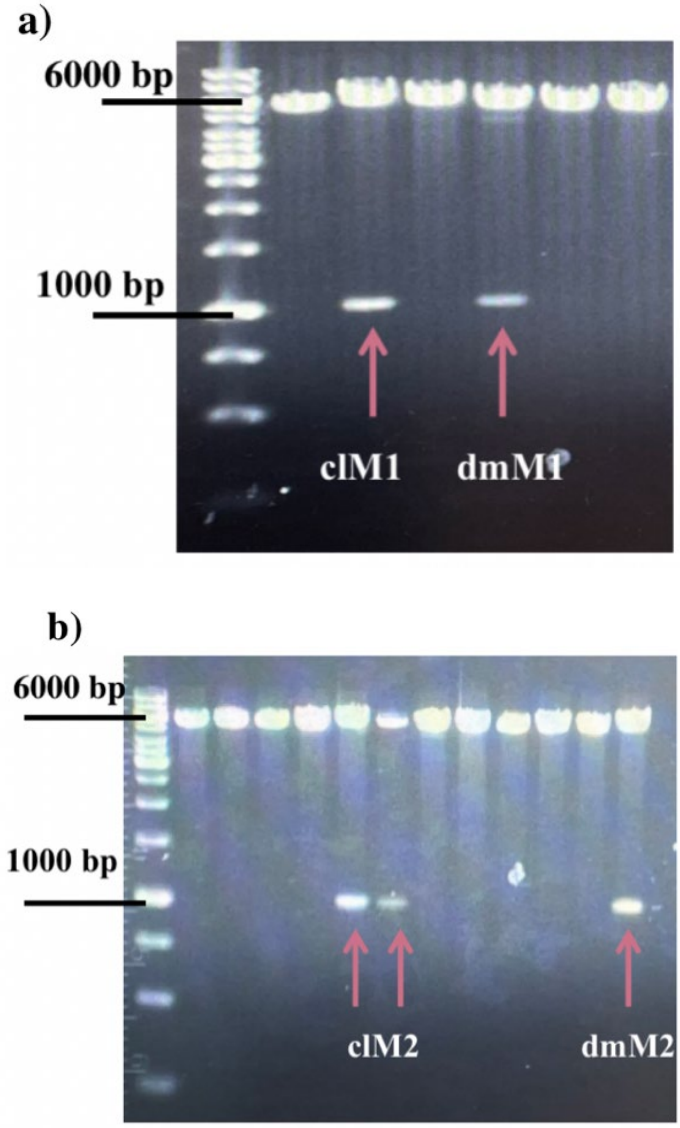

Figure 6-10 Confirmation of MagR fused aspB-M1/M2 recombinant plasmids by restriction digestion.

(a) Restriction digestion of pET24a-clMagR-M1 and pET24a-dmMagR-M1 using NdeI. From left to right: Lane 1: 1 kb gene ruler; Lanes 2-4: pET24a-clMagR-M1 (colonies 1 to 3); Lanes 5-7: pET24a-dmMagR-M1 (colonies 1 to 3). Clear bands corresponding to the clM1 and dmM1 fragments (~1000 bp) confirm successful ligation.

(b) Restriction digestion of pET24a-clMagR-M1/M2 and pET24a-dmMagR-M1/M2 using NdeI. From left to right: Lane 1: 1 kb gene ruler; Lanes 2-4: pET24a-clMagR-M1 (colonies 1 to 3); Lanes 5-7: pET24a-clMagR-M2 (colonies 1 to 3); Lanes 8-10: pET24a-dmMagR-M1 (colonies 1 to 3); Lanes 11-13: pET24a-dmMagR-M2 (colonies 1 to 3). Bands around 1000 bp for clM1, clM2, dmM1, and dmM2 indicate successful plasmid construction.

6.2.5 Analysis of fusion expressed MagR and AspB-M1/M2.

The expression of MagR fused with AspB-M1/M2 was analyzed following transformation of the recombinant plasmids pET24a-clMagR-M1, pET24a-dmMagR-M1, pET24a-clMagR-M2, and pET24a-dmMagR-M2 into BL21(DE3) and C41(DE3) strains of *E. coli* using the $CaCl_2$ transformation method. After transformation, successful colony formation was observed on kanamycin-supplemented agar plates for all constructs. In contrast, no colony growth was observed on negative control plates, where the host cells BL21(DE3) and C41(DE3) were transformed without plasmids. This confirmed that the kanamycin resistance was plasmid-specific, and that selection was effective, ensuring the successful transformation of recombinant plasmids.

Protein expression was induced in the transformed cells using 1 mM IPTG under varying temperature and incubation time conditions to optimize expression. These conditions included incubation at 18°C for 16 hours and 30°C for 20 hours. Protein expression was evaluated via SDS-PAGE analysis using 10% denaturing gels (Figure 6-11). In BL21(DE3), a distinct band corresponding to the AspB-M1/M2 fusion protein (~55 kDa) was observed at both induction temperatures, indicating successful expression. However, the results from C41(DE3) revealed reduced protein expression levels under identical induction conditions, suggesting that BL21(DE3) is a more suitable host for expressing MagR-AspB fusion constructs.

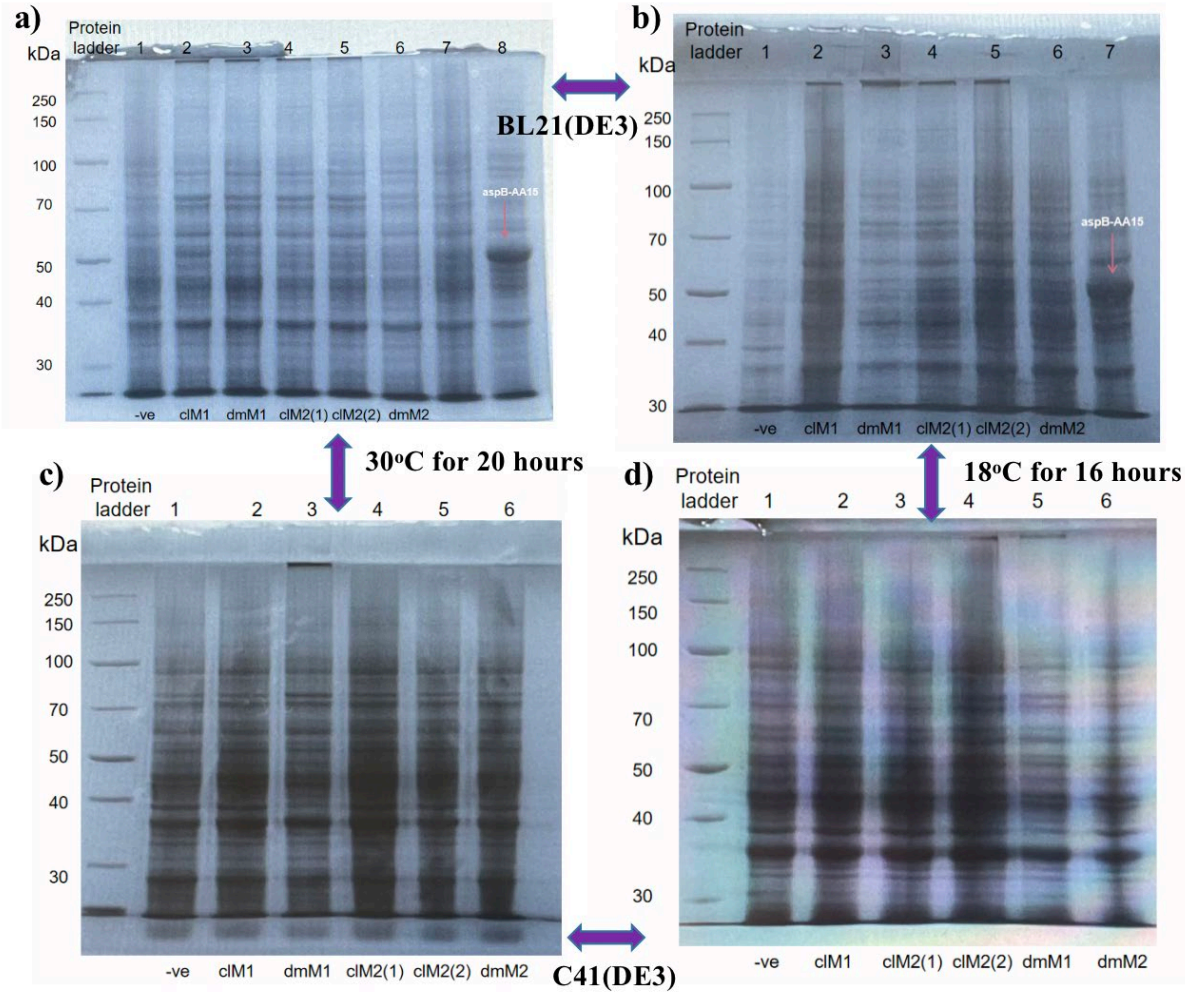

Figure 6-11 Analysis of MagR fused AspB-M1/M2 mutants expression under different conditions.

(a) Protein expression in BL21(DE3) cells induced at 30°C for 20 hours. Lane 1: Protein ladder; Lane 2: Negative control (-ve); Lane 3: pET24a-clMagR-M1; Lane 4: pET24a-dmMagR-M1; Lane 5-6: pET24a-clMagR-M2 (colonies 1 and 2); Lane 7: pET24a-dmMagR-M2. A distinct band near 55 kDa in lane 8 corresponds to aspB-AA15.

(b) Protein expression in BL21(DE3) cells induced at 18°C for 16 hours. Lane assignments are identical to panel (a).

(c) Protein expression in C41(DE3) cells induced at 30°C for 20 hours. Lane 1: Protein ladder; Lane 2: Negative control (-ve); Lane 3: pET24a-clMagR-M1; Lane 4: pET24a-dmMagR-M1; Lane 5-6: pET24a-clMagR-M2 (colonies 1 and 2); Lane 7: pET24a-dmMagR-M2. Lower levels of protein expression are observed compared to BL21(DE3).

(d) Protein expression in C41(DE3) cells induced at 18°C for 16 hours. Lane assignments are identical to panel (c). Protein expression levels are lower than the conditions shown in (a) and (b).

Notably, protein aggregation was observed in several SDS-PAGE lanes, particularly in constructs containing *dmMagR*, as evidenced by faint but aggregated bands near the top of the gel. This aggregation could indicate challenges in protein solubility or folding during expression, especially at higher temperatures. The fusion of AspB-M1/M2 (~41 kDa) to MagR introduces additional complications through steric effects. The substantial bulk added to MagR's C-terminus may interfere with the proper formation of its N-terminal iron-sulfur cluster-binding domain. This structural misalignment likely destabilizes MagR's overall architecture, contributing to its tendency to aggregate. The impact of this fusion-induced strain appears particularly pronounced for dmMagR, suggesting its structure is more sensitive to perturbation than clMagR. Temperature conditions during expression significantly influence protein aggregation patterns. At 30°C, the rapid rate of protein synthesis appears to exceed the capacity of *E. coli*'s folding machinery, resulting in inclusion body formation. While lowering the expression temperature to 18°C helps slow protein synthesis and generally promotes better folding, dmMagR's inherent instability seems to persist, leading to partial aggregation even under these more favorable conditions. This temperature sensitivity highlights the challenging nature of expressing this eukaryotic protein in a bacterial system, where even optimized conditions may not fully overcome its structural complexity and folding requirements.

On the other hand, the use of high IPTG concentration (1 mM) likely led to excessive induction of the T7 system, overwhelming the cell's protein production machinery and contributing to protein misfolding. This situation was further complicated by the extended induction period of 16-20 hours, which placed sustained metabolic stress on the cells, particularly challenging for fusion proteins that require precise folding conditions.

6.3 Optimizing expression conditions for MagR and MAgR-fused AspB mutants

To optimize the expression conditions for MagR-fused aspartase variants, several parameters were systematically varied. Induction temperatures were lowered to 25°C and 18°C to enhance protein solubility and reduce aggregation, while the induction duration was limited to 16 hours to minimize the risk of protein degradation.

Additionally, a range of IPTG concentrations (0.1–1 mM) was tested to balance expression levels with solubility. Despite these efforts, no visible protein bands corresponding to MagR or MagR-fused AspB-B19 were observed in the SDS-PAGE analysis, indicating challenges in achieving detectable expression under the tested conditions.

To further optimize protein expression, an alternative *E. coli* strain, C41(DE3), was employed to assess its potential for improving MagR expression and solubility. Analysis using a 15% denaturing SDS-PAGE gel revealed a prominent band corresponding to dmMagR aggregation at the top of the gel in lane 4, which strongly suggests the presence of insoluble or misfolded protein (Figure 6-12). This observation aligns with previous reports of MagR's propensity to aggregate under certain conditions. Notably, AspB-B19 protein bands were not visible in the same gel, suggesting that BL21(DE3) remains the preferred host strain for achieving better expression and solubility of AspB-B19, compared to C41(DE3).

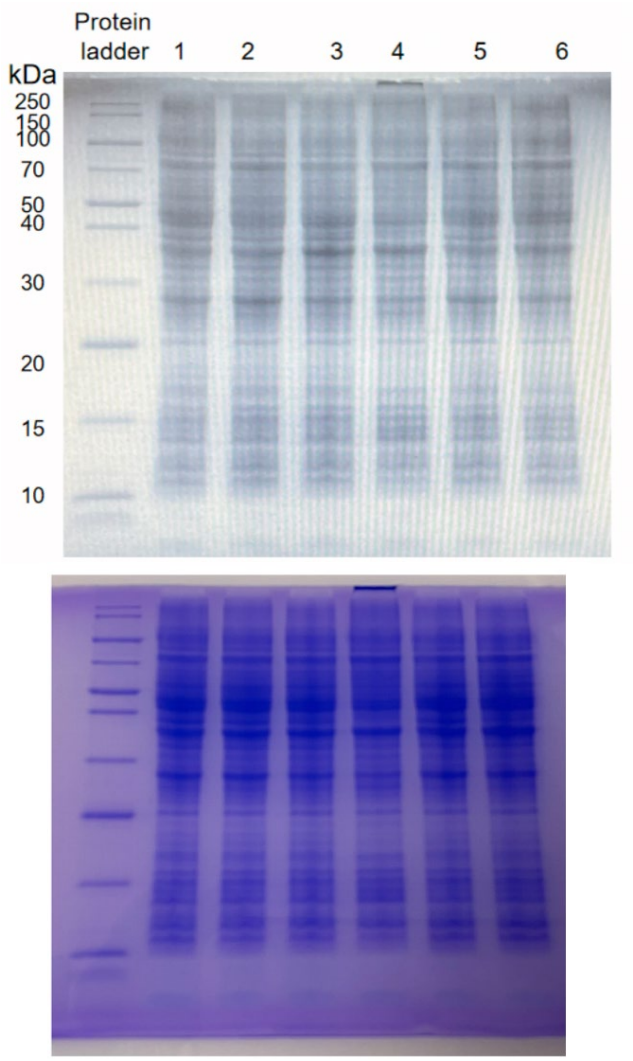

Figure 6-12 Analysis of protein expression in C41(DE3) cells by 15% denaturing SDS-PAGE gel.

Protein expression was induced by adding IPTG (final concentration of 1 mM) when OD600 reached 0.5–0.6 and analyzed using a 15% denaturing SDS-PAGE gel. Lane 1: C41(DE3) -ve control (no plasmid); Lane 2: pET28a-AspB-B19 +ve control (expected ~51 kDa); Lane 3: pET24a-clMagR (~14 kDa, not visible under these conditions); Lane 4: pET24a-dmMagR (~14 kDa, not visible under these conditions); Lane 5: pET24a-clMagR-aspB-B19 (~66 kDa); Lane 6: pET24a-dmMagR-aspB-B19 (~66 kDa).

To improve protein expression and solubility, other expression strain such as BL21(DE3) pLysS or Rosetta™ could be used in the future to enhance the folding of disulfide-rich proteins like dmMagR through improved thioredoxin/glutathione pathways or rare tRNA supplementation. Refinement of induction conditions by reducing IPTG concentration to 0.1-0.5 mM could help moderate expression rates,

while shorter induction times (4-6 hours at 30°C or less than 16 hours at 18°C) might better balance protein yield and solubility. Solubility enhancement strategies should include exploring fusion tags by cloning MagR-AspB into vectors like pET28a for N-terminal His-tags, along with co-expression of chaperone proteins such as GroEL/ES or Trigger Factor. Media optimization could also significantly impact protein quality through the addition of specific supplements. Including $FeSO_4$ to support iron-sulfur cluster assembly and redox additives like cysteine/glutathione could improve MagR folding. The use of autoinduction media might provide more gradual, less stressful protein production conditions. Aggregation mitigation strategies should incorporate solubilizing agents such as arginine (0.5-1 M) or glycerol (5%) in lysis buffers, while pulse-chase experiments could help identify optimal harvest times.

6.4 Discussion and conclusions

In this chapter, the construction of universal vectors harboring MagR genes (clMagR and dmMagR) and subsequent cloning of aspartase B mutants (aspB-B19, aspB-M1, and aspB-M2) was demonstrated. The successful construction of plasmids was confirmed through restriction digestion and electrophoretic analyses, validating the accuracy of the molecular cloning steps. The pET24-based vectors exhibited lower plasmid concentrations compared to pUC-based vectors. This disparity can be attributed to differences in their origin of replication and intended purpose. pET24 vectors utilize a pBR322-derived origin, which results in a low to medium copy number, thereby reducing the metabolic burden on host cells during protein expression. In contrast, pUC vectors employ a modified ColE1 origin, designed for high-copy replication, producing significantly higher plasmid yields. Additionally, pET24 vectors are optimized for controlled protein expression through the T7 promoter, whereas pUC vectors are primarily designed for cloning purposes, allowing uncontrolled replication. The host strain used further influences plasmid yield, as pET24 vectors are commonly propagated in strains like BL21(DE3), optimized for protein expression, while pUC vectors are typically replicated in high-yield strains such as DH5α (Mairhofer *et al.* 2013).

Protein expression of MagR and MagR-fused AspB mutants was explored under various conditions, including changes in induction temperature, IPTG concentration, and host strain. However, clMagR, dmMagR, and their fusion proteins were either not visible or displayed aggregation on SDS-PAGE analysis. These results are consistent with findings in the literature discussed in Section 1.5.4, where significant debate surrounds the intrinsic magnetic properties of MagR and its underlying immobilization mechanism. While the literature proposes ionic interactions as a

possible factor contributing to immobilization efficiency, the observed aggregation and expression challenges suggest that the MagR variants themselves may influence solubility and functionality. For instance, as reported in literature (Pekarsky *et al.* 2021), clMagR expressed in *E. coli BL21(DE3)* was predominantly insoluble. This limited solubility is likely due to MagR's amino acid sequence, which contains surface-exposed hydrophobic residues, promoting aggregation through hydrophobic interactions. Furthermore, the presence of iron-sulfur ([2Fe–2S]) clusters within MagR may significantly influence protein folding and stability, contributing to its insolubility.

As discussed in the section 6.2 and 6.3, the inclusion bodies were observed on SDS-PAGE results. High overexpression at 30–37 °C in T7 systems frequently exceeds the folding capacity of *E. coli*, driving polypeptides into inclusion bodies (IBs). For the MagR fusions, aggregation is plausible from three angles: (i) oligomerization propensity of MagR that can nucleate self-association of the fusion; (ii) electrostatic and hydrophobic mismatch at the fusion interface; and (iii) insufficient maturation of iron–sulfur clusters, which destabilizes the polypeptide during translation. IB formation masks true catalytic yield; therefore, qualitative whole-lysate bands cannot be interpreted as productive expression without solubility-resolved analytics.

To transform the current expression data from qualitative to quantitative, systematic analysis of soluble and insoluble fractions is essential. A rigorous workflow should involve lysis under non-denaturing conditions, centrifugation, and loading equal cell equivalents of supernatant and pellet fractions onto SDS-PAGE, followed by densitometric analysis to calculate a solubility index (soluble/[soluble + insoluble]) across biological replicates ($n \geq 3$). Band identity can be confirmed by Western blotting with anti-His or anti-MagR antibodies. For proteins in the soluble fraction, further biophysical characterization is crucial. Size-exclusion chromatography (SEC), combined with SEC–MALS or dynamic light scattering (DLS), can determine oligomeric state and aggregation, with a mono-disperse peak at the expected molecular weight correlating with functional folding. Because MagR is predicted to bind Fe–S clusters, iron/sulfur loading should also be measured using UV–Vis spectroscopy (A420/A450), colorimetric assays, or ICP-MS, as poor loading may rationalize instability. These biochemical and structural data must ultimately be tied to function by reporting specific activity ($U \cdot mg^{-1}$) for the soluble pool. If refolding is attempted, pre- and post-refold activity should be directly compared to evaluate recovery. For any immobilization claims, inclusion of negative controls is essential—such as samples lacking enzyme, using non-MagR enzymes, or beads alone—to demonstrate specific MagR-mediated capture. Mass balance analyses of bound versus unbound protein, alongside activity assays performed both on-bead and in solution, would allow functional retention to be quantified.

To address the problem of inclusion bodies (IBs), expression conditions such as temperature, induction duration, and inducer concentration are critical factors influencing MagR solubility. The aggregation observed in this study highlights the inherent challenges of expressing MagR in bacterial systems. Optimizing expression conditions (e.g., reducing induction temperature, co-expression with chaperones, or altering growth media) or engineering the MagR protein sequence (e.g., mutating hydrophobic residues or truncating insoluble regions) may improve solubility and functional expression. Another promising route is co-expression with molecular chaperones. Plasmids encoding GroEL/ES, DnaK/DnaJ/GrpE, or Trigger Factor could be introduced to enhance folding of oligomeric enzymes. Since Fe–S cluster maturation is relevant for MagR, co-expression of isc/suf operons, together with microaerobic cultivation and supplementation with Fe^{2+} and cysteine, could improve cofactor incorporation and protein stability.

Because MagR is central to the one-step purification and immobilization concept, analytical strategies must also directly test binding specificity and functional retention on solid supports. Capture efficiency can be quantified by magnetic pull-down assays coupled with mass balance, comparing protein levels in flow-through, wash, and eluates using SDS-PAGE densitometry. Retained enzyme activity should be measured on-bead and compared with free enzyme to confirm functional immobilization. It would also be instructive to benchmark MagR-mediated capture against established immobilization chemistries, including His–Ni^{2+} affinity, SpyTag/SpyCatcher, HaloTag, or biotin–streptavidin systems, to clarify whether MagR offers unique advantages beyond its current solubility bottleneck. These results emphasize the complexity of achieving soluble MagR-fused constructs and underscore the need for further exploration into strategies to overcome these challenges. Such advancements would enable functional characterization and applications of MagR-fused aspartase mutants for one-step purification and immobilization in biocatalysis. If E. coli optimization remains insufficient, alternative expression systems may be necessary. Periplasmic targeting via PelB leaders could reduce aggregation by exploiting the oxidizing environment and chaperone network of the periplasm. Eukaryotic hosts such as Pichia pastoris could provide oxidative folding support and glyco-tolerance, while insect cell systems offer a platform for assembling complex oligomers. Codon optimization or expression in rare tRNA-supplemented hosts (e.g., Rosetta) may also reduce ribosomal pausing that exacerbates aggregation.

In summary, the findings of this study have illuminated significant challenges in expressing and characterizing MagR variants and their fusion proteins with AspB mutants, revealing complex interactions between vector design, expression conditions, and protein properties that influence successful protein production. The observed aggregation and solubility issues of MagR constructs align with previous literature

reports, suggesting inherent difficulties in expressing these proteins in bacterial systems. The presence of surface-exposed hydrophobic residues and iron-sulfur clusters in MagR significantly impacts protein folding and stability. Moving forward, several optimization strategies could address these challenges. The expression system could be enhanced by exploring alternative expression vectors that combine controlled expression with solubility-enhancing features, testing different host strains optimized for challenging protein expression, and implementing co-expression systems with molecular chaperones. Protein engineering approaches might include designing rational mutations to reduce surface hydrophobicity of MagR, considering truncation variants to identify and eliminate aggregation-prone regions, and exploring alternative fusion strategies or linker designs to minimize structural interference. Process development optimization should focus on cultivation conditions including temperature, pH, and media composition, while fine-tuning induction parameters and investigating the impact of iron supplementation on iron-sulfur cluster assembly. Analytical development would benefit from implementing more sensitive detection methods for low-expression proteins, developing improved solubility screening approaches, and establishing robust activity assays for functional characterization. Additionally, stability enhancement could be achieved by testing various buffer compositions and additives, exploring the use of stabilizing agents during expression and purification, and investigating the role of redox conditions in protein folding and stability.

7 General Conclusions and Future Work.

7.1 Major observations and overall conclusion

This study represents a comprehensive effort to engineer enzymes for the production of β-amino acids and unnatural amino acids, focusing on AspB, AspA, MAL, and MagR. The work not only evaluated catalytic potential and substrate scope but also addressed critical challenges in protein expression, solubility, and multifunctional protein design. Collectively, these findings contribute to the growing field of biocatalysis and provide insights into the opportunities and bottlenecks that must be addressed for industrial implementation.

The successful engineering of AspB mutants, particularly the M2 variant, illustrates the power of rational design and targeted mutagenesis to improve catalytic activity and substrate specificity. Mutations such as T187C, M321I, K324L, and N326A enhanced the conversion of crotonic acid into (R)-β-aminobutanoic acid, validating computational predictions and demonstrating the utility of structure-guided approaches. Importantly, these results parallel successes in other engineered lyases, such as fumarase and phenylalanine ammonia lyase variants, where rational design has yielded mutants with broadened substrate tolerance for unnatural amino acid production. However, the solubility and aggregation issues encountered in AspB variants reinforce a recurring theme in enzyme engineering: functional improvements often come at the expense of structural stability. Unlike some other lyase systems expressed successfully in high-yield hosts such as *E. coli* BL21(DE3) or optimized in Pichia pastoris, several AspB mutants displayed inclusion body formation, underscoring the need for balancing activity and foldability in future design strategies.

The investigation of AspA further demonstrated the value of comparative enzymology, where lessons from AspB could be extended to homologous systems. Despite the absence of a resolved AspA–substrate structure, the parallels in active-site architecture allowed transfer of engineering logic across enzyme families. This comparative approach mirrors work on homologous transaminases and decarboxylases, where insights gained from one system have accelerated engineering across related scaffolds. Such strategies broaden the applicability of protein engineering efforts and suggest that cumulative knowledge from homologues can generate families of tailored biocatalysts.

The investigation of DtMAL from *Dictyoglomus thermophilum* reinforces the critical role of thermostable enzymes in industrial biocatalysis. While the wild-type DtMAL showed promising activity in converting fumaric acid to aspartic acid, the significant activity loss in engineered variants (e.g., DtMAL-SM) highlights the challenges in maintaining thermostability while engineering new functionalities. The varying

success rates across different substrates and enzyme variants highlight the inherent trade-offs in enzyme engineering. While some variants showed enhanced activity for specific substrates, others demonstrated reduced catalytic efficiency, suggesting that highly specialized enzymes may come at the cost of broader substrate compatibility. These findings indicate several critical areas for future investigation, including the development of improved computational tools for predicting protein stability alongside functional modifications, investigation of alternative strategies for multi-functional protein design that minimize aggregation and misfolding, and exploration of novel approaches to maintain thermal stability while engineering new substrate specificities.

MagR introduced an innovative dimension to this thesis, combining magnetoreceptor functionality with enzyme engineering. The integration of MagR with AspB mutants aimed to simplify enzyme purification and enable immobilization. While MagR exhibited promising magnetic-responsive properties, issues such as aggregation and misfolding during expression limited its practical utility. These findings reflect the complexity of designing multifunctional protein constructs and the need for improved stabilization techniques.

In conclusion, this thesis has advanced the understanding and engineering of AspB, novel AspA, novel MAL, and MagR for industrial applications. It has demonstrated the feasibility of rational design and structural insights in developing biocatalysts with enhanced activity and substrate specificity.

However, beyond the specific findings on AspB, AspA, MAL, and MagR, this work also highlights broader technical gaps that must be addressed to improve accessibility of enzyme engineering workflows. A recurring limitation lies in the incomplete integration of solubility analytics and quantitative folding assessments into early-stage protein engineering. While catalytic activity was the main benchmark, parallel analysis of soluble versus insoluble fractions, folding efficiency, and cofactor incorporation would have provided a more complete picture of protein quality. Addressing this gap with systematic solubility indices, biophysical assays (CD, DSC, nanoDSF), and cofactor quantification would not only improve reliability for specialists but also create standardized benchmarks that can be readily compared across studies.

Another gap is the accessibility of expression systems. Much of this work relied on *E. coli* BL21(DE3) or C41(DE3), which, while convenient, often fail with multi-domain or Fe–S–binding proteins. Expanding accessibility will require diversifying into alternative hosts (e.g., Pichia pastoris, insect cells, or engineered chaperone-rich E. coli strains) that can better accommodate complex protein architectures. Streamlining protocols for these systems and providing clear performance comparisons would enable researchers from outside the protein engineering field — for example,

synthetic chemists or process engineers — to adopt biocatalytic methods with fewer barriers.

Finally, bridging to interdisciplinary contexts requires translating enzyme engineering results into metrics that resonate across fields. For instance, reporting turnover numbers, space–time yields, and fold-changes in activity relative to chemical routes would allow direct comparison with catalytic and process-engineering benchmarks. Similarly, including robust negative controls, mass balances, and immobilization efficiencies would make the data more transparent and interpretable by non-specialists. By addressing these technical gaps and focusing on accessible, standardized methodologies, future work will not only refine the science for enzyme engineering experts but also make it easier for interdisciplinary researchers in chemistry, materials science, and industrial biotechnology to adopt and apply these findings.

7.2 Future direction.

7.2.1 Analysis of enzymatic assay methods: current limitations and future approaches.

Current spectrophotometric and NMR methods for enzymatic assay analysis, while valuable, present several key limitations that impact data quality and experimental efficiency. Spectrophotometric analysis at OD235, which monitors the depletion of conjugated double bonds, is limited by interference from protein absorbance and other UV-active compounds in the reaction mixture, potentially masking subtle changes in substrate conversion. Additionally, this approach cannot distinguish between similar structural isomers or side products, potentially leading to overestimation of product formation. The requirement for continuous monitoring also makes this method less suitable for high-throughput screening of multiple enzyme variants or reaction conditions. NMR analysis, while providing detailed structural information about substrates and products, also presents significant limitations. The technique requires relatively high sample concentrations (typically >0.1 mM), which may not reflect physiologically relevant conditions or may exceed substrate solubility limits. The time-intensive nature of NMR data collection makes it impractical for real-time monitoring of reaction kinetics, particularly for rapid transformations. Furthermore, the need for deuterated solvents can affect enzyme behavior and stability, potentially altering the reaction dynamics being studied. The method also requires significant sample preparation time and specialized expertise for data interpretation, limiting its utility for routine analysis.

Several advanced analytical approaches, such as High-Performance Liquid Chromatography coupled with Mass Spectrometry offers superior sensitivity and specificity compared to spectrophotometric methods. Multiple Reaction Monitoring Mass Spectrometry enables simultaneous quantification of multiple reaction components, including intermediates and side products, with detection limits in the picomolar range. This approach could be particularly valuable for identifying novel products formed by engineered enzyme variants or for detecting unexpected side reactions. Time-resolved X-ray crystallography represents another powerful tool for understanding enzyme mechanisms. This technique can capture structural snapshots of enzyme-substrate complexes during catalysis, providing direct visualization of conformational changes and helping validate computational predictions of substrate binding modes. While technically challenging, recent advances in X-ray free-electron laser technology enable collection of structural data on microsecond to millisecond timescales, potentially revealing previously unobserved catalytic intermediates. Microfluidic platforms coupled with real-time detection methods offer exciting possibilities for high-throughput enzyme characterization. Droplet-based microfluidics can encapsulate individual enzyme variants with substrates and fluorogenic reporters, enabling rapid screening of thousands of reactions in parallel. Integration with fluorescence-activated droplet sorting would allow direct selection of improved variants based on activity. This approach could be particularly valuable for directed evolution experiments, significantly accelerating the optimization of enzyme function.

Additionally, Surface Plasmon Resonance and Bio-Layer Interferometry provide label-free, real-time monitoring of enzyme-substrate interactions. These techniques can measure binding kinetics and affinity constants directly, offering insights into how mutations affect substrate recognition. These methods require minimal sample volumes and can detect interactions at physiologically relevant concentrations. Integration with automated sampling systems would enable high-throughput characterization of multiple enzyme variants or substrate combinations. Isothermal Titration Calorimetry offers direct measurement of reaction thermodynamics, providing detailed insights into the energetics of enzyme-catalyzed reactions. This technique can reveal subtle changes in binding mechanisms resulting from protein engineering, helping optimize enzyme-substrate interactions. Modern Isothermal Titration Calorimetry instruments with automated sampling capabilities enable systematic characterization of multiple variants or reaction conditions.

The implementation of these advanced analytical methods should be complemented by robust data analysis pipelines. Machine learning algorithms can help process and interpret complex datasets, identifying patterns in enzyme behavior and predicting promising engineering strategies. Integration of multiple analytical techniques

through automated workflows would enable comprehensive characterization of engineered enzymes while minimizing manual intervention.

7.2.2 Advanced methodologies for optimizing engineered enzymes.

Future research should address the challenges identified in this study by enhancing catalytic efficiency, substrate compatibility, and the industrial applicability of engineered enzymes such as AspB mutants and MAL variants. The optimization of engineered enzymes like AspB mutants and MAL variants requires a multi-faceted approach combining computational predictions with experimental validation. Molecular dynamics (MD) simulations can provide detailed insights into enzyme-substrate interactions at atomic resolution, revealing the dynamic behavior of the active site during catalysis. For AspB mutants, MD simulations should focus on analyzing the conformational changes during substrate binding, particularly how mutations like T187C and M321I affect the positioning of β-amino acid precursors. These simulations can be performed using software packages such as GROMACS or AMBER, with specific attention to water networks and hydrogen bonding patterns that influence substrate orientation. Long-timescale simulations (>100 ns) would be particularly valuable for understanding the complete catalytic cycle and identifying rate-limiting steps that could be targeted for improvement.

High-resolution crystallographic studies serve as a crucial complement to MD simulations by providing structural validation of predicted conformational changes. For MAL variants, obtaining crystal structures of enzyme-substrate complexes would be particularly valuable for understanding how mutations affect substrate binding. The structures should be determined at resolutions better than 2.0 Å to clearly visualize water molecules and subtle conformational changes in the active site. Time-resolved crystallography could potentially capture intermediate states during catalysis, providing unprecedented insights into the reaction mechanism. These structural studies should prioritize complexes with both native and non-native substrates to understand the molecular basis of substrate specificity.

Additionally, the application of Rosetta for enzyme redesign offers powerful capabilities for predicting beneficial mutations. The RosettaDesign module can be used to optimize the packing of residues around the active site while maintaining critical catalytic interactions. For AspB mutants, Rosetta's enzyme design protocols should focus on redesigning substrate-binding pockets to accommodate larger or more sterically hindered substrates while maintaining proper orientation of catalytic residues. The approach should involve multiple rounds of design, starting with a focused library of mutations within 8 Å of the substrate binding site, followed by broader searches that consider second-shell residues that might influence active site dynamics. Energy calculations using RosettaMatch can help identify optimal amino

acid combinations that stabilize the transition state. FoldX complements Rosetta by providing rapid calculations of mutation effects on protein stability. This tool is particularly valuable for screening large numbers of potential mutations before experimental validation. For MAL variants, FoldX calculations should focus on identifying stabilizing mutations that could compensate for the destabilizing effects of active site modifications. The analysis should consider both single mutations and combinations of mutations, with special attention to regions that showed instability in previous engineering attempts. Integration of FoldX predictions with evolutionary conservation data can help identify mutations that are likely to be tolerated while improving stability.

Alternative expression systems should be explored to overcome solubility and stability challenges. For instance, expressing these enzymes in *Pichia pastoris* or employing molecular chaperone co-expression in *E. coli* could improve protein folding and reduce aggregation. Additionally, cell-free protein synthesis systems provide a promising host-independent platform for producing soluble, active enzymes, especially for challenging targets such as MagR-fused proteins. This approach could bypass host-related metabolic limitations, such as the native metabolism of fumaric acid observed in *E. coli*, thereby enhancing enzyme activity and yield. Thermostabilization strategies are essential to improve the performance of these enzymes under industrial conditions. Introducing stabilizing mutations or optimizing linker regions in fusion proteins could mitigate thermal denaturation and aggregation. Reaction parameters, including buffer composition, pH, ionic strength, and temperature, must also be optimized to maximize enzymatic performance. Bioreactor-based studies, which simulate large-scale production conditions, will provide invaluable insights into improving catalytic efficiency and operational stability.

The experimental validation of computationally predicted mutations should follow a systematic approach combining high-throughput screening with detailed kinetic characterization. Initial screening can utilize colorimetric or fluorogenic assays to rapidly identify promising variants. For AspB mutants, a particular focus should be placed on developing screening methods that can detect improved activity toward sterically hindered substrates. The most promising variants should undergo comprehensive kinetic characterization, including determination of kcat and KM values under various conditions to understand how the mutations affect different steps of the catalytic cycle.

Directed evolution strategies can be employed to further optimize promising variants identified through rational design. For both AspB and MAL variants, iterative rounds of random mutagenesis focused on beneficial mutations identified by computational approaches can help fine-tune activity and stability. Error-prone PCR libraries should be created with moderate mutation rates (1-3 mutations per gene) to maintain library

quality while exploring sequence space. The integration of machine learning approaches can help guide library design by identifying patterns in successful mutations and predicting promising combinations. Additionally, the development of microfluidic screening platforms could significantly increase the throughput of directed evolution experiments, allowing for more comprehensive exploration of mutation combinations.

7.2.3 Expand substrate scope and enhance biocatalyst robustness.

To expand the substrate scope, computational tools such as AutoDock Vina, Rosetta, and Molecular Dynamics (MD) simulations enable precise modeling of enzyme-substrate interactions, identifying steric and electronic barriers to non-canonical substrates. These tools facilitate substrate docking simulations to analyze the binding of target substrates to the active site of aspartases or ammonia lyases, helping identify clashes with residues like Leu382 in DtMAL or analogous positions in related enzymes. Through iterative mutagenesis, mutations can be designed to enlarge the active site or introduce complementary functional groups, such as replacing bulky residues with smaller ones or introducing aromatic residues for π-π stacking with phenyl substrates. Validation of predicted mutants via site-directed mutagenesis and kinetic assays, such as HPLC monitoring of β-amino acid formation, provides crucial experimental confirmation of computational predictions.

The diversification of amine donors represents another crucial strategy for expanding product range. Traditional ammonia-dependent enzymes limit product diversity, but incorporating alternative amine donors enables the synthesis of N-substituted β-amino acids. This approach involves screening substituted amines and amides in kinetic assays, where using compounds like hydroxylamine could yield valuable β-hydroxy-β-amino acids for peptidomimetics. Active-site modifications, such as AspB-K326A, can relax donor specificity, while high-throughput assays using colorimetric or fluorometric readouts enable rapid assessment of donor compatibility. These advances have significant industrial relevance, particularly in pharmaceutical applications for accessing N-alkylated β-amino acids and in agrochemical production of chiral β-aminonitriles.

Using thermophilic enzymes provides a robust platform for industrial applications. Enzymes from thermophiles, such as *Dictyoglomus thermophilum*, exhibit inherent stability under extreme conditions—a critical trait for industrial scalability. Bioprospecting efforts can identify novel aspartases and ammonia lyases using BLAST or hidden Markov models, while directed evolution of thermophilic scaffolds under selective pressure can yield variants with desired activities. The integration of these enzymes into continuous flow reactors operated at elevated temperatures enhances substrate solubility and reduces contamination risks, as demonstrated by

engineering DtMAL variants for activity at moderate temperatures while maintaining thermostability. The integration of computational precision, donor diversification, and thermophilic enzyme robustness presents a comprehensive approach to accessing diverse unnatural amino acids. In the future studies, the machine learning-guided enzyme design and industrial-scale validation are important to create sustainable manufacturing solutions. This multi-pronged strategy not only expands the toolkit for biocatalysis but also establishes a framework for continuous innovation in enzyme engineering.

7.2.4 Application of functionalized magnetic beads for MagR-mediated enzyme immobilization and purification.

The integration of MagR-fused enzymes with functionalized magnetic beads represents a transformative approach to biocatalyst engineering, enabling streamlined one-step purification and immobilization. This strategy relies on MagR's innate ability to bind magnetic nanoparticles (MNPs) while leveraging functional groups on bead surfaces to enhance enzyme stability, orientation, and reusability. The versatility of functionalized magnetic beads offers diverse interaction modes with MagR-fused enzymes, enabling customization for specific applications through various functional groups (Table 17). Hydroxyl (-OH) groups provide hydrophilic surfaces that minimize non-specific binding and are ideal for enzymes requiring aqueous environments, facilitating hydrogen bonding with polar residues on MagR or the fused enzyme. Amine ($-NH_2$) groups, positively charged at neutral pH, enable electrostatic interactions with negatively charged regions of MagR or AspB, particularly useful for enzymes operating at neutral-to-acidic pH. Carboxyl (-COOH) groups create negatively charged surfaces that bind cationic regions of MagR-fusion proteins via ionic interactions, offering versatility through pH-modulated binding. C18 (Octadecyl) chains provide hydrophobic surfaces that interact with nonpolar regions of MagR or fused enzymes, making them suitable for lipases or enzymes requiring hydrophobic microenvironments.

The process implementation follows a modular workflow that begins with expressing MagR-fused enzymes in *E. coli*. Post-lysis, the crude extract is mixed with functionalized magnetic beads, where magnetic capture occurs as MagR's iron-sulfur clusters bind MNPs, while functional groups on beads provide secondary interactions to stabilize enzyme orientation. Through magnetic separation, non-target proteins and cellular debris are removed, retaining only the immobilized enzyme-bead complex. This streamlined approach eliminates chromatography, reducing costs and processing

time by more than 50%, enabling direct deployment of the immobilized enzyme in bioreactors without additional purification steps.

The optimization of bead properties plays a crucial role in meeting industrial demands. Pore size considerations include large-pore beads (50–100 nm) to accommodate bulky fusion proteins without steric hindrance, and small-pore beads (10–30 nm) ideal for smaller enzymes, offering high surface area for dense enzyme loading. Magnetic core composition options range from standard iron oxide (Fe_3O_4) for most applications to silica-coated MNPs for enhanced chemical resistance in organic solvents or extreme pH conditions. For instance, C18-functionalized silica-coated beads could immobilize MagR-lipase fusions for biodiesel production, where hydrophobic interactions stabilize the enzyme in non-aqueous reaction mixtures.

The modularity of MagR-bead systems extends to the design of spatially organized multi-enzyme reactors, enabling co-immobilization through functionalized beads with mixed surface groups for reaction cascades. Magnetic recovery allows for post-reaction separation, washing, and reuse for more than 10 cycles without significant activity loss (Jiang *et al.* 2017).

Several challenges require specific optimization strategies for successful implementation. Aggregation mitigation can be achieved through pre-treatment of beads with blocking agents like BSA or PEG to reduce non-specific protein adsorption. Solubility enhancement may involve co-immobilization with chaperones on COOH beads to improve folding of aggregation-prone fusions. Scalability considerations necessitate bead size uniformity to ensure consistent fluid dynamics in large-scale reactors. The integration of functionalized magnetic beads with MagR-fused enzymes offers a versatile platform that successfully unifies purification and immobilization processes. Through careful tailoring of bead chemistry and physical properties, this system can be optimized for diverse industrial processes, from pharmaceutical synthesis to biofuel production. Future development requires high-throughput screening of bead-enzyme combinations to identify optimal pairings, advancing toward the creation of plug-and-play biocatalytic modules for sustainable manufacturing.

Table 17 Megnetic beads designed with various functional group.

Supplier	Functional Group	Product name and Pore size
Beaver (Silica Magnetic Beads	OH	Mag OH-500 (500 nm)
		Mag OH-1000 (1000 nm)

(SiO_2)		Mag OH-500 single dispersion (500 nm)
	NH_2	Mag NH_2-500 (500 nm)
	COOH	Mag COOH-S500 (500 nm)
		Mag COOH-SC300 (300 nm)
		Mag COOH-NS500 (500 nm)
Bioneer	NH_2	AccuNanoBead™ NH_2 Magnetic Nanobeads (400 nm)
	COOH	AccuNanoBead™ COOH Magnetic Nanobeads (400 nm)
	Just silica coated	AccuBead™ Silica Magnetic Nanobeads (400 nm)
Creative Diagnostics (Silica Magnetic Particles)	OH	Catalog：SMP-NM01 (350 nm)
		Catalog：SMP-NM05 (250 nm)
		Catalog：SMP-UM02 (1.5 μm)
		Catalog：SMP-UM15 (6 μm)
	NH_2	Catalog: SMP-NM03 (250 nm)
		Catalog: SMP-UM03 (1.5 μm)
		Catalog: SMP-UM16 (6 μm)
	COOH	Catalog: SMP-NM04 (250 nm)
		Catalog: SMP-UM04 (1.5 μm)
		Catalog: SMP-UM17 (6 μm)
	C18 (Octadecyl)	Catalog: SMP-NM06 (250 nm)
		Catalog: SMP-UM14 (1.5 μm)
	NHS	Catalog: SMP-UM07 (1.5 μm)

G-Biosciences	Silica Magnetic Beads	Catalog: 786-915 (2.5-4.5µm particle size)
	NH_2 Magnetic Beads	Catalog: 786-906 (1 µm particle size)
	COOH Magnetic Beads	Catalog: 786-906 (1 µm particle size)

8 BIBLIOGRAPHY

Adhikari, B.-R., et al. (2017). "A high-performance enzyme entrapment platform facilitated by a cationic polymer for the efficient electrochemical sensing of ethanol." The Analyst **142 14**: 2595-2602.

Aissaoui, N., et al. (2014). "Enzyme immobilization on silane-modified surface through short linkers: fate of interfacial phases and impact on catalytic activity." Langmuir : the ACS journal of surfaces and colloids **30 14**: 4066-4077.

Akhtar, M., et al. (1987). "Enantiospecific synthesis of 3-substituted aspartic acids via enzymic amination of substituted fumaric acids." Tetrahedron **43**(24): 5899-5908.

Akimaru, M., et al. (2015). "Temperature-responsive Solid-phase Extraction Column for Biological Sample Pretreatment." Anal Sci **31**(9): 881-886.

Akram, W., et al. (2019). "POLYELECTROLYTE COMPLEXATION AND IONOTROPIC GELLATION: THE POTENTIAL NOVEL APPROACH TO DESIGN HYDROGEL PARTICULATE FOR SUSTAINED, MODULATED DRUG DELIVERY SYSTEM: A REVIEW." **10**: 3563.

Al-Dulaimy, E. A. M. and M. A. Jasim (2022). "Effect Of Non-Protein Amino Acid (BABA) On Gastrointestinal Tissues Of Male Rats And Some Negative Enterobacteria." Journal of Pharmaceutical Negative Results: 219-225.

Alpert, A. J. (1990). "Hydrophilic-interaction chromatography for the separation of peptides, nucleic acids and other polar compounds." Journal of Chromatography A **499**: 177-196.

Asano, Y. and Y. Kato (1994). "Crystalline 3-methylaspartase from a facultative anaerobe, Escherichia coli strain YG1002." FEMS Microbiology Letters **118**(3): 255-258.

Asano, Y., et al. (2005). "Alteration of substrate specificity of aspartase by directed evolution." Biomolecular Engineering **22**(1): 95-101.

Asuncion, M., et al. (2002). "The Structure of 3-Methylaspartase from Clostridium tetanomorphum Functions via the Common Enolase Chemical Step *." Journal of Biological Chemistry **277**(10): 8306-8311.

Ayyar, B. V., et al. (2012). "Affinity chromatography as a tool for antibody purification." Methods **56**(2): 116-129.

Babbitt, P. C., et al. (1996). "The enolase superfamily: a general strategy for enzyme-catalyzed abstraction of the alpha-protons of carboxylic acids." Biochemistry **35**(51): 16489-16501.

Bai, Q., et al. (2018). "Protein separation using a novel silica-based RPLC/IEC mixed-mode stationary phase modified with N-methylimidazolium ionic liquid." Talanta **185**: 89-97.

Barker, H. A., et al. (1959). "The purification and properties of beta-methylaspartase." J Biol Chem **234**(2): 320-328.

Barth, H. G. (2018). "Size Exclusion Chromatography: A Teaching Aid for Physical Chemistry." Journal of Chemical Education **95**(7): 1125-1131.

Baskaran, D., et al. (2018). "Partitioning of crude protein from aqua waste using PEG 600-inorganic salt Aqueous Two-Phase Systems." Chemical Data Collections **15-16**: 143-152.

Bet-moushoul, E., et al. (2016). "TiO2 nanocomposite based polymeric membranes: A review on performance improvement for various applications in chemical engineering processes." Chemical Engineering Journal **283**: 29-46.

Blaskovich, M. A. (2016). "Unusual Amino Acids in Medicinal Chemistry." J Med Chem **59**(24): 10807-10836.

Bornscheuer, U. T., et al. (2012). "Engineering the third wave of biocatalysis." Nature **485**(7397): 185-194.

Brady, D. and J. Jordaan (2009). "Advances in enzyme immobilisation." Biotechnology Letters **31**(11): 1639-1650.

Buß, O., et al. (2018). "FoldX as Protein Engineering Tool: Better Than Random Based Approaches?" Comput Struct Biotechnol J **16**: 25-33.

Cai, W., et al. (2017). "Top-Down Proteomics of Large Proteins up to 223 kDa Enabled by Serial Size Exclusion Chromatography Strategy." Analytical Chemistry **89**(10): 5467-5475.

Cárdenas-Fernández, M., et al. (2015). "Co-immobilised aspartase and transaminase for high-yield synthesis of l-phenylalanine." Biochemical Engineering Journal **93**: 173-178.

Cheng, Q., et al. (2023). "Bionic Magnetic Sensor Based on the MagR/Cry4 Complex-Configured Graphene Transistor with an Integrated On-Chip Gate." ACS sensors **8**.

Cheng, R. P., et al. (2001). "β-Peptides: From Structure to Function." Chemical Reviews **101**(10): 3219-3232.

Clerici, F., et al. (2016). "Non-standard amino acids and peptides: From self-assembly to nanomaterials." Tetrahedron Letters **57**(50): 5540-5550.

Cohen, Y. R. (2002). "β-Aminobutyric Acid-Induced Resistance Against Plant Pathogens." Plant Disease **86**(5): 448-457.

Córdova, A., et al. (2002). "A Highly Enantioselective Route to Either Enantiomer of Both α- and β-Amino Acid Derivatives." Journal of the American Chemical Society **124**(9): 1866-1867.

Corso, G., et al. (2017). "Reproducible and scalable purification of extracellular vesicles using combined bind-elute and size exclusion chromatography." Scientific Reports **7**(1): 11561.

Cox, B. M., et al. (2009). "Enhanced Conversion of Racemic α-Arylalanines to (R)-β-Arylalanines by Coupled Racemase/Aminomutase Catalysis." The Journal of organic chemistry **74**(18): 6953-6959.

Cui, Y., et al. (2021). "Development of a versatile and efficient C–N lyase platform for asymmetric hydroamination via computational enzyme redesign." Nature Catalysis **4**(5): 364-373.

D'Cunha, G. B., et al. (1994). "Novel direct synthesis of l-phenylalanine methyl ester by using Rhodotorula glutinis phenylalanine ammonia lyase in an organic-aqueous biphasic system." Enzyme and Microbial Technology **16**(4): 318-322.

Dahal, Y. R. and J. D. Schmit (2018). "Ion Specificity and Nonmonotonic Protein Solubility from Salt Entropy." Biophys J **114**(1): 76-87.

de Villiers, M., et al. (2012). "Catalytic Mechanisms and Biocatalytic Applications of Aspartate and Methylaspartate Ammonia Lyases." ACS Chemical Biology **7**(10): 1618-1628.

Drienovská, I., et al. (2018). "A designer enzyme for hydrazone and oxime formation featuring an unnatural catalytic aniline residue." Nature Chemistry **10**(9): 946-952.

Drienovská, I. and G. Roelfes (2020). "Expanding the enzyme universe with genetically encoded unnatural amino acids." Nature Catalysis **3**(3): 193-202.

El-Naggar, N. E.-A., et al. (2016). "Purification, characterization, cytotoxicity and anticancer activities of L-asparaginase, anti-colon cancer protein, from the newly isolated alkaliphilic Streptomyces fradiae NEAE-82." Scientific Reports **6**(1): 32926.

Emery, T. F. (1963). "Aspartase-Catalyzed Synthesis of N-Hydroxyaspartic Acid*." Biochemistry **2**(5): 1041-1045.

Emin, C., et al. (2018). "Polyarylsulfone-based blend ultrafiltration membranes with combined size and charge selectivity for protein separation." Separation and Purification Technology **193**: 127-138.

Fawole, F. J., et al. (2018). "Effects of detoxified Jatropha curcas protein isolate on growth performance, nutrient digestibility and physio-metabolic response of Labeo rohita fingerlings." Aquaculture Nutrition **24**(4): 1223-1233.

Fernandez-Lorente, G., et al. (2020). "Immobilization of Lipases by Adsorption on Hydrophobic Supports: Modulation of Enzyme Properties in Biotransformations in Anhydrous Media." Methods in molecular biology **2100**: 143-158.

Fibriansah, G., et al. (2011). "Structural Basis for the Catalytic Mechanism of Aspartate Ammonia Lyase." Biochemistry **50**(27): 6053-6062.

Forró, E. and F. Fülöp (2007). "The first direct enzymatic hydrolysis of alicyclic β-amino esters: A route to enantiopure cis and trans β-amino acids." Chemistry: A European Journal **13**: 6397-6401.

Fujii, T., et al. (2003). "Crystal Structure of Thermostable Aspartase from Bacillus sp. YM55-1: Structure-based Exploration of Functional Sites in the Aspartase Family." Journal of Molecular Biology **328**(3): 635-654.

Gallart-Palau, X., et al. (2015). "Extracellular vesicles are rapidly purified from human plasma by PRotein Organic Solvent PRecipitation (PROSPR)." Scientific Reports **5**(1): 14664.

Gan, J., et al. (2020). "Covalent organic frameworks as emerging host platforms for enzyme immobilization and robust biocatalysis - A review." International journal of biological macromolecules.

Gao, W., et al. (2017). "Rh/DuanPhos-Catalyzed Asymmetric Hydrogenation of β-Acetylamino Vinylsulfides: An Approach to Chiral β-Acetylamino Sulfides." Organic Letters **19**(11): 2877-2880.

García-Nicolás, M., et al. (2023). "Dispersive Magnetic Solid-Phase Extraction as a Novelty Sample Treatment for the Determination of the Main Aflatoxins in Paprika." Toxins (Basel) **15**(2).

Glasner, M. E., et al. (2006). "Evolution of enzyme superfamilies." Current Opinion in Chemical Biology **10**(5): 492-497.

Grom, M., et al. (2018). "Protein A affinity chromatography of Chinese hamster ovary (CHO) cell culture broths containing biopharmaceutical monoclonal antibody (mAb): Experiments and mechanistic transport, binding and equilibrium modeling." J Chromatogr B Analyt Technol Biomed Life Sci **1083**: 44-56.

Grossmann, L., et al. (2018). "Effect of precipitation, lyophilization, and organic solvent extraction on preparation of protein-rich powders from the microalgae Chlorella protothecoides." Algal Research **29**: 266-276.

Guichard, G. and I. Huc (2011). "Synthetic foldamers." Chemical Communications **47**(21): 5933-5941.

Hall, M. (2018). Chapter 21 - Size Exclusion Chromatography (SEC). Biopharmaceutical Processing. G. Jagschies, E. Lindskog, K. Łącki and P. Galliher, Elsevier**:** 421-432.

Han, C., et al. (2015). "Nitrilase-catalyzed hydrolysis of 3-aminopropionitrile at high concentration with a tandem reaction strategy for shifting the reaction to β-alanine formation." Journal of Molecular Catalysis B: Enzymatic **115**: 113-118.

Han, J.-L., et al. (2020). "Separation and Purification of Sialylglycopeptide from Egg Yolk Based on Cotton Hydrophilic Chromatography." Chinese Journal of Analytical Chemistry **48**(1): 34-39.

Hao, X., et al. (2024). "Recent Advances in the Strategies of Simultaneous Enzyme Immobilization Accompanied by Nanocarrier Synthesis." Applied Sciences.

Harden, A. (1901). "LXIV.—The chemical action of Bacillus coli communis and similar organisms on carbohydrates and allied compounds." Journal of the Chemical Society, Transactions **79**(0): 610-628.

He, F.-S., et al. (2017). "The facile and stereoselective synthesis of pyrrolidine β-amino acids via copper(i)-catalyzed asymmetric 1,3-dipolar cycloaddition." Organic Chemistry Frontiers **4**(1): 52-56.

He, J., et al. (2018). "Recyclable aqueous two-phase system based on two pH-responsive copolymers and its application to porcine circovirus type 2 Cap protein purification." Journal of Chromatography A **1555**: 113-123.

Helmchen, G. and A. Pfaltz (2000). "PhosphinooxazolinesA New Class of Versatile, Modular P,N-Ligands for Asymmetric Catalysis." Accounts of Chemical Research **33**(6): 336-345.

Hosseini, S., et al. (2018). "Covalent Immobilization of Cellulase Using Magnetic Poly(ionic liquid) Support: Improvement of the Enzyme Activity and Stability." Journal of agricultural and food chemistry **66 4**: 789-798.

Ida, N. and M. Tokushige (1985). "L-Aspartate-induced activation of aspartase." J Biochem **98**(1): 35-39.

Ilicheva, N. V., et al. (2018). "Development and characterization of polyclonal antibodies against the linker region of the telomere-binding protein TRF2." Electronic Journal of Biotechnology **32**: 1-5.

Imam, H., et al. (2023). "Supramolecular Ionic Liquid Gels for Enzyme Entrapment." ACS Sustainable Chemistry & Engineering **11**: 6829-6837.

Jayasekera, M. M. K., et al. (1997). "Evaluation of Functionally Important Amino Acids in l-Aspartate Ammonia-Lyase from Escherichia coli." Biochemistry **36**(30): 9145-9150.

Jesionowski, T., et al. (2014). "Enzyme immobilization by adsorption: a review." Adsorption **20**: 801-821.

Jiang, M., et al. (2017). "Novel Application of Magnetic Protein: Convenient One-Step Purification and Immobilization of Proteins." Scientific Reports **7**(1): 13329.

Jie, O., et al. (2020). "Enzymatic hydrolysate of geniposide directly acts as cross-linking agent for enzyme immobilization." Process Biochemistry **99**: 187-195.

Jisha, K. C. and J. T. Puthur (2016). "Seed priming with BABA (β-amino butyric acid): a cost-effective method of abiotic stress tolerance in Vigna radiata (L.) Wilczek." Protoplasma **253**(2): 277-289.

Juaristi, E. and H. López-Ruiz (1999). "Recent Advances in the Enantioselective Synthesis of β-Amino Acids." Current Medicinal Chemistry.

Juaristi, E., et al. (1996). "Enantioselective synthesis of β-amino acids. 7. Preparation of enantiopure α-substituted β-amino acids from 1-benzoyl-2(S)-tert-butyl-3-methylperhydropyrimidin-4-one.1,2." Tetrahedron: Asymmetry **7**(8): 2233-2246.

Kahle, J. and H. Wätzig (2018). "Interlaced Size Exclusion Chromatography for faster protein analysis." European Journal of Pharmaceutics and Biopharmaceutics **126**: 101-103.

Kang, J., et al. (2021). "Molecular Diagnostic System Using Engineered Fusion Protein-Conjugated Magnetic Nanoparticles." Analytical Chemistry **93**(50): 16804-16812.

Karsten, W. E., et al. (1986). "Kinetic studies of L-aspartase from Escherichia coli: substrate activation." Biochemistry **25**(6): 1299-1303.

Kato, Y. and Y. Asano (1995). "3-Methylaspartate ammonia-lyase from a facultative anaerobe, strain YG-1002." Applied Microbiology and Biotechnology **43**(5): 901-907.

Katorcha, E. and I. V. Baskakov (2018). Analysis of Covalent Modifications of Amyloidogenic Proteins Using Two-Dimensional Electrophoresis: Prion Protein and Its Sialylation. Amyloid Proteins: Methods and Protocols. E. M. Sigurdsson, M. Calero and M. Gasset. New York, NY, Springer New York**:** 241-255.

Kawata, Y., et al. (2000). "Cloning and over-expression of thermostable Bacillus sp. YM55-1 aspartase and site-directed mutagenesis for probing a catalytic residue." Eur J Biochem **267**(6): 1847-1857.

Kawata, Y., et al. (1999). "Purification and characterization of thermostable aspartase from Bacillus sp. YM55-1." Arch Biochem Biophys **366**(1): 40-46.

Kidambi, P. R., et al. (2017). "Nanoporous Atomically Thin Graphene Membranes for Desalting and Dialysis Applications." Advanced Materials **29**(33): 1700277.

Kim, S.-H., et al. (2022). "Optimizing Parameters for the Downscaling of Daily Precipitation in Normal and Drought Periods in South Korea." Water **14**: 1108.

King, C., et al. (2018). "Characterization of recombinant monoclonal antibody variants detected by hydrophobic interaction chromatography and imaged capillary isoelectric focusing electrophoresis." J Chromatogr B Analyt Technol Biomed Life Sci **1085**: 96-103.

Kinugasa, T., et al. (2023). "Precipitation and recovery of lysozyme denatured by urea and guanidine hydrochloride using anionic surfactant and acetone." Journal of Chemical Engineering of Japan **56**(1): 2181033.

Koen, E., et al. (2014). "β-Aminobutyric Acid (BABA)-Induced Resistance in Arabidopsis thaliana: Link with Iron Homeostasis." Molecular Plant-Microbe Interactions® **27**(11): 1226-1240.

Kotz, S., et al. (2018). "Optimized two-dimensional gel electrophoresis in an alkaline pH range improves the identification of intracellular CFDA-cisplatin-protein adducts in ovarian cancer cells." ELECTROPHORESIS **39**(12): 1488-1496.

Kress, C., et al. (2017). "Solubilization of proteins in aqueous two-phase extraction through combinations of phase-formers and displacement agents." European Journal of Pharmaceutics and Biopharmaceutics **112**: 38-44.

Kritzer, J. A., et al. (2004). "Helical β-Peptide Inhibitors of the p53-hDM2 Interaction." Journal of the American Chemical Society **126**(31): 9468-9469.

Krug, D. and R. Müller (2009). "Discovery of Additional Members of the Tyrosine Aminomutase Enzyme Family and the Mutational Analysis of CmdF." ChemBioChem **10**(4): 741-750.

Kurzbaum, E., et al. (2020). "Phenol biodegradation by bacterial cultures encapsulated in 3D microfiltration-membrane capsules." Environmental Technology **41**(22): 2875-2883.

Levy, C. W., et al. (2002). "Insights into Enzyme Evolution Revealed by the Structure of Methylaspartate Ammonia Lyase." Structure **10**(1): 105-113.

Li, N., et al. (2023). "Transfection of clMagR/clCry4 imparts MR-T(2) imaging contrast properties to living organisms (E. coli) in the presence of Fe(3+) by endogenous formation of iron oxide nanoparticles." Front Mol Biosci **10**: 1119356.

Li, R., et al. (2018). "Computational redesign of enzymes for regio- and enantioselective hydroamination." Nature Chemical Biology **14**(7): 664-670.

Li, T., et al. (2019). "Purification of lactoperoxidase from bovine milk by integrating the technique of salting-out extraction with cation exchange chromatographic separation." Journal of Food Measurement and Characterization **13**(2): 1400-1410.

Liang, X., et al. (2021). "Immobilized enzymes in inorganic hybrid nanoflowers for biocatalytic and biosensing applications." Journal of materials chemistry. B **9 37**: 7597-7607.

List, B., et al. (2002). "The proline-catalyzed direct asymmetric three-component Mannich reaction: scope, optimization, and application to the highly enantioselective synthesis of 1,2-amino alcohols." J Am Chem Soc **124**(5): 827-833.

Liu, C. C. and P. G. Schultz (2010). "Adding new chemistries to the genetic code." Annu Rev Biochem **79**: 413-444.

Liu, D.-M., et al. (2017). "Tyrosinase immobilization on aminated magnetic nanoparticles by physical adsorption combined with covalent crosslinking with improved catalytic activity, reusability and storage stability." Analytica chimica acta **1006**: 90-98.

Liu, P., et al. (2020). "Immobilized metal affinity chromatography matrix modified by poly (ethylene glycol) methyl ether for purification of angiotensin I-converting enzyme inhibitory peptide from casein hydrolysate." Journal of Chromatography B **1143**: 122042.

Liu, Z., et al. (2022). "Functional Immobilization of a Biofilm-Releasing Glycoside Hydrolase Dispersin B on Magnetic Nanoparticles." Applied Biochemistry and Biotechnology **194**(2): 737-747.

Lou, Y., et al. (2018). "Secretory expression and scale-up production of recombinant human thyroid peroxidase via baculovirus/insect cell system in a wave-type bioreactor." Protein Expression and Purification **149**: 7-12.

Luca, G., et al. (2010). "Chemical Modifications Designed to Improve Peptide Stability: Incorporation of Non-Natural Amino Acids, Pseudo-Peptide Bonds, and Cyclization." Current Pharmaceutical Design **16**(28): 3185-3203.

Lyu, X., et al. (2021). "Immobilization of Enzymes by Polymeric Materials." Catalysts.

Maghraby, Y., et al. (2023). "Enzyme Immobilization Technologies and Industrial Applications." ACS Omega **8**: 5184-5196.

Mairhofer, J., et al. (2013). "Comparative Transcription Profiling and In-Depth Characterization of Plasmid-Based and Plasmid-Free Escherichia coli Expression Systems under Production Conditions." Applied and Environmental Microbiology **79**: 3802-3812.

Manjare, S. D. and K. Dhingra (2019). "Supercritical fluids in separation and purification: A review." Materials Science for Energy Technologies **2**(3): 463-484.

Martinek, T. A. and F. Fülöp (2012). "Peptidic foldamers: ramping up diversity." Chemical Society Reviews **41**(2): 687-702.

Mavencamp, T. L., et al. (2008). "Synthesis and preliminary pharmacological evaluation of novel derivatives of l-β-threo-benzylaspartate as inhibitors of the neuronal glutamate transporter EAAT3." Bioorganic & Medicinal Chemistry **16**(16): 7740-7748.

Meister, M. (2016). "Physical limits to magnetogenetics." eLife **5**: e17210.

Meyer, A., et al. (2006). "AtGAT1, a High Affinity Transporter for γ-Aminobutyric Acid in Arabidopsis thaliana*." Journal of Biological Chemistry **281**(11): 7197-7204.

Montclare, J. K. and D. A. Tirrell (2006). "Evolving Proteins of Novel Composition." Angewandte Chemie International Edition **45**(27): 4518-4521.

Moser, A. C., et al. (2018). "Studies of antibody-antigen interactions by capillary electrophoresis: A review." Methods **146**: 66-75.

Naghshbandi, M. P. and H. Moghimi (2020). "Stabilization of phytase on multi-walled carbon nanotubes via covalent immobilization." Methods in enzymology **630**: 431-451.

Ni, Z.-F., et al. (2021). "Structure-guided protein engineering of ammonia lyase for efficient synthesis of sterically bulky unnatural amino acids." Bioresources and Bioprocessing **8**(1): 103.

Ni, Z.-F., et al. (2020). "Characterization of a Novel Methylaspartate Ammonia Lyase from E. coli O157:H7 for Efficient Asymmetric Synthesis of Unnatural Amino Acids." ACS Sustainable Chemistry & Engineering **8**(1): 329-334.

Nuijens, T., et al. (2009). "Enzymatic synthesis of C-terminal arylamides of amino acids and peptides." The Journal of organic chemistry **74 15**: 5145-5150.

Oki, T., et al. (1989). "Cispentacin, a new antifungal antibiotic. II. In vitro and in vivo antifungal activities." J Antibiot (Tokyo) **42**(12): 1756-1762.

Orrego, A., et al. (2018). "Stabilization of Immobilized Lipases by Intense Intramolecular Cross-Linking of Their Surfaces by Using Aldehyde-Dextran Polymers." International Journal of Molecular Sciences **19**.

Özkan, A., et al. (2018). "Protein ion-exchange chromatography on a biomacromolecule-immobilized monolithic cryogel." Turkish Journal of Chemistry **42**.

Paizs, C., et al. (2006). "Chemoenzymatic One-Pot Synthesis of Enantiopure L-Arylalanines from Arylaldehydes." European Journal of Organic Chemistry **2006**(5): 1113-1116.

Parmeggiani, F., et al. (2018). "Synthetic and Therapeutic Applications of Ammonia-lyases and Aminomutases." Chemical Reviews **118 1**: 73-118.

Pekarsky, A., et al. (2021). "Revisiting the Potential Functionality of the MagR Protein." Magnetochemistry **7**: 147.

Pereira, A. M., et al. (2018). "High protein ingredients of microalgal origin: Obtainment and functional properties." Innovative Food Science & Emerging Technologies **47**: 187-194.

Porter, E. A., et al. (2002). "Mimicry of Host-Defense Peptides by Unnatural Oligomers: Antimicrobial β-Peptides." Journal of the American Chemical Society **124**(25): 7324-7330.

Puthan Veetil, V., et al. (2012). "Aspartase/Fumarase Superfamily: A Common Catalytic Strategy Involving General Base-Catalyzed Formation of a Highly Stabilized aci-Carboxylate Intermediate." Biochemistry **51**(21): 4237-4243.

Puthan Veetil, V., et al. (2009). "Site-directed mutagenesis, kinetic and inhibition studies of aspartate ammonia lyase from Bacillus sp. YM55-1." The FEBS Journal **276**(11): 2994-3007.

Qin, S., et al. (2016). "A magnetic protein biocompass." Nature Materials **15**(2): 217-226.

Quastel, J. H. and B. Woolf (1926). "The Equilibrium between l-Aspartic Acid, Fumaric Acid and Ammonia in Presence of Resting Bacteria." Biochemical Journal **20**(3): 545-555.

Raj, H. and G. Poelarends (2013). "The roles of active site residues in the catalytic mechanism of methylaspartate ammonia-lyase." FEBS Open Bio **3**: 285-290.

Raj, H. and G. J. Poelarends (2013). "The roles of active site residues in the catalytic mechanism of methylaspartate ammonia-lyase." FEBS Open Bio **3**(1): 285-290.

Raj, H., et al. (2012). "Characterization of a thermostable methylaspartate ammonia lyase from Carboxydothermus hydrogenoformans." Appl Microbiol Biotechnol **94**(2): 385-397.

Raj, H., et al. (2012). "Engineering methylaspartate ammonia lyase for the asymmetric synthesis of unnatural amino acids." Nature Chemistry **4**(6): 478-484.

Raj, H., et al. (2009). "Alteration of the Diastereoselectivity of 3-Methylaspartate Ammonia Lyase by Using Structure-Based Mutagenesis." ChemBioChem **10**(13): 2236-2245.

Ramos-Payán, M., et al. (2018). "Recent trends in capillary electrophoresis for complex samples analysis: A review." ELECTROPHORESIS **39**(1): 111-125.

Reetz, M. T. (2011). "Laboratory Evolution of Stereoselective Enzymes: A Prolific Source of Catalysts for Asymmetric Reactions." Angewandte Chemie International Edition **50**(1): 138-174.

Rehman, S., et al. (2016). "Cross-linked enzyme aggregates (CLEAs) of Pencilluim notatum lipase enzyme with improved activity, stability and reusability characteristics." International journal of biological macromolecules **91**: 1161-1169.

Rodler, A., et al. (2018). "Hydrophobic interaction chromatography of proteins: Studies of unfolding upon adsorption by isothermal titration calorimetry." Journal of Separation Science **41**(15): 3069-3080.

Rodrigues, R., et al. (2021). "Stabilization of enzymes via immobilization: Multipoint covalent attachment and other stabilization strategies." Biotechnology advances: 107821.

Röhm, K. H. and R. L. van Etten (1985). "Stereospecific synthesis of L-[1,4-13C2]aspartic acid, L-β-([13C]cyano)alanine and L-[4-13C]aspartic acid." Journal of Labelled Compounds and Radiopharmaceuticals **22**(9): 909-915.

Rother, C. and B. Nidetzky (2014). Enzyme Immobilization by Microencapsulation: Methods, Materials, and Technological Applications. Encyclopedia of Industrial Biotechnology**:** 1-21.

Rudolph, F. B. and H. J. Fromm (1971). "The purification and properties of aspartase from Escherichia coli." Archives of Biochemistry and Biophysics **147**(1): 92-98.

Saeed Gulzar, M., et al. (1997). "Preparation of N-substituted aspartic acids via enantiospecific conjugate addition of N-nucleophiles to fumaric acids using methylaspartase: synthetic utility and mechanistic implications1." Journal of the Chemical Society, Perkin Transactions 1(5): 649-656.

Sahebani, N., et al. (2011). "The effects of β-amino-butyric acid on resistance of cucumber against root-knot nematode, Meloidogyne javanica." Acta Physiologiae Plantarum **33**(2): 443-450.

Sannino, F., et al. (2020). "Covalent Immobilization of β-Glucosidase into Mesoporous Silica Nanoparticles from Anhydrous Acetone Enhances Its Catalytic Performance." Nanomaterials **10**.

Santos-Moriano, P., et al. (2016). "Vinyl sulfone-activated silica for efficient covalent immobilization of alkaline unstable enzymes: application to levansucrase for fructooligosaccharide synthesis." RSC Advances **6**: 64175-64181.

Sattar, H., et al. (2018). "Agar-agar immobilization: An alternative approach for the entrapment of protease to improve the catalytic efficiency, thermal stability and recycling efficiency." International journal of biological macromolecules **111**: 917-922.

Schejbal, J. and Z. Glatz (2018). "Immobilized-enzyme reactors integrated with capillary electrophoresis for pharmaceutical research." Journal of Separation Science **41**(1): 323-335.

Seebach, D. and J. Gardiner (2008). "Beta-peptidic peptidomimetics." Acc Chem Res **41**(10): 1366-1375.

Shi, W., et al. (1997). "The Structure of l-Aspartate Ammonia-Lyase from Escherichia coli." Biochemistry **36**(30): 9136-9144.

Shibasaki, M. and M. Kanai (2008). "Asymmetric Synthesis of Tertiary Alcohols and α-Tertiary Amines via Cu-Catalyzed C−C Bond Formation to Ketones and Ketimines." Chemical Reviews **108**(8): 2853-2873.

Shimamoto, K. (2008). "Glutamate transporter blockers for elucidation of the function of excitatory neurotransmission systems." Chem Rec **8**(3): 182-199.

Shindo, M., et al. (2002). "Anionic Inverse Electron-Demand 1,3-Dipolar Cycloaddition of Nitrones with Ynolates. Facile Stereoselective Synthesis of 5-Isoxazolidinones Leading to β-Amino Acids." Organic Letters **4**(18): 3119-3121.

Sieber, S., et al. (2017). "Immobilization of Enzymes on PLGA Sub-Micrometer Particles by Crosslinked Layer-by-Layer Deposition." Macromolecular bioscience **17 8**.

Spengler, J., et al. (2010). "Synthesis of orthogonally protected l-threo-β-ethoxyasparagine." Amino Acids **39**(1): 161-165.

Strompen, S. (2012). "Process development of a solvent-free, chemoenzymatic reaction sequence for the enantioselective synthesis of beta-amino acid esters."

Sun, J., et al. (2017). "Stability and activity of immobilized trypsin on carboxymethyl chitosan-functionalized magnetic nanoparticles cross-linked with carbodiimide and glutaraldehyde." Journal of chromatography. B, Analytical technologies in the biomedical and life sciences **1054**: 57-63.

Suo, H., et al. (2020). "Ionic liquids-modified cellulose coated magnetic nanoparticles for enzyme immobilization: Improvement of catalytic performance." Carbohydrate polymers **234**: 115914.

Takov, K., et al. (2019). "Comparison of small extracellular vesicles isolated from plasma by ultracentrifugation or size-exclusion chromatography: yield, purity and functional potential." Journal of Extracellular Vesicles **8**(1): 1560809.

Tang, C., et al. (2014). "Cross-linked polymer nanofibers for hyperthermophilic enzyme immobilization: approaches to improve enzyme performance." ACS applied materials & interfaces **6 15**: 11899-11906.

Teng, M.-Y., et al. (2006). "Effect of ultrasound on the separation of binary protein mixtures by cross-flow ultrafiltration." Desalination **200**(1): 280-282.

Thammasena, R., et al. (2020). "Evaluation of nutrient content, physicochemical and functional properties of desalted duck egg white by ultrafiltration as desalination." Animal Science Journal **91**(1): e13339.

Tian, Z. (2019). Aspartic enzyme mutant and application thereof. China, Yikelai Biotechnology Group Co ltd.

Tizchang, S., et al. (2021). "Immobilization of β-galactosidase by halloysite-adsorption and entrapment in a cellulose nanocrystals matrix." Biochimica et biophysica acta. General subjects: 129896.

Trivedi, H., et al. (2023). "Immobilization of Protease on Synthesized Beads of K-Carrageenan by Entrapment: its use in Commercial Activity like Juice Purification." International Journal of Research Publication and Reviews.

Tu, X., et al. (2018). "Comparison of salting-out and sugaring-out liquid-liquid extraction methods for the partition of 10-hydroxy-2-decenoic acid in royal jelly and

their co-extracted protein content." J Chromatogr B Analyt Technol Biomed Life Sci **1073**: 90-95.

Turner, N. J. (2009). "Directed evolution drives the next generation of biocatalysts." Nature Chemical Biology **5**(8): 567-573.

Turner, N. J. (2011). "Ammonia lyases and aminomutases as biocatalysts for the synthesis of α-amino and β-amino acids." Curr Opin Chem Biol **15**(2): 234-240.

Vaghari, H., et al. (2015). "Application of magnetic nanoparticles in smart enzyme immobilization." Biotechnology Letters **38**: 223-233.

Varghese, A., et al. (2018). "Remediation of heavy metals and dyes from wastewater using cellulose-based adsorbents." Environmental Chemistry Letters **17**: 867-877.

Velasco-Lozano, S. (2020). "Immobilization of Enzymes as Cross-Linked Enzyme Aggregates: General Strategy to Obtain Robust Biocatalysts." Methods in molecular biology **2100**: 345-361.

Voeten, R. L. C., et al. (2018). "Capillary Electrophoresis: Trends and Recent Advances." Anal Chem **90**(3): 1464-1481.

Vogel, A., et al. (2014). "Converting Aspartase into a β-Amino Acid Lyase by Cluster Screening." ChemCatChem **6**(4): 965-968.

Wang, L., et al. (2019). "Isolation and quantitation of exosomes isolated from human plasma via hydrophobic interaction chromatography using a polyester, capillary-channeled polymer fiber phase." Analytica chimica acta **1082**: 186-193.

Wang, L., et al. (2006). "EXPANDING THE GENETIC CODE." Annual Review of Biophysics **35**(Volume 35, 2006): 225-249.

Wang, L., et al. (2019). "Magnetic immobilization of a quorum sensing signal hydrolase, AiiA." MicrobiologyOpen **8**(8): e00797.

Wang, S., et al. (2024). "Unexpected divergence in magnetoreceptor MagR from robin and pigeon linked to two sequence variations." Zool Res **45**(1): 69-78.

Wang, W., et al. (2024). "Chitosan-Based Charge-Controllable Supramolecular Carrier for Universal Immobilization of Enzymes with Different Isoelectric Points." Journal of agricultural and food chemistry.

Wang, Y., et al. (2020). "Surface charge-based rational design of aspartase modifies the optimal pH for efficient β-aminobutyric acid production." International journal of biological macromolecules **164**: 4165-4172.

Wani, M. C., et al. (1971). "Plant antitumor agents. VI. Isolation and structure of taxol, a novel antileukemic and antitumor agent from Taxus brevifolia." Journal of the American Chemical Society **93**(9): 2325-2327.

Warburton, M., et al. (2015). "OneClick: A Program for Designing Focused Mutagenesis Experiments." AIMS Bioengineering **2**: 126-143.

Watanabe, M., et al. (2002). GABA and GABA Receptors in the Central Nervous System and Other Organs. International Review of Cytology. K. W. Jeon, Academic Press. **213:** 1-47.

Weaver, T., et al. (1997). "Mutations of fumarase that distinguish between the active site and a nearby dicarboxylic acid binding site." Protein Sci **6**(4): 834-842.

Weiner, B., et al. (2008). "Biocatalytic Enantioselective Synthesis of N-Substituted Aspartic Acids by Aspartate Ammonia Lyase." Chemistry – A European Journal **14**(32): 10094-10100.

Wennemers, H. (2011). "Asymmetric catalysis with peptides." Chemical Communications **47**(44): 12036-12041.

Winklhofer, M. and H. Mouritsen (2016). "A room-temperature ferrimagnet made of metallo-proteins?" bioRxiv: 094607.

Won, K., et al. (2005). "Optimization of lipase entrapment in Ca-alginate gel beads." Process Biochemistry **40**(6): 2149-2154.

Wu, J., et al. (2015). "Enhanced enzyme stability through site-directed covalent immobilization." Journal of biotechnology **193**: 83-90.

Wu, Y., et al. (2014). "Adsorption of Trametes versicolor laccase to soil iron and aluminum minerals: enzyme activity, kinetics and stability studies." Colloids and surfaces. B, Biointerfaces **114**: 342-348.

Wubbolts, M. (2002). Addition of Amines to C = C Bonds. Enzyme Catalysis in Organic Synthesis**:** 866-872.

Xi, H., et al. (2018). "Expression and purification of pneumococcal surface protein a of clade 4 in Escherichia coli using hydroxylapatite and ion-exchange column chromatography." Protein Expr Purif **151**: 56-61.

Xie, J., et al. (2007). "A Genetically Encoded Bidentate, Metal-Binding Amino Acid." Angewandte Chemie International Edition **46**(48): 9239-9242.

Xiong, C., et al. (2018). "Preparation and evaluation of a hydrophilic interaction and cation-exchange chromatography stationary phase modified with 2-methacryloyloxyethyl phosphorylcholine." Journal of Chromatography A **1546**: 56-65.

Xue, L., et al. (2020). "A Novel Biomimetic Magnetosensor Based on Magneto-Optically Involved Conformational Variation of MagR/Cry4 Complex." Advanced Electronic Materials **6**: 1901168.

Yang, J., et al. (2018). "Detection of plant protein adulterated in fluid milk using two-dimensional gel electrophoresis combined with mass spectrometry." J Food Sci Technol **55**(7): 2721-2728.

Yen, C.-H., et al. (2015). "A Novel Method for Separation of Caseins from Milk by Phosphates Precipitation." Preparative Biochemistry & Biotechnology **45**(1): 18-32.

Yoon, M. Y., et al. (1995). "Acid-base chemical mechanism of aspartase from Hafnia alvei." Arch Biochem Biophys **320**(1): 115-122.

Zasloff, M. (1987). "Magainins, a class of antimicrobial peptides from Xenopus skin: isolation, characterization of two active forms, and partial cDNA sequence of a precursor." Proceedings of the National Academy of Sciences **84**(15): 5449-5453.

Zhang, D., et al. (2015). "Development of β-Amino Acid Dehydrogenase for the Synthesis of β-Amino Acids via Reductive Amination of β-Keto Acids." ACS Catalysis **5**: 2220-2224.

Zhang, J., et al. (2024). "On the evolutionary trail of MagRs." Zool Res **45**(4): 821-830.

Zhang, L., et al. (2018). "Biocompatible magnetic nanoparticles grafted by poly(carboxybetaine acrylamide) for enzyme immobilization." International journal of biological macromolecules **118 Pt A**: 1004-1012.

Zhang, Y., et al. (2024). "Mitochondrial targeting sequence of magnetoreceptor MagR: More than just targeting." Zool Res **45**(3): 468-477.

Zhao, K. (2021). Synthesis and purification method of (R) -3-aminobutyric acid

. China, Third Institute of Oceanography MNR.

Zhao, M., et al. (2019). "Adsorption of cholesterol oxidase and entrapment of horseradish peroxidase in metal-organic frameworks for the colorimetric biosensing of cholesterol." Talanta **200**: 293-299.

Zhou, Y., et al. (2023). "Towards magnetism in pigeon MagR: Iron- and iron-sulfur binding work indispensably and synergistically." Zool Res **44**(1): 142-152.

Zhu, Y.-T., et al. (2014). "Covalent immobilization of porcine pancreatic lipase on carboxyl-activated magnetic nanoparticles: characterization and application for enzymatic inhibition assays." Materials science & engineering. C, Materials for biological applications **38**: 278-285.

Zimmerli, L., et al. (2000). "Potentiation of pathogen-specific defense mechanisms in Arabidopsis by beta -aminobutyric acid." Proc Natl Acad Sci U S A **97**(23): 12920-12925.

9 APPENDICES

Appendix 1: Gene Sequences Used in This Study

The gene sequences utilized in this study were selected for enzyme engineering and protein expression, aiming to broaden the enzymatic toolbox for the synthesis of β-amino acids and unnatural amino acids. This appendix presents the complete DNA sequences flanked with restriction site on both sides, for each protein investigated in the project, spanning from the ATG start codon to the TAA or TGA stop codon. These sequences were integral to the exploration of enzymatic activities, protein engineering, and the development of biocatalysts with enhanced industrial relevance.

Gene name	DNA sequence
clMagR	CAT ATG CTT CAC ATT CTG GTT TGC GCA AGT ACT CAT TGC AAA CAG AAG AAT ACC CAG ATT GAC CTG TAT GTG TTC GTC TTT CAG ACT CCA TCA GCG GTA CAG AAA ATC AAA GAA CTC CTG AAA GAC AAA CCG GAA CAT GTG GGC GTT AAA GTC GGA GTT CGC ACA CGT GGC TGT AAT GGC CTG TCT TAC ACC TTA GAG TAC ACG AAG TCG AAA GGG GAT TCG GAT GAA GAA GTT GTC CAA GAT GGT GTA CGC GTG TTT ATC GAG AAG AAA GCC CAA TTG ACC CTG TTA GGG ACG GAA ATG GAC TAT GTG GAG GAT AAA CTG TCC AGC GAA TTT GTG TTC AAC AAT CCG AAC ATC AAA GGC ACC TGT GGT TGC GGT GAA AGC TTC AAC ATT GGA TCC TAA GAA TTC
dmMagR	CAT ATG GCT ACA CGC GTA GTT GCG ACC GCT ACC GTT CGT GCC GTC AAA GGT CGC AAA CTG ATT CCT ACT CGT GCA GCG TTA ACC TTG ACT CCA GCA GCC GTC TTA CGG ATC AAA ACC CTG CTG CAG GAT AAA CCG GAT ATG GTG GGC TTG AAA GTA GGG GTT CGC CAA CGT GGG TGC AAT GGC CTG TCA TAC ACG CTG GAT TAT GCC AGT CAG AAG GAC AAA CTG GAT GAG GAA GTT GTG CAG GAT GGT GTG AAG GTG TTC ATT GAC AAG AAA GCG CAA CTG TCT CTG CTT GGC ACG GAA ATG GAC TTT GTC GAA TCC AAA CTC TCG AGC GAG TTT GTG TTC AAC AAT CCG AAC ATC AAA GGC ACG TGT GGT TGC GGA GAA TCG TTT AGC ATG GGA TCC TAA GAA TTC
AspB-M2	atgGGCAATACCGATGTGCGCATCGAAAAAGATTTTCTGGGC GAAAAAGAAATCCCGAAAGATGCCTATTATGGTGTTCAGAC CATTCGTGCAACCGAAAACTTTCCGATTACCGGTTATCGTAT TCATCCGGAACTGATTAAAAGCCTGGGCATTGTGAAAAAAA GCGCAGCACTGGCAAATATGGAAGTTGGTCTGCTGGATAAA

	GAAGTGGGTCAGTATATTGTTAAAGCAGCCGATGAAGTGAT TGAAGGCAAATGGAATGATCAGTTTATTGTGGACCCGATTC AAGGTGGTGCAGGCACCAGCATTAATATGAATGCAAATGAA GTTATTGCCAACCGTGCACTGGAACTGATGGGTGAAGAAA AAGGTAACTATAGCAAAATCAGCCCGAATAGCCATGTTAATA TGAGCCAGAGCACCAATGATGCATTTCCGACCGCAACACAT ATTGCAGTTCTGAGCCTGCTGAACCAGCTGATTGAAACCAC CAAATATATGCAGCAAGAATTTATGAAAAAAGCGGACGAAT TTGCCGGTGTGATTAAAATGGGTCGTTGTCATCTGCAGGAT GCAGTTCCGATTCTGCTGGGTCAAGAATTTGAAGCATATGC ACGTGTTATTGCCCGTGATATTGAACGTATTGCAAATACCCG CAATAACCTGTATGATATCAATATGGGTGCAACCGCAGTTGG CACCGGTCTGAATGCAGATCCGGAATATATCAGCATTGTTAC CGAACATCTGGCCAAATTTAGCGGTCATCCGCTGCGTAGCG CACAGCATCTGGTTGATGCAACCCAGAATACCGATTGTTATA CCGAAGTTAGCAGCGCACTGAAAGTGTGCATGATTAACATG AGCAAAATTGCCAATGATCTGCGTCTGATGGCAAGCGGTCC GCGTGCAGGTCTGAGCGAAATTGTTCTGCCTGCACGTCAGC CTGGTAGCAGCATTATTCCTGGTATGGTTTGTCCGGTTATGC CGGAAGTTATGAATCAGGTTGCATTTCAGGTGTTTGGTAAC GATCTGACCATTACCAGCGCAAGCGAAGCAGGTCAGTTTG AACTGAATGTTATGGAACCGGTGCTGTTTTTCAATCTGATTC AGAGCATTAGCATCATGACCAACGTGTTTAAATCCTTTACCG AGAATTGCCTGAAAGGCATTAAAGCCAATGAAGAACGCAT GAAAGAATATGTGGAAAAGAGCATTGGTATCATCACCGCAA TTAATCCGCATGTTGGTTATGAAACCGCAGCAAAACTGGCA CGTGAAGCCTATCTGACCGGTGAAAGCATTCGTGAACTGTG TATCAAATATGGTGTGCTGACCGAAGAACAGCTGAATGAAA TTCTGAATCCGTATGAAATGACCCATCCGGGTATTGCAGGTC GTAAAGAAAATCTGTATTTTCAGGGTCATCATCACCATCACC ACTAA
PmAspA	CATATGACCGTTACTCGCAAAGAGGTGGACTTACTGGGTGA ACGGGAAGTACCGGCAGATGCGTATTGGGGCATCCATACCC TGCGTGCTGTCGAAAACTTCAACATCTCTAATGCTGTCATTA GCGACGTGCCGGACTTTGTTCGTGGCATGGTGATGGTCAAG AAAGCGACCGCATTAGCCAATGGCGAACTCGGCGCAATTCC AGACAAAATCGCAAAGGCGATTGTTGCAGCATGTGATGAG ATTCTGACGACTGGTAAATGCCTGGATCAGTTTCCGAGTGA CATTTATCAGGGTGGTGCCGGAACAAGTGTCAATATGAACA

	CGAACGAAGTTGTGGCCAATCTGGCCTTGGAACTGCTGGG ACACAAGAAAGGCGAATACCAGTACTTAGACCCGATGGATC ATGTGAATGCGTCCCAATCCACGAATGATGCGTATCCGACC GGTTTTCGCATTGCGGTGTATAACTCGATCATGAAATTGGTG GCCAAGGTGCTGTACCTTCAACAGGGCTTCGAAAACAAAG CCAAAGAATTTTCCCACATTCTGAAAATGGGCCGCACCCAG TTACAGGATGCTGTACCTATGACTGTAGGTCAGGAGTTTAA AGCGTTCAGTGTCTTGCTTGATGAGGAAGTACGTAACTTAA CTCGCACAGCTGAATATCTGCTGGAAGTTAATCTGGGTGCG ACCGCCATTGGCACCGGGCTGAACACGCCTAAAGGGTATG CCCCATTGGCGGTTAAATACCTGAGCGAAGTAACAGGCCTC CCTTGTGTGCTGGCAGAGAACCTGATTGAGGCGACGTCTGA TTGTGGAGCGTACGTGATGGTGCATGGTGCACTGAAACGCA CTGCGGTGAAACTGTCAAAGGTGTGCAACGATCTGCGCTTA CTGAGCTCTGGTCCACGTGCTGGCCTGAATGAGATCAACCT TCCCGAACTTCAAGCAGGGAGCTCAATTATGCCGGCGAAA GTCAATCCGGTTGTTCCGGAAGTCGTGAACCAGGTGTGCTA TAAAGTAATGGGCAACGATACAACCATCACCTTTGCCGCTG AAGCTGGACAGTTACAACTCAATGTCATGGAACCGGTCATT GCGCAAGCGATGTTTGAGTCGATTGACATCCTTACCAATGC GTGTGTTAATCTGCGCGACAAATGCATTGATGGCATCACCG TTAACAAGGAAACGTGCGAAAATTATGTGTTCAATTCGATT GGCATCGTTACCTATCTGAACCCGTTCATCGGTCACCATAAT GGGGATCTGGTGGGCAAAATCTGCGCCAAAACCGGTCGTG GGGTTAAAGAAGTAGTGCTGGAGAAAGGTCTGCTCACGGA AGCCGAACTCGATGATATTTTGAGCGTCGAGAACTTGATGA ACCCCACGTACAAGGCCAAACTGAACAAATAAGAATTC
6H-PmAspA-QM	CAT**ATG**CATCACCATCATCACCACACAGTAACTCGCAAAGAAGTGGA CTTGTTGGGTGAACGCGAAGTTCCAGCTGATGCCTATTGGGGCATTC ATACCCTGCGTGCGGTCGAAAACTTCAACATCAGTAACGCGGTGATT TCTGATGTCCCGGATTTTGTTCGCGGTATGGTCATGGTAAAGAAAGC AACCGCATTAGCCAATGGTGAACTGGGCGCAATTCCGGATAAAATCG CGAAAGCCATCGTTGCCGCCTGTGACGAGATTCTGACTACCGGCAAA TGCCTGGATCAGTTTCCGTCGGACATTTACCAAGGTGGTGCTGGTAC GTCCGTTAACATGAACACGAACGAAGTTGTCGCGAATTTAGCCCTGG AATTGCTCGGACATAAGAAAGGCGAATACCAGTATCTCGATCCTATG GACCATGTGAATGCAAGCCAGTCTACGAATGATGCGTATCCGACCGG ATTTCGCATTGCCGTCTACAACAGCATCATGAAGCTGGTAGCTAAAG TGCTGTATCTGCAACAGGGCTTTGAGAACAAAGCGAAAGAATTTTC GCACATTCTGAAGATGGGTCGTTGCCAGCTGCAGGATGCAGTCCCGA TGACGGTAGGACAGGAGTTCAAAGCCTTTAGCGTGTTACTTGACGA

	AGAAGTTCGCAACCTTACGCGTACGGCCGAATACCTGTTGGAGGTTA ATCTGGGCGCAACTGCGATTGGGACAGGCTTAAATACCCCGAAAGG ATATGCTCCCCTGGCGGTCAAATATCTGTCAGAGGTGACTGGGCTCC CTTGTGTGCTGGCGGAAAACCTGATTGAAGCAACCTCGGATTGTGG CGCTTATGTGATGGTTCACGGTGCCTTAAAACGTACGGCAGTGAAGC TGTCCAAAGTTTGCAACGATCTGCGCCTTTTATCTAGTGGCCCACGC GCCGGTTTGAACGAAATCAACTTACCGGAACTGCAAGCGGGCTCAT CCATTATCCCGGCTATGGTATGCCCAGTTGTTCCGGAAGTGGTCAATC AGGTTTGCTACAAAGTCATGGGCAATGACACGACCATCACATTTGCG GCGGAAGCCGGTCAACTCCAGCTGAACGTCATGGAACCTGTGATTG CGCAAGCGATGTTCGAAAGCATTGACATTCTGACCAATGCATGTGTG AATCTTCGGGATAAATGCATTGATGGGATCACCGTAAACAAAGAGAC ATGTGAGAATTATGTGTTCAACAGCATCGGCATTGTGACCTACCTGA ACCCCTTCATTGGTCACCATAACGGCGATCTTGTGGGCAAAATCTGC GCTAAAACCGGGCGTGGGGTAAAAGAGGTGGTGCTGGAAAAGGGT CTGCTGACTGAGGCGGAGTTGGATGACATCCTCAGTGTGGAAAATCT GATGAATCCGACCTATAAAGCGAAACTGAATAAG**TAA**GAATTC
DtMAL	CATATGACCGTTACTCGCAAAGAGGTGGACTTACTGGGTGAACGGG AAGTACCGGCAGATGCGTATTGGGGCATCCATACCCTGCGTGCTGTC GAAAACTTCAACATCTCTAATGCTGTCATTAGCGACGTGCCGGACTT TGTTCGTGGCATGGTGATGGTCAAGAAAGCGACCGCATTAGCCAATG GCGAACTCGGCGCAATTCCAGACAAAATCGCAAAGGCGATTGTTGC AGCATGTGATGAGATTCTGACGACTGGTAAATGCCTGGATCAGTTTC CGAGTGACATTTATCAGGGTGGTGCCGGAACAAGTGTCAATATGAAC ACGAACGAAGTTGTGGCCAATCTGGCCTTGGAACTGCTGGGACACA AGAAAGGCGAATACCAGTACTTAGACCCGATGGATCATGTGAATGCG TCCCAATCCACGAATGATGCGTATCCGACCGGTTTTCGCATTGCGGT GTATAACTCGATCATGAAATTGGTGGCCAAGGTGCTGTACCTTCAAC AGGGCTTCGAAAACAAAGCCAAAGAATTTTCCCACATTCTGAAAAT GGGCCGCACCCAGTTACAGGATGCTGTACCTATGACTGTAGGTCAGG AGTTTAAAGCGTTCAGTGTCTTGCTTGATGAGGAAGTACGTAACTTA ACTCGCACAGCTGAATATCTGCTGGAAGTTAATCTGGGTGCGACCGC CATTGGCACCGGGCTGAACACGCCTAAAGGGTATGCCCCATTGGCGG TTAAATACCTGAGCGAAGTAACAGGCCTCCCTTGTGTGCTGGCAGAG AACCTGATTGAGGCGACGTCTGATTGTGGAGCGTACGTGATGGTGCA TGGTGCACTGAAACGCACTGCGGTGAAACTGTCAAAGGTGTGCAAC GATCTGCGCTTACTGAGCTCTGGTCCACGTGCTGGCCTGAATGAGAT CAACCTTCCCGAACTTCAAGCAGGGAGCTCAATTATGCCGGCGAAA GTCAATCCGGTTGTTCCGGAAGTCGTGAACCAGGTGTGCTATAAAGT AATGGGCAACGATACAACCATCACCTTTGCCGCTGAAGCTGGACAG TTACAACTCAATGTCATGGAACCGGTCATTGCGCAAGCGATGTTTGA GTCGATTGACATCCTTACCAATGCGTGTGTTAATCTGCGCGACAAATG CATTGATGGCATCACCGTTAACAAGGAAACGTGCGAAAATTATGTGT

	TCAATTCGATTGGCATCGTTACCTATCTGAACCCGTTCATCGGTCACC ATAATGGGGATCTGGTGGGCAAAATCTGCGCCAAAACCGGTCGTGG GGTTAAAGAAGTAGTGCTGGAGAAAGGTCTGCTCACGGAAGCCGAA CTCGATGATATTTTGAGCGTCGAGAACTTGATGAACCCCACGTACAA GGCCAAACTGAACAAATAAGAATTC
6H-DtMAL-SM	CAT**ATG**CATCATCATCACCACCATATTAAGGACGCGTTTTAT AGCATCGGTCTTAGTGGCTTTTACTTTGACGATCAACGTGC CATCAAAGCTGGTGCCAAAGAAGATGGCTTTGCGTATCGCG GTGTTCCGTTGACATCGGGTTATGAAGCCGTTCGCCAGAAA GGAGAAAGCATTTCAGTGATGCTCTTCCTGGATGACGGCCA AATCGCGTTTGGGGACTGTGCGGCTATCCAGTATTCTGGTG CCGGTGGGCGTGAACCCCTGTTCAAAGCGCGTGATTTAGCG AAAGATCTTGAGAAAGTCGTGTTCCCGTTCCTGATGAACGA GAAATGGAGCAGCTTTCGCGAAATGTGTCAGAAACTGGAA GATTTACGCGTGAATGGAAAGAAACTGCACACGGCAATTC GGTACGGTGTTTCACAGGTGATCCTGGATACGTTTGCTAAG TACTACAAGAAAACCATGACCGAGATCATTCGCGATGAGTA TTCTCTGAATTTCGAAATTAAGAAAGTCCCGATTTTCGCGC AGTCCGGAGATGAGCGCTATATTAATGCGGACAAAATGATC CTCAAACGTGTCGATGTACTGCCACATGCCCTGATCAACAA CGTGGAAACCAAGTTAGGTTGGCGCGGTGAAAAGCTTATT GAATATCTGGGCTGGTTGAAAGAACGCGTTCGGATCTTAGG AGGTGACAACTATTACCCAGTGTTTCACATTGATGTGTACG GGACCATTGGGATTGCCTTTCAGTACAATGTGGACGAAATT GCGGAGTATCTCGGCCGTTTAGAGAAAATTTGCTATCCGTAT AAACTGCGCATTGAAGGCCCTGTCGACATGGAATCCAAAG AATTGCAGATTGAATTTCTGTCGAAACTGCGCAAGAAACTG AAAGAGAAAGGCATCAAAGTAGACATTGTGGCGGATGAAT GGTGTAACAGTCTGAACGATATCAAAGATTTCATCAAAGCG GAGGCTGTAGACATGATTCAGATCAAAACCCCGGTACTGGG GTCGATTCACAACAGCATTGAAGCCGTGCTGTATTGCAAAG AAAACAACATTGGCGCATACCTTGGTGGCTCCTGCAATGAA ACGGATCGTTCTGCACAAGTTAGTGTTCATGTGGCACTGGC CACTCAAGCAGACCAAATCGCTGCAAAACCTGGCATGGGC GTCGATGAAGGCCTCATGATTGTCTACAATGAGATGATGCGT ACTCTGCGCATCCTGAAACGTAAGGGCTTGAATGTTATCGA TGATTAAGAATTC

Appendix 2: NMR Spectra for Enzymatic Conversion Reactions

The appendix 2 presents the detailed nuclear magnetic resonance (NMR) analysis conducted to validate enzymatic conversions performed by AspB and its engineered mutants. The experiments were conducted using various substrates under optimized conditions.

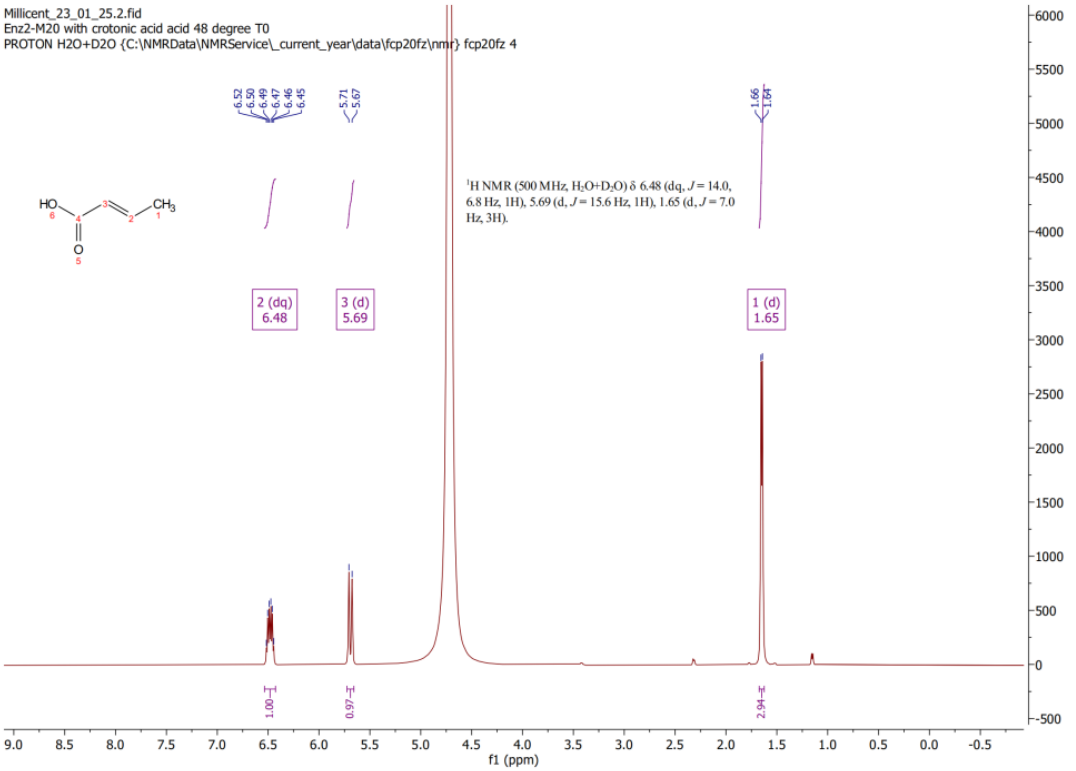

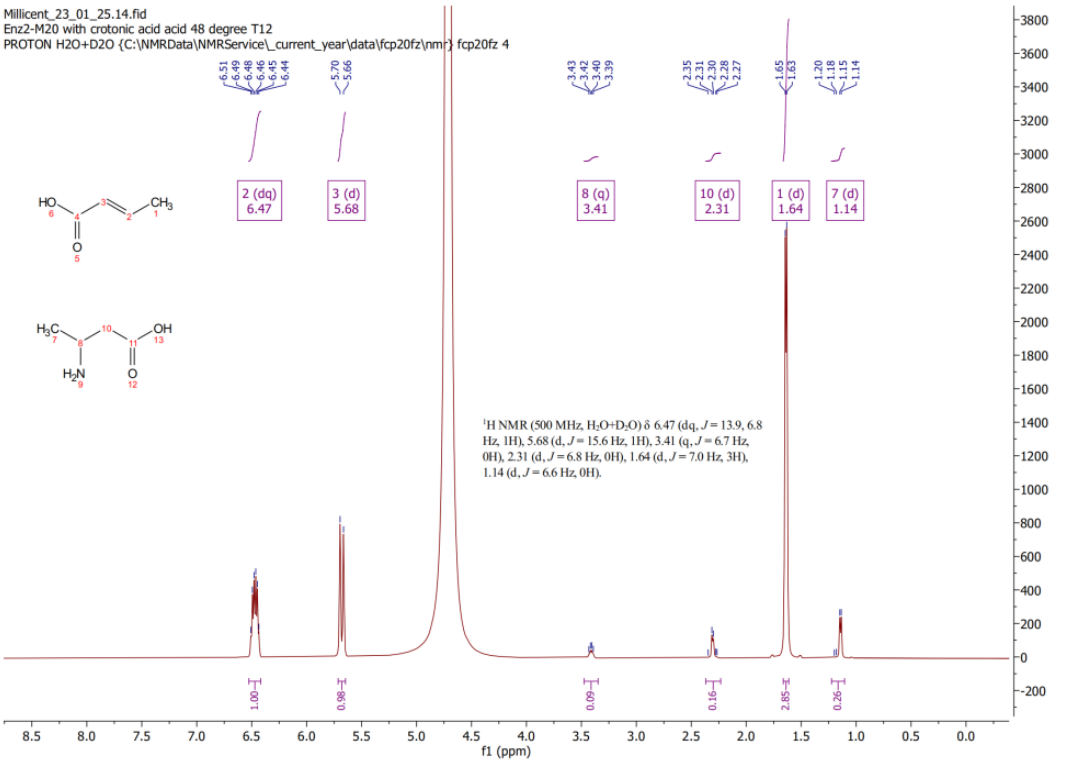

Figure A2.1:

Substrate: 300 g/L Crotonic Acid, pH 9.0 (adjusted by 35% NH_4OH)

Conditions: Reaction at 48°C with enzymatic monitoring every 2 hours, over 24 hours reaction time.

Enzyme Used: AspB-Enz2M20

Observation: NMR spectra reveal the gradual conversion of crotonic acid, evidenced by the diminishing vinyl proton peaks at δ6.46 ppm and δ5.68 ppm at the beginning of the reaction (*Top*) and the appearance of new product peaks at δ3.41 ppm, δ2.31 ppm, and δ1.65 ppm at 24 hours of the reaction (*bottom*).

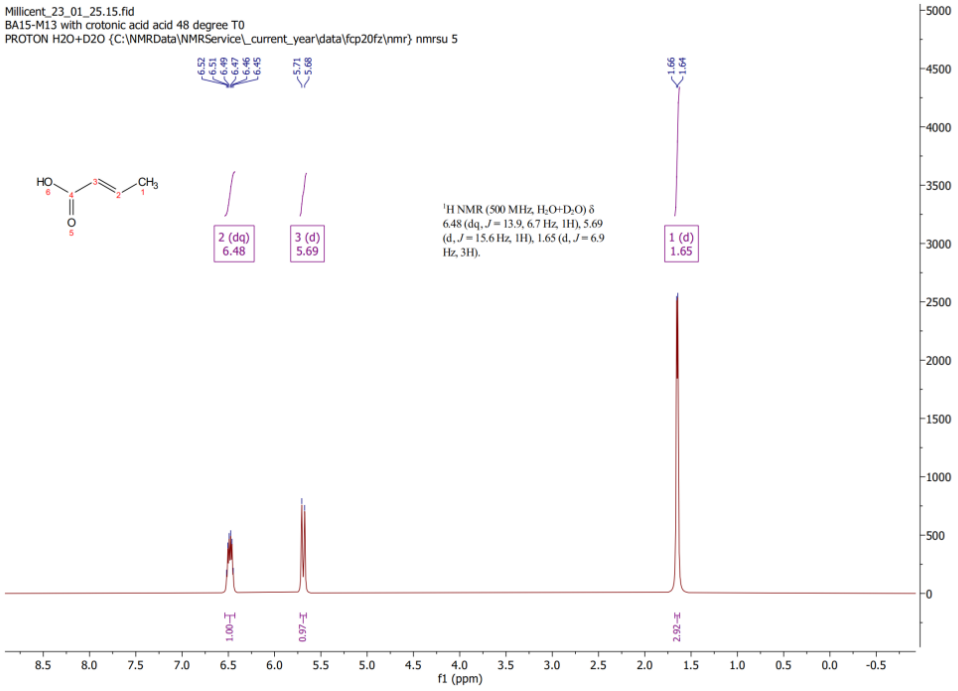

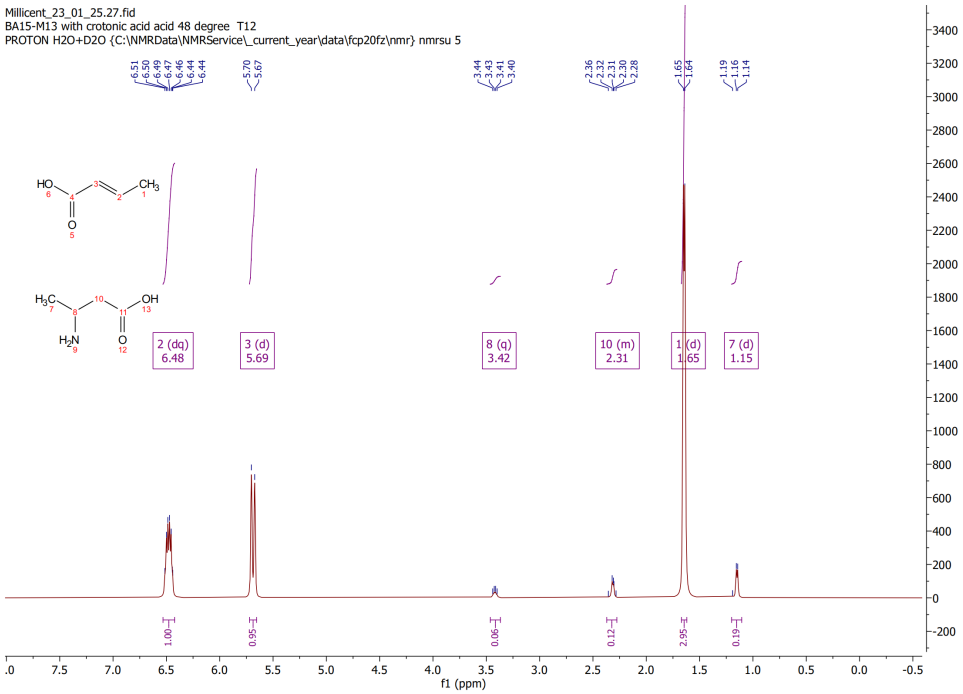

Figure A2.2:

Substrate: 300 g/L Crotonic Acid, pH 9.0 (adjusted by 35% NH_4OH)

Conditions: Reaction at 48°C with NMR monitoring every 2 hours, over 24 hours.

Enzyme Used: AspB-BA15-M13

Observation: The top spectra represent the beginning of reaction and the bottom represent the reaction after 24 hours. The spectra show a decrease in crotonic acid peaks (δ6.48 ppm and δ5.69 ppm) and the emergence of new product peaks corresponding to R-BABA (e.g., δ3.42 ppm, δ2.31 ppm, and δ1.15 ppm), indicating enzymatic activity.

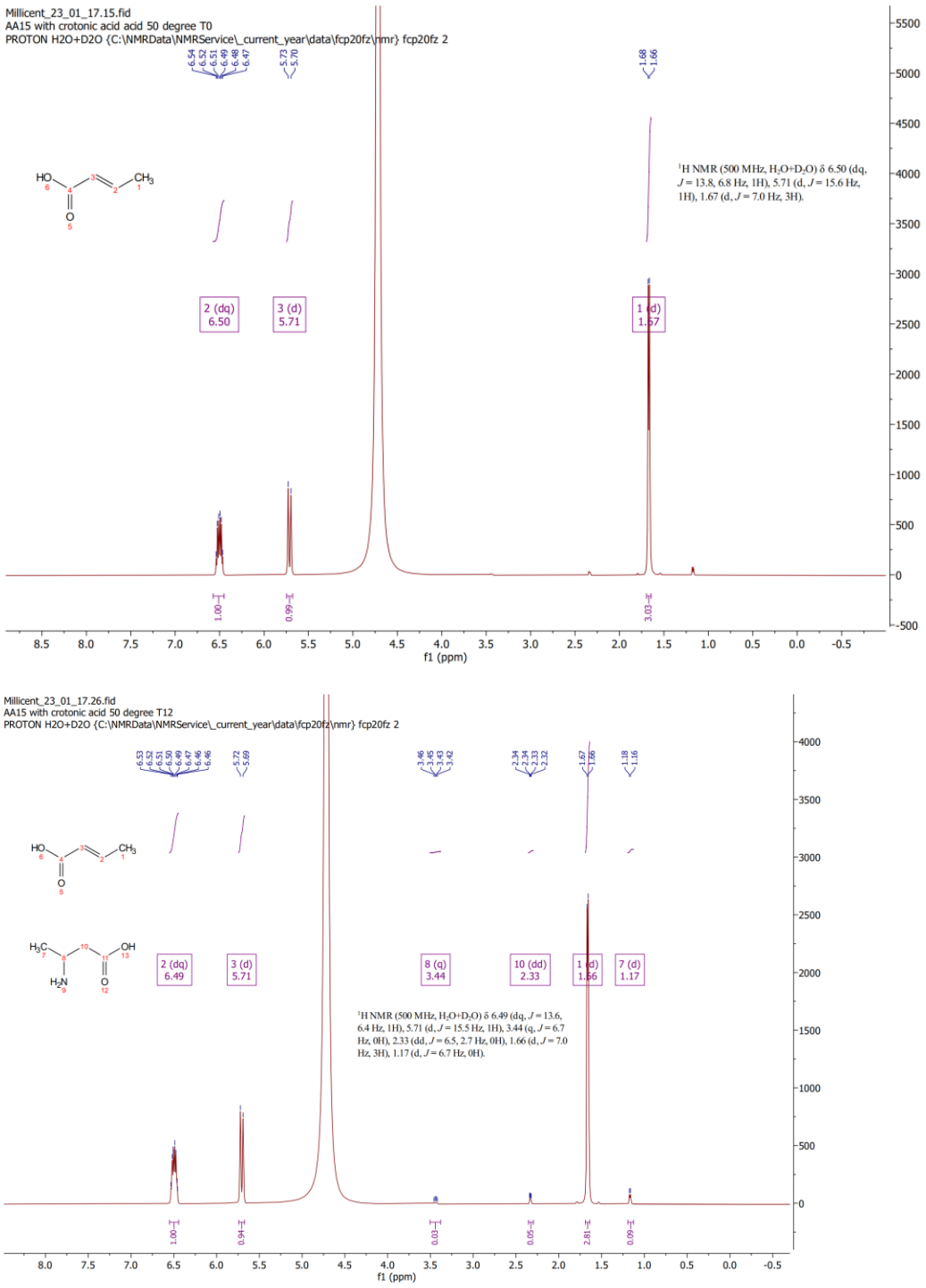

Figure A2.3:

Substrate: 300 g/L Crotonic Acid, pH 9.0 (adjusted by 35% NH_4OH)

Conditions: Reaction at 50°C with NMR monitoring every 2 hours, over 24 hours reaction time.

Enzyme Used: AspA-AA15

Observation: The top spectra represent the beginning of reaction and the bottom represent the reaction after 24 hours. The spectra show a decrease in crotonic acid peaks (δ6.48 ppm and δ5.69 ppm) and the emergence of new product peaks

corresponding to R-BABA (e.g., δ3.42 ppm, δ2.31 ppm, and δ1.15 ppm), indicating enzymatic activity.

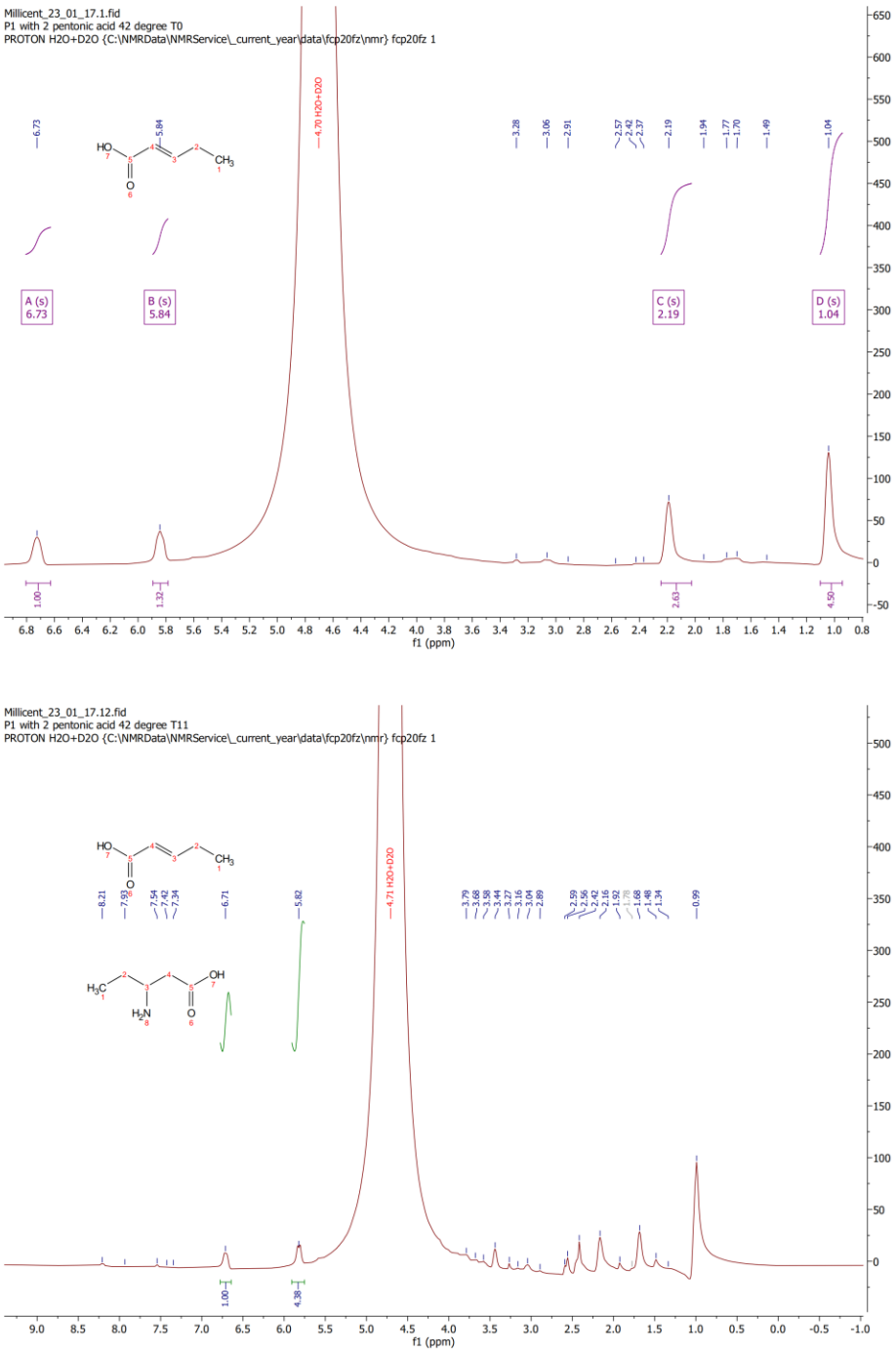

Figure A2.4:

Substrate: 80 g/L 2-Pentenoic Acid, pH 9.0 (adjusted by 35% NH_4OH)

Conditions: Reaction at 42°C with NMR monitoring every 2 hours, over 24 hours.

Enzyme Used: AspB-P1

Observation: The peaks displayed in this spectrum are not very clear may due to the interference of water peak.

Appendix 3: Analysis of purified 6H-PmAspA-QM and 6H-DtMAL-SM protein via ÄKTA Pure chromatography system.

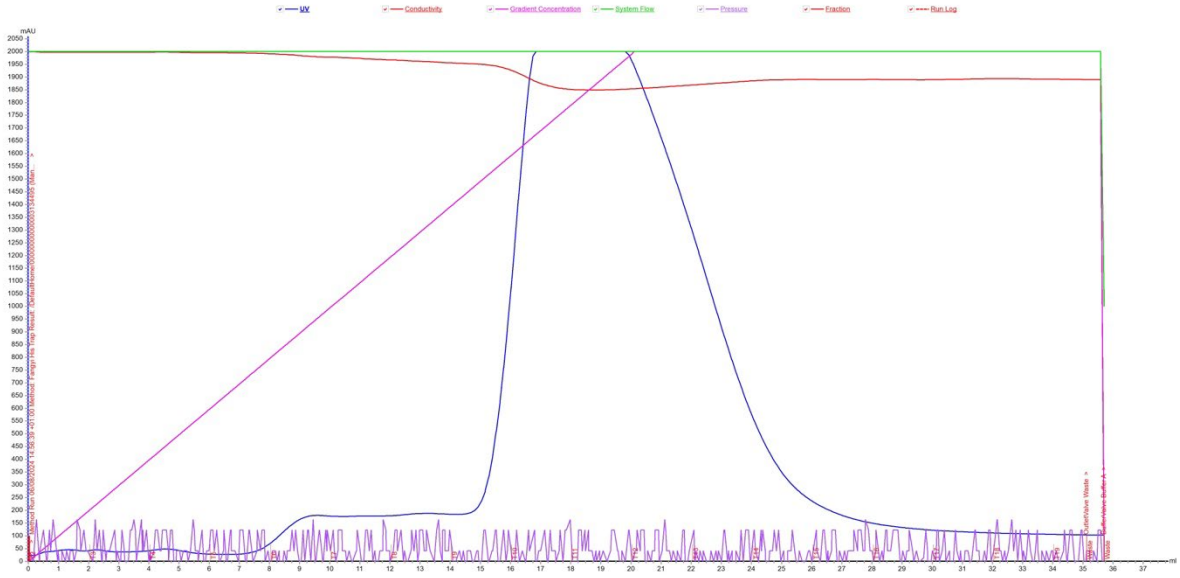

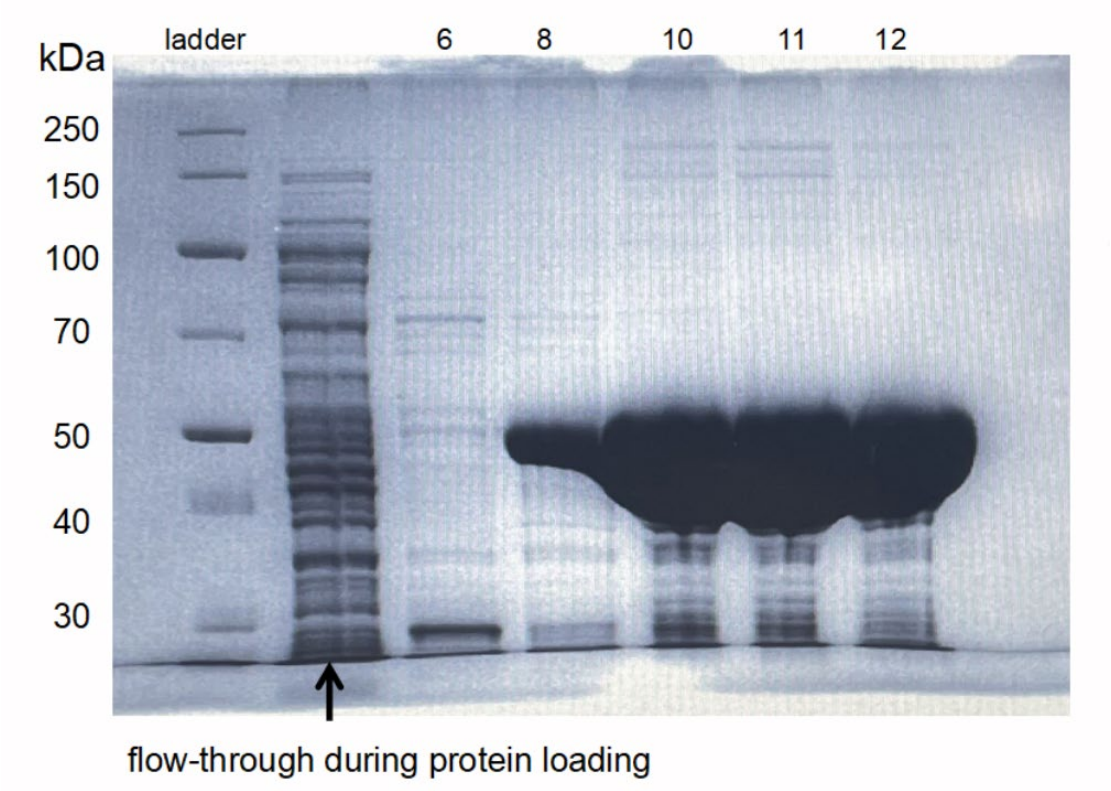

Figure A3.1:

SDS-PAGE gel displaying the purification of 6H-PmAspA-QM protein using the ÄKTA Pure chromatography system. The "flow-through" lane represents unbound proteins collected during column loading. Lanes 6, 8, 10, 11 12 correspond to elution fractions, with distinct bands at approximately 52 kDa, indicating successful purification of 6H-PmAspA-QM. Molecular weight markers (ladder) are shown in the first lane for reference.

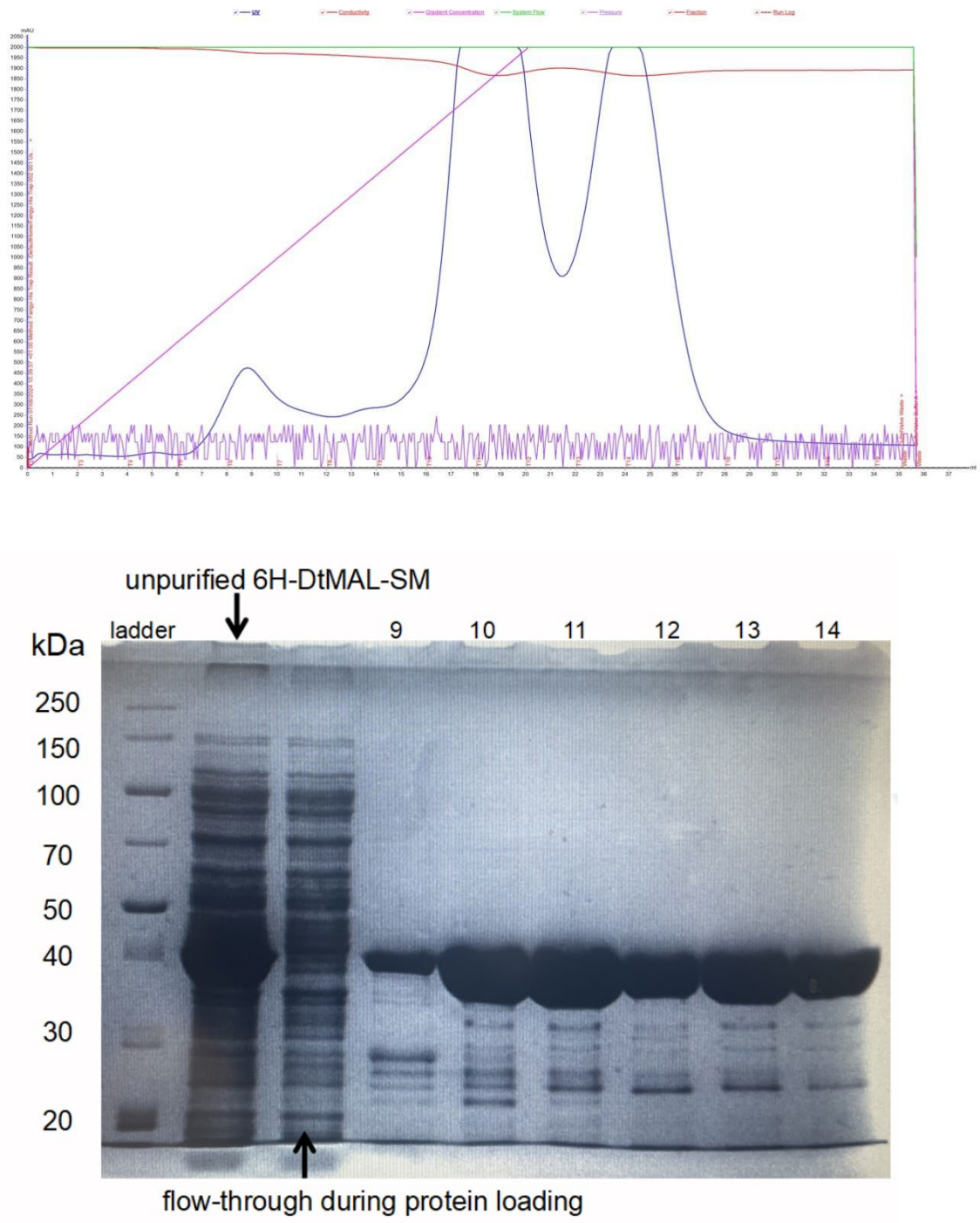

Figure A3.2:

SDS-PAGE gel displaying the purification of 6H-DtMAL-SM protein using the ÄKTA Pure chromatography system. The "unpurified" lane contains the crude protein extract prior to purification, while the "flow-through" lane represents unbound proteins collected during column loading. Lanes 9 to 14 correspond to elution fractions, with distinct bands at approximately 48 kDa, indicating successful purification of 6H-DtMAL-SM. Molecular weight markers (ladder) are shown in the first lane for reference.